Martin Treiber, Arne Kesting

# Traffic Flow Dynamics

## Data, Models and Simulation

March 27, 2025

Springer

# Contents

# Part I
# Traffic Data

# Part II
# Traffic Flow Modeling

# Chapter 16
# Stability Analysis

*Mathematics is the key and door to the sciences.* Galileo Galilei

**Abstract** Second-order macroscopic models and most car-following models are able to reproduce traffic waves or other observed instabilities of traffic flow. After an intuitive introduction, we define the relevant stability concepts such as local instability, convective and absolute string and flow instability, or Ljapunov and asymptotic stability. We give general analytic criteria for the occurrence of these instabilities for microscopic and macroscopic models. For microscopic models, we compare the approaches via Fourier analysis and transfer functions. The formulation is more comprehensive than the various accounts in the specialized literature and can be evaluated for any traffic flow model with a well-defined acceleration function, and also for models with explicit time delays or considering several vehicles ahead (multi-anticipation) or one in the back. The stability criteria allow us to characterize the influencing factors of traffic flow instabilities and answer the question of if, and in which way, the driving behavior (or advanced driver-assistance systems) influence traffic flow stability.

## 16.1 Formation of Stop-and-Go Waves

Instabilities of traffic flow resulting in *traffic waves*, also termed *stop-and-go waves*, are caused by the delays in adapting the speed to the actual traffic conditions. These *delays* are the consequence of finite acceleration and braking capabilities, and also result from finite reaction times of the drivers. If traffic density is sufficiently high, this delay leads to a positive feedback on density and speed perturbations.[1] We will now intuitively explain this *vicious circle* with the help of Fig. 16.1 (see also Fig. 16.8):

[1] Generally, delays in a feedback control system favor instabilities. This can be experienced intuitively when taking a shower and controlling the water temperature, particularly, if the response time between the controlling action and the result (a change of the water temperature) is rather long.

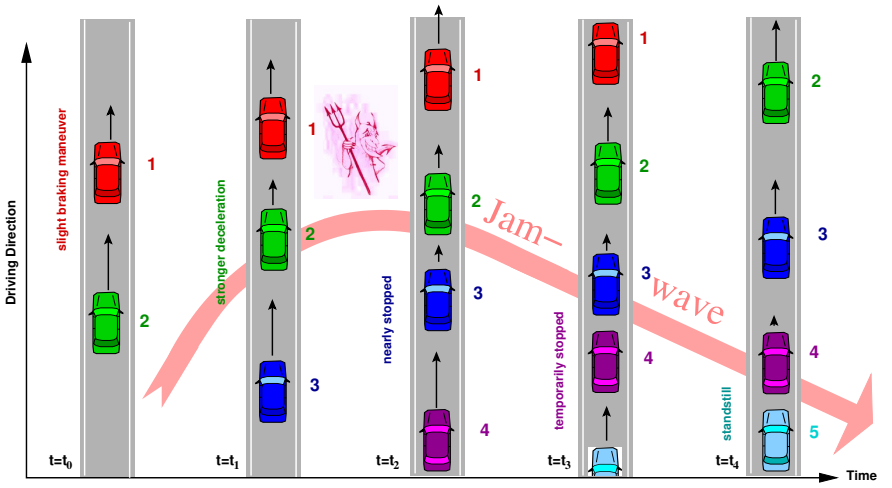


**Fig. 16.1** The vicious circle: In order to regain the safety gap, the driver of every following vehicle needs to brake harder than his or her predecessor. The numbers beside the vehicles denote the vehicle index.

- The scenario starts with a platoon of cars initially in steady-state equilibrium at speed $v_e$. At time $t = t_0$, the driver of car 1 brakes slightly (for whatever reason) and continues driving at a slightly lower speed $v_1 < v_e$.
- As a result, the new optimal speed for car 2 is given by $v_1$ as well. So the driver of this car reduces his or her speed from $v_e$ to $v_1$ in a finite time interval ending at time $t_1$.
- If traffic is sufficiently dense, or if the speed adaptation time is sufficiently long, the gap of car 2 at time $t_1$ is smaller than the steady-state gap $s_e(v_1)$ at the speed of the leading car 1. In order to regain his or her desired gap, the driver of car 2 has to brake *more*, i.e., he or she decelerates temporarily to a speed $v_2 < v_1$ in the time interval between $t_1$ and $t_2$. The degree of this *overreaction* increases with the sensitivity to changes of the gap which is given by $|v_e'(s)|$ and $V_e'(\rho)$ for microscopic and macroscopic models, respectively.
- Since the driver of the next car 3 also needs some time to adapt the speed, the gap between car 2 and car 3 may become smaller than the steady-state gap $s_e(v_2)$. Therefore, the driver of car 3 decelerates further to a minimum speed $v_3 < v_2$ at time $t_2$.
- This positive feedback continues when going to the next car 4 which has to stop completely (time $t_3$).
- The resulting traffic wave dissolves only if the number of new vehicles approaching the wave from behind decreases.

As a result, a stop-and-go wave emerges "out of thin air" giving rise to the name *phantom jam* for this phenomenon (see also Section 21.2 and the right diagram of Fig. 16.11). At sufficiently low traffic density, or when traffic consists predominantly of agile drivers, the vicious circle is broken. In this case, the drivers have

already equilibrated their speed to the new situation at the time where a new vehicle comes within interaction distance, so the stop-and-go mechanism is not effective. As a result, all drivers following car 1 decelerate to $v_1$ but not further (see the left diagram of Fig. 16.11 for an example). From the qualitative consideration, it follows that the stop-and-go mechanism is never effective in models describing instantaneous speed adaptations and zero reaction times as in first-order macroscopic models (LWR models), or in Newell's microscopic model. As a result, density perturbations never grow in such models, so they cannot describe traffic instabilities.[2]

In summary, the qualitative argumentation suggests that the tendency to traffic flow instabilities increases with

- increasing speed adaptation time,
- increasing traffic density,
- and increasing sensitivity $|v_e'(s)|$ or $V_e'(\rho)$ for changes of the gap.

The stability analysis expounded below agrees with this reasoning.[3]

## 16.2 Mathematical Classification of Traffic Flow Instabilities

We emphasize that all types of instabilities discussed in this chapter describe a tendency to oscillations, traffic waves, stop-and-go traffic and the like. However, they do *not* correspond to accidents (which would be characterized by negative gaps or densities exceeding the maximum density $\rho_{\max}$ in the microscopic and macroscopic descriptions, respectively). Generally, simulated accidents only occur if the instability thresholds are exceeded extremely. However, in some models representing "short-sighted" drivers (such as the OVM), accidents may happen even for parameters corresponding to *perfectly stable* traffic.

Moreover, the *physical* instabilities of real traffic discussed below have to be distinguished from *numerical instabilities*. The latter result from integration steps being too large, or by applying an unsuitable numerical update method (see Sections 10.5 and 11.3 for details). In contrast, real traffic instabilities are the consequence of physical delays due to finite accelerations and reaction times.[4]

---

[2] The only way to generate a traffic breakdown in such models is by simulating a bottleneck and assuming upstream boundary conditions corresponding to an inflow exceeding the bottleneck capacity. Then, as soon as the flow at the bottleneck exceeds its capacity, the density immediately upstream of the bottleneck jumps to the congested branch of the fundamental diagram at a flow corresponding to the bottleneck capacity (cf. Section 9.6).

[3] Notice that, in some models, the speed adaptation time may depend on traffic density getting shorter for increased density. This can more than compensate for the destabilizing effects of traffic density itself, so congested traffic may be unstable for most densities but *restabilize* for high densities near the maximum.

[4] In particular, both physical and numerical instabilities include so-called *convective instabilities* which are discussed in the Sections 10.5 and 16.6, respectively. Convective physical and numerical instabilities have no commonalities, whatsoever.

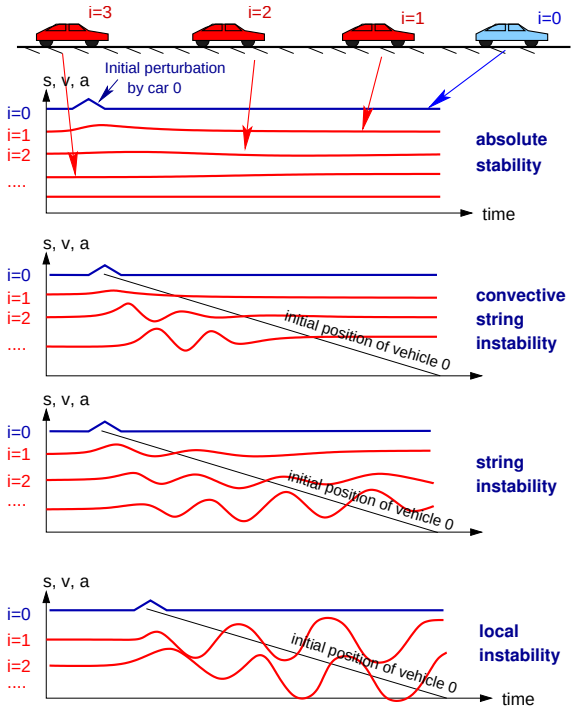


**Fig. 16.2** Schematic sketch of the different instability concepts in terms of speed time series of single vehicles: If traffic flow is *convectively string unstable*, perturbations grow but propagate only upstream. Consequently, all vehicles drive smoothly at the time they pass the location of the initial perturbation (indicated by the thin black line). If traffic flow is absolutely string unstable, the perturbation eventually spreads everywhere but any given vehicle eventually drives smoothly, i.e., it can follow a vehicle with predetermined trajectory without sustained oscillations (platoon stability) In the presence of *local instabilities* or *platoon instabilities*, even following a single vehicle leads to sustained oscillations.

In the following, we distinguish categories of traffic instabilities depending on criteria for their existence and the type of resulting congestion pattern.

**Evolution in time or over vehicles: local versus string instability.** Local instability relates to the car-following dynamics of a single or a few vehicles following a leader with a predetermined trajectory (typically introducing a perturbation by a temporary speed drop or fluctuation while driving at constant speed for the rest of the time).

To define local stability, we require that the leader $j = 0$[5] only introduces perturbations for times $t < t_0 < \infty$, i.e., the deviation $u_0(t)$ from the final steady state

[5] To avoid confusions with the imaginary unit $i$ needed later on, we will denote the vehicle index as $j$ throughout this chapter.

satisfies $u_0(t) = 0$ for $t > t_0$ while generally $u_j(t) \neq 0$ for all followers $j > 0$.[6] Then, this system is (asymptotically) *locally stable*, if the gap and speed fluctuations of any given follower eventually decay to zero for $t \to \infty$. Otherwise, it is locally unstable (cf. Fig. 16.2).[7]

In mathematical terms, a platoon of $n$ followers is (asymptotically) locally stable if the deviations $u_j(t)$ of any follower $j = 1, \ldots, n$ satisfy

$$\lim_{t\to\infty} u_j(t) = 0 \text{ if } u_0(t) = 0 \text{ for all } t > t_0. \tag{16.1}$$

Since this definition refers to a (finite) platoon of followers, one also speaks of *platoon (in)stability*. Notice that this definition does *not* exclude cases where fluctuations may *temporarily* increase from follower to follower as illustrated by the second set of trajectories of Fig. 16.2 (convectively string unstable but locally stable): The maximum perturbation amplitude increases from follower 1 to 2 to 3 but eventually, all perturbations decay to zero. The trajectories of Fig. 16.4 show another example of this situation. Later on, we will mathematically describe such an increase by the absolute value of the transfer function (16.71).

Obviously, this stability concept is only applicable for microscopic models. For practical purposes, it is relevant when developing the feedback controllers of ACC systems.[8]

In contrast, the ubiquitous traffic waves are the result of *string instability*. In defining string instability, we consider how an *infinitely long* vehicle platoon on an infinite homogeneous road responds to a local and temporary perturbation. Traffic flow is (asymptotically) string stable if such a perturbation eventually decays *everywhere*:

$$\lim_{t\to\infty} \max_j (u_j(t)) = 0. \tag{16.2}$$

Otherwise, it is string unstable.

We emphasize that the definitions (16.1) and (16.2) for local and string stability only differ if the system is infinite or if it is closed (ring road). Mathematically speaking, only local stability is well defined in open finite systems, i.e., in real-world road networks. Does this mean that string instability is irrelevant in open systems? Not necessarily since (i) even for a temporary initial perturbation of the leader, the definition of local stability allows for a temporary growth of perturbations which is excluded if the system is string stable, (ii) for practical purposes, a string of a few hundred vehicles is sufficient to generate traffic waves, i.e., it represents already a

[6] In general dynamic systems texts, stability types are typically defined in terms of a system response to initial conditions with the system left to its own devices, afterwards. However, in the driven open systems considered here, a nontrivial steady state implies a leader with a fixed trajectory at all times. Therefore, we adapted the definitions correspondingly.

[7] It may also be Ljapunov stable, i.e., the perturbations remain limited. However, this type of stability does not play a role in this context, see also page 352.

[8] At least, if the penetration level of ACC equipped vehicles is sufficiently small. Otherwise, the influence of ACC-driven vehicles on the string instability becomes relevant as will be discussed in the main text below.

good approximation of an "infinite" system,[9] (iii) when considering the response to *sustained* (rather than temporary) perturbations of a leader, string stability rather than local stability determines whether perturbations grow when propagating from follower to follower as will be shown in Sect. 16.4.3 below.

Considering the responses to sustained perturbations of a leader in open systems and heterogeneous vehicles, three categories of string stabilities are distinguished:

- *Head-to-tail* string stability: The last follower of a finite heterogeneous platoon shows smaller perturbations than the leader although perturbations may grow from vehicle to vehicle in between.
- *Strict* string stability: Perturbations always decrease from follower to follower.
- *Asymptotic* string stability: string stability of an infinite or closed system, i.e., string stability in the stricter sense.

Furthermore, a string *in*stability can be of a convective or absolute nature, see page 354 below.

As illustrated by Fig. 16.3, string stability is a much more restrictive concept compared to local stability: Traffic flow may be string unstable even if speed fluctuations within a vehicle platoon of finite size decay quickly, or even if there are *no local oscillations at all*. An example of this latter case is given in the two sketched situations in the middle of Fig. 16.2, in the simulations of Fig. 16.6, and particularly in Problem 16.3. This has immediate practical implications for developers of ACC controllers: Even if the ACC is optimized to be perfectly free of oscillations when following a "test hare vehicle" driving a prescribed speed profile, traffic flow mainly consisting of such ACC vehicles may be *absolutely string unstable*.

Since string instability is defined in terms of a collective phenomenon, it can be applied to both microscopic and macroscopic models. To emphasize its macroscopic nature, one also speaks of *collective instability*, or *flow instability*.[10]

**Types of perturbation and asymptotic state: Ljapunov, asymptotic and structural stability.** If we require that any sort of sufficiently small initial perturbations remain small forever, we speak of *Ljapunov stability*. If we additionally require that sufficiently small perturbations tend to zero for $t \to \infty$, the system is *asymptotically stable*. If we allow not only initial perturbations but also small persistent fluctuations and all trajectories remain close to the unperturbed trajectories, the system is *structurally stable*. These stability concepts are mainly used by mathematicians[11]

[9] For a driver driving through stop-and-go traffic, it is little consolidation that the perturbations will decay in the limit $t \to \infty$.

[10] Some authors stress that there is a conceptual difference between string instability (relevant for microscopic models), and flow instability (macroscopic models). However, observed differences are merely a consequence of an imperfect equivalence between microscopic and macroscopic models with respect to macroscopic phenomena (notice that microscopic models can describe macroscopic phenomena but not vice versa). The unified instability criteria to be developed in the next sections show that the concepts of string and flow instability are identical in a precisely defined sense: For each microscopic model displaying string instabilities in a subset of the space spanned by the model parameters and the steady-state traffic density, there exists a micro-macro relation to a macroscopic model displaying flow instability for exactly the same subset.

[11] We do not give the precise mathematical definitions.

and apply to arbitrary dynamical systems. For the traffic flow models with smooth acceleration functions considered here, Ljapunov and asymptotic stability are equivalent concepts.[12] Since Ljapunov and asymptotic stability are defined in terms of sufficiently small but otherwise arbitrary initial and asymptotic perturbations, these concepts refer to linear string (or flow) stability when applied to traffic flow models. When explicitly defining the latter in Eq. (16.4), we refer to asymptotic rather than Ljapunov stability, i.e., we require that all small perturbations have negative growth rates, i.e., they tend to zero.

**Amplitude of perturbation: linear versus nonlinear instability.** If arbitrarily small perturbations increase in the course of time, one speaks of *linear instability*. If small perturbations decay but sufficiently severe perturbations (caused, e.g., by hard braking maneuvers or inconsiderate lane changes) develop to persistent traffic waves, this corresponds to *nonlinear instability*. As illustrated in Fig. 16.3, car-following models or second-order macroscopic models generally have parameter ranges where, for a certain range of steady-state densities, traffic flow is linearly stable and simultaneously nonlinearly unstable, i.e., small perturbations decay and larger ones develop to stop-and-go waves. This is termed *metastability*. As a consequence of this type of instability, the future dynamics depends not only on the present and future exogenous conditions but also on the past – for arbitrarily long times. For example, given the same traffic demand profile, there may be growing regions of congested traffic (a traffic breakdown occurred in the past), or completely free traffic (no breakdown in the past). This dependence on the past ("path dependence") is also called *hysteresis* .

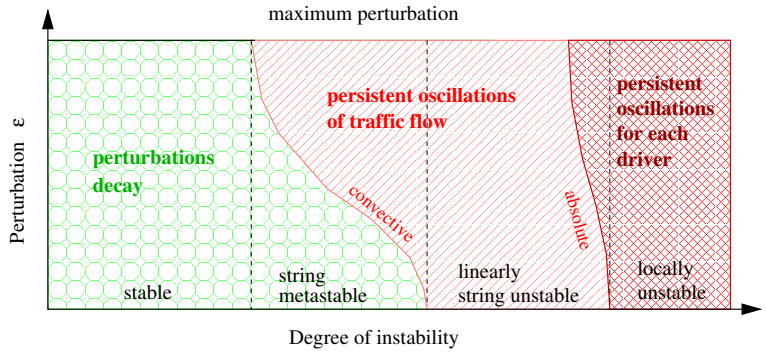


**Fig. 16.3** Sequence of stability types as a function of the inherent tendency to instabilities (horizontal axis) and the amplitude of the initial perturbation. The string instability is convective in the limit of reaching the boundary to stability, and absolute at the boundary of local instability.

[12] The distinction may become relevant for models with non-smooth or even non-continuous acceleration functions. Typically, this is the case when the model formulation involves several distinct traffic regimes (e.g., Gipps' model or the Wiedemann model). Such models may be Ljapunov but not asymptotically stable.

In order that a perturbation can develop to a persistent jam, the outflow from the congested region must be smaller than the inflow, i.e., the bottleneck capacity under congested conditions (also known as *active* or *activated bottleneck*) must be smaller than the maximum possible flow through the bottleneck under free-flow conditions (*static capacity*). Observed values for the difference between the static and dynamic capacities, the so-called *capacity drop*, are of the order of 10% (cf. Chapter 5.5). Consequently, the fundamental diagram is not unique for densities in the metastable range. Instead, there are two values for the flow, a higher one for free traffic, and a lower one for congested traffic. For the graph of the fundamental diagram, this leads to the characteristic shape of a mirrored Greek $\lambda$, also referred to as the *inverse lambda* shape,[13] cf. Fig. 5.16 and 5.17.

Formally, we define linear and nonlinear string instability in macroscopic terms by considering an infinite system initially in steady state at density $\rho_e$ and looking at the spatiotemporal development of the response $U(x,t)$ of a temporary and localized perturbation $U_\varepsilon(x,0)$ of amplitude $\varepsilon$ denoting, e.g., the difference between the actual and steady-state local speed fields. If the initial perturbation corresponds to a sudden change $\varepsilon$ of speed of a single vehicle located at $x = 0$, the macroscopic initial perturbation $U_\varepsilon(x,0)$ of the speed field is

$$U_\varepsilon(x,0) = U_\varepsilon(x) = \begin{cases} \varepsilon & \text{if } |x| < \frac{1}{2\rho_e}, \quad \varepsilon > 0, \ \ x \in I\!R, \\ 0 & \text{otherwise.} \end{cases} \tag{16.3}$$

This means, the speed field is changed by $\varepsilon$ in a region whose width $\Delta x = 1/\rho_e$ corresponds to the distance between two vehicles, i.e., to the effective space attributed to one vehicle. Traffic flow is linearly unstable if

$$\lim_{t\to\infty} \max_x U(x,t) > 0 \quad \text{for all } \varepsilon > 0. \tag{16.4}$$

It is nonlinearly unstable or *metastable*, if there exists a minimum perturbation amplitude $\varepsilon_{\text{nl}} > 0$ such that

$$\lim_{t\to\infty} \max_x U(x,t) = \begin{cases} U_0 > 0 & \text{if } \varepsilon > \varepsilon_{\text{nl}}, \\ 0 & \text{if } \varepsilon \in [0, \varepsilon_{\text{nl}}]. \end{cases} \tag{16.5}$$

As illustrated in Fig. 16.3, the limit between linear instability and metastability is defined by $\varepsilon_{\text{nl}} \to 0$, while the limit between metastability and absolute stability is given by Eq. (16.5) for the limit of a maximum perturbation, e.g., $|\varepsilon| = V$ (braking to a complete stop).[14]

**Propagation of the perturbation: absolute versus convective instability.** If traffic flow is (linearly or nonlinearly) string unstable, the region of perturbations as considered from a stationary observer can propagate in both directions (*absolute*

[13] Although this is not correct: The Greek $\lambda$ is mirrored and not upside down.

[14] To make the perturbation more massive, the duration of the perturbation must be increased such that it results in a fully-formed initial jam.

*string instability*), or exclusively upstream or downstream which is termed *upstream* and *downstream convective instability*, respectively (see Fig. 16.4).

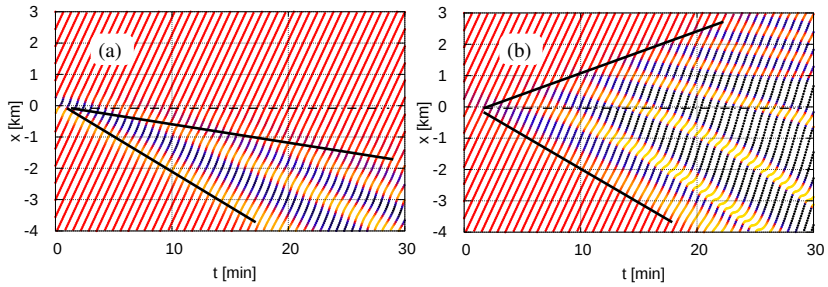


**Fig. 16.4** Visualization of the spatiotemporal evolution of (a) convective upstream string instability, and (b) absolute string instability by vehicle trajectories in a space-time plot. Shown are IDM simulations with $l = 5\,\mathrm{m}$, $v_0 = 120\,\mathrm{km/h}$, $s_0 = 2\,\mathrm{m}$, and $b = 1.5\,\mathrm{m/s^2}$, $T = 1.5\,\mathrm{s}$, and acceleration parameters $a = 1.1\,\mathrm{m/s^2}$ and $a = 0.9\,\mathrm{m/s^2}$ for the plots (a) and (b), respectively. Shown are the trajectories of every 20th vehicle.

Convective instabilities were originally observed in open systems of fluid flows such as water in pipes. In this case, the convective instability is of the downstream type: perturbations leave the system together with the fluid after some time, i.e., they are *convected out* of the system.[15]

In traffic flow, however, one observes that perturbations generally grow *against* the driving direction and leave the system, i.e., the road section under consideration, by the upstream boundary. Of course, this is particularly true for stop-and-go traffic waves moving backwards at a constant velocity (cf. Section 21.3). We emphasize that this propagation direction is not obvious: While the asymmetric interactions of drivers (reacting essentially to the leading and hardly to the following vehicle) ensure that, when considering a system *comoving with the drivers*, string instability is always of the upstream convective type[16] (cf. Figs. 16.4(a) and 16.11) both types of convective instability are theoretically plausible in the fixed system. In fact, both types can be reproduced in simulations. However, downstream convective instability is not robust against nonlinear effects (cf. Fig. 16.5), so only upstream convective instability is actually observed.

The distinction between convective and absolute instability is relevant since traffic flow relates to an *open system* where absolute and convective instability leads to qualitatively different congestion patterns:

- If traffic flow is absolutely string unstable, the perturbed region will sooner or later cover the whole road section under consideration.

[15] This technical term originates from the Latin *convehi*: to move together.

[16] At least, if traffic flow is locally stable which is safe to assume.

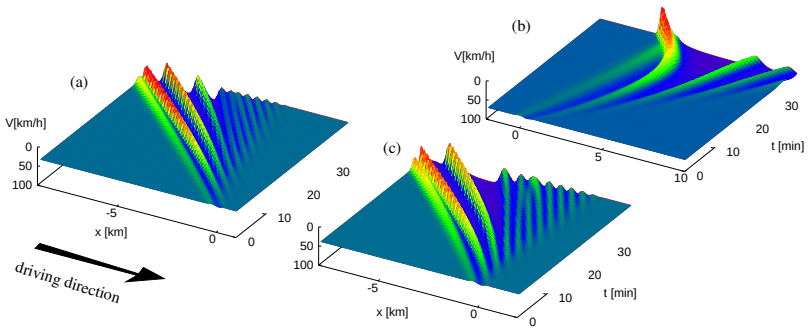


**Fig. 16.5** Speed response functions for the initial localized perturbation (16.3). Shown are IDM simulations of (a) convective instability propagating upstream, (b) linear convective instability propagating downstream which is destroyed by nonlinearities, and of (c) the limit between convective and absolute instability.

- If traffic flow is convectively string unstable, the perturbations eventually will leave the system. Thus, in a given section, oscillations resulting from temporary perturbations are not persistent *even in the presence of linear instability*. If there are persistent local perturbations (e.g., lane changes near ramps or lane closures), the oscillations are, of course, persistent as well. However, they are small near the location of the perturbations (generally at a bottleneck), and increase in amplitude further upstream. All this is markedly different in closed systems (ring roads) where there is no qualitative long-term difference between these stability types.

Convective instability is a widespread phenomenon. For example, *all* oscillations and traffic waves on the German highway A5 (Fig. 6.1) are the consequence of convective instability driven by persistent perturbations near the bottlenecks. In contrast, city traffic flow generally is stable and stop-and-go conditions are the trivial consequence of the operations of traffic lights. In Section 16.6 we show that string instability *always* starts as a convective instability (cf. Fig. 16.3). From a multitude of observations, we conclude the following:

The vast majority of all instabilities of highway traffic flow is of the convective type.

Formally, one can define convective instability in terms of the dynamics of the perturbation field $U(x,t)$ for a given localized and temporary initial perturbation $U_\varepsilon(x)$ according to Eq. (16.3): Homogeneous flow is convectively unstable with respect to this perturbation, if

$$\lim_{t\to\infty} \max_x U(x,t) > 0 \quad \text{and} \quad \lim_{t\to\infty} U(0,t) = 0. \tag{16.6}$$

The first condition is true if traffic flow is (linearly or nonlinearly) string unstable, i.e., the initial perturbation does not decay to zero, at least somewhere in the system. The second condition states that the perturbations eventually vanish at the location of the initial triggering point.[17]

By analogy one can define absolute string instability by requiring the first condition to be true, and the second to be false. By suitably combining these conditions with Eq. (16.5), one can define in a straightforward way convective and absolute linear instability and metastability (nonlinear instability).

**Stability in stochastic models.** We can determine the behavior in the presence of acceleration noise or other fluctuations described by stochastic models from the above definitions of convective and nonlinear instability:

- If the noise is of sufficiently low amplitude to allow a linear analysis, we obtain persistent fluctuations for any type of linear string or flow instability. In contrast, if a deterministic model describes convectively unstable traffic flow in open systems, all initial perturbations are eventually convected out of the system. This means, small fluctuations change the qualitative behavior in such systems while they have not much influence, otherwise.
- If the noise is of sufficient amplitude to warrant a nonlinear description, it can trigger nonlinear instabilities. This means, larger-amplitude noise can change the qualitative system behavior with respect to the deterministic description if the system is convectively or absolutely metastable.

**Wavelength of the perturbations.** Since traffic flow represents an extended system which can be abstracted to an infinitely long homogeneous road, there is, in principle, an infinite multitude of perturbations leading to instabilities. In Section 16.4, we show, that the perturbations can be arranged in two branches or "modes" of periodic perturbations with arbitrary real-valued wavelengths. However, we can only observe the perturbations becoming first unstable when increasing the traffic density (or making the model more unstable): Once nonlinearities become effective (saturation, capacity drop, reversal of the propagation velocity), all other perturbations are suppressed.

Depending on the nature of the onset of the "first" instability, we distinguish two categories: In the presence of *short-wavelength instabilities*, the first instability has a finite and typically short wavelength of only a few vehicle distances, i.e., each wave consists of only a few vehicles. In contrast, if there is a *long-wavelength instability*, the wavelength of the "first" unstable perturbation tends to infinity. Since vehicle conservation implies that the growth rate tends to zero when the wavelength tends to infinity *regardless of the degree of (in-)stability*, the practically observed waves originating from long-wavelength instabilities, i.e., the perturbations with maximum growth rate, are large but finite (of the order of 1 km or more). Mathematicians have shown that instabilities are always of the long-wavelength type

- for continuous-in-time car-following models containing no explicit reaction time (such as the OVM or the IDM)

[17] More generally, the perturbations eventually vanish at *any* fixed location $x$ for $t \to \infty$.

- for second-order local macroscopic models such as Payne's model or the Kerner-Konhäuser model.

In contrast, the instability may be (but need not to be) of the short-wavelength type if

- time is discrete (iterated maps, e.g., Gipps' model),
- explicit reaction times are modeled (HDM, cf. Section 13.2),
- or nonlocal macroscopic models (such as the GKT model) are considered.

This means, the first instability may be of the short-wavelength type if the model contains some nonlocalities in space or time. Since observed instabilities are always of the long-wavelength type, one can restrict the further analysis to this category. Conversely, if one observes short-wavelength instabilities in the simulations,[18] this must be considered as an artifact of the model, or the consequence of an erroneous (or erroneously parameterized) numerical integration method.

## 16.3 Local Stability

We consider a situation where a leading vehicle drives at constant speed and investigate small changes $y(t)$ and $u(t)$ of the gap and speed of a single follower with respect to the steady-state equilibrium:

$$s(t) = s_e + y(t), \tag{16.7}$$

$$v(t) = v_e + u(t). \tag{16.8}$$

When analyzing local stability, it is essential that the leading vehicle does not exhibit persistent perturbations since the question whether persistent perturbations are amplified when transferred to the following vehicles refers to string instability. Furthermore, instead of considering an initial perturbation of the leader, we can investigate an unperturbed leader and an initial perturbation of the follower as specified above. Inserting this ansatz into the general formulation (11.3), (11.6) of time-continuous models, we obtain, in zeroth order of the perturbations ($y = u = 0$), the steady-state conditions

$$f(s_e, v_e, v_e) = 0 \quad \text{and} \quad \tilde{f}(s_e, v_e, 0) = 0 \tag{16.9}$$

for the two forms $f$ and $\tilde{f}$ of the acceleration function, respectively (cf. Section 11.4). These conditions define the *microscopic fundamental diagram* in terms of the steady-state gap $s_e$ for a certain constant speed $v_e$ which can be written as $v_e(s_e)$ (steady-state speed for a given gap), or $s_e(v_e)$ (steady-state gap for a given speed).

In first order of the perturbations $y$ and $u$ of the follower, we obtain, for models defined by the acceleration function $f$, the following system of ordinary linear

[18] For example, Gipps' model in its original formulation exhibits a short-wavelength instability with the smallest possible wavelength of two car distances.

differential equations:

$$\frac{\mathrm{d}y}{\mathrm{d}t} = u_l - u = -u, \tag{16.10}$$

$$\frac{\mathrm{d}u}{\mathrm{d}t} = f_s y + f_v u + f_l u_l = f_s y + f_v u. \tag{16.11}$$

Notice that the assumed constant speed of the leading vehicle implies $u_l = 0$. The coefficients $f_s$, $f_v$, and $f_l$ of the linearization originate from a first-order Taylor expansion of the acceleration function $f$ with respect to its three independent variables around the steady-state equilibrium,

$$f(s, v, v_l) = f(s_e, v_e, v_e) + f_s y + f_v u + f_l u_l + \text{ higher orders} \tag{16.12}$$

with, by definition, $f(s_e, v_e, v_e) = 0$ and the expansion coefficients

$$\boxed{f_s = \left.\frac{\partial f}{\partial s}\right|_e, \quad f_v = \left.\frac{\partial f}{\partial v}\right|_e, \quad f_l = \left.\frac{\partial f}{\partial v_l}\right|_e.} \tag{16.13}$$

The subscript $e$ denotes that the derivatives are evaluated at the steady-state point $s = s_e$ and $v = v_l = v_e(s_e)$.

By virtue of condition (16.9) describing a one-dimensional manifold of steady-state solutions $v_e(s)$, the three Taylor coefficients are not independent of each other. Moving along the space of steady-state solutions by simultaneously changing $s$ and $v = v_l$ must not change the acceleration (which is always zero), i.e.,

$$f_s \mathrm{d}s_e + (f_v + f_l)\,\mathrm{d}v_e = f_s \mathrm{d}s_e + (f_v + f_l)\,v_e'(s_e)\mathrm{d}s_e = 0 \tag{16.14}$$

resulting in

$$v_e'(s_e) = -\frac{f_s}{f_v + f_l}. \tag{16.15}$$

Expanding the general acceleration equation (11.3) for the alternative acceleration function $\tilde{f}(s, v, \Delta v)$ to first order leads to the linear system

$$\frac{\mathrm{d}y}{\mathrm{d}t} = u_l - u = -u, \tag{16.16}$$

$$\frac{\mathrm{d}u}{\mathrm{d}t} = \tilde{f}_s y + \left(\tilde{f}_v + \tilde{f}_{\Delta v}\right) u - \tilde{f}_{\Delta v} u_l = \tilde{f}_s y + \left(\tilde{f}_v + \tilde{f}_{\Delta v}\right) u. \tag{16.17}$$

with the Taylor expansion coefficients

$$\boxed{\tilde{f}_s = \left.\frac{\partial \tilde{f}}{\partial s}\right|_e, \quad \tilde{f}_v = \left.\frac{\partial \tilde{f}}{\partial v}\right|_e, \quad \tilde{f}_{\Delta v} = \left.\frac{\partial \tilde{f}}{\partial \Delta v}\right|_e.} \tag{16.18}$$

Comparing Eq. (16.11) with Eq. (16.17), it is evident that one needs to consider only one formulation of the acceleration function which we chose to be $f(s, v, v_l)$.

Formulations for the alternative acceleration function $\tilde{f}(s, v, \Delta v)$ can be obtained from that for $f$ by the following set of replacements:[19]

$$\boxed{f_s = \tilde{f}_s, \quad f_v = \tilde{f}_v + \tilde{f}_{\Delta v}, \quad f_l = -\tilde{f}_{\Delta v}.} \tag{16.19}$$

This is valid for all expressions in this chapter, including these for string instability. As an example, when applying the replacement rules to the steady-state condition (16.15), we obtain following relation for the microscopic fundamental diagram:

$$v_e'(s) = -\frac{\tilde{f}_s}{\tilde{f}_v} = -\frac{f_s}{f_v + f_l}. \tag{16.20}$$

### *16.3.1 Single Leader-Follower Pair*

Equations (16.10) and (16.11) describe a harmonic damped oscillator. To see this explicitly, we write them as a single second-order differential equation by taking the time derivative of Eq. (16.10) and inserting Eq. (16.11),

$$\frac{\mathrm{d}^2 y}{\mathrm{d}t^2} + 2\eta \frac{\mathrm{d}y(t)}{\mathrm{d}t} + \omega_0^2 y(t) = 0. \tag{16.21}$$

The damping constant $\eta$ and the angular oscillation frequency $\omega_0$ are given by

$$\eta = -\frac{f_v}{2} = -\frac{\left(\tilde{f}_v + \tilde{f}_{\Delta v}\right)}{2}, \quad \omega_0^2 = f_s = \tilde{f}_s. \tag{16.22}$$

Assuming the exponential ansatz

$$y = y_0 \mathrm{e}^{\lambda t} \tag{16.23}$$

we arrive at the quadratic equation

$$\lambda^2 + 2\eta\lambda + \omega_0^2 = 0 \tag{16.24}$$

for the (generally complex) growth rate $\lambda = \sigma + \mathrm{i}\omega$ ($\mathrm{i} = \sqrt{-1}$ is the imaginary unit) with the solutions

$$\lambda_{1/2} = -\eta \pm \sqrt{\eta^2 - \omega_0^2}. \tag{16.25}$$

The dynamics of the follower is locally stable if both solutions decay, i.e., the real parts are negative, $\sigma_{1/2} = \mathrm{Re}(\lambda_{1/2}) \leq 0$. This is satisfied if $\eta > 0$, or, with the definitions (16.22)

[19] We emphasize that we have defined the relative speed $\Delta v = v - v_l$ as the approaching rate. Some publications define it as the negative approaching rate which means that all signs of $\Delta v$ and $\tilde{f}_{\Delta v}$ are swapped.

$$\boxed{f_v < 0 \quad \text{or} \quad \tilde{f}_v + \tilde{f}_{\Delta v} < 0 \quad \text{Local stability.}} \tag{16.26}$$

Since, by virtue of condition (12.1), $f_v < 0$ for all plausible models, we conclude that time-continuous car-following models without additional delay by explicit reaction times are unconditionally locally stable.

As a more restrictive condition on the local behavior, we can require that all deviations from the steady-state decay are without oscillations, not even damped ones. This is the case if the imaginary parts of the growth rates are zero leading to $\omega_0^2 < \eta^2$, or $f_s \leq f_v^2/4$. Expressing $f_s$ by the sensitivity $v_e'(s)$ to changes of the gap, we obtain the following no-oscillation conditions (cf. the left column of Fig. 16.6):

$$\boxed{f_s \leq \frac{f_v^2}{4} \quad \text{or} \quad v_e'(s) \leq \frac{-\tilde{f}_v}{4}\left(1 + \frac{\tilde{f}_{\Delta v}}{\tilde{f}_v}\right)^2 \quad \text{No local oscillations.}} \tag{16.27}$$

Here, the transformation rules (16.19) and (16.20) have been applied to arrive at the second condition for models given in terms of the acceleration function $\tilde{f}(s, v, \Delta v)$. In summary, we can make the following statements on local instability:

- Since $f_v < 0$ for all sensible models and the above considerations are valid for time-continuous car-following models without explicit reaction-time delay, such models are *always* locally stable. However, this need not to be the case for iterated maps (Gipps' Model), or when considering explicit reaction times by delay-differential equation as in the HDM.
- The more restrictive no-oscillation or *overdamped* oscillator condition (16.27) is not always satisfied. For example, we obtain for the Optimal Velocity Model[20] the condition
$$v_e'(s)_{\text{OVM}} < \frac{1}{4\tau}. \tag{16.28}$$
This condition is more restrictive as the condition $v_e'(s)_{\text{OVM}} < 1/(2\tau)$ for string stability to be derived in the following section. As can be seen by the derivation, this relation between the thresholds of over-damped local stability and string stability is valid for any car-following model without sensitivity to speed differences that is formulated by ordinary differential equations.
- Near the threshold to string instability, the oscillations of a single vehicle when approaching the local steady state are hardly recognizable (cf. right column of Fig. 16.6). Reasoning in the converse direction, we conclude that when a vehicle driving with adaptive cruise control shows recognizable oscillations, it is nearly certain that traffic flow consisting of such vehicles is string unstable, even if the oscillations of the single vehicle are strongly damped. Considering models with the speed difference as exogenous factor, the model may even be *completely* free of oscillations in the local context, and simultaneously string unstable when considering traffic flow with many vehicles (cf. Problem 16.3).

[20] The partial derivatives of the acceleration function are $f_v = -1/\tau$, $f_l = 0$, $f_s = -v_e'(s) f_v$.

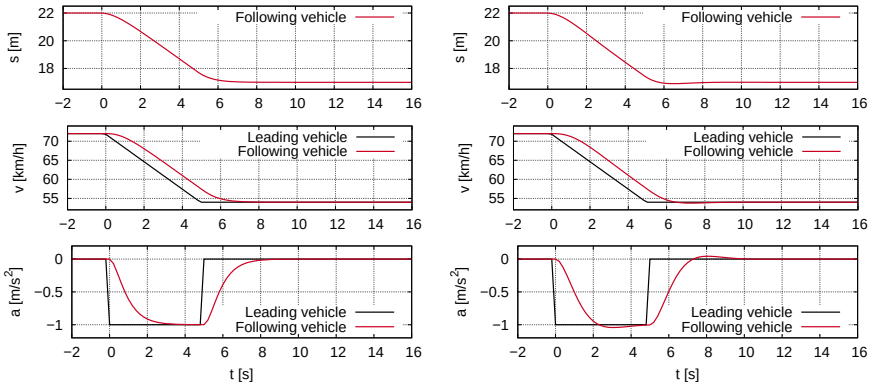


**Fig. 16.6** Response of an OVM vehicle to a speed reduction of the leading vehicle (driving a fixed speed profile) from 72 km/h to 54 km/h. Left: At the limit of an oscillation-free response ($v_e' = 1\,\mathrm{s}^{-1}$, $\tau = 0.25\,\mathrm{s}$). Right: Limit of string instability ($v_e' = 1\,\mathrm{s}^{-1}$, $\tau = 0.5\,\mathrm{s}$).

### *16.3.2 More Than One Follower*

For reasons of simplicity, the derivation above was restricted to a single follower, for example, a car with adaptive cruise control (ACC) following another car. The question arises if the condition for local stability changes when considering more than one follower. To investigate this case, we need to consider the full linearized equations for vehicle $j$ including the leading vehicle $j-1$. Assuming identical vehicles and drivers, we generalize the system (16.10), (16.11) to

$$\frac{\mathrm{d}y_j}{\mathrm{d}t} = u_{j-1} - u_j, \tag{16.29}$$

$$\frac{\mathrm{d}u_j}{\mathrm{d}t} = f_s y_j + f_v u_j + f_l u_{j-1}. \tag{16.30}$$

Now we differentiate (16.30) and apply (16.29) to the right-hand side of the resulting equation to obtain a coupled differential equation solely in $u_j$ and $u_{j-1}$,

$$\frac{\mathrm{d}^2 u_j}{\mathrm{d}t^2} = f_s \frac{\mathrm{d}y_j}{\mathrm{d}t} + f_v \frac{\mathrm{d}u_j}{\mathrm{d}t} + f_l \frac{\mathrm{d}u_{j-1}}{\mathrm{d}t} = f_s(u_{j-1} - u_j) + f_v \frac{\mathrm{d}u_j}{\mathrm{d}t} + f_l \frac{\mathrm{d}u_{j-1}}{\mathrm{d}t}$$

For each vehicle $j$, this is an inhomogeneous second-order linear ordinary differential equation with the respective leader acting as the inhomogeneity:

$$\left(\frac{\mathrm{d}^2}{\mathrm{d}t^2} - f_v \frac{\mathrm{d}}{\mathrm{d}t} + f_s\right) u_j = \left(f_l \frac{\mathrm{d}}{\mathrm{d}t} + f_s\right) u_{j-1} \tag{16.31}$$

The same differential equation is also valid for the gap deviations $y_j$. According to the definition (16.1) of local stability, the perturbation of the leader $u_0(t) = 0$ for all $t > t_0$. For the first follower $j = 1$, this means that, for $t > t_0$, (16.31) reverts to

a homogeneous differential equation which, in fact, is equivalent to (16.21). This means that $u_1(t)$ decays to zero if the local stability criterion (16.26) is satisfied. Applying this reasoning recursively to the next followers, we find that $u_j(t) = 0$ for $t \to \infty$ as long as (16.26) is valid and $j$ remains *finite:*

The criterion (16.26) for local stability is valid for any finite number of followers.

### *16.3.3 Models with Delay*

In contrast to time-continuous models of the form (11.3) as discussed above, time-continuous models with delay, i.e., delay-differential equations of the form (13.1) modeling a *finite reaction time*, or time-discrete models (iterated maps) of the form (11.7) may become locally unstable. Performing the same stability analysis as above for models of the form (13.1), i.e., models whose acceleration equation is of the form $\frac{\mathrm{d}}{\mathrm{d}t} v(t+T_r) = \tilde{f}(s(t), v(t), \Delta v(t))$, we obtain

$$\lambda^2 + \mathrm{e}^{-\lambda T_r} \left(2\eta\lambda + \omega_0^2\right) = 0. \tag{16.32}$$

In spite of its simple appearance, solving this equation for the growth rate $\lambda = \sigma + \mathrm{i}\,\omega$ is nontrivial and can be done only numerically. For sufficiently high delay times (more than 2.0 s for the IDM with the highway parameters of Table 12.2), the real part $\sigma$ of the most unstable solution becomes positive for some steady-state situations, i.e., the model becomes locally unstable (Fig. 16.7).

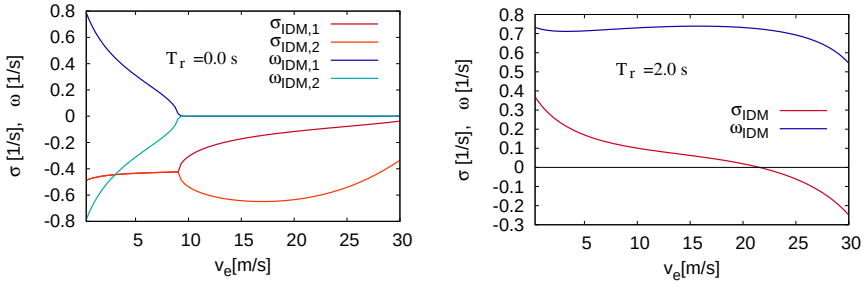


**Fig. 16.7** *Left:* The two branches of the linear growth rate $\lambda = \sigma + \mathrm{i}\,\omega$ according to Eq. (16.25) for the conventional IDM with the standard highway parameters of Table 12.2 as a function of the steady-state speed. *Right:* Most unstable branch of the solutions to Eq. (16.32) for the IDM with an additional delay by the reaction time $T_r = 2.0\,\mathrm{s}$ (no other human driver properties added).

## 16.4 String Stability of Car-Following Models

Even if a system consisting of a single or a few vehicles following a leader with a fixed speed profile is well within the stable range, the oscillations may increase with each following vehicle, i.e., traffic flow is *string unstable* (cf. Figs. 16.1, 16.2 and 16.8).

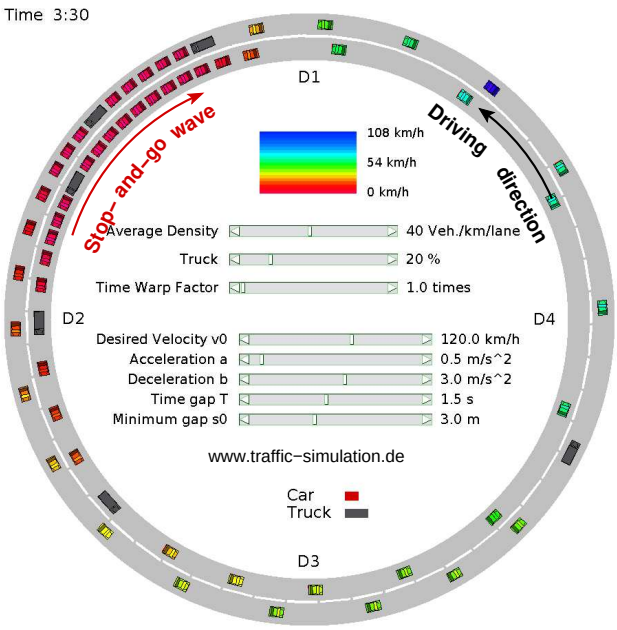


**Fig. 16.8** Interactive simulation of stop-and-go waves with the Intelligent Driver Model (IDM) on the authors' website https://traffic-simulation.de.

Generally, the resulting oscillations or waves have a wavelength of 1 km or more, i.e., a single wave contains many vehicles corresponding to a *long-wavelength instability* This is fortunate since it allows compact analytical expressions for the stability thresholds of time-continuous car-following models and macroscopic models.

### *16.4.1 String Stability Criteria*

We start with the general formulation (11.3), (11.6) of time-continuous car-following models without delay and without multi-anticipation. Furthermore, we consider identical driver-vehicles on a homogeneous infinite road, i.e., the same acceleration functions and identical parameter sets for all vehicles. The set of coupled equations for the gap $s_j$ and the speed $v_j$ reads

$$\frac{\mathrm{d}s_j}{\mathrm{d}t} = v_{j-1} - v_j, \tag{16.33}$$

$$\frac{\mathrm{d}v_j}{\mathrm{d}t} = f\left(s_j(t), v_j(t), v_{j-1}(t)\right). \tag{16.34}$$

As in the analysis for local instability, we assume, for all vehicles $j$, small deviations $y_j$ and $u_j$ from the steady-state gap $s_e$ and speed $v_e$, respectively,

$$s_j = s_e + y_j(t), \tag{16.35}$$

$$v_j = v_e + u_j(t). \tag{16.36}$$

In zeroth order with respect to $y_j$ and $u_j$, we obtain the same result as for the local analysis: The microscopic fundamental diagram $v_e(s)$ and the relations (16.15), (16.19) and (16.20) remain valid.

In first order, we obtain the following system of coupled linear differential equations with constant coefficients:

$$\frac{\mathrm{d}y_j}{\mathrm{d}t} = u_{j-1} - u_j, \tag{16.37}$$

$$\frac{\mathrm{d}u_j}{\mathrm{d}t} = f_s y_j + f_v u_j + f_l u_{j-1}, \tag{16.38}$$

where the partial derivatives $f_s$, $f_v$, and $f_l$ are given by (16.13). Formally, this is the same set as (16.29) and (16.30). However, we now consider these equations as an infinite coupled set with initial perturbations everywhere rather than a finite sequence of differential equations with a temporary perturbation of a single leader, only. The appropriate approach is therefore the *Fourier-Ansatz*

$$\begin{pmatrix} y_j(t) \\ u_j(t) \end{pmatrix} = \begin{pmatrix} \hat{y} \\ \hat{u} \end{pmatrix} \mathrm{e}^{\lambda t + \mathrm{i} jk} \tag{16.39}$$

corresponding to linear waves of strict periodicity whose Fourier amplitudes $\hat{y}(k)$ and $\hat{u}(k)$ are determined by the initial perturbations. This ansatz contains the following elements:

- $\mathrm{i} = \sqrt{-1}$ is the imaginary unit.
- $\lambda = \sigma + \mathrm{i}\omega$ is the complex growth rate. The real part $\sigma$ denotes the growth rate of the oscillation amplitude while the imaginary part $\omega$ indicates the angular frequency *from the perspective of the driver*. The driver passes a complete wave in the time $2\pi/\omega$.[21]
- The dimensionless *wave number* $k \in [-\pi, \pi]$ indicates the phase shift of the traffic waves from one vehicle to the next at a given time instant. Consequently, the number of vehicles per wave is given by $2\pi/k$. Since the steady-state distance

[21] Since $\omega$ is defined with respect to the vehicle index which is increasing for decreasing $x$, we have defined the imaginary part of the wave exponent to be $\omega t + kj$ rather than the conventional ansatz $\omega t - kj$. Thus, $\omega t + kj$ corresponds to $\omega_{\mathrm{mac}} t - kx$, see Eq. (16.115) below and both $\omega$ and $\omega_{\mathrm{mac}}$ are generally negative reflecting waves travelling upstream.

between the front bumpers of two vehicles is equal to $s_e + l = 1/\rho_e$, the physical wavelength is given by $(s_e + l)2\pi/k$.

- The phase velocity is defined by the movement of points of constant phase, i.e., by a constant imaginary part $\omega t + jk$ of the exponent of Eq. (16.39). This gives rise to following quantities:
  - The *passing rate*
    $$\dot{j} = -\frac{\omega}{k} \tag{16.40}$$
    denotes the vehicle flux through the waves in a coordinate system moving with the waves,[22] i.e., with points of constant phase $\omega t + jk$. Since $\omega(k) < 0$ for $k > 0$, the passing rate is positive: The waves propagate in the direction of increasing vehicle indices, i.e., opposite to the movement of the vehicles.
  - In physical space, the relative propagation velocity *in the system comoving with the vehicles* is given by[23]
    $$\tilde{c}_{\mathrm{rel}}(k) = (s_e + l)\frac{\omega}{k} = \frac{\omega}{\rho_e k}. \tag{16.41}$$
  - In the fixed system of a stationary observer at the road side, the positive steady-state speed of the vehicles has to be added to the negative relative velocity,
    $$\tilde{c}(k) = v_e(s_e) + \tilde{c}_{\mathrm{rel}}(k). \tag{16.42}$$
    This road-based propagation velocity is the one that can be derived from traffic data. In order to be consistent with observations, the long-wavelength limit $\tilde{c} = \lim_{k\to 0} \tilde{c}(k)$ should be of the order of $-15\,\mathrm{km/h}$, in congested situations.
- The traffic waves include periodic changes of both gap and speed. The fraction $\hat{u}/\hat{y}$ of the prefactors indicates the relation between the respective amplitudes. For example, a traffic wave described by $\hat{u} = 0$ would consist of gap changes, only.

Inserting the *traffic wave ansatz* (16.39) in the linear system (16.37), Eq. (16.38) results in
$$\begin{pmatrix} \lambda & 1 - \mathrm{e}^{-\mathrm{i}k} \\ -f_s & \lambda - \left(f_v + f_l \mathrm{e}^{-\mathrm{i}k}\right) \end{pmatrix} \cdot \begin{pmatrix} \hat{y} \\ \hat{u} \end{pmatrix} = 0. \tag{16.43}$$
This linear-homogeneous $2 \times 2$ system for the amplitudes has only nontrivial solutions if the determinant of the matrix of coefficients is equal to zero. The resulting solvability condition assumes the form of a quadratic equation
$$\lambda^2 + p(k)\lambda + q(k) = 0 \tag{16.44}$$
for the complex growth rate $\lambda$ with solutions given by (cf. Fig. 16.9)

[22] This technical term has to be distinguished from passing in the sense of overtaking which is completely unrelated.

[23] Since the vehicle index is decreasing for increasing $x$, the sign is reversed with respect to Eq. (16.40). With $\omega/k < 0$, the waves propagate upstream, i.e., in negative $x$ direction.

$$\lambda_{1/2}(k) = -\frac{p(k)}{2}\left(1 \pm \sqrt{1 - \frac{4q(k)}{p^2(k)}}\right) \tag{16.45}$$

where

$$\begin{aligned} p(k) &= -f_v - f_l \mathrm{e}^{-\mathrm{i}k}, \\ q(k) &= f_s\left(1 - \mathrm{e}^{-\mathrm{i}k}\right). \end{aligned} \tag{16.46}$$

Typically, one solution is fast decaying ($\mathrm{Re}\,\lambda$ is strongly negative) while the other, also called the "slow mode", decays more slowly, or even grows. Only the latter is relevant for investigating string stability. We therefore define the complex, real, and imaginary growth rate of the slow mode as follows:

$$\lambda(k) = \begin{cases} \lambda_1(k) \ \mathrm{Re}(\lambda_1(k)) \geq \mathrm{Re}(\lambda_2(k)) \\ \lambda_2(k) \ \text{otherwise.} \end{cases} \tag{16.47}$$

$$\sigma(k) = \mathrm{Re}(\lambda(k)) \tag{16.48}$$

$$\omega(k) = \mathrm{Im}(\lambda(k)) \tag{16.49}$$

For a given phase shift $k$ between two consecutive vehicles, the actual solution $(\hat{y}, \hat{u})$ of the slow mode (the *eigenvector*) gives the amplitudes and the phases of the gap and speed oscillations. Since the eigenvector is only defined up to a (complex) common factor, it essentially gives the relation of the amplitudes and the relative phase between the speed and gap oscillations.

We can now define string stability:

A car-following model is *string stable* (a macroscopic model is flow stable) if $\sigma(k) \leq 0$ for all relative phase shifts (wave numbers) in the range $k \in [-\pi, \pi]$.

Furthermore, we distinguish the type of instability as follows:

When making the model more unstable by changing a control parameter (e.g., the acceleration parameter $a$) the emerging string instability ($\sigma(k) > 0$) is of the *long-wavelength* type if it arises at $k \to 0$. If the first instability appears at a finite phase shift (wave number) $k_0$, it is of the *short-wavelength* type.

In Sect. 16.4.3, we will prove that the first instability of time-continuous models without delay times is always of the long-wavelength type. Since only waves of a finite wavelength can have finite growth rates, the resulting wavelengths are finite but consist of many vehicles and the onset of instability is very slow. We illustrate this by Figure 16.9: The middle curve corresponds to a maximum of the growth rate at $k_0 \approx 0.13$ corresponding to $2\pi/k_0 \approx 50$ vehicles per wave, in agreement with observations of real traffic waves.

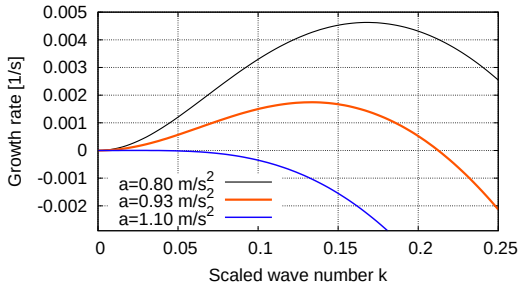


**Fig. 16.9** Linear growth rate $\sigma(k)$ of a congested steady state ($v_e = 48\,\mathrm{km/h}$, $v_e/v_0 = 0.4$) according to (16.48) for the Intelligent Driver Model (IDM) as a function of the scaled wave number (phase shift) $k$ for three values of the IDM acceleration parameter $a$. The remaining IDM parameters are $v_0 = 120\,\mathrm{km/h}$, $T = 1.5\,\mathrm{s}$, $s_0 = 2\,\mathrm{m}$, $b = 1.3\,\mathrm{m/s^2}$, and the vehicle length is $l = 5\,\mathrm{m}$.

Restricting the further investigations to wave numbers $|k| \ll \pi$, we expand the coefficients of the quadratic equation for $\lambda(k)$ in a Taylor series around $k = 0$:[24]

$$\begin{aligned} p(k) &= p_0 + p_1 k + \mathcal{O}(k^2), \\ q(k) &= q_1 k + q_2 k^2 + \mathcal{O}(k^3), \end{aligned} \tag{16.50}$$

with

$$\begin{aligned} p_0 &= -(f_v + f_l) = -\tilde{f}_v, \\ p_1 &= \mathrm{i} f_l = -\mathrm{i}\tilde{f}_{\Delta v}, \\ q_1 &= \mathrm{i} f_s = \mathrm{i}\tilde{f}_s = \mathrm{i} v_e'(s_e) p_0, \\ q_2 &= \frac{f_s}{2} = \frac{\tilde{f}_s}{2} = \frac{v_e'(s_e)}{2} p_0. \end{aligned} \tag{16.51}$$

The prefactors $p_0$ and $q_2$ are real-valued while $p_1$ and $q_1$ are purely imaginary. Notice that the expressions for $q_1$ and $q_2$ on the right-hand sides of the last equal sign follow from Eq. (16.15) and Eq. (16.20). Since there are no zero-order terms of $q(k)$, and the general criteria for sensible microscopic models imply that $p_0 = -\tilde{f}_v$ is strictly positive, the real part of $\lambda$ can (in lowest order) become positive only for the solution with the negative sign of the square root of Eq. (16.47). Expanding this solution around $k = 0$ to quadratic order making use of the expansion

$$\sqrt{1-\varepsilon} = 1 - \frac{1}{2}\varepsilon - \frac{1}{8}\varepsilon^2 + \mathcal{O}(\varepsilon^3) \tag{16.52}$$

for complex-valued $\varepsilon$, we arrive at the general expression

[24] The "order" symbol $\mathcal{O}(\cdot)$ defines how fast the symbolized contributions converge to zero. Specifically, if a contribution $f(k)$ is of the order $\mathcal{O}(k^\gamma)$, then $\lim_{k\to 0} k^{-\gamma} f(k)$ is finite, and $\lim_{k\to 0} k^{-\gamma+\varepsilon} f(k) = 0$ for any positive real-valued $\varepsilon$.

$$\lambda(k) = -\frac{q_1}{p_0}k + \left(\frac{q_1 p_1}{p_0^2} - \frac{q_2}{p_0} - \frac{q_1^2}{p_0^3}\right)k^2 + \mathcal{O}(k^3), \tag{16.53}$$

which is also valid for the second-order macroscopic models to be discussed below.

A long-wavelength string instability is characterized by a positive (always real) second-order coefficient of the more unstable solution $\lambda(k)$,

$$\sigma''(0) = \lambda''(0) = \frac{p_0 q_1 p_1 - p_0^2 q_2 - q_1^2}{p_0^3}. \tag{16.54}$$

So a necessary (and for homogeneous traffic flow without reaction times sufficient) string stability criterion is given by a nonpositive value of this coefficient. Because the general plausibility criteria (Sect. 12.1) imply $p_0 > 0$, the general criterion for string stability (and macroscopic flow stability) can be expressed as

$$\boxed{p_0 q_1 p_1 - p_0^2 q_2 - q_1^2 \leq 0 \quad \text{String stability.}} \tag{16.55}$$

Inserting the expansion coefficients (16.51) in terms of the sensitivities $f_s$, $f_v$, and $f_l$ of time-continuous microscopic models into Eq. (16.53) gives

$$\lambda = -\mathrm{i}v_e'(s_e)\,k + \frac{v_e'(s_e)}{f_v + f_l}\left[\frac{1}{2}(f_l - f_v) - v_e'(s_e)\right]k^2 + \mathcal{O}(k^3). \tag{16.56}$$

The growth rate $\lambda$ tends to zero for $k = 0$. This is a direct consequence of the continuity equation. By virtue of the conservation of the number of vehicles, traffic waves of infinite wavelength (or wave number $k = 0$) cannot dissolve since there is simply no way for the vehicles to leave the wave.

The contribution linear in $k$ is purely imaginary and therefore describes the *propagation properties* of the waves for small phase shifts between consecutive vehicles. Since we have set $\lambda = \sigma + \mathrm{i}\omega$, we have $\omega = -v_e'(s_e)k + \mathcal{O}(k^3)$ and arrive at the following simple expression for the relative (Lagrangian) propagation velocity (16.41) of the traffic waves:

$$\tilde{c}_{\mathrm{rel}}(k) = (s_e + l)\frac{\omega}{k} = -(s_e + l)v_e'(s_e) + \mathcal{O}(k^2). \tag{16.57}$$

Notice that, in this equation, the acceleration function of the model enters only indirectly via the gradient $v_e'(s) = -\tilde{f}_s/\tilde{f}_v = -f_s/(f_v + f_l)$ of the microscopic fundamental diagram $v_e(s)$. Since $v_e'(s) \geq 0$ and, consequently, $\tilde{c}_{\mathrm{rel}} \leq 0$, the waves propagate against the direction of the flow, at least in the coordinate system comoving with the drivers. This is plausible since the considered class of car-following models represents drivers reacting only to the leading but not to the following vehicle. In the limit of completely interaction-free traffic corresponding to $v_e = v_0$, $v_e'(s) = 0$, we have $\tilde{c}_{\mathrm{rel}} = 0$, i.e., the waves move with the vehicles. In fact, the waves can be interpreted as independently moving vehicle clusters, in this limiting case.

The second-order contribution of the growth rate (16.56) is purely real, and therefore describes the *growth properties* of the waves. In particular, traffic flow is long-

wavelength string stable if this term is negative. Inserting into (16.55) the expansion coefficients (16.51) results in the following criterion for string stability:

$$\boxed{v_e'(s_e) \leq \frac{1}{2}\,(f_l - f_v) \quad \text{String stability for } \dot{v}_j = f(s, v, v_l).} \tag{16.58}$$

For models whose acceleration function is of the form $\tilde{f}(s, v, \Delta v)$, we apply the replacements (16.19) and obtain the alternative condition[25]

$$\boxed{v_e'(s_e) \leq -\frac{\tilde{f}_v}{2} - \tilde{f}_{\Delta v} \quad \text{String stability for } \dot{v} = \tilde{f}(s, v, \Delta v).} \tag{16.59}$$

**Formulation in terms of linear sensitivities alone.** Since many publications give the string stability in terms of the linear sensitivities of the microscopic model alone, we will also provide them here, for reference. Replacing $v_e'(s_e)$ with the sensitivities using (16.20) gives the alternative criteria

$$2f_s - f_v^2 + f_l^2 \leq 0, \tag{16.60}$$

$$2\tilde{f}_s - \tilde{f}_v^2 - 2\tilde{f}_v\tilde{f}_{\Delta v} \leq 0. \tag{16.61}$$

**Discussion.** The above criteria for string stability directly point to the three main factors determining the stability of traffic flow with respect to collective perturbations. It is most convenient to extract these factors from the formulation (16.59).

Firstly, a necessary condition for string *instability* is a sufficient sensitivity $v_e'(s) \geq 0$ to changes of the gap (left-hand side of Eq. (16.59)): Without this sensitivity, there is no feedback, and the instability mechanism discussed qualitatively in Section 16.1 would break down already in the first step. The drivers simply ignore the vehicles in front of them. Since this is a plausible behavior for low traffic densities, only, it explains why a minimum traffic flux and density is necessary for generating traffic flow instabilities.

Secondly, string instability implies that the sensitivity $-\tilde{f}_v/2 > 0$ to speed changes, i.e., the first term of the right-hand side of Eq. (16.59) remains below a certain threshold $v_e'(s_e) + \tilde{f}_{\Delta v}$. In terms of the driver's behavior this means that *responsive* or *agile* drivers corresponding to high values of $-\tilde{f}_v$ tend to suppress string instabilities.

Thirdly, string instabilities are only possible if the sensitivity $-\tilde{f}_{\Delta v}$ to speed *differences* remains below a certain threshold. In agreement with common sense, drivers without any sensitivity to speed differences drive very short-sightedly and tend to make traffic flow more unstable. Since future gaps can be estimated by speed differences, one can conclude that $-\tilde{f}_{\Delta v}$ describes a simple form of anticipation.

In summary, the stability analysis shows that the factors favoring string instability are (i) sufficiently dense or congested traffic, (ii) drivers with little agility,

[25] We reiterate that there are two conventions for the relative speed $\Delta v$. If it is defined as $\Delta v = v_l - v$ instead of the approaching rate $\Delta v = v - v_l$, the signs of $\tilde{f}_{\Delta v}$ reverse while the conditions (16.58) and (16.60) are unchanged.

and (iii) a driving style characterized by little anticipation. This observation can be used as a starting point for increasing traffic flow stability by driver-assistance systems (cf. Section 25.4), or for formulating rules for effective driving to be taught in driving schools. Even if stop-and-go conditions prevail, anticipative drivers (or suitable ACC systems) react earlier to braking maneuvers of the preceding vehicles than their more short-sighted peers thereby reducing the inflow to the traffic waves. Moreover, responsive and anticipative drivers (or ACC-driven vehicles) leave traffic waves faster than their more sluggish and short-sighted contemporaries. With less inflow and more outflow, even existing traffic waves eventually will dissolve.

**Interactive simulations.** All three factors of string instability can be interactively simulated at the authors' website[26] using the ring-road scenario depicted in Fig. 16.8. In the default setting, traffic flow is unstable and traffic waves emerge after some time. These waves can be suppressed by each of the following actions:

- Reducing the "average density" via the top scrollbar. This reduces the overall interactions and thus the positive destabilizing feedback characterized by $v_e'(s)$.
- Increasing the "acceleration $a$" by controlling the corresponding scrollbar. This makes the drivers more agile and corresponds to increasing the sensitivity $-\tilde{f}_v$ (see also Fig. 16.9).
- Decreasing the (comfortable) "deceleration $b$". Since one needs to react earlier in order to reduce decelerations, this corresponds to increasing the level of anticipation $-\tilde{f}_{\Delta v}$.

The latter two actions can also be applied to the other simulation scenarios.

### *16.4.2 Extension to Multi-Anticipation*

When modeling human drivers (Chapter 13) or adaptive-cruise control (ACC) with communication to other vehicles (cooperative ACC, CACC), the driving response does not only depend on the immediate leader but extends to the *next-nearest leaders* further ahead. Since information in vehicle platoons generally travels backwards,[27] looking further ahead gains valuable time to respond to new situations. Here, we analyze to which extent this will stabilize traffic flow.

**Generalized form of multi-anticipative models.** In contrast to car-following models in the stricter sense, it is more efficient to formulate general multi-anticipative models in terms of position differences rather than gaps. Since, regarding stability, we can set all vehicle lengths equal to zero,[28] both representations are equivalent if we replace the independent variables "positional differences" by the sum of all gaps

[26] see: https://traffic-simulation.de

[27] Since we are in the moving-observer (Lagrangian) perspective, this even applies to noncongested traffic.

[28] The vehicle itself is just a rigid body without internal dynamic effects through which the information propagates instantaneously.

(cf. Eq. (13.11)). Since microscopic stability and the growth rate, e.g., Eq. (16.47), is formulated in terms of the phase shift or scaled wavenumber $k$, the vehicle length enters only when transforming the scaled wavenumber to a physical wave number via $k_{\text{phys}} = (s_e(v) + l_{\text{veh}})k$. This affects the onset of convective instability (see Sect. 16.6) but not the onset of string stability as such.

In addition to a response to multiple leaders, we will also include a response to the *immediate* follower since it can also influence the driving behavior, e.g., by light signals or the horn.

Inserting the speed definition $v_j = \dot{x}_j$, the general multi-anticipative car-following model for $M$ leaders and one follower can be written as a set of coupled second-order differential equations for the positions $x_j$,[29]

$$\ddot{x}_j = f\left(x_{j+1} - x_j, x_{j-1} - x_j, \ldots, x_{j-M} - x_j, \dot{x}_{j+1}, \dot{x}_j, \dot{x}_{j-1}, \ldots, \dot{x}_{j-M}\right). \tag{16.62}$$

**Linearization.** The homogeneous steady state defining the microscopic fundamental diagram $v_e(\Delta x_e)$ is given by

$$0 = f(-\Delta x_e, \Delta x_e, \ldots, M\Delta x_e, v_e, \ldots, v_e). \tag{16.63}$$

Linearizing (16.62) around the small positional perturbations $y_j$ of each vehicle $j$ defined by $x_j(t) = v_e t - j\Delta x_e + y_j(t)$ gives

$$\ddot{y}_j = \sum_{m=-1}^{M} \left(f_{sm}(y_{j-m} - y_j) + f_{vm}\dot{y}_{j-m}\right) \tag{16.64}$$

with

$$f_{sm} = \left(\frac{\partial f}{\partial(x_{j-m} - x_j)}\right)_e, \; -1 \le m \le M, \quad f_{s0} = 0 \tag{16.65}$$

and

$$f_{vm} = \left(\frac{\partial f}{\partial v_{j-m}}\right)_e, \; -1 \le m \le M. \tag{16.66}$$

Inserting the wave ansatz $y_j(t) = \hat{y}\exp(\lambda t + ijk)$ results in a quadratic equation for the dispersion relation $\lambda(k)$ that is formally equivalent to (16.44),

$$\lambda^2 + p(k)\lambda + q(k) = 0,$$

with the functions

$$p(k) = -\sum_{m=-1}^{M} f_{vm} e^{-imk}, \quad q(k) = \sum_{m=-1}^{M} f_{sm}\left(1 - e^{-imk}\right). \tag{16.67}$$

[29] In case of heterogeneity, the functions $f(\cdot) = f_j(\cdot)$ are different for each vehicle but we will not consider this further, here (cf. Sect. 16.4.3).

Notice that for the special case of a classical single-leader car-following model with $M = 1$, $f_{v,-1} = f_{s,-1} = f_{s0} = 0$, $f_{v0} = f_v$, $f_{v1} = f_l$, and $f_{s1} = f_s$, we revert to the relations (16.46) derived earlier.

As in the single-leader case, the first instability is a long-wavelength one and string stability is characterized by a nonpositive quadratic Taylor coefficient in (16.44), i.e., by (16.55) with

$$p_0 = -\sum_m f_{vm}, \quad p_1 = \mathrm{i}\sum_m m f_{vm}, \quad q_1 = \mathrm{i}\sum_m m f_{sm}, \quad q_2 = \frac{1}{2}\sum_m m^2 f_{sm}. \quad (16.68)$$

### 16.4.3 String Stability for Open Systems: Transfer Function

While the wave ansatz (16.39) is suitable for infinite systems (continuous wave number $k$) and closed systems (the system length is a multiple of the wavelength $2\pi/k$), a different approach is suitable for open systems where the dynamics of a finite or infinite sequence of followers of a given leader trajectory is to be investigated. Specifically, the perturbation is no longer momentary and everywhere (initial condition) but permanently sustained and localized (a single leader is perturbed). Consequently, we decompose the perturbation into temporal rather than spatial Fourier modes. This ansatz also allows more easily the generalization to heterogeneous platoons, time delays, and lower-level controllers. The stability of multi-anticipative models, however, is better analyzed using the wave ansatz (Sect. 16.4.2).

For finite platoons we have already derived that the local stability of a finite platoon is the same as that of a single follower, i.e., that a finite-time perturbation of the leader will not lead to permanent perturbations of any follower (Sect. 16.3.2). Here, we investigate the related but different problem that the leader has permanent perturbations (that can be decomposed in a temporal Fourier series) and how these perturbations propagate from follower to follower.

We start with the *Laplace transformation* ansatz $u_j(t) = \hat{u}_j e^{\lambda t}$ for the speed perturbations of follower $j$ with the complex growth rate $\lambda = \sigma + i\omega$.[30] Inserting this into (16.31) results in

$$\left(\lambda^2 - \lambda f_v + f_s\right)\hat{u}_j = \left(\lambda f_l + f_s\right)\hat{u}_{j-1}, \quad (16.69)$$

which can be formulated in terms of a complex *transfer function*

$$G(\lambda) = \frac{\hat{u}_j}{\hat{u}_{j-1}} = \frac{\hat{y}_j}{\hat{y}_{j-1}} = \frac{\lambda f_l + f_s}{\lambda^2 - \lambda f_v + f_s} \quad (16.70)$$

relating the perturbations of the follower to that of the leader. Assuming that the perturbations of the leader can be decomposed into temporal Fourier components

[30] Often, the variable $s$ is used in the control theory literature. However, in order to avoid confusion with the gap variable $s$ and consistent with other locations in this chapter, we name the complex growth rate $\lambda$.

$\hat{u}_0 e^{i\omega t}$, we can set $\lambda = i\omega$ resulting in the stationary transfer function

$$G(\mathrm{i}\omega) = \frac{\mathrm{i}\omega f_l + f_s}{-\omega^2 - \mathrm{i}\omega f_v + f_s}. \tag{16.71}$$

For each harmonic component of the leader's oscillation, the next follower responds

- with a phase shift $\arctan\left[\mathrm{Im}(G(\mathrm{i}\omega))/\mathrm{Re}(G(\mathrm{i}\omega))\right]$,
- and a growth factor $|G(\mathrm{i}\omega)|$ where

$$|G(\mathrm{i}\omega)|^2 = \frac{f_s^2 + f_l^2\omega^2}{(f_s - \omega^2)^2 + f_v^2\omega^2}\,. \tag{16.72}$$

For $\omega \to 0$ (oscillations with durations tending to infinity), we have $G(i\omega) \to 1$, i.e., the phase shift tends to zero and the growth factor to unity. This is to be expected in view of vehicle conservation and finite follower response times.

In order to investigate string instability of infinite platoons, we determine the conditions for which at least one frequency mode has a growth factor exceeding unity, i.e., we look for the maximum of $|G(i\omega)|^2$. A necessary condition for a maximum (which we will call a "resonance condition") is given by setting the derivative of $|G(i\omega)|^2$ with respect to $\omega^2$ equal to zero resulting, after a lengthy calculation, to

$$\omega_{\mathrm{res}}^2 = \frac{f_s}{f_l^2}\left(-f_s + \sqrt{f_s^2 + f_l^2(f_l^2 - f_v^2 + 2f_s)}\right). \tag{16.73}$$

This has several consequences:

- A maximum of $|G|$ in $\omega^2 > 0$ only exists if $f_l^2 - f_v^2 + 2f_s \geq 0$, i.e., the infinite platoon is string unstable or *neutrally stable* (otherwise, $\omega_{\mathrm{res}}$ is imaginary).[31]
- At string instability, $f_l^2 - f_v^2 + 2f_s > 0$, one can show that (16.73) corresponds to a unique maximum of the growth factor $|G_{\mathrm{res}}| = |G(i\omega_{\mathrm{res}})| > 1$. Furthermore, both the growth factor and the resonance frequency of the fastest growing mode increase strictly monotonously with $f_l^2 - f_v^2 + 2f_s$.
- At neutral stability, the resonance frequency $\omega_{\mathrm{res}}$ of the maximum growth tends to zero justifying the ansatz (16.50) made earlier for the infinite system.[32]

In summary, long-wavelength perturbations decay from follower to follower if $2f_s - f_v^2 + f_l^2 < 0$ which is precisely the condition (16.60) for string stability:

An infinite homogeneous vehicle platoon is asymptotically string stable if all oscillations decay when propagating backwards from vehicle to vehicle.

[31] This means that there is no horizontal tangent in $\omega^2$. However, in $\omega$, there is a horizontal tangent corresponding to a maximum $|G_{\mathrm{res}}| = 1$ at $\omega = 0$.

[32] Here, we take the limit $\omega^2 \to 0$ while in (16.50), we assumed the wavenumber $k \to 0$. However, for a finite propagation velocity, these two limits are interchangeable.

This is plausible since any *temporary* perturbation (as required by the definition of string instability) can be decomposed into Fourier components, and the dephasing of the components when going from follower to follower will lead to permanent fluctuations unless the components decay to zero for $j \to \infty$. In this sense, the transfer function (Laplace) ansatz leads to the same string stability criterion as the wave ansatz.

**Heterogeneous strings.** Without multi-anticipation (i.e., looking only at the immediate leader), the transfer function (16.70) exclusively depends on the model parameters of the considered follower, irrespective of the composition of the leaders and further followers. This makes it easy to define the strict and head-to-tail string stability for such car-following models.

The *strict* string stability is satisfied if every single follower has a growth factor of at most one for all frequencies $\omega$,

$$|G_j(i\omega)| \leq 1 \ \forall \omega \geq 0, \ j = 1, ..., n, \tag{16.74}$$

where $G_j(\lambda)$ is the transfer function (16.70) for the sensitivities $f_{js}$, $f_{jv}$, and $f_{jl}$ corresponding to the model and parameters of follower $j$ for a given steady state $(s_e, v_e)$.[33]

For formulating the *head-to-tail* string stability, we first define the *head-to-tail* transfer function as

$$G_{n1}(\lambda) = \frac{\hat{u}_n}{\hat{u}_0} = \prod_{j=1}^{n} G_j(\lambda). \tag{16.75}$$

A finite heterogeneous platoon satisfies *weak* or *head-to-tail* string stability is

$$|G_{n1}(i\omega)| \leq 1 \ \ \forall \omega \geq 0. \tag{16.76}$$

Assuming that the first instability arises at $\omega^2 \to 0$ in the heterogeneous case as well, we can evaluate head-to-tail stability according to

[33] Notice that even different models of the form (11.3), (11.6) are allowed, e.g., a mixture of human-driven and automated vehicles with their respective models.

$$
\begin{aligned}
0 &\geq \frac{\mathrm{d}}{\mathrm{d}\omega^2}\left(\prod_j |G_j(i\omega)|^2\right)_{\omega=0} \\
&= \frac{\mathrm{d}}{\mathrm{d}\omega^2}\ln\left(\prod_j |G_j(i\omega)|^2\right)_{\omega=0} \\
&= \frac{\mathrm{d}}{\mathrm{d}\omega^2}\left(\sum_j \ln|G_j(i\omega)|^2\right)_{\omega=0} \\
&= \sum_j \frac{1}{|G_j(0)|^2}\frac{\mathrm{d}}{\mathrm{d}\omega^2}|G_j(i\omega)|^2_{\omega=0} \\
&= \sum_j \left(\frac{1}{f_{js}^2}\right)\left(f_{jl}^2 - f_{jv}^2 + 2f_{js}\right),
\end{aligned}
$$

where we have made use of the strict monotonicity of the logarithm function and that $|G_j(i\omega)|^2 \to 1$ for $\omega \to 0$. This means that a heterogeneous platoon is long-wavelength head-to-tail string stable if the arithmetic average of the individual string instability criteria $f_{jl}^2 - f_{jv}^2 + 2f_{js}$ weighted with $1/f_{js}^2$ is nonpositive. However, this popular formula is only a necessary, not a sufficient condition for head-to-tail string stability because, for some configurations including string stable and string unstable followers, the first instability in the heterogeneous platoon may arise at finite frequencies. Then, we need to evaluate (16.76) which is exact.

Obviously, for homogeneous platoons, the head-to-tail and strict string stability criteria coincide and are given by the conventional string stability criterion (16.60).

**Explicit time delays and lower-level control.** Presently, most semi-automated cars with longitudinal adaptive-cruise control (ACC) are not string stable. While this is irrelevant for low penetration levels as long as they are locally stable, it matters for larger levels. Since, for physical reasons, a vehicle cannot implement a prescribed acceleration immediately (cf. Sect. 12.5.3 for details), we need to consider the *control path* of the vehicle powertrain as well. This means the ACC is composed of two components,

- the *commanded* acceleration given by the *higher-level controller*, typically a car-following model with transfer function $G(\lambda)$,
- the mapping of the commanded to the physical acceleration given by a *lower-level controller* with transfer function $H(\lambda)$.

In the simplest case, the lower-level controller is modeled by a first-order lag according to

$$
\frac{\mathrm{d}a_{\mathrm{phys}}}{\mathrm{d}t} = \frac{a_{\mathrm{cmd}}(t) - a_{\mathrm{phys}}(t)}{\tau_a}, \quad H(\lambda) = H_1(\lambda) = \frac{1}{\tau_a\lambda + 1},
$$

where $H_1(\lambda)$ is the transfer function of this "PT1 element". Alternatively or additionally, one can also model an explicit reaction time delay

$$\frac{\mathrm{d}a_{\mathrm{phys}}}{\mathrm{d}t} = a_{\mathrm{cmd}}(t-\tau_d), \quad H(\lambda) = H_2(\lambda) = e^{-\tau_d \lambda},$$

or combine both elements (cf. Eq. (12.41))

$$\frac{\mathrm{d}a_{\mathrm{phys}}}{\mathrm{d}t} = \frac{a_{\mathrm{cmd}}(t-\tau_d) - a_{\mathrm{phys}}(t-\tau_d)}{\tau_a}, \quad H(\lambda) = H_1(\lambda)H_2(\lambda).$$

The total transfer function of an ACC controller with a car-following model, a PT1 element and a delay element as vehicle control path is then given by

$$G_{\mathrm{ACC}}(\lambda) = G(\lambda)H(\lambda). \tag{16.77}$$

This use case demonstrates the strength of the transfer function approach: the general string stability criteria (16.74) and (16.76) remain valid, just the evaluation in terms of $f_s$, $f_v$, $f_l$, $\tau_a$ and $\tau_d$ becomes more involved. In particular, for explicit delays $\tau_d > 0$, the first instability often arises at a finite frequency. This is similar to the situation for local instabilities, cf. Fig. 16.7.

### *16.4.4 Application to Specific Car-Following Models*

In the following, we apply the general stability criteria to some of the car-following models presented in the Chapters 11 to 13.

**Optimal Velocity Model and extensions.** We analyze the Full Velocity Difference Model (FVDM) presented in Section 11.8 which is a generalization of the Optimal Velocity Model (OVM). Its acceleration function $\tilde{f}(s,v,\Delta v) = (v_{\mathrm{opt}}(s)-v)/\tau - \gamma\Delta v$ is of the form $\tilde{f}(s,v,\Delta v)$, so Eq. (16.59) is the suitable criterion for string stability. With $\tilde{f}_v = -1/\tau$ and $\tilde{f}_{\Delta v} = -\gamma$, we obtain

$$v_e'(s) \le \frac{1}{2\tau} + \gamma. \tag{16.78}$$

For bound and congested traffic, the left-hand side $v_e'(s)$ is of the order of the inverse of the time gap. Specifically, for the optimal-velocity relation (11.24), it is directly given by the inverse $1/T$ of the desired time gap $T$.

Traffic flow modeled with the OVM ($\gamma$=0) is only string stable if $\tau < \frac{1}{2}v_e'(s)$, i.e., the speed adaptation time $\tau$ must be smaller than half the time gap of the order of 1-2 s. Since this implies unrealistically agile drivers and unphysically high accelerations, the OVM cannot describe realistic driving behavior. The speed difference sensitivity $\gamma$ of the FVDM partially resolves this problem since sensitivities $\gamma$ of the order of $1\,\mathrm{s}^{-1}$ are realistic in car-following mode if speed differences are not too large. However, as discussed in Section 11.8, the FVDM is not complete since the sensitivity to speed differences does not tend do zero when gaps tend to infinity.

**Newell's model.** Newell's model (11.28) is formulated in terms of an iterated coupled map, so the results of Section 16.4.1 cannot be applied directly. Proceeding as in this section, the resulting solvability condition for the growth rate $\lambda$ contains algebraic terms but also exponentials $e^{\lambda \Delta t}$ and, therefore, cannot be solved analytically.[34] As a consequence, no compact analytic stability criterion can be derived. Moreover, in contrast to models formulated as differential equations but similarly to time-delay differential equations, the first instability may be of a short-wavelength type.

If one assumes *a priori* that short-wavelength instabilities are not relevant, it is a good approximation to replace difference quotients by time derivatives using Eq. (11.13). Thus, Newell's speed update rule $v_j(t+T) = v_e(s_j(t))$ can approximately be formulated by the time-continuous acceleration equation

$$f^{\text{Newell}}(s,v) = \frac{v_e(s) - v}{T}. \tag{16.79}$$

It is identical to the OVM if one identifies the speed adaptation time $\tau$ with the update (reaction) time $T$. We conclude that Newell's model is stable with respect to long-wavelength string instabilities if

$$v_e'(s) \le \frac{1}{2T}. \tag{16.80}$$

**Gipps' model.** For reference, Gipps' model (12.9) has the acceleration equation

$$f(s,v,v_l) = \min\left(a_{\text{free}}(v), \frac{v_{\text{safe}}(s,vl) - v}{\tau}\right)$$

with a monotonously decreasing free-flow acceleration $a_{\text{free}}(v)$ and the safe speed (making the usual assumption $\theta = \tau/2$ for the safety time cushion)

$$v_{\text{safe}}(v,v_l,s) = -b\tau + \sqrt{b^2\tau^2 + b\left[2(s-s_0) - v\tau + v_l^2/b_l\right]}.$$

For free flow, the steady state is at $v_0$ with $v_f = a_{\text{free}}'(v_0) < 0$ and $v_e'(s) = f_s = f_l = 0$. Hence, the stability criterion (16.58), $0 < 0.5 f_v$, is always satisfied.

For congested flow, we assume that the minimum leading deceleration $b_l$ satisfies (12.21) because the model does not give plausible results, otherwise. Under this conditions, the steady-state gap $s_e(v)$, Eq. (12.17), is strictly monotonously increasing within its application range $v < v_0$ resulting in the gradient

$$v_e'(s) = \frac{1}{s_e'(v)} = \frac{1}{1.5\tau + \frac{v_e(s)}{b}\left(1 - \frac{b}{b_l}\right)} > 0\,.$$

The sensitivities needed for the stability criterion (16.58) are

[34] The equation for $\lambda$ is of a similar form as the condition (16.32) for local instability of time-delay differential equations.

$$f_v = -\frac{v_e + 1.5b\tau}{\tau(v_e + b\tau)}, \quad f_l = \frac{b}{b_l}\,\frac{v_e}{\tau(v_e + b\tau)},$$

and the model is string stable according to (16.58) if

$$v_e'(s) \le \frac{\left(2 + \frac{b}{b_l}\right) v_e + 3b\tau}{2\tau(v_e + b\tau)}. \tag{16.81}$$

For $b = b_l$, this simplifies to

$$\frac{2}{3\tau} \le \frac{3}{2\tau}$$

which, obviously, is always satisfied. For $b_l > b$, the drivers get more conservative (because they assume that the leader can brake harder) and the stability condition is satisfied even with a greater margin. If, however, Condition (12.21) for $b_l$ tends to its limits, the denominator of $v_e'(s)$ for $v_e \to v_0$ tends to zero, the gradient $v_e'(s)$ to infinity and the stability criterion is violated (cf. Fig. 16.10).

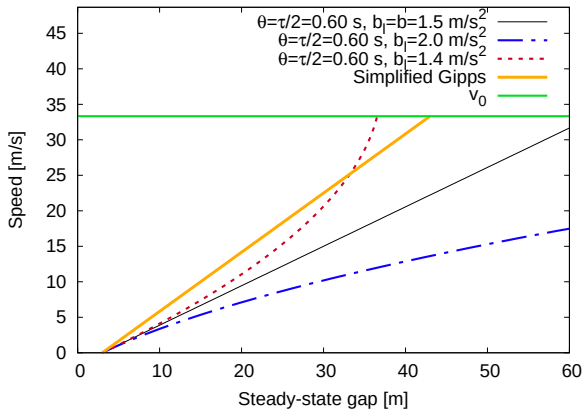


**Fig. 16.10** Steady-state speed $v_e(s)$ for different variants and parameterizations of the Gipps model. The parameters not given in the plot are the highway parameters of Table 12.1 ($v_0 = 120\,\mathrm{km/h}$, $s_0 = 3\,\mathrm{m}$, $\tau = 1.2\,\mathrm{s}$, and $a = b = 1.5\,\mathrm{m/s^2}$).

In summary, as expected, the stability condition depends essentially on the ratio $b/b_l$. If $b/b_l \le 1$, congested flow is always stable. However, if $b_l$ is only somewhat smaller than $b$, string instability sets in near $v = v_0$, particularly for high desired speeds. Finally (not shown but the derivation is straightforward), congested flow without a safety cushion ($\theta = 0$), is always string stable if $b/b_l < 1$, marginally stable if $b/b_l = 1$, or unstable if $b/b_l > 1$.

**Simplified Gipps' model.** The simplified Gipps' model has the same general structure (12.9) as the original model but the safe speed (12.16) does not depend on the actual speed and is given by $v_{\mathrm{safe}}(s, v_l) = -b\tau + \sqrt{b^2\tau^2 + v_l^2 + 2b(s - s_0)}$.

For free traffic at $v_0$, we have $v_e'(s) = 0$, $f_v = -1/\tau$ and $f_l = 0$ and the string stability criterion (16.58), $v_e' \le (f_l - f_v)/2$ or $0 \le 1/\tau$, is satisfied.

For interacting or congested traffic at the homogeneous steady state, we have $v = v_{\text{safe}} < v_0$, the microscopic fundamental diagram $v_e(s) = \max(0, (s - s_0)/\tau)$, and the gradient $v_e'(s)$ and the sensitivities needed for the criterion (16.58) and for (16.47) evaluate to

$$v_e'(s) = \frac{1}{\tau}, \quad f_s = \frac{b}{\tau(b\tau + v_e)}, \quad f_v = -\frac{1}{\tau}, \quad f_l = \frac{v_e}{\tau(b\tau + v_e)} \tag{16.82}$$

resulting in the string stability condition

$$\frac{1}{\tau} \le \frac{1}{2\tau}\left(1 + \frac{v_e}{v_e + b\tau}\right) \quad \Rightarrow \quad b\tau \le 0\,. \tag{16.83}$$

Since both the driver's braking deceleration $b$ and the response time $\tau$ are strictly positive, this is never satisfied, i.e., congested traffic represented by this model is *always* unstable. However, the instabilities are always of the convective type (cf. Section 16.6). Moreover, for reasonable values of the deceleration parameter $b$, the maximum growth rate $\sigma(k)$ according to (16.48) is of the order of one hour and the perturbations need several kilometers of propagation to grow significantly (cf. Fig. 12.5). In many cases, the critical road sections are shorter, so the perturbations leave these sections before growing into fully developed traffic waves. As a result, the model is de facto *marginally stable* if $b\tau \ll v_e$ which is satisfied unless traffic flow is nearly stopped.[35]

**Intelligent Driver Model.** The IDM acceleration function is of the type $\tilde{a}(s, v, \Delta v)$. Since the partial derivative $\tilde{f}_v$ with respect to the vehicle speed would result in a markedly longer analytic expression than the derivative with respect to the gap $s$, we make use of relation (16.20) and set $\tilde{f}_v = -\tilde{f}_s / v_e'(s_e)$. Then, Eq. (16.59) reads

$$v_e'(s_e) \le \frac{\tilde{f}_s}{2v_e'(s_e)} - \tilde{f}_{\Delta v}. \tag{16.84}$$

With the partial derivatives

$$\tilde{f}_s^{\text{IDM}} = \frac{2a(s_0 + v_e T)^2}{s_e^3}, \quad \tilde{f}_{\Delta v}^{\text{IDM}} = -\sqrt{\frac{a}{b}}\left(\frac{(s_0 + v_e T)v_e}{s_e^2}\right), \tag{16.85}$$

we obtain the string stability criterion (Fig. 16.11)

$$(v_e'(s_e))^2 \le \frac{a(s_0 + v_e T)}{s_e^2}\left[\frac{s_0 + v_e T}{s_e} + \frac{v_e v_e'(s_e)}{\sqrt{ab}}\right], \tag{16.86}$$

where the IDM steady-state gap (12.29) is given by $s_e(v) = (s_0 + vT)/\sqrt{1 - (v/v_0)^\delta}$. For reference and for using (16.60) and (16.61), we also give the partial derivative

[35] For $v_e = 0$ and $s \le s_0$, traffic flow restabilizes.

of the IDM acceleration with respect to the speed, and the partial derivatives of the IDM in the formulation $f(s,v,v_l)$. For a later use in the multi-anticipative IDM, we have split $f_v$ and $\tilde{f}_v$ into a free and interacting contribution:

$$\tilde{f}_v^{\mathrm{IDM}} = \tilde{f}_v^{\mathrm{IDM,free}} + \tilde{f}_v^{\mathrm{IDM,int}}, \tag{16.87}$$

$$\tilde{f}_v^{\mathrm{IDM,free}} = -\frac{a\delta v_e^{\delta-1}}{v_0^{\delta}}, \quad \tilde{f}_v^{\mathrm{IDM,int}} = \frac{-2aT(s_0+v_eT)}{s_e^2}, \tag{16.88}$$

$$f_v^{\mathrm{IDM,free}} = \tilde{f}_v^{\mathrm{IDM,free}}, \quad f_v^{\mathrm{IDM,int}} = \tilde{f}_v^{\mathrm{IDM,int}} + \tilde{f}_{\Delta v}^{\mathrm{IDM}}, \tag{16.89}$$

$$f_s^{\mathrm{IDM}} = \tilde{f}_s^{\mathrm{IDM}}, \quad f_l^{\mathrm{IDM}} = -\tilde{f}_{\Delta v}^{\mathrm{IDM}}. \tag{16.90}$$

Condition (16.86) reflects the three influencing factors for string stability discussed in Section 16.4.1 on page 370:

- The tendency to instability increases with the sensitivity $v_e'(s)$ to changes of the gap fueling the feedback mechanism.
- The tendency to instability decreases with the driver's agility characterized by the acceleration parameter $a$.
- And it decreases with decreasing comfortable deceleration $b$, i.e., with increasing level of anticipation.

Notice that $v_e'(s_e) \approx 1/T$ for $v \ll v_0$, so the desired time gap $T$ is the main influencing factor to the gap sensitivity (besides the actual traffic state): Lower values of $T$ lead to higher sensitivities $v_e'(s_e)$ and to a higher tendency to instabilities. In agreement with common sense, traffic flow becomes more unstable if the time gaps in car-following mode are comparatively short.[36]

For the limiting case $v_e \to 0$, or equivalently, $s_e \to s_0$ and $v_e'(s_0) = 1/T$, we obtain the simple explicit stability condition

$$a \geq \frac{s_0}{T^2}\,. \tag{16.91}$$

If the stability condition (16.91) is satisfied but traffic flow is string unstable for congested traffic of finite steady-state speed $v_e$, one speaks of *restabilization*. In this case, mildly congested traffic resulting from comparatively small bottlenecks is unstable while nearly standing traffic behind severe bottlenecks is stable, creeping slowly. This will be discussed in Section 18.2.

**Optimal Velocity Model with impatient followers.** Sometimes, drivers are urged from behind by light and horn signals from impatient followers. To model this in the simplest possible way, the OVM (11.21) is first separated into a free and interacting force,

$$\frac{\mathrm{d}v}{\mathrm{d}t} = \frac{v_{\mathrm{opt}}(s)-v}{\tau} = \frac{v_0-v}{\tau} + \frac{v_{\mathrm{opt}}(s)-v_0}{\tau} = f^{\mathrm{free}}(v) + f^{\mathrm{int}}(s,v), \tag{16.92}$$

[36] On the other hand, short gaps lead to a higher dynamic capacity, see Section 12.3.6.

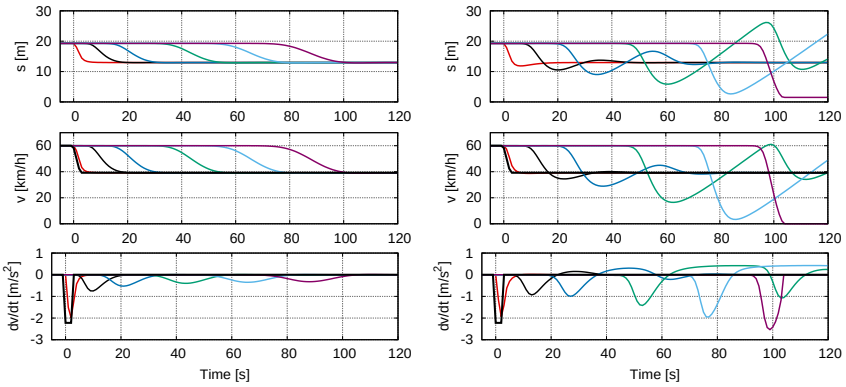


**Fig. 16.11** String instability of the IDM visualized by the reaction of a sequence of vehicles driving in steady-state equilibrium far below the desired speed ($v_0 = 120\,\mathrm{km/h}$) behind a leading vehicle whose driver reduces his or her speed from 60 km/h to 40 km/h. Shown is the first vehicle (leader) and the 10th, 20th, 40th, 60th, and 80th vehicle. *Left:* Traffic flow is string stable ($T = 1\,\mathrm{s}$, $s_0 = 2\,\mathrm{m}$, $a = b = 2\,\mathrm{m/s^2}$). *Right:* Traffic flow becomes unstable by reducing the IDM acceleration parameter from $a = 2\,\mathrm{m/s^2}$ to $a = 0.6\,\mathrm{m/s^2}$.

and then augmented with a "pushing" force from the follower of the subject vehicle corresponding to *its* interaction force but reversed in sign and weakened by a factor $\lambda < 1$,

$$\frac{\mathrm{d}v_j}{\mathrm{d}t} = \frac{v_0 - v}{\tau} + \frac{v_{\mathrm{opt}}(x_{j-1} - x_j) - v_0}{\tau} - \lambda \frac{v_{\mathrm{opt}}(x_j - x_{j+1}) - v_0}{\tau}. \tag{16.93}$$

In the special case $\lambda = 0$, this model reverts to the OVM while, for $\lambda = 1$, we have momentum conservation of the interactions. The general steady state is given by $v_e(s) = (1-\lambda)v_{\mathrm{opt}}(s) + \lambda v_0$. The sensitivities of the general linearization (16.64) are given by

$$\begin{aligned} f_{v0} &= f_v = -\frac{1}{\tau}, \\ f_{v1} &= f_{v,-1} = 0, \\ f_{s1} &= f_s = \frac{v'_{\mathrm{opt}}(\Delta x_e)}{\tau}, \\ f_{s,-1} &= \lambda \frac{v'_{\mathrm{opt}}(\Delta x_e)}{\tau} \end{aligned}$$

resulting in the Taylor coefficients (16.68)

$$p_0 = \frac{1}{\tau}, \quad p_1 = 0, \quad q_1 = \frac{i(1-\lambda)v'_{\mathrm{opt}}(\Delta x_e)}{\tau}, \quad q_2 = \frac{(1+\lambda)v'_{\mathrm{opt}}(\Delta x_e)}{2\tau},$$

and, with (16.55), to the long-wavelength string stability criterion

$$v'_{\text{opt}}(s) \leq \frac{1+\lambda}{2\tau(1-\lambda)^2}\,. \tag{16.94}$$

Notice that, for the special case of no impatient followers ($\lambda = 0$), this condition reverts to the normal OVM string stability condition (16.78). Remarkably, the effect of impatient followers *suppresses* string instability. However, this model is not suitable for very congested or standing traffic (cf. Problem 16.5).

**Multi-anticipative IDM.** We consider the multi-anticipative extension (13.14) of the IDM, i.e., the Human-Driver Model (HDM) without temporal anticipation and estimation errors. In this model, the interaction forces of all $M$ leaders are added according to

$$\frac{\mathrm{d}v_j}{\mathrm{d}t} = f^{\text{free}}(v_j) + \sum_{m=1}^{M} f^{\text{int}}(x_{j-m} - x_j, v_j, v_{j-m}) \tag{16.95}$$

with

$$f^{\text{free}}(v_j) = a\left(1 - \left(\frac{v_j}{v_0}\right)^{\delta}\right), \quad f^{\text{int}}(\cdot) = \left(\frac{s_0 + v_j T + \frac{v_j(v_j - v_{j-m})}{2\sqrt{ab}}}{x_{j-m} - x_j}\right)^2. \tag{16.96}$$

Without loss of generality, we consider a vehicle length $l_{\text{veh}} = 0$, so, in steady state $(v_e, s_e(v_e))$, we have $x_{j-m} - x_j = m s_e$. For nonzero vehicle length, this relation remains unchanged if we assume that the independent space variable of the $m^{\text{th}}$ leader is the sum of all gaps instead of $x_{j-m} - x_j$ which is consistent with Eq. (13.11).

This means that, in steady state, the interacting forces decrease with $1/m^2$ and the steady state is given by

$$s_e(v) = C_2 s_e^{\text{IDM}}(v), \tag{16.97}$$

where

$$C_n = \sum_{m=1}^{M} \frac{1}{m^n}\,. \tag{16.98}$$

Since, according to (12.29), the IDM steady-state gap $s_e^{\text{IDM}}(v) = (s_0 + vT)(1 - (v/v_0)^{\delta})^{-1/2}$, the multi-anticipative IDM has the same microscopic fundamental diagram (steady-state relation) as the original IDM when setting

$$s_0^{\text{multi}} = s_0/C_2, \quad T^{\text{multi}} = T/C_2. \tag{16.99}$$

The fact that the steady-state interactions decrease with $1/m^2$ directly leads to following multi-anticipative sensitivities of the linearized model,

$$f_{\text{sm}} = \frac{1}{m^3} f_s^{\text{IDM}}, \quad f_{\text{vm}} = \frac{1}{m^2} f_l^{\text{IDM}}, \quad m = 1, \ldots, M \tag{16.100}$$

and to

$$f_{v0} = f_v = f_v^{\text{IDM,free}} + C_2 f_v^{\text{IDM,int}} \tag{16.101}$$

where $f_v^{\mathrm{IDM}}$, $f_s^{\mathrm{IDM}}$, and $f_l^{\mathrm{IDM}}$ are given by (16.89) and (16.90). This leads to the same expression for the growth rate as (16.47) with the general functions (16.67) given by

$$\begin{aligned} p(k) &= -f_v^{\mathrm{IDM}} - f_l^{\mathrm{IDM}} \sum_{m=1}^{M} \frac{\mathrm{e}^{-\mathrm{i}mk}}{m^2}, \\ q(k) &= f_s^{\mathrm{IDM}} \sum_{m=1}^{M} \frac{1-\mathrm{e}^{-\mathrm{i}mk}}{m^3}. \end{aligned} \tag{16.102}$$

Hence, the Taylor coefficients (16.68) to determine the analytic stability criterion (16.55) are

$$\begin{aligned} p_0 &= -f_v^{\mathrm{IDM,free}} - C_2 f_v^{\mathrm{IDM,int}} - C_2 f_l^{\mathrm{IDM}}, & p_1 &= \mathrm{i}C_1 f_l^{\mathrm{IDM}}, \\ q_1 &= \mathrm{i}C_2 f_s^{\mathrm{IDM}}, & q_2 &= \frac{C_1}{2} f_s^{\mathrm{IDM}}, \end{aligned} \tag{16.103}$$

with $C_1$ and $C_2$ given by (16.98).

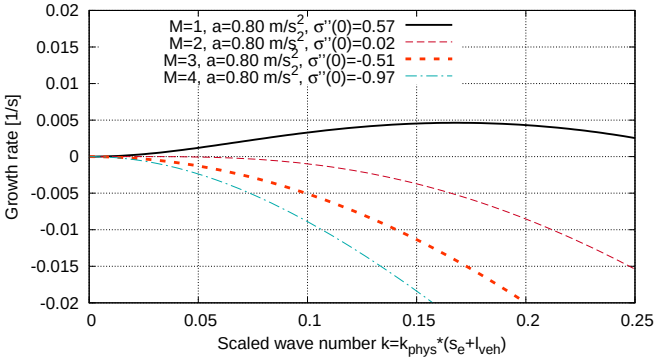


**Fig. 16.12** Linear growth rate of the more unstable branch of perturbations (16.47) of a steady state corresponding to congested traffic ($v_e = 48\,\mathrm{km/h}$) for the multi-anticipative IDM with $M = 1$ (normal IDM), 2, 3, and 4 leaders as a function of the scaled wave number (phase shift) $k$ for the IDM acceleration parameter $a = 0.8\,\mathrm{m/s^2}$. Also given are the values of the second-order Taylor coefficient $\sigma''(0)$, Eq. (16.54) with (16.103) (a positive value means string instability). The remaining IDM parameters are given in the caption of Fig. 16.9.

Remarkably, the expansion terms of the multi-anticipative IDM growth rate differ from that of the single-leader IDM just by factors 1, $C_1$, or $C_2$ and by the steady-state gap (16.97) to be used when calculating sensitivities $f_s$, $f_v$ and $f_l$ which is larger than that of the single-leader IDM by a factor of $C_2$.

Figure 16.12 shows the resulting growth rate $\sigma(k)$, Eq. (16.48), for a parameterization leading to the same fundamental diagram as in Fig. 16.9, i.e., evaluating everything with the minimum gap $s_0^{\mathrm{multi}} = s_0/C_2$ and $T^{\mathrm{multi}} = T/C_2$. In order to show the stabilizing effect, a low acceleration parameter $a = 0.8\,\mathrm{m/s^2}$ is chosen such that

the $M = 1$ curve corresponds to the most unstable curve in Fig. 16.9. While this figure clearly shows a stabilizing effect of multi-anticipation, its true power comes into play when considering finite reaction times since multi-anticipation simply "buys time" to respond.

## 16.5 Flow Stability of Macroscopic Models

For investigating macroscopic flow instability, i.e., the equivalent of the microscopic string instability, we start from the general acceleration equation (10.1) of second-order macroscopic models combined with the continuity equation (10.10) for homogeneous road sections,[37] including possible diffusion terms.

### *16.5.1 Generalized Linear Formulation of Second-Order Models*

We rewrite the acceleration equation such that all partial derivatives and nonlocalities contributing to actual accelerations appear explicitly as independent variables of the acceleration function. Together with the continuity equation, this gives

$$\frac{\partial \rho}{\partial t} + \frac{\partial (\rho V)}{\partial x} = D \frac{\partial^2 \rho}{\partial x^2}, \tag{16.104}$$

$$\frac{\partial V}{\partial t} + V \frac{\partial V}{\partial x} = A\left(\rho, V, \rho_a, V_a, \rho_x, V_x, \rho_{xx}, V_{xx}\right). \tag{16.105}$$

The partial derivatives and nonlocalities of the density field are given by

$$\rho_x = \frac{\partial \rho(x,t)}{\partial x}, \quad \rho_{xx} = \frac{\partial^2 \rho(x,t)}{\partial x^2}, \quad \rho_a(x,t) = \rho(x_a,t) \;\text{ with }\; x_a > x. \tag{16.106}$$

The derivatives $V_x$, $V_{xx}$ and nonlocalities $V_a$ of the speed field are defined in analogy.

As for the microscopic models, we expand Eqs. (16.104) and (16.105) around the steady-state solution $(\rho_e, V_e)$. The steady-state condition itself defines the fundamental speed-density relation $V_e = V_e(\rho)$ by

$$A\left(\rho, V_e(\rho), \rho, V_e(\rho), 0, 0, 0, 0\right) = 0. \tag{16.107}$$

Moving along the one-dimensional space of steady-states,

$$\mathrm{d}A = \left(A_\rho + A_{\rho_a}\right) \mathrm{d}\rho + \left(A_V + A_{V_a}\right) \frac{\mathrm{d}V_e}{\mathrm{d}\rho} \mathrm{d}\rho = 0, \tag{16.108}$$

[37] Otherwise, Fourier modes cannot be used and the analysis becomes more complicated.

we obtain the following relation between the partial derivatives of the acceleration function:

$$\frac{\mathrm{d}V_e(\rho)}{\mathrm{d}\rho} = V_e' = -\frac{A_\rho + A_{\rho_a}}{A_v + A_{V_a}}. \tag{16.109}$$

Here, the partial derivatives of the acceleration function (including these appearing in Eq. (16.114) below) are given by

$$A_\rho = \left.\frac{\partial A}{\partial \rho}\right|_e, \quad A_{\rho_a} = \left.\frac{\partial A}{\partial \rho_a}\right|_e, \quad A_{\rho_x} = \left.\frac{\partial A}{\partial \rho_x}\right|_e, \quad A_{\rho_{xx}} = \left.\frac{\partial A}{\partial \rho_{xx}}\right|_e. \tag{16.110}$$

The derivatives $A_V$, $A_{V_a}$, $A_{V_x}$, and $A_{V_{xx}}$ are defined in analogy. The subscript "$e$" denotes that the functions are evaluated at the steady-state point $(\rho_e, V_e(\rho_e))$. Linearizing Eqs. (16.104) and (16.105) using the ansatz

$$\rho(x,t) = \rho_e + \tilde{\rho}(x,t), \tag{16.111}$$

$$V(x,t) = V_e + \tilde{V}(x,t), \tag{16.112}$$

leads to the linear partial (and possibly nonlocal) differential equations

$$\frac{\partial \tilde{\rho}}{\partial t} = -\rho_e \frac{\partial \tilde{V}}{\partial x} - V_e \frac{\partial \tilde{\rho}}{\partial x} + D\frac{\partial^2 \tilde{\rho}}{\partial x^2}, \tag{16.113}$$

$$\begin{aligned}\frac{\partial \tilde{V}}{\partial t} = &-V_e \frac{\partial \tilde{V}}{\partial x} + A_\rho \tilde{\rho} + A_V \tilde{V} + A_{\rho_a}\tilde{\rho}_a + A_{V_a}\tilde{V}_a \\ &+ A_{\rho_x}\frac{\partial \tilde{\rho}}{\partial x} + A_{V_x}\frac{\partial \tilde{V}}{\partial x} + A_{\rho_{xx}}\frac{\partial^2 \tilde{\rho}}{\partial x^2} + A_{V_{xx}}\frac{\partial^2 \tilde{V}}{\partial x^2}\end{aligned} \tag{16.114}$$

which $\tilde{\rho}_a(x,t) = \tilde{\rho}(x_a,t)$ and $\tilde{V}_a(x,t) = \tilde{V}(x_a,t)$.

### *16.5.2 Linear Stability Analysis*

The general ansatz to solve this system of equations consists of linear waves (*Fourier modes*) of wave number $k$ and a growth rate $\lambda(k)$,

$$\begin{pmatrix} \tilde{\rho}_k(x,t) \\ \tilde{V}_k(x,t) \end{pmatrix} \propto \begin{pmatrix} \hat{\rho} \\ \hat{V} \end{pmatrix} \mathrm{e}^{\lambda t - \mathrm{i}kx} = \begin{pmatrix} \hat{\rho} \\ \hat{V} \end{pmatrix} \mathrm{e}^{(\sigma + \mathrm{i}\omega)t - \mathrm{i}kx}. \tag{16.115}$$

In contrast to the microscopic ansatz (16.39), the macroscopic Fourier modes are defined in the stationary (road) system. Furthermore, the quantity $k$ is dimensional with the unit $\mathrm{m}^{-1}$. Specifically:

- The wavelength is given by $2\pi/k$, i.e., $k$ is consistent with the physical definition of a *wave number*. This has to be contrasted with the physical wavelength $2\pi(s_e + l)/k$ of microscopic models.
- With $I$ lanes, a wave contains $I\rho_e 2\pi/k$ vehicles.

- The points of constant phase $\phi = \omega t - kx$ (the waves), move with the velocity $\tilde{c}(k) = \omega/k$ in the stationary system. This has to be contrasted with the physical propagation velocity $\tilde{c}_{\mathrm{mic}}(k) = v_e(s_e) + (s_e + l)\frac{\omega}{k}$ of microscopic waves in the stationary system.

Similarly to the analysis of car-following models, inserting the ansatz (16.115) into Eqs. (16.113) and (16.114) results in an algebraic linear system of equations for the amplitudes $\hat{\rho}$ and $\hat{V}$ of the density and speed oscillations, respectively:

$$\begin{aligned}
\lambda\hat{\rho} &= (\mathrm{i}kV_e - Dk^2)\hat{\rho} + \mathrm{i}k\rho_e\hat{V},\\
\lambda\hat{V} &= \left(A_\rho + A_{\rho_a}\mathrm{e}^{-\mathrm{i}ks_a} - \mathrm{i}kA_{\rho_x} - k^2A_{\rho_{xx}}\right)\hat{\rho}\\
&\quad + \left(\mathrm{i}kV_e + A_V + A_{V_a}\mathrm{e}^{-\mathrm{i}ks_a} - \mathrm{i}kA_{V_x} - k^2A_{V_{xx}}\right)\hat{V}.
\end{aligned}$$

Here, $s_a = x_a - x$ is the anticipation distance of nonlocal models.

As in the analysis of the car-following models, the solvability condition for this homogeneous linear system leads to a quadratic equation of the form (16.44) for $\lambda$. The long-wavelength expansion of the more unstable branch (given by Eq. (16.47) with the negative sign of the square root) around $k = 0$ proceeds in exact analogy to the analysis of car-following models in Section 16.4.1. Again, the result takes on the general form (16.53) but now with the macroscopic expansion coefficients

$$\begin{aligned}
p_0 &= -(A_V + A_{V_a}),\\
p_1 &= \mathrm{i}(A_{V_x} + s_aA_{V_a} - 2V_e),\\
q_1 &= \mathrm{i}V_e(A_V + A_{V_a}) - \mathrm{i}\rho_e(A_\rho + A_{\rho_a}) = -\mathrm{i}Q'_ep_0,\\
q_2 &= V_e(A_{V_x} + s_aA_{V_a}) - \rho_e(A_{\rho_x} + s_aA_{\rho_a}) - V_\mathrm{e}^2 - D(A_V + A_{v_a}).
\end{aligned} \tag{16.116}$$

To arrive at the second equality sign of the expression for $q_1$, we have applied Eq. (16.109):

$$q_1 = -\mathrm{i}V_ep_0 + \mathrm{i}\rho_ep_0\frac{A_\rho + A_{\rho_a}}{A_V + A_{V_a}} = -\mathrm{i}p_0(V_e + \rho_eV'_e) = -\mathrm{i}Q'_ep_0. \tag{16.117}$$

In first order of the wave number $k$, the general long-wavelength expansion (16.53) yields a purely imaginary contribution and results in the phase velocity

$$\tilde{c}(k) = \frac{\omega}{k} = -\frac{q_1}{p_0} + \mathscr{O}(k^2) = Q'_e + \mathscr{O}(k^2). \tag{16.118}$$

As in the LWR models, the propagation speed of waves of low wave number ($k \ll \pi$) is given by the gradient $Q'_e$ of the fundamental diagram. In contrast to these models where $\tilde{c} = Q'_e$ is valid for any perturbation, the wave velocity of second-order macroscopic models changes with the wavelength and $\tilde{c} = \lim_{k\to 0}\tilde{c}(k) = Q'_e$ is only a linear and long-wavelength approximation. In Problem 16.2 we will show that expression (16.118) for the physical phase velocity in the road-based system also applies to the considered car-following models.

As in the microscopic analysis, the second-order term of Eq. (16.53) providing the stability properties is purely real and the string stability criterion is given by (16.55). Inserting (16.117), $q_1 = -\mathrm{i}Q'_e p_0$, into (16.55) results in the simple, still general macroscopic flow stability condition

$$(Q'_e)^2 - \mathrm{i}p_1 Q'_e - q_2 \leq 0. \tag{16.119}$$

Notice that $p_0$ dropped out completely in this relation.

**Local models.** Local macroscopic models are defined by $A_{\rho_a} = A_{V_a} = 0$. Inserting the macroscopic expansion coefficients (16.116) for $p_1$ and $q_2$ and replacing $Q'_e = V_e + \rho_e V'_e$, we obtain the stability condition

$$\boxed{(\rho_e V'_e)^2 \leq -\rho_e \left(V'_e A_{V_x} + A_{\rho_x}\right) - DA_V \quad \begin{array}{l}\text{Flow stability for}\\ \text{local macroscopic models.}\end{array}} \tag{16.120}$$

With (16.109), this condition can also be formulated purely in terms of derivatives of the acceleration function,

$$\left(\frac{\rho_e A_\rho}{A_v}\right)^2 \leq \frac{\rho_e A_\rho A_{v_x}}{A_v} - \rho_e A_{\rho_x} - DA_V. \tag{16.121}$$

We emphasize that this criterion does not depend on $A_{V_{xx}}$ or $A_{\rho_{xx}}$. So, contrary to intuition, flow stability is *not* enhanced by diffusion terms in the equation for the speed field. It is enhanced, however, by the diffusion term proportional to $D$ in the density equation. Remarkably, without diffusion, the form (16.120) does also not depend directly on the acceleration sensitivities $A_\rho$ and $A_v$ with respect to density or speed, respectively, since they only appear in the combination $V'_e = -A_\rho/A_v$. If the macroscopic model can be written in the form (10.11), i.e., the acceleration function does not contain speed gradients, and all other gradients can be written in terms of a complete differential $-\frac{1}{\rho}\partial P/\partial x$ of a *traffic pressure* $P(\rho(x,t))$ depending on density, only, Eq. (16.120) assumes the form

$$(\rho_e V'_e)^2 \leq P'_e - DA_V \quad \text{where} \quad P'_e = P'(\rho_e). \tag{16.122}$$

**Nonlocal models.** Since the nonlocal terms containing $\rho_a(x,t) = \rho(x+s_a,t)$ or $V_a(x,t) = V(x+s_a,t)$ constitute anticipative elements ($s_a = x_a - x > 0$), they play the role of the gradient terms of the local models and it does not make sense to include the latter in nonlocal models: After all, nonlocal models have been proposed to overcome some conceptual and numerical problems that are inherent to the gradients of local models.[38] Therefore, we can set $A_{\rho_x} = 0$, $A_{V_x} = 0$, and $D = 0$. However, this applies to gradients related to accelerations of single vehicles, only. Gradients arising from kinematic reasons (the advective term $V\frac{\partial V}{\partial x}$), or representing

[38] Diffusion terms imply infinite speeds. Furthermore, in the presence of speed gradients, negative speeds cannot be excluded. Moreover, local models are numerically more unstable than gradient-free nonlocal models.

purely statistical effects (pressure term $-1/\rho \frac{\partial P}{\partial x}$, cf. Section 10.3.4) are retained. Consequently, the nonlocal models considered in the following (including the GKT model) have acceleration equations of the form

$$\frac{\partial V}{\partial t} + V\frac{\partial V}{\partial x} + \frac{1}{\rho}\frac{\partial P(\rho)}{\partial x} = A\left(\rho, V, \rho_a, V_a\right). \tag{16.123}$$

Evaluating the general stability condition (16.119) for this model class leads to

$$\boxed{(\rho_e V_e')^2 \leq P_e' - \rho_e s_a \left(V_e' A_{V_a} + A_{\rho_a}\right) \quad \text{Stability condition for nonlocal macro-models.}} \tag{16.124}$$

**Discussion.** As for the microscopic models, macroscopic models tend to become more instable with increasing gap sensitivity $|V_e'(\rho)|$ representing the degree of interaction between drivers, i.e., completely free traffic is never unstable. Furthermore, like in car-following models, anticipation in the form of gradients ($A_{V_x} > 0, A_{\rho_x} < 0$) or nonlocalities ($A_{V_a} > 0, A_{\rho_a} < 0$) enhance stability. By comparing the stability conditions (16.124) and (16.120) it becomes evident that the nonlocalities $A_{\rho_a}$, $A_{V_a}$ of the nonlocal models directly correspond to the gradients $A_{\rho_x}$, $A_{V_x}$ of the local models.

In contrast to microscopic models, the speed sensitivity $A_V$ alone does not influence stability since it appears only in combination with the density diffusion $D$ which is zero, in most macroscopic models. We conclude:

Without gradients or nonlocalities, macroscopic models are unconditionally unstable.

Furthermore, linear stability does not depend on diffusion terms characterized by $A_{\rho_{xx}}$ and $A_{V_{xx}}$ but only on density diffusion characterized by the coefficient $D$. Nevertheless, diffusion terms in the speed equation tend to stabilize perturbations of higher amplitude and/or frequency that are outside the limits of this linear long-wavelength analysis. Therefore, such terms are included into some local macroscopic models, e.g., the Kerner-Konhäuser model (10.21).

### *16.5.3 Application to Specific Macroscopic Models*

In the following, we apply the general criteria to three models of Chapter 10, Payne's model, Kerner-Konhäuser model, and the GKT model. Furthermore, the investigate a modified *Aw-Rascle model*

**Payne's model.** The acceleration function of Payne's model (10.18) is given by

$$A(x,t) = \frac{V_e(\rho) - V}{\tau} + \frac{V_e'(\rho)}{2\rho\tau}\frac{\partial \rho}{\partial x}.$$

With the partial derivatives $A_{\rho_x} = V_e'/(2\rho\tau)$, $A_{V_x} = 0$ and $D = 0$, the macroscopic stability condition (16.120) for local models gives

$$\rho V_e'^2 \leq -A_{\rho_x} = -\frac{V_e'}{2\rho\tau}$$

and (watch the signs keeping in mind that $V_e' = V_e'(\rho) < 0$)

$$-V_e'(\rho) = |V_e'(\rho)| \leq \frac{1}{2\rho^2\tau}. \tag{16.125}$$

Again, stability of traffic flow increases with increasing agility of the drivers (decreasing speed adaptation time $\tau$), and decreasing sensitivity $|V_e'(\rho)|$ to density changes which is the macroscopic equivalent to the microscopic gap sensitivity $v_e'(s)$.

Notice that this result could also be obtained directly from the formulation of Payne's model with a pressure gradient, $\frac{\mathrm{d}V}{\mathrm{d}t} = \frac{V_e - V}{\tau} - \frac{1}{\rho}\frac{\partial P}{\partial x}$ with $P = -V_e/(2\rho)$. Applying (16.122) gives $(\rho_e V_e')^2 \leq P_e' = -V_e'/(2\rho\tau)$

**LWR models.** In the limiting case $\tau \to 0$, Payne's model tends to the LWR model with diffusion (cf. Section 10.4.1). According to Eq. (16.125), this model is *unconditionally stable*. In contrast, the stability properties of the classical LWR model without diffusion terms are undefined. However, since even the smallest finite diffusion makes the model unconditionally stable and integration schemes typically introduce a finite amount of *numerical diffusion* (cf. Sect. 10.5.7), the LWR models can be considered as unconditionally stable, for practical purposes.

**Kerner-Konhäuser model.** For reference, the model formulation (10.22) in terms of the traffic pressure is given by

$$\frac{\partial V}{\partial t} + V\frac{\partial V}{\partial x} = \frac{V_e(\rho) - V}{\tau} - \frac{1}{\rho}\frac{\partial P(\rho)}{\partial x} + \frac{\mu}{\rho}\frac{\partial^2 V}{\partial x^2}, \quad P(\rho) = \rho c_0^2.$$

It is convenient to apply the form (16.122) of the stability criterion. With $P'(\rho) = c_0^2$ and $D = 0$,[39] we obtain

$$\left(\rho_e V_e'\right)^2 \leq P_e'(\rho) = c_0^2. \tag{16.126}$$

As in Payne's model, flow stability is enhanced by decreasing the sensitivity $|V_e'(\rho)|$ to density changes. Furthermore, stability grows with the drivers' level of anticipation which is characterized by the prefactor $c_0^2$ of the traffic pressure.[40] We emphasize that, at variance with expectations, the model parameter $\tau$ representing the driver's agility drops out of the stability condition. This makes the model somewhat counterintuitive.

---

[39] Notice that the speed diffusion $A_{V_{xx}} = \mu/\rho$ does not contribute to linear stability.

[40] In a statistical interpretation, $c_0^2$ formally denotes the speed variance in analogy to the corresponding term $\theta = \alpha(\rho)V^2$ of the GKT model. However, in the Kerner-Konhäuser model, $c_0^2$ is usually interpreted as a purely phenomenological anticipation term.

**A modified Aw-Rascle model.** For theoretical investigations, the Aw-Rascle model is often used because it is fully flow conservative. However, it does not describe realistic traffic flow, so some "generalizations" have been proposed, e.g., one with the acceleration equation

$$\frac{\partial V}{\partial t} + \left( V - \frac{1}{\rho T} \right) \frac{\partial V}{\partial x} = 0. \tag{16.127}$$

Obviously, this model allows for any two-dimensional combination of $\rho$ and $Q = \rho V$ as a steady state because it contains only gradients. Moreover, its flow stability is undefined because the relevant stability criterion (16.120) depends on the existence of a fundamental diagram to form the gradient $V_e'(\rho) = -A_\rho / A_V$. By adding a relaxation term and writing the acceleration equation term in the form

$$\frac{\partial V}{\partial t} + V \frac{\partial V}{\partial x} = \frac{1}{\rho T} \frac{\partial V}{\partial x} + \frac{V_e(\rho) - V}{\tau},$$

its stability is defined. With $A_v = -1/\tau$, $A_{V_x} = 1/(\rho T)$, $A_\rho = V_e'(\rho)/\tau$, and $A_{\rho_x} = 0$ and inserting this in (16.120) considering $V_e'(\rho) \leq 0$, we obtain the flow stability condition

$$V_e'(\rho_e) \geq -\frac{1}{\rho_e^2 T}.$$

Notice that, as in the Kerner-Konhäuser model, the relaxation time $\tau$ drops out.

**GKT model.** In spite of the more complex GKT acceleration function given by the right-hand side of Eq. (10.25), the partial derivatives necessary for the nonlocal stability criterion (16.124) can be expressed in a compact form,

$$A_{\rho_a} = \frac{\partial A}{\partial \rho_a} = -\frac{2(V_0 - V_e)\rho_{\max}}{\tau \rho_e (\rho_{\max} - \rho_e)}, \tag{16.128}$$

$$A_{v_a} = \frac{\partial A}{\partial V_a} = \frac{2(V_0 - V_e)}{\tau \sigma_V(\rho_e)\sqrt{\pi}}. \tag{16.129}$$

Here, the speed variance $\sigma_V^2(\rho) = \alpha(\rho) V_e^2(\rho)$ is given by Eq. (10.23). Inserting the partial derivatives into the stability criterion results in the following condition for GKT flow stability

$$\left(\rho_e V_e'\right)^2 \leq P_e' + \frac{2 s_a (V_0 - V_e)}{\tau} \left[ \frac{\rho_{\max}}{\rho_{\max} - \rho_e} - \frac{\rho_e V_e'}{\sigma_V \sqrt{\pi}} \right] \tag{16.130}$$

where $s_a = \gamma V_e T$ and $P_e' = \sigma_V^2 + \rho \alpha'(\rho) V_e^2$ are taken at steady-state conditions. Notice that, in the limit of zero anticipation ($\gamma \to 0$), the GKT flow stability criterion reverts to that for the Kerner-Konhäuser Model but the stability increases for increasing anticipation distance $s_a = \gamma v_e T$ and increasing driver agility $1/\tau$, in agreement with the general qualitative discussion on the influencing factors of string stability in Section 16.4.1 on page 370.

Near the maximum density, we can approximate this GKT stability criterion and express it in terms of a simple condition for the anticipation factor $\gamma$ (cf. Prob-

lem 16.7),

$$\gamma > \frac{\tau}{2T^2\rho_{\max}V_0\left(1+(\alpha_{\max}\pi)^{-1/2}\right)}. \tag{16.131}$$

This condition makes explicit that, in the GKT model, stability

- increases with $\gamma$ characterizing the level of anticipation,
- decreases with increasing $\tau$, i.e., reducing the driver's agility $a = V_0/tau$ corresponding to the maximum acceleration in the vehicle reference frame,
- increases with increasing desired time gap $T$, i.e., reducing the aggressiveness,
- increases with the desired speed $V_0$, i.e., increasing the agility $V_0/\tau$,
- and increases with the sensitivity to speed differences which is characterized by $\alpha^{-1/2}$.

Notice that all influencing factors are plausible, i.e., change the stability in the expected direction.

## 16.6 Convective Instability and Signal Velocities

In order to arrive at an approximate analytical criterion between convective and absolute instability, we start directly with definition (16.6) and investigate whether an initial transient and localized perturbation propagates in both directions (absolute instability), or only in one direction (upstream or downstream convective instability). Since all considerations are based on Eq. (16.44) and this quadratic equation applies equally to car-following and macroscopic models (cf. Eqs. (16.46) and the solvability condition derived from Eq. (16.116), respectively), the analysis to be developed below applies to macroscopic flow stability as well as to microscopic string stability. The macroscopic approach allows for a more compact analytical representation, so we will use it in the following.

We recall that Eq. (16.44) has two solution branches (linear complex dispersion relations) $\lambda_{1/2}(k)$ of which one is always decaying. Since we are interested in growing perturbations, we will consider the more unstable branch, only, by setting

$$\lambda(k) = \begin{cases} \lambda_1(k) & \text{if } \mathrm{Re}(\lambda_1(k)) > \mathrm{Re}(\lambda_2(k)), \\ \lambda_2(k) & \text{otherwise.} \end{cases} \tag{16.132}$$

Generally, the more unstable branch is given by Eq. (16.47) with the negative sign of the square root.

In contrast to the investigations on the instability threshold, the growth rates will no longer be expanded around the wave number $k = 0$ of the *firstly unstable* perturbation but around the wave number

$$k_0 = \arg\max_k(\mathrm{Re}\ \lambda(k)) \tag{16.133}$$

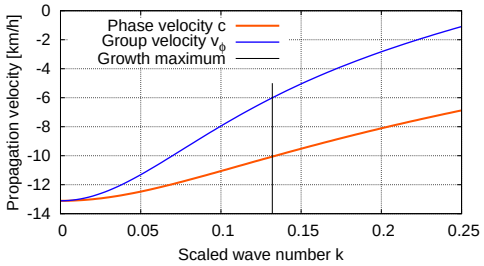


**Fig. 16.13** Propagation velocity $\tilde{c}(k)$ and group velocity $v_g(k)$ for the IDM with acceleration parameter $a = 0.93\,\mathrm{m/s^2}$. The steady-state speed $v_e$ and the other IDM parameters are given in the caption of Fig. 16.9.

of the *fastest growing* perturbation. Since this investigation only makes sense if there is a linear instability at all, the associated maximum growth rate

$$\sigma_0 = \sigma(k_0) = \mathrm{Re}\,\lambda(k_0) \tag{16.134}$$

is positive. Due to vehicle conservation, waves of infinite wavelength corresponding to $k = 0$ always have a growth rate of zero, so the wave number $k_0$ of the fastest growing mode is nonzero as well. We emphasize that determining the argument $k_0$ of the fastest growing mode is the only numerical step required in this section.[41] The qualitative picture is exemplified by Fig. 16.9 displaying the growth rate $\sigma(k) = \mathrm{Re}\,\lambda(k)$ for the IDM as a function of the wave number $k$ and the distance from the linear instability threshold (corresponding to an IDM acceleration parameter $a = 1.10\,\mathrm{m/s^2}$):

- For reasons of symmetry, not only $\sigma(0)$ is 0 but also the tangent slope $\sigma'(0) = 0$.
- At the instability threshold, the first unstable mode has a wave number $k \to 0$, so $k_0 \to 0$. Above the linear threshold, $k_0$ grows with increasing distance.
- For reasonable parameter settings, the instability retains its long-wavelength nature also above the threshold. In the example of Fig. 16.9, the wave number $k_0$ of the fastest growing mode at the limit between convective and absolute instability (corresponding to the middle curve) represents traffic waves of wavelength $(l_{\mathrm{veh}} + s_e)2\pi/k_0 \approx 1.3\,\mathrm{km}$. In other words, each wave contains $2\pi/k_0 \approx 47$ vehicles. Furthermore, although significantly above the threshold, the associated growth rate $\sigma_0 = 0.0017\,\mathrm{s^{-1}}$ corresponds to a remarkably slow growth by a factor of $\mathrm{e}^1$ every ten minutes.[42]

[41] The analytic derivation of the resonance frequency (16.73) is of little help here because this equation determines the oscillation frequency for a maximum growth rate from vehicle to vehicle for sustained leading vehicle oscillations while here the wave number for a maximum growth rate $\mathrm{Re}\,\lambda$ of a spatially infinite harmonic wave field is needed. In spite of the simple appearance of (16.45) for $\lambda(k)$, it is extremely cumbersome to calculate analytically.

[42] Notice that this is another hint that it may take some time until an initial perturbation develops to high-amplitude traffic waves, or a traffic breakdown.

In order to determine the limits of convective instability, we determine the spatiotemporal evolution $U(x,t)$ of the perturbation amplitude, and check whether it spreads only upstream, only downstream, or in both directions. The amplitude $U(x,t)$ is defined by the system (16.113), (16.114) of linear partial differential equations to be solved in the infinitely extended system with the localized initial perturbation (16.3), or the corresponding microscopic linear equations. This initial-value problem is approximately solved in the following steps:

- The initial perturbation $U(x,0)$ is partitioned into linear waves by Fourier transforming the initial condition with respect to space. Since the initial perturbation is localized within the space available for one vehicle and the interesting Fourier modes have much greater wavelengths, the integral over $x$ determining the complex amplitude of the modes (Fourier transform) is the same for all relevant modes, and can be set to unity.
- The Fourier modes are evolved in time by the Eqs. (16.39) or (16.115) for microscopic and macroscopic models, respectively
- In the case of microscopic models, the Fourier modes are transformed in a fixed system with dimensional space coordinates. In any case, the development of the complex speed components of the Fourier modes is now given by $\tilde{V}_k(x,t) = \mathrm{e}^{\lambda t - \mathrm{i}kx}$ (cf. Eq. (16.115)).
- Summing over the speed components $\tilde{V}_k(x,t)$ of the Fourier modes, i.e., performing an inverse Fourier transformation, gives the complex perturbation amplitude $\tilde{U}(x,t) = \int \tilde{V}_k(x,t)\mathrm{d}k$. Taking the real part finally gives the spatiotemporal evolution $U(x,t) = \mathrm{Re}\,\tilde{U}(x,t)$.

While the first three steps are straightforward, the last step can only be evaluated analytically if one expands the complex growth rate to second order around $k = k_0$ and solves the resulting complex Gaussian integral. This rather lengthy calculation results in (cf. Fig. 16.14)

$$U(x,t) = \mathrm{Re}(\tilde{U}(x,t)), \tag{16.135}$$

$$\tilde{U}(x,t) \propto \exp\left[\mathrm{i}(k_0^{\mathrm{phys}}x - \omega_0 t)\right] \exp\left[\left(\sigma_0 - \frac{\left(v_g - \frac{x}{t}\right)^2}{2(\mathrm{i}\omega_{kk} - \sigma_{kk})}\right)t\right]. \tag{16.136}$$

The expansion coefficients are summarized in the following table:

| Quantity in Eq. (16.136) | Microscopic models | Macroscopic models |
|---|---|---|
| $k_0^{\text{phys}}$ | $\rho_e k_0 = \rho_e \arg\max_k \text{Re}\,\lambda(k)$ | $k_0 = \arg\max_k \text{Re}\,\lambda(k)$ |
| $\sigma_0$ | $\text{Re}\,\lambda(k_0)$ | $\text{Re}\,\lambda(k_0)$ |
| $\omega_0$ | $v_e\rho_e k_0 + \text{Im}\;\lambda(k_0)$ | $\text{Im}\,\lambda(k_0)$ |
| $v_g$ | $v_e + \text{Im}\,\lambda'(k_0)/\rho_e$ | $\text{Im}\,\lambda'(k_0)$ |
| $\sigma_{kk}$ | $\text{Re}\,\lambda''(k_0)/\rho_e^2$ | $\text{Re}\,\lambda''(k_0)$, |
| $\omega_{kk}$ | $\text{Im}\,\lambda''(k_0)/\rho_e^2$ | $\text{Im}\,\lambda''(k_0)$. |

As visualized by Fig. 16.14, expression (16.136) represents a localized group of waves with the following properties:

- Single waves propagate with the *phase velocity* $v_\phi = \tilde{c}(k_0) = \omega_0/k_0^{\text{phys}}$ (first factor of $\tilde{U}(x,t)$).
- The center of the perturbation propagates with the *group velocity* $v_g$ (second factor).
- The amplitude at the center of the perturbation grows with the rate $\sigma_0$.

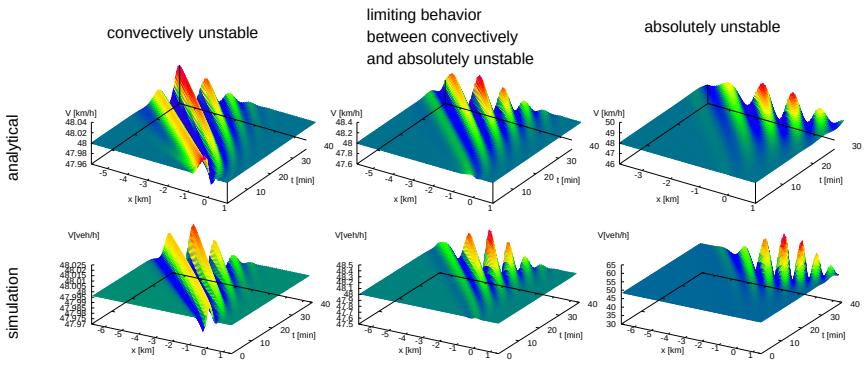


**Fig. 16.14** Spatiotemporal propagation $U(x,t)$ of a localized perturbation of the steady-state traffic flow (speed $v_e = 48\,\text{km/h}$) as simulated with the IDM. The parameter settings of the left column (acceleration parameter $a = 1\,\text{m/s}^2$, further IDM parameters as in Fig. 16.9) correspond to convectively unstable traffic, the right column ($a = 0.85\,\text{m/s}^2$) to absolutely unstable traffic, and the middle column ($a = 0.93\,\text{m/s}^2$) to the limit between convective and absolute instability. For each parameter settings, the analytical result Eq. (16.136) (top row) is compared with an IDM simulation (bottom row).

Figures 16.13 and 16.15 show that phase and group velocity are different from each other (and also different from the LWR propagation speed $\tilde{c} = \lim_{k\to 0}\tilde{c}(k)$): Since $v_g$ is larger (less negative) than $v_\phi$, the waves emerge at the downstream boundary of the perturbation, propagate through the perturbed region, and vanish

at the upstream boundary.[43] In spite of the many approximations made in deriving Eq. (16.136), this analytical expression agrees with the simulation result *in fine detail*.

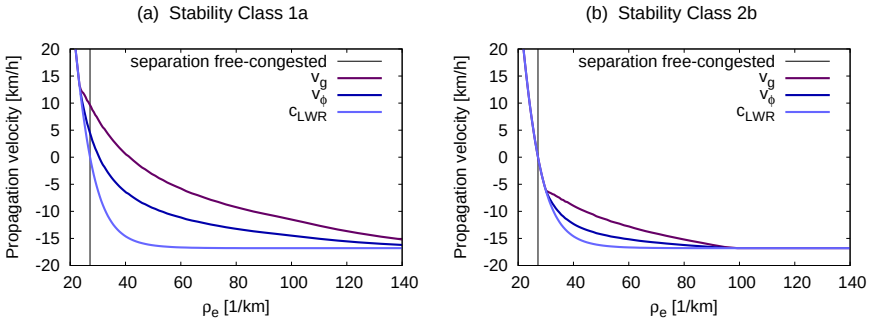


**Fig. 16.15** Propagation velocities of linear perturbations as a function of the steady-state density $\rho_e$. Shown are the group velocity $v_g$, the phase velocity $v_\phi$ and, for comparison, the LWR propagation velocity $Q'_e(\rho)$ for the IDM. In Plot (a), traffic flow at capacity is unstable (stability class 1, $a = 0.8\,\mathrm{m/s^2}$, the other parameters are as in Fig. 16.9) while, in diagram (b), traffic flow at capacity is linearly stable (stability class 2, $a = 1.1\,\mathrm{m/s^2}$).

By applying the definition (16.6) of convective instability to the solution (16.136), we finally arrive at the following analytic criteria for convective instability:

$$\boxed{0 < \sigma_0 \leq \frac{v_g^2}{2D_2}, \quad D_2 = -\sigma_{kk}\left(1 + \frac{\omega_{kk}^2}{\sigma_{kk}^2}\right) \qquad \text{Convective instability.}} \tag{16.137}$$

The first inequality sign states that traffic flow must be linearly (string or flow) unstable while the second inequality ensures that the perturbations propagate in only one direction. Notice that Eq. (16.137) depends only on the square of the group velocity, so it does not distinguish between upstream and downstream convective instability. The latter information is directly contained in the analytical solution (16.136): A steady-state flow satisfying Eq. (16.137) is convectively upstream unstable if $v_g < 0$, and convectively downstream unstable, otherwise.

Remarkably, the range of growth rates corresponding to convective instability increases with the *square* of the group velocity $v_g$ and with the inverse of the second-order effective dispersion coefficient $D_2$:[44] If $v_g \approx 0$ (corresponding to the transition between free and congested traffic or to congested traffic of comparatively low density, cf. Fig. 16.15(a), the instability is always absolute. For congested traffic sufficiently far away from the transition point, $v_g < 0$ and the instabilities are *nearly*

[43] This is similar to a group of water waves triggered by a localized perturbation, e.g., by a stone thrown at the water surface.

[44] This dispersion has the same unit, order of magnitude ($100\,\mathrm{m^2/s}$), and effect, as the diffusion terms of some macroscopic models.

*always* of an upstream convective nature. Finally, if the model parameter settings imply linear instabilities on the left-hand side of the fundamental diagram ("dense" but technically free traffic flow, $v_g > 0$), Eq. (16.137) allows for convective downstream instabilities, similarly to the original hydrodynamic systems where the concept of convective instability comes from. However, unlike the upstream type, downstream convective instabilities are not robust with respect to nonlinear effects: Downstream propagating growing waves reverse their propagation direction once nonlinearities kick in so the system effectively becomes absolutely unstable (cf. Fig. 16.5). This reversal, also called the *boomerang effect* can also be observed in traffic data (cf. Fig. 21.4). We conclude that, unlike upstream convective instabilities, downstream convective instabilities are not relevant for traffic flow dynamics.

**Signal velocities.** The signal velocities are defined as the slopes of rays $x = c_s t$ in spacetime along which the linear amplitude of instabilities triggered by a localized and instantaneous perturbation at $x = t = 0$ neither grows nor shrinks. Generally, there are two such velocities representing the motion of the two boundaries of the instability region. In Fig. 16.4, these boundaries are indicated by solid black lines

In order to extract the signal velocities from the perturbation field $U(x,t)$, we consider the amplitude of $U(x,t)$ along rays $x = c_s t$ and determine $c_s$ such that the growth of the amplitude along this ray is equal to zero. This means, we replace $x = c_s t$ in the expression (16.135) for $U(x,t)$ and set the real part of its exponent equal to zero:

$$\sigma_0 - \mathrm{Re}\left(\frac{(v_g - c_s)^2}{2(\mathrm{i}\omega_{kk} - \sigma_{kk})}\right) = \sigma_0 - \left(\frac{(v_g - c_s)^2}{2D_2}\right) = 0.$$

For $\sigma_0 > 0$ (i.e., traffic flow is string unstable which we require anyway), this leads to two signal velocities,

$$c_\mathrm{s}^\pm = v_\mathrm{g} \pm \sqrt{2D_2\sigma_0}. \tag{16.138}$$

From this relation, we learn the following:

- The center of the region of significantly perturbed traffic flow propagates with the group velocity.
- The perturbed region grows spatially at a constant rate $2\sqrt{2D_2\sigma_0}$.
- As expected, the spatial growth rate increases with the overall level of instability $\sigma_0$ and with the effective dispersion coefficient $D_2$.
- The special case $c_s = 0$ leads us to the threshold condition $\sigma_0 = v_g^2/(2D_2)$ between absolute and convective instability which agrees with (16.137).

The latter point indicates that signal velocities are related to convective instability. Moreover, they provide an intuitive, and yet mathematically stringent, approach to distinguish between the upstream and downstream types of convective instability:

$$\text{traffic flow is} \begin{cases} \text{absolutely string unstable} & c_\mathrm{s}^- < 0 < c_\mathrm{s}^+ \\ \text{upstream convectively unstable} & c_\mathrm{s}^- < 0, c_\mathrm{s}^+ < 0 \\ \text{downstream convectively unstable} & c_\mathrm{s}^- > 0, c_\mathrm{s}^+ > 0. \end{cases} \tag{16.139}$$

The upstream type of convective instability (Fig. 16.4 left) is often observed in the traffic flow context while the downstream type is related to the hydrodynamic context where the very concept of convective instability originates.

## 16.7 Nonlinear Instability and the Stability Diagram

The analytical investigation of the previous sections refer to small perturbations, i.e., to *linear instability*. Few analytical results are available for large-amplitude perturbations or fully developed traffic waves.[45] Instead, one investigates nonlinear effects directly by simulations of well-defined systems that are as simple as possible. The most popular of such *toy systems* is a closed single-lane ring road populated which identical drivers and vehicles.[46] In order to avoid *finite-size effects*, the system should contain more than 500 vehicles. As a further abstraction, one can also consider a ring road with a circumference tending to infinity or, equivalently, an infinitely extended homogeneous road. The only *control parameter* is the global (average) density $\rho_e$. By simulating the qualitative system dynamics in the full range $[0, \rho_{\max}]$ of possible values for the control parameter, one obtains a *stability diagram*.

We emphasize that a ring road does not represent a realistic abstraction of real road networks: Real road networks are open, so the inflow (traffic demand) rather than the density acts as control parameter. Furthermore, bottlenecks are missing on the idealized ring road. Nevertheless, their investigation allows us to draw far-reaching conclusions on more realistic open systems with bottlenecks. A big advantage of stability diagrams derived from ring roads is that they reflect the dynamical properties of a given model-parameter combination independently of the properties of the road network, or the traffic state.

To obtain stability diagrams as that of Fig. 16.17(a), (b), or (d), we scan the whole range of global densities $\rho_e \in [0, \rho_{\max}]$. For a given global density, we simulate two scenarios: One is initialized with a very small perturbation, and one with the maximum possible perturbation. Instead of the "linear" scenario initialized with the small perturbation, one could also use the analytical results. However, simulating them represents a good combined test of the simulator code, and of the approximations and assumptions made during the analytical derivations. For each scenario, we check whether the initial perturbation dissolves, or evolves into persistent traffic waves. Generally, the resulting stability diagram is subdivided into the following regions:

- Absolute stability for global densities $\rho_e$ below the lower nonlinear threshold $\rho_1$.

[45] There is a large body of literature proposing and investigating solitary nonlinear waves which can be investigated analytically. However, the conditions to derive equations for such waves (e.g., a *modified Korteweg-de-Vries equation*) are extremely restrictive and nearly never satisfied in real traffic situations.

[46] A ring road must not be confused with a roundabout which, in contrast to the former, represents a comparatively complex network node.

- *Metastability* in a range $\rho_1 \leq \rho_e < \rho_2$ between the lower nonlinear and linear thresholds. In this range, sufficiently small initial perturbations eventually dissolve while higher-amplitude perturbations develop to persistent traffic waves (Fig. 16.16, see also Fig. 16.8).
- Absolute linear instability in a range $\rho_2 \leq \rho_e < \rho_{\mathrm{cv}}$.
- Convective linear instability in the range $\rho_{\mathrm{cv}} \leq \rho_e < \rho_3$.[47]
- Convective metastability in the range $\rho_3 \leq \rho_e < \rho_4$ between the upper linear and nonlinear density thresholds.
- And absolute instability for $\rho_e \geq \rho_4$.

Which subset of the above stability types is actually realized when scanning the global density depends on the model-parameter combination. Since this determines the qualitative behavior of congested states in real open road networks (and in particular whether this behavior is realistic or not), the most relevant subsets are attributed to *stability classes* that will be discussed in the next section.

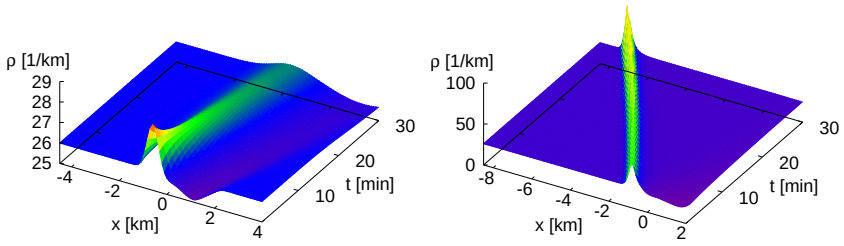


**Fig. 16.16** Metastable traffic flow on a ring road with the global density $\rho = 26\,\mathrm{veh/km}$ for IDM parameters as in Fig. 16.17(d). Small perturbations dissolve (left) while a larger initial perturbation develops to a persistent traffic wave propagating around the ring road (right). Notice the different scales of the $z$-axes.

## 16.8 Stability Classes

While the density regions for the different instability types appear (with few exceptions) always in the order $\rho_1 \leq \rho_2 \leq \rho_{\mathrm{cv}} \leq \rho_3 \leq \rho_4$,[48] not all density regions are realized, in general. Particularly, there may be no restabilization for high densities

[47] Strictly speaking, convective instability is only well-defined in an infinite or open system. However, for practical purposes, the circumference of the ring must be sufficiently large such that no vehicle drives around the complete ring during the simulation time.

[48] For rare combinations of models and parameters, we obtain a region of absolute instability embedded on both sides by regions of convective downstream and upstream instabilities, respectively.

(Fig. 16.17(a)), no absolute instability ($\rho_2 = \rho_{cv}$, Fig. 16.17(a), (b)), or no instability at all ($\rho_1 = \rho_4 = \rho_{max}$). In principle, all ranges apart from the first one ($\rho < \rho_1$) may vanish independently from each other. It is hard, however, to find model-parameter combinations showing metastable regimes but no linear instability at any density.

Analyzing real open systems with bottlenecks, it turns out that the qualitative spatiotemporal behavior, i.e., the set of possible congestion patterns, depends on only a few combinations of existing regimes. Additionally, the relative position of the thresholds with respect to the density $\rho_K$ at capacity (the density where the maximum flow is observed) plays an essential role. This leads to the definition of the following *stability classes*:

**Class 1a:** When increasing the density, traffic flow becomes linearly unstable for densities corresponding to dense but technically yet free traffic. Furthermore, it remains unstable for all higher densities: $\rho_1 \leq \rho_2 < \rho_K$, $\rho_3 = \rho_4 = \rho_{max}$. Since the propagation velocity $v_g$ is 0 for a steady-state density $\rho_e \approx \rho_K$, Equation (16.137) implies that this class includes density ranges of absolute instability. Typically, the instability remains absolute up to moderately congested traffic and becomes convective for severe congestions near the maximum density.

**Class 1b:** Traffic flow *restabilizes* for high densities, i.e., traffic flow becomes smoothly creeping rather than oscillatory if severely congested.[49]

**Class 2a:** Only congested traffic flow (on the "right-hand side" of the fundamental diagram) can become unstable, and there is no restabilization: $\rho_2 > \rho_K$, $\rho_3 = \rho_4 = \rho_{max}$. Typically, the instability is always of a convective nature. However, a small range of absolutely unstable traffic is possible for congested traffic of comparatively low density.

**Class 2b:** As Class 2a, but with restabilization, $\rho_3 < \rho_{max}$.

**Class 3:** Absolute stability everywhere, $\rho_1 = \rho_{max}$.

Comparing the patterns simulated in realistic open systems with observations (cf. Chapter 21), we conclude the following:

Realistic model-parameter combinations for highway traffic flow correspond to stability classes 2a or 2b.

Depending on the parameter set, one and the same model can belong to different stability classes. Figure 16.17 shows that the IDM can assume *all* classes. With the help of this model, we will now discuss the influencing factors leading to the different classes.

[49] We are aware that, in vehicles with manual transmission, it is hard to drive smoothly at very low speeds where the clutch must be operated even when driving in first gear. While this is considered in sub-microscopic models, it is ignored for the models considered here. In effect, the difficulty to drive very slowly leads to persistent noise at a sub-microscopic level. However, if traffic flow is stable at a microscopic or macroscopic level, these perturbations are not collectively amplified, i.e., traffic data show strong fluctuations but no deterministic signal.

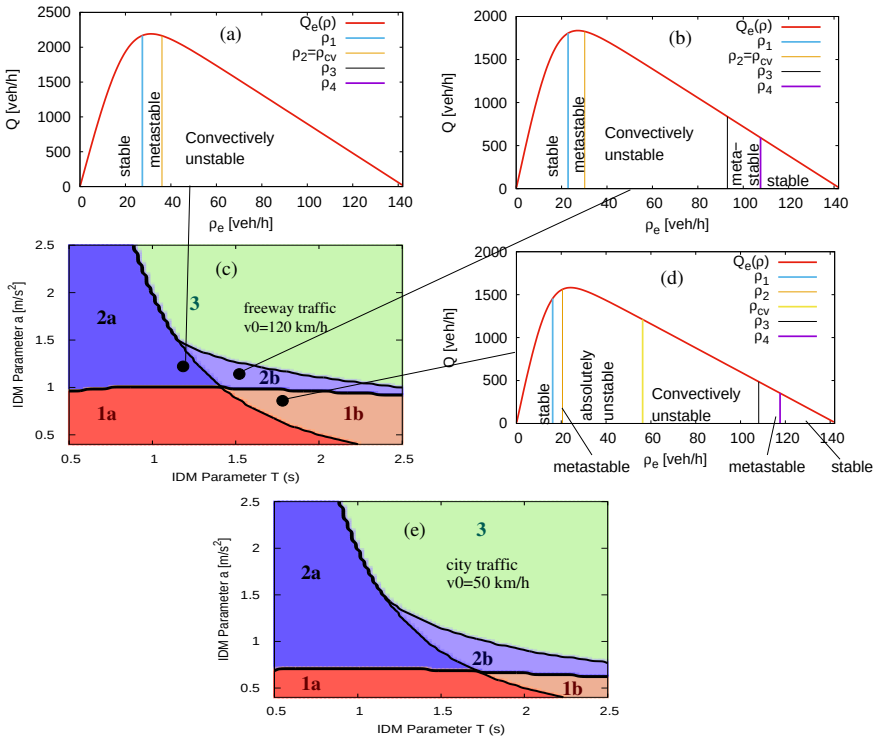


**Fig. 16.17** (c) Class diagram of the IDM as a function of the time gap $T$ and acceleration $a$. The other IDM parameters and the vehicle length 5 m are the same as in Fig. 16.9. (a), (b), (d) stability diagrams for three points of the class diagram corresponding to the classes 2a, 2b, and 1b, respectively. (e) class diagram for city traffic ($v_0$ reduced to 50 km/h, everything else unchanged).

**Agility.** Agility or responsiveness corresponds to the acceleration parameter $a$. Starting with low agility and increasing the agility by increasing the parameter $a$, the stability class changes from Class 1 (instabilities are possible even for dense but uncongested traffic), to Class 2 (only congested traffic can become unstable) to Class 3 (no instability anywhere). Notice that in some other microscopic or macroscopic models, the agility corresponds to the inverse of the speed adaptation time $\tau$.

**Time gap.** The capacity of traffic flow (maximum flow) increases with decreasing time gap $T$ in car-following mode. Simultaneously, reducing $T$ also reduces the time margin of the drivers to react to changing situations, so traffic flow generally becomes more unstable. Remarkably, this does not influence the transition between Classes 1 and 2 which essentially is determined by the acceleration $a$.

**Anticipation.** By scaling the IDM appropriately (cf. Problem 16.8), one can show that the dynamics, and particularly the stability class, remains unchanged when simultaneously

- increasing the anticipation by decreasing the comfortable deceleration $b$ by a factor $f_b < 1$,
- decreasing the agility by reducing $a$ by a factor of $f_b$,
- increasing the time gap $T$ by a factor $1/\sqrt{f_b}$,
- decreasing the desired speed $v_0$ by a factor of $\sqrt{f_b}$, and
- leaving $s_0$ unchanged.

As expected, this means that a decrease of agility is compensated for by increasing the responsiveness. Moreover, exact compensation is reached if the ratio $a/b$ remains unchanged. Remarkably, the restabilization properties (subclasses 1a, 2a vs. 1b, 2b, 3) do not depend on the anticipation at all. To see this, we notice that the IDM corresponds to stability subclass a (1a, or 2a) if and only if

$$a < \frac{s_0}{T^2} \tag{16.140}$$

(and to one of the classes 1b, 2b, or 3, otherwise), and that this distinction criterion does not contain $b$ as influencing factor.

## 16.9 Short-Wavelength Collective Instabilities

When discussing the collective instabilities discussed in the Sections 16.4 – 16.8, we have assumed long-wavelength instabilities, i.e., the first instability is always one with respect to waves whose wave number tends to zero and the associated wavelength tends to infinity. Mathematically, it can be shown that this is true for all time-continuous car-following models without explicit reaction time formulated by coupled ordinary differential equations, and for all macroscopic local second-order models, i.e., formulated by partial differential equations for the density and speed fields.

However, many popular models do not belong to one of these mathematical classes. Examples include iterated coupled maps, time-continuous car-following models with reaction times, or nonlocal macroscopic models. Figure 16.18 shows the simultaneous occurrence of long-wavelength and short-wavelength collective instabilities for the IDM with an explicit delay by a reaction time $T_r = 1.2\,\mathrm{s}$ (but no other human driving aspect of Chapter 13 added). We observe that the short-wavelength instabilities propagate faster than the long-wavelength instabilities, so that they "collide" into each other. However, neither these collisions nor the propagation velocity of the short-wavelength modes (about $-30\,\mathrm{km/h}$) are realistic. We conclude that short-wavelength instabilities should not occur for realistic model-parameter combinations.

Finally, we emphasize that, for realistic parameters, the first instability of models including potential short-wavelength instabilities is generally of the long-wavelength type. Since it is not possible to test or prove this mathematically, simulations are necessary to check this property.

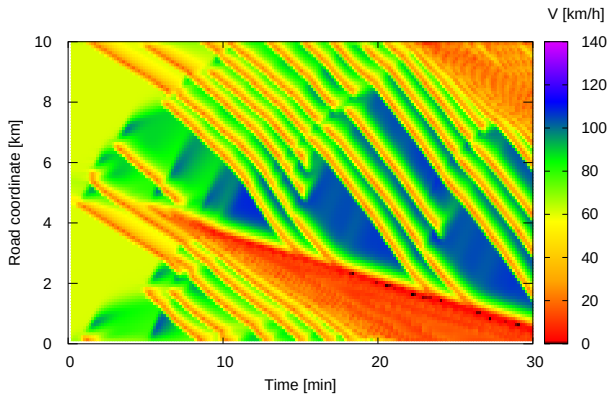


**Fig. 16.18** Simultaneous appearance of long-wave and short-wave instabilities in the IDM with reaction time $T_r = 1.2\,\mathrm{s}$ for initially steady-state traffic at $\rho_e = 30\,\mathrm{km}^{-1}$ with a small perturbation. The IDM parameters are $v_0 = 120\,\mathrm{km/h}$, $T = 1.5\,\mathrm{s}$, $a = 1\,\mathrm{m/s^2}$, $b = 1.3\,\mathrm{m/s^2}$, $s_0 = 2\,\mathrm{m}$, and the vehicle length $l = 5\,\mathrm{m}$.

## Problems

### 16.1. Characterizing the Type of Instability

Consider the dynamics schematically shown in Fig. 16.1. Is it a local or string instability? If the latter is true: Is the instability absolute or convective, linear or nonlinear?

### 16.2. Propagation Velocity of Traffic Waves in Microscopic Models

Show that the long-wavelength limit (16.57) of the microscopic propagation velocity corresponds macroscopically to the gradient $\tilde{c} = Q_e'(\rho)$ of the fundamental diagram. To this purpose, scale the microscopic propagation velocity to dimensional physical units, and transform it from the system comoving with the vehicles to a road-based fixed system. Finally, express the microscopic quantities in terms of macroscopic variables.

### 16.3. Instability Limits for the Full Velocity Difference Model

Consider the acceleration equation (11.25) of the FVDM with a speed adaptation time $\tau = 5\,\mathrm{s}$ and a triangular fundamental diagram given by the microscopic relation $v_e(s) = \min(s/T, v_0)$, $T = 1\,\mathrm{s}$. What is the minimum value of the sensitivity $\gamma$ to speed differences to ensure (i) local stability, (ii) no (damped) oscillations when a single vehicle follows a leader with at a given speed profile, (iii) string stability?

### 16.4. Stability Properties of the Optimal Velocity Model Compared to Payne's Model

Consider the OVM and Payne's model for general, but equivalent, optimal-velocity (steady-state) relations and show that the conditions for collective (string or flow)

stability of both models are equivalent. *Hint:* Find the macroscopic equivalent $V_e(\rho)$ of the microscopic steady-state relation $v_e(s)$, derive a relation between the derivatives $v_e'(s)$ and $V_e'(\rho)$, express the OVM stability condition in macroscopic terms, and compare it with the condition (16.125) for Payne's model.

**16.5. OVM with "Pushing" from Behind**

Consider the model (16.93) and show that, for $\lambda = 0.5$, the OV gradient $V'(s)$ at neutral stability (boundary between string stability and instability) becomes six times as large as that for the normal OVM greatly increasing stability. Now consider the triangular fundamental relation $v_{\text{opt}}(s) = \min((s - s_0)/T, v_0)$ and show that this model still leads to collisions for any platoon of $\geq 3$ vehicles if the leader stops and $\lambda > (1 + v_0 T/s_0)^{-1}$ which typically is the case already for values as small as $\lambda = 0.05$.

**16.6. Flow Instability in Payne's Model and in the Kerner-Konhäuser Model**

Consider Payne's model and the Kerner-Konhäuser model with a triangular fundamental diagram $Q_e(\rho) = \min(V_0\rho, 1/T(1 - l_{\text{eff}}\rho))$ and the parameters $l_{\text{eff}} = 6\,\text{m}$, $V_0 = 144\,\text{km/h}$ and $T = 1.1\,\text{s}$. (i) Show that Payne's model is unconditionally linearly stable if $\tau < T/2$, and flow unstable in the congested regions, otherwise. (ii) For the Kerner-Konhäuser model, determine the parameter $c_0^2$ such that this model is string unstable in the density range $\rho \in [20\,\text{vehicles/km}, 50\,\text{vehicles/km}]$.

**16.7. Flow Instability of the GKT Model**

Consider sufficiently congested traffic such that the speed variation coefficient $\sigma_V/v = \sqrt{\alpha(\rho_{\max})}$ can be considered as constant. Show that, in the local limit of zero anticipation distance ($\gamma = s_a = 0$), the GKT model is unconditionally unstable in this situation for all reasonable parameter values. Furthermore, show that anticipation stabilizes traffic flow by deriving the approximate Condition (16.131) for densities near the maximum density.

**16.8. IDM Stability Class Diagram for Other Parameter Values**

Calculate the stability class diagram as in Fig. 16.17(c) but assume a comfortable deceleration $b^* = 2\,\text{m/s}^2$ instead of $b = 1.5\,\text{m/s}^2$, and $v_0^* = 139\,\text{km/h}$ instead of 120 km/h. Is it possible to use this diagram without recalculating anything, just by scaling the axes appropriately?

*Hint:* Formulate the IDM model equations in scaled units by scaling time in multiples of the unit time $\sqrt{s_0/b}$ (of the order of 1 s), and space in multiples of the minimum gap $s_0$. Show that the scaled model depends on only three dimensionless parameters

$$\tilde{v}_0 = \frac{v_0}{\sqrt{bs_0}}, \quad \tilde{f} = \frac{a}{b}, \quad \tilde{T} = T\sqrt{\frac{b}{s_0}},$$

and on the scaled vehicle length $\tilde{l}_{\text{veh}} = l_{\text{veh}}/s_0$. Now use the fact that all dynamic properties (and, in particular, the stability class) depend on the scaled parameters and the scaled vehicle length, only. Find appropriate scalings for the two axes of the class diagram.

**16.9. Fundamental Diagram with Hysteresis**
Given are the following characteristics of highway traffic flow: Average vehicle length $l = 4.67\,\mathrm{m}$, average gap in car-following situations $s = s_0 + vT$ where $s_0 = 2\,\mathrm{m}$ and $T = 1.6\,\mathrm{s}$, average free-flow speed 120 km/h, and critical density at traffic breakdown (free $\rightarrow$ congested) $\rho_c = 20\,\mathrm{veh/km}$ per lane. From these data it follows that two values of traffic flow are possible in a certain density range.

1. At which traffic flow does a breakdown occur, i.e., where does the free branch of the fundamental diagram end?
2. Determine the "congested branch" of the fundamental diagram and the density at which it intersects with the free branch. For which density range can free and congested traffic exist simultaneously?
3. The outflowing region of congestions is characterized by the intersection $(\rho_{\mathrm{out}}, Q_{\mathrm{out}})$ of the free and congested branches of the fundamental diagram. Indicate $\rho_{\mathrm{out}}$ and calculate $Q_{\mathrm{out}}$. Also calculate the *capacity drop* as the difference between the maximum flow of free traffic and $Q_{\mathrm{out}}$
4. Make a graph of the fundamental diagram showing its mirrored $\lambda$-shape.

## Further Reading


- Peppard, L.: String stability of relative-motion PID vehicle control systems. IEEE Transactions on Automatic Control **19** (1974) 579–581
- Montanino, M., Punzo, V.: On string stability of a mixed and heterogeneous traffic flow: A unifying modelling framework Transportation Research Part B: Methodological **144** (2021) 133–154
- Zhang, X., Sun, J., Zheng, Z., Sun, J.: On the string stability of neural network-based car-following models: A generic analysis framework. Transportation Research Part C: Emerging Technologies **160** (2024) 104525.
- Huerre, P., Monkewitz, P.: Local and global instabilities in spatially developing flows. Annual Review of Fluid Mechanics **22** (1990) 473–537
- Ngoduy, D.: Linear stability of a generalized multi-anticipative car following model with time delays. Communications in Nonlinear Science and Numerical Simulation **22** (2015) 420–426.
- Treiber, M., Kesting, A.: Evidence of convective instability in congested traffic flow: A systematic empirical and theoretical investigation. Transportation Research Part B: Methodological **45** (2011) 1362–1377
- Wilson, R.: Mechanisms for spatio-temporal pattern formation in highway traffic models. Philosophical Transactions of the Royal Society A: Mathematical, Physical, Engineering Sciences **366** (2008) 2017–2032
- Treiber, M., Kesting, A.: Validation of traffic flow models with respect to the spatiotemporal evolution of congested traffic patterns. Transportation Research Part C: Emerging Technologies **21** (2012) 31–41

# Part III
# Applications of Traffic Flow Theory

# Solutions to the Problems

## Problems of Chapter 2

### 2.1 Edie's Definitions

1. The depicted spatiotemporal area is $A = 3,200\,\mathrm{m\,s}$. The total time of the trajectories spent inside $A$ is given by

$$t^{\mathrm{tot}} = 40\,\mathrm{s} + 4\,\mathrm{s}\sum_{j=1}^{10} j = 40 + 4 \cdot 55\,\mathrm{s} = 260\,\mathrm{s}.$$

The total distance covered by the trajectories with parts inside $A$ are given by

$$x^{\mathrm{tot}} = 35\,\mathrm{m} + 5\,\mathrm{m}\sum_{j=1}^{10} j = 310\,\mathrm{m}.$$

Hence, Edie's density, flow, and average speed are given by

$$\rho_{\mathrm{Edie}} = \frac{t^{\mathrm{tot}}}{A} = 81.3\,\mathrm{veh/km}, \quad Q_{\mathrm{Edie}} = \frac{x^{\mathrm{tot}}}{A} = 0.0969\,\mathrm{veh/s},$$
$$V^{\mathrm{Edie}} = \frac{Q_{\mathrm{Edie}}}{\rho_{\mathrm{Edie}}} = 1.19\,\mathrm{m/s}.$$

2. Macroscopic flow at $x = 40\,\mathrm{m}$ inside $A$ (counting the vehicle passing at $t = 0$ but not the one stopping at $x = 40\,\mathrm{m}$):

$$Q = \frac{7\,\mathrm{veh}}{40\,\mathrm{s}} = 0.175\,\mathrm{veh/s}\,.$$

The time mean speed $V$ in $A$ is near the maximum speed of 10 m/s since the stopped vehicle did not yet pass, i.e., it does not count. Hence, the density estimated by temporal quantities is given by

$$\hat{\rho} = \frac{Q}{V} = 17.5\,\text{veh/km},$$

which is less than 25% of Edie's density.

3. At $t = 20\,\text{s}$, $n = 6$ vehicles are inside $A$, hence $\rho = 75\,\text{veh/km}$, near Edie's density. The space-average speed is given by

$$V_s \approx \frac{2 \cdot 10\,\text{m/s}}{n} = 3.33\,\text{m/s}.$$

4. The situation is not stationary, so the condition for $V_s = V^{\text{H}}$ is not satisfied. In fact, the temporal harmonic mean $V^{\text{H}}$ at $x = 40\,\text{m}$ is near 10 m/s without counting the vehicle stopping at $x = 40\,\text{m}$ (as in part 2), and undefined when including it.

## Problems of Chapter 3

### 3.1 Analysis of Empirical Trajectory Data

*1. Flow, density, and speed.* Using the spatiotemporal region $[10\,\text{s}, 30\,\text{s}] \times [20\,\text{m}, 80\,\text{m}]$ suggested for a representative free-flow situation, we obtain by trajectory counting:

$$Q_{\text{free}} = \frac{11\,\text{veh}}{20\,\text{s}} = 1,980\,\text{veh/h}, \quad \rho_{\text{free}} = \frac{3\,\text{veh}}{60\,\text{m}} = 60\,\text{veh/km}.$$

The speed can be deduced either from the gradient of the trajectories or from the hydrodynamic relation $Q/\rho$:

$$V_{\text{free}}^{\text{gradient}} = \frac{60\,\text{m}}{5\,\text{s}} = 43.2\,\text{km/h}, \quad V_{\text{free}}^{\text{hyd}} = \frac{Q_{\text{free}}}{\rho_{\text{free}}} = 39.6\,\text{km/h}.$$

This discrepancy is tolerable in view of the reading accuracy (one may also count 12 vehicles in 20 s, yielding $Q = 2,160\,\text{veh/h}$ and thus $\rho = 43.2\,\text{km/h}$). For congested traffic, we use, again, the suggested spatiotemporal region $[50\,\text{s}, 60\,\text{s}] \times [40\,\text{m}, 100\,\text{m}]$ and obtain analogously

$$Q_{\text{cong}} = \frac{2\,\text{veh}}{10\,\text{s}} = 720\,\text{veh/h}, \quad \rho_{\text{cong}} = \frac{6\,\text{veh}}{60\,\text{m}} = 1,000\,\text{veh/km},$$
$$V_{\text{cong}}^{\text{hyd}} = \frac{Q_{\text{cong}}}{\rho_{\text{cong}}} = 7.2\,\text{km/h}.$$

*2. Propagation velocity.* The stop-and-go wave can be identified by the spatiotemporal region with nearly horizontal trajectories. First, we observe that, in the diagram, the gradient of the (essentially parallel) upstream and downstream wave boundaries are negative, i.e., the wave propagates *against* the direction of traffic. To determine the propagation velocity, we estimate from the diagram

$$c \approx -\frac{140\,\mathrm{m}}{(60-33)\,\mathrm{s}} = -5.2\,\mathrm{m/s} = -19\,\mathrm{km/h}.$$

*3. Travel time increase.* Without being obstructed by the traffic wave, the considered vehicle entering at $t = 50\,\mathrm{s}$ into the investigated road section ($x = 0$) would leave the section ($x = L = 200\,\mathrm{m}$) after about 16 s. This can be deduced either by linearly extrapolating the first seconds of the trajectory, or by the quotient $L/V_{\mathrm{free}}$. The *actual* vehicle leaves the investigated region at $t = 86\,\mathrm{s}$. Thus, the delay imposed by this traffic wave on the vehicle is 20 s.

*4. Lane-changing rate.* By counting all lane changes entering and leaving the considered lane in the spatiotemporal region $[0\,\mathrm{s}, 80\,\mathrm{s}] \times [0\,\mathrm{m}, 140\,\mathrm{m}]$, i.e., trajectories beginning or ending inside this region[1], we obtain the lane-changing rate by

$$r \approx \frac{6\ \text{changes}}{80\,\mathrm{s}\ 140\,\mathrm{m}} = 0.00054\,\frac{\text{changes}}{\mathrm{m\ s}} \approx 1{,}900\,\frac{\text{changes}}{\mathrm{km\ h}}.$$

### 3.2 Trajectory Data of "Obstructed" Traffic Flow

1. The trajectory data shows a queue at a traffic light. The horizontal bar marks the position of the traffic light and the duration of the red light phase.
2. Flow $Q_{\mathrm{in}}$ = 5 trajectories per 20 s = 0.25 veh/s = 900 veh/h.
3. Following the trajectory which starts at $x = -80\,\mathrm{m}$, $t = -16\,\mathrm{s}$ and which ends at $(x,t) = (80\,\mathrm{m}, 0\,\mathrm{s})$, we get the speed

$$v_{\mathrm{in}} = \frac{160\,\mathrm{m}}{16\,\mathrm{s}} = 10\,\mathrm{m/s} = 36\,\mathrm{km/h}.$$

   The density is read off the diagram as one trajectory per 40 m or is calculated using $\rho = Q/v$. Either way yields $\rho = 25\,\mathrm{veh/km}$.
4. Density in the congested area: 8 horizontal trajectories per 40 m $\Rightarrow \rho_{\mathrm{jam}} = 200\,\mathrm{veh/km}$.
5. Outflow after the red light turns green: The best way is to count the number of lines within a 20 s interval above the blue dots marking the end of the acceleration phase, giving 10 lines per 20 s and thus $Q_{\mathrm{out}} = 0.5\,\mathrm{veh/s} = 1{,}800\,\mathrm{veh/h}$. The speed is the same as in free traffic (the trajectories are parallel to those further upstream), i.e., $V = 36\,\mathrm{km/h}$. The density is obtained again by counting trajectories (two lines per 40 m) or via the hydrodynamic relation, yielding $\rho = 50\,\mathrm{veh/km}$.
6. Propagation velocities of the fronts can be read off the chart as the gradient of the front lines (marked by the dots) or using the continuity equation (cf. Chapter 8):

[1] Outside this region, a positive bias is unavoidable because real lane changes cannot be distinguished from the begin/end of recorded trajectories.

$$\text{free} \to \text{congested:} \quad v_g^{\text{up}} = \frac{\Delta Q}{\Delta \rho} = \frac{-900\,\text{veh/h}}{175\,\text{veh/km}} = -5.17\,\text{km/h},$$
$$\text{congested} \to \text{free:} \quad v_g^{\text{down}} = \frac{\Delta Q}{\Delta \rho} = \frac{1,800\,\text{veh/h}}{-150\,\text{veh/km}} = -12\,\text{km/h}.$$

7. Without the red light the vehicle entering at $x = -80\,\text{m}$ and $t = 20\,\text{s}$ would have reached the "end" (upper border) of the diagram ($x = 100\,\text{m}$) at $t_{\text{end}} = 38\,\text{s}$. De facto, it arrives at $x = 100\,\text{m}$ at time $t = 69\,\text{s}$, thus delayed by 31 s.
8. The braking distance is $s_b = 25\,\text{m}$, while the distance covered during the acceleration phase is $s_a = 50\,\text{m}$. Thus

$$b = \frac{v^2}{2s_b} = 2\,\text{m/s}^2, \quad a = \frac{v^2}{2s_a} = 1\,\text{m/s}^2.$$

Alternatively, we can calculate the braking distance using the definition of the acceleration and the duration $\Delta t$ of the acceleration/deceleration:

$$b = -\frac{\Delta v}{\Delta t} = -\frac{-10\,\text{m/s}}{10\,\text{s}} = 2\,\text{m/s}^2, \quad a = \frac{\Delta v}{\Delta t} = \frac{10\,\text{m/s}}{10\,\text{s}} = 1\,\text{m/s}^2.$$

### 3.3 Trajectories of City Traffic

1. Signalized intersections are expected to be a little bit downstream of the vehicles stopping without a leader, i.e., at about $x_1 = 50\,\text{m}$ and $x_2 = 250\,\text{m}$ (and possibly at $x_3 = 355\,\text{m}$). The red phase starts when the first leader about to stop behind the traffic light *begins* to decelerate and ends a little bit before the first vehicle starts to accelerate (reaction time), i.e., 317 s - 350 s at $x_1$ and 317 s - 378 s at $x_2$ (and 310 s - 335 s at $x_3$ but the red phase may have started earlier)
2. Beginning trajectories: lane changes 3-2 and 1-2; ending trajectories: lane changes 2-3 and 2-1
3. Wave velocity (sequence of the first eight starting vehicles between 380 s and 390 s): $w = \frac{-60\,\text{m}}{10\,\text{s}} = -21.6\,\text{km/h}$.

### 3.4 Bicycle Trajectory Data

1. Shown is a moving traffic wave of stopped bicycles that is neither growing nor shrinking, so outflow $\approx$ inflow. Theoretically, the moving cyclists could be in a maximum-flow state at the boundary between free and congested traffic. However, in view of their close distance of about 4 m, this region is congested as well.
2. Inside the "stop" region: $\rho_{\max} = 24/40\,\text{m} = 0.6\,/\text{m}$, $Q = 0$, $V = 0$; in the regions outside the jam, e.g., at $t = 190\,\text{s}$: $\rho = 13/40\,\text{m} = 0.325\,/\text{m}$, $Q = 13/40\,\text{s} = 0.325\,/\text{s}$, $V = Q/\rho = 1\,\text{m/s}$.
3. Region $A = 20\,\text{s} \cdot 10\,\text{m} = 200\,\text{m s}$, $t^{\text{tot}} = 6 \cdot 20\,\text{s}$, so $\rho_{\text{Edie}} = 120\,\text{s}/200\,\text{m s} = 0.6\,/\text{m}$.
4. $w = -40\,\text{m}/27\,\text{s} \approx -1.5\,\text{m/s}$.
5. Time gap $T = (\Delta x - l_{\text{eff}})/V = (1/\rho - 1/\rho_{\max})/V = (3.08\,\text{m} - 1.67\,\text{m})/1\,\text{m/s} = 1.41\,\text{s}$.

## Problems of Chapter 4

### 4.1 Map Matching

According to the problem statement, the vehicle can only be on road 1 with lateral position $y_1 = 0$, or on road 2 at $y_2 = 30\,\text{m}$. Since the GNSS position $\hat{Y}$ is assumed to be unbiased and Gaussian distributed with a standard deviation $\sigma = 10\,\text{m}$, we have the two conditional probability densities[2]

$$f_1(\hat{y}) = \frac{1}{\sigma}\phi\left(\frac{\hat{y}}{\sigma}\right), \quad f_2(\hat{y}) = \frac{1}{\sigma}\phi\left(\frac{\hat{y}-y_2}{\sigma}\right)$$

with the density of the standard normal distribution $\phi(z) \propto \exp(-z^2/2)$. Thus, the conditional probabilities for the measuring event

$$\text{E: ``the GNSS position } \hat{Y} \text{ is in the range } [\hat{y}-\Delta y/2, \hat{y}+\Delta y/2]\text{''}$$

provided the true position is on road $r_1$ ($y = y_1$) or on $r_2$ ($y = y_2$), are given, for sufficiently small $\Delta y$, by

$$P(E|r_1) = f_1(\hat{y})\Delta y, \quad P(E|r_2) = f_2(\hat{y})\Delta y.$$

The small interval $\Delta y$ is only introduced to avoid a "divided by zero" situation.

1. The desired probability $P(r_1|E) = P(y = y_1|E)$ can be calculated using Bayes' Theorem:

$$\begin{aligned} P(r_1|E) &= \frac{P(E|r_1)P(r_1)}{P(E)} \\ &= \frac{P(E|r_1)P(r_1)}{P(E|r_1)P(r_1)+P(E|r_2)P(r_2)} \\ &= \frac{f_1(\hat{y})P(r_1)}{f_1(\hat{y})P(r_1)+f_2(\hat{y})P(r_2)} \\ &= \frac{\exp(-2)}{\exp(-2)+\exp(-1)} = 18\%, \end{aligned}$$

   where we have used the non-informative priors $P(r_1) = P(r_2) = 1/2$. We conclude that, without any prior information, the best map matching is to road 2. It will be correct in 82% of all cases.
2. The prior information that the density on road 1 is nine times higher than that on road 2 means that, when blindly picking a vehicle, it is on road 1 in nine out of ten cases, $P(r_1) = 0.9$ and $P(r_2) = 1 - P(r_1) = 0.1$. Using the flow instead of the density for estimating the priors would give a bias towards the road with the faster speed (presumably road 1). Updating the priors in the second to last

[2] As per convention, we denote random variables in uppercase letters ($\hat{Y}$) and realizations (measurements) in lowercase ($\hat{y}$).

line of problem part 1 gives

$$P(r_1|E) = \frac{0.9 f_1(\hat{y})}{0.9 f_1(\hat{y}) + 0.1 f_2(\hat{y})} = \frac{0.9 \exp(-2)}{0.9 \exp(-2) + 0.1 \exp(-1)} = 67\%.$$

With this prior information, there is now a two-thirds chance that mapping onto road 1 is correct, although it is more distant to the GNSS position than road 2.

3. The best clues can be obtained from the fact of continuity: a car does not jump. So, past position with nonambiguous map matching, or the position where the device was switched off after the previous trip, are good bets. By using the Hidden Markov approach, Sect. 4.5 transforms these clues into a formal model.

### 4.2 Floating-Car Data

GPS data provide space-time data points and anonymized IDs of the equipped vehicles. We can obtain their *trajectories* by connecting the data points in a space-time diagram (via a map-matching process). From the trajectories, we can directly obtain the travel time and infer the instantaneous speed by taking the gradients. Low speeds on a highway (e.g., 30 km/h) usually indicate a *traffic jam*. Since the data provide spatiotemporal positions of the vehicles, we can deduce the location of congested zones, including their upstream and downstream boundaries. With a sampling rate of two per minute, the vehicle can cover 1 km and more between a data point in free traffic. Fortunately, in congestions, the points are naturally closer and jam fronts are resolved at a high spatial resolution whenever an equipped vehicle "floats" through. The temporal resolution depends on the penetration level of probe vehicles. GNSS measurements are only accurate to the order of 10 m and careful map-matching/error checking is necessary to exclude, for example, stopped vehicles on the shoulder or vehicles on a parallel road (see Problem 4.1). Therefore, GNSS data do *not* reveal lane information, nor information on *lane changes*. If the percentage of probe vehicles providing positional data is low, variable, and unknown, we can *not* deduce extensive quantities like traffic density and flow from this type of data. To wrap it up: (1): yes, (2): no, (3): no, (4): no, (5): yes, (6): yes, (7): yes.

### 4.3 Relative Errors of Probe-Based Flow Estimations

1. For a Poisson distributed variable, the expectation value and the variance are given by $\mu$, so that the relative error is $\delta n = 1/\sqrt{\mu} = 1/\sqrt{n}$, and, together with Eq. (4.1), $\delta n = 1/\sqrt{q\Delta t}$. With the partial volumes $q = \theta Q$ the relative error is given by $\delta n = 1/\sqrt{\theta Q \Delta t}$. On the one hand it is attractive to report flow estimates within short aggregation intervals. On the other hand, the relative errors become smaller with longer aggregation intervals as more probe vehicles are observed. FCD-based flow estimates work best for high penetration rates and high traffic flows, e.g., on multi-lane highways and/or at times of heavy traffic.
2. With $\theta = 0.1$ and $\Delta t = 0.25$ h, we obtain $\delta n \approx 14\%$ for $Q = 2{,}000$ /h, $\delta n \approx 45\%$ for 200 /h, and $\delta n \approx 8\%$ for 6,000 /h.

3. With $\Delta t = 1/(\theta Q \delta n^2)$ and the values from above the aggregation interval needed for a relative error of 10% is 30 min. A doubling of the penetration level $\theta$ halves the value.

### 4.4 Traffic State Estimation Using Floating-Car Data

1. With a penetration level $\theta = 1\%$ of floating cars, the partial density over all four lanes as a function of the one-lane density $\rho$ is given by

$$\rho_{\mathrm{FC}}^{\mathrm{tot}} = 4\theta\rho,$$

   so $\rho_{\mathrm{FC}}^{\mathrm{tot}} = 0.8\,\mathrm{veh/km}$ for the uncongested, and $\rho_{\mathrm{FC}}^{\mathrm{tot}} = 3\,\mathrm{veh/km}$ for the congested regions, respectively.
2. On average, there are $4\,\mathrm{km} \cdot 3\,\mathrm{veh/km} = 12$ vehicles inside the congestion.
3. If the traffic jam fronts are stationary, the flow through the jam fronts free $\rightarrow$ congested and congested $\rightarrow$ free is equal to $Q^{\mathrm{tot}} = 6,000\,\mathrm{veh/h}$. If, furthermore, the average speed of the floating cars is the same as that of all vehicles, the partial flow is given by $pQ^{\mathrm{tot}} = 60\,\mathrm{veh/h}$.[3] So, we have an average rate of one update of the jam-front positions and the segment travel time per minute. We conclude that even for a very small penetration level of 1%, we have a sufficient update rate.

### 4.5 Analysis of Extended Floating-Car Data

1. Here, the episode $t > 225\,\mathrm{s}$ is most revealing since the leader already shows oscillations. While the speed amplitude (from the local minimum to the local maximum) of the leader is on average about 3 m/s, that of the follower increases to about 5 m/s for the last follower. Hence, there is evidence for flow instabilities (more precisely, the following behavior is locally stable but string unstable as described in more detail in Sections 16.3 and 16.4).
2. The maxima and minima of the speed curves of the leader and the last follower are shifted by about 5 s. Thus, the average delay in an individual follower's response is of the order of 1.5 s to 2 s.[4]
3. Between $t \approx 214\,\mathrm{s}$ and 218 s, the speed drops from about $11\,\mathrm{m/s}$ to 1 m/s corresponding to a maximum deceleration of $b = 2.5\,\mathrm{m/s^2}$. The maximum acceleration (between $t \approx 222\,\mathrm{s}$ and 224 s) has the same order.
4. The last driver (vehicle 4) follows most closely with time gaps $s_i/v_i$ strongly varying but generally below 1 s. The shortest minimum gap (about 1 m), however, is observed for the driver of vehicle 3.

[3] If, for example, the average floating car speeds are lower, the partial flow would be lower as well by virtue of Edie's relation (2.8).

[4] This is not necessarily due to reaction times. In Chapters 11 and 12, we will see that even models with zero reaction times display such a delay.

# Problems of Chapter 5

## 5.1 Data Aggregation at a Cross-Section

*1. Flow and speed.* With an aggregation interval $\Delta t = 30\,\mathrm{s}$ and $n_1 = 6$, $n_2 = 4$ measured vehicles on lanes 1 and 2, respectively, the flow and time mean speed on the two lanes are

$$Q_1 = \frac{n_1}{\Delta t} = 0.2\,\mathrm{veh/s} = 720\,\mathrm{veh/h}, \quad Q_2 = \frac{n_2}{\Delta t} = 0.133\,\mathrm{veh/s} = 480\,\mathrm{veh/h},$$
$$V_1 = \frac{1}{n_1}\sum_i v_{1i} = 25.8\,\mathrm{m/s}, \qquad V_2 = \frac{1}{n_2}\sum_i v_{2i} = 34.0\,\mathrm{m/s}.$$

*2. Density.* When assuming zero correlations between speeds and time headways, the covariance $\mathrm{Cov}(v_i, \Delta t_i) = 0$. With Eq. (5.23), this means that calculating the true (spatial) densities by $Q/V$ using the arithmetic (time) mean speed gives no bias:

$$\rho_1 = \frac{Q_1}{V_1} = 7.74\,\mathrm{veh/km}, \quad \rho_2 = \frac{Q_2}{V_2} = 3.92\,\mathrm{veh/km}\,.$$

*3. Both lanes combined.* Density and flow are *extensive quantities* increasing with the number of vehicles. Therefore, building the total quantities by simple summation over the lanes makes sense:

$$\rho^{\mathrm{tot}} = \rho_1 + \rho_2 = 11.66\,\mathrm{veh/km}, \quad Q^{\mathrm{tot}} = Q_1 + Q_2 = 1,200\,\mathrm{veh/h}\,.$$

Since speed is an *intensive* quantity (it does not increase with the vehicle number), summation over lanes makes no sense. Instead, we define the effective aggregated speed by requiring the hydrodynamic relation to be valid for total flow and total density as well:

$$V = \frac{Q^{\mathrm{tot}}}{\rho^{\mathrm{tot}}} = \frac{\rho_1 V_1 + \rho_2 V_2}{\rho^{\mathrm{tot}}} = \frac{Q^{\mathrm{tot}}}{Q_1/V_1 + Q_2/V_2} = 28.5\,\mathrm{m/s} = 102.9\,\mathrm{km/h}.$$

By its derivation from the hydrodynamic relation, this effective speed is the space mean speed rather than the time mean speed measured directly by the detectors. We notice that the effective speed is simultaneously the *arithmetic mean* weighted with the densities, and the *harmonic mean* weighted with the flows. However, the weighting with the densities requires that the density estimates itself are known without bias. This is the case here but not generally. Since flows can always be estimated without systematic errors from stationary detectors, the harmonic mean weighted with the flows is preferable.

*4. Fraction of trucks.* Two out of six (33%) are in the right lane, none in the left, two out of ten (20%) total. Notice again that the given percentages are the fraction of trucks *passing* a fixed location (*time mean*). In the same situation, we expect the fraction of trucks observed by a "snapshot" of a road section at a fixed time (*space mean*) to be higher, at least if trucks are generally slower than cars.

### 5.2 Determining Macroscopic Quantities from Single-Vehicle Data

The distance headway $\Delta x_i = 60\,\mathrm{m}$ is constant on both lanes. All vehicles are of the same length $l = 5\,\mathrm{m}$ and all vehicles on a given lane $l$ (left) or $r$ (right) have the same speed $v_i^{\mathrm{l}} = 144\,\mathrm{km/h} = 40\,\mathrm{m/s}$ and $v_i^{\mathrm{r}} = 72\,\mathrm{km/h} = 20\,\mathrm{m/s}$, respectively.

*1. Time gap / headway.* The headways $\Delta t_i = \Delta x_i / v_i$ are

$$\Delta t_i^{\mathrm{l}} = \frac{60\,\mathrm{m}}{40\,\mathrm{m/s}} = 1.5\,\mathrm{s}, \quad \Delta t_i^{\mathrm{r}} = \frac{60\,\mathrm{m}}{20\,\mathrm{m/s}} = 3.0\,\mathrm{s}.$$

The time gaps $T_i$ are equal to the headway minus the time needed to cover a distance equal to the length of the leading vehicle, $T_i = \Delta t_i - \frac{l_{i-1}}{v_{i-1}}$. Since all vehicle lengths are equal, this results in

$$T_i^{\mathrm{l}} = \frac{60\,\mathrm{m} - 5\,\mathrm{m}}{40\,\mathrm{m/s}} = 1.375\,\mathrm{s}, \quad T_i^{\mathrm{r}} = \frac{60\,\mathrm{m} - 5\,\mathrm{m}}{20\,\mathrm{m/s}} = 2.75\,\mathrm{s}.$$

*2. Macroscopic quantities.* We assume an aggregation time interval $\Delta t = 60\,\mathrm{s}$. However, due to the stationary situation considered here, any other aggregation interval will lead to the same results. Directly from the definitions of flow, occupancy, and time-mean speed, we obtain for each lane

$$Q^{\mathrm{l}} = \frac{1}{\Delta t_i^{\mathrm{l}}} = \frac{1}{1.5\,\mathrm{s}} = 2{,}400\,\mathrm{veh/h}, \qquad Q^{\mathrm{r}} = \frac{1}{\Delta t_i^{\mathrm{r}}} = \frac{1}{3\,\mathrm{s}} = 1{,}200\,\mathrm{veh/h}.$$

$$\mathscr{O}^{\mathrm{l}} = \frac{0.125}{1.5} = 0.083 = 8.3\%, \qquad \mathscr{O}^{\mathrm{r}} = \frac{0.25}{3.0} = 0.083 = 8.3\%.$$

$$V^{\mathrm{l}} = 144\,\mathrm{km/h}, \qquad V^{\mathrm{r}} = 72\,\mathrm{km/h}.$$

Due to the homogeneous traffic situation, the arithmetic and harmonic time-mean speed are the same and directly given by the speed of the individual vehicles.

*Totals and averages of both lanes.* As already discussed in Problem 5.1 summing over the lanes to obtain a total quantity makes only sense for extensive quantities ($Q$, $\rho$) but not for the intensive ones ($V$, $\mathscr{O}$).

Flow:

$$Q_{\mathrm{tot}} = \frac{\Delta N}{\Delta t} = \frac{\Delta N^{\mathrm{l}} + \Delta N^{\mathrm{r}}}{\Delta t} = 3{,}600\,\mathrm{veh/h}, \quad Q = \frac{Q_{\mathrm{tot}}}{2} = 1{,}800\,\mathrm{veh/h}.$$

Occupancy:

$$\mathscr{O} = \mathscr{O}^{\mathrm{l}} = \mathscr{O}^{\mathrm{r}} = 0.083.$$

Arithmetic time mean speed:

$$V = \frac{1}{\Delta N} \sum_i v_i = \frac{40 \cdot 40\,\mathrm{m/s} + 20 \cdot 20\,\mathrm{m/s}}{60} = 120\,\mathrm{km/h}.$$

Harmonic time mean speed:

$$V_{\mathrm{H}} = \frac{\Delta N}{\sum 1/v_i} = \frac{60}{\frac{40}{40\,\mathrm{m/s}} + \frac{20}{20\,\mathrm{m/s}}} = 108\,\mathrm{km/h}.$$

We observe that the arithmetic mean is larger than the harmonic mean.

*3. Which mean?* In traffic flow, there are four sensible ways to average, consisting of the four combinations of (i) one of two physical ways (time mean and space mean), (ii) one of two mathematical ways (arithmetic and harmonic).

- *Time mean* means averaging at a fixed location over some time interval as done by stationary detectors.
- *Space mean* means averaging at a fixed time over some space interval (road section), e.g., when making a snapshot of the traffic flow.

For the *space mean*, we have (cf. the previous problem)

$$V = \frac{\rho_1 V_1 + \rho_2 V_2}{\rho^{\mathrm{tot}}} = \frac{Q^{\mathrm{tot}}}{Q_1/V_1 + Q_2/V_2}$$

while, for the time mean, we simply have

$$V = \frac{Q_1 V_1 + Q_2 V_2}{Q^{\mathrm{tot}}}.$$

The time mean is generally larger than the space mean because, at the same partial densities, the class of faster vehicles passes the cross-section more often within the aggregation interval than the vehicles of the slower class do. The arithmetic average is generally larger than the harmonic average which can be shown for any data. Only for the trivial case of identical data, both averages agree.

Here, $\rho_1 = \rho_2$ but $Q_1 \neq Q_2$, so the simple (not weighted) arithmetic average over lanes applies for the space mean speed.

*4. Speed variance between lanes.* Because of identical speeds on either lane, the total variance of the speeds in the left and right lane is the same as the inter-lane variance sought after:

$$\begin{aligned}\sigma_V^2 &= E(v_i - E(v_i))^2 \\ &= \frac{1}{60}\left(40[40-33.3]^2 + 20[20-33.3]^2\right) \\ &= 88.9\,\mathrm{m}^2/\mathrm{s}^2\,.\end{aligned}$$

*Total speed variance.* We divide the speed variance

$$\sigma_V^2 = \frac{1}{N}\sum_i (v_i - V)^2$$

into two sums over the left and right lane, respectively:

$$\sigma_V^2 = \frac{1}{N}\left[\sum_{i_1=1}^{N_1}(v_{i_1}-V)^2 + \sum_{i_2=1}^{N_2}(v_{i_2}-V)^2\right].$$

Now we expand the two squares:

$$(v_{i_1}-V)^2 = (v_{i_1}-V_1+V_1-V)^2 = (v_{i_1}-V_1)^2 + 2(v_{i_1}-V_1)(V_1-V) + (V_1-V)^2,$$

where $V_1$ is the average over lane 1. We proceed analogously for $(v_{i_2}-V)^2$. Inserting this into the expression for $\sigma_V^2$ and recognizing that

$$\sum_{i_1}(v_{i_1}-V_1)(V_1-V) = 0, \quad \sum_{i_2}(v_{i_2}-V_2)(V_2-V) = 0$$

and

$$\sigma_{V_1}^2 = \frac{1}{N_1}\sum_{i_1=1}^{N_1}(v_{i_1}-V_1)^2$$

and similarly for $\sigma_{V_2}^2$, we obtain

$$\sigma_V^2 = \frac{N_1}{N}\left[\sigma_{V_1}^2 + (V_1-V)^2\right] + \frac{N_2}{N}\left[\sigma_{V_2}^2 + (V_2-V)^2\right].$$

With $p_1 = N_1/N$ and $p_2 = N_2/N = 1-p_1$, we get the formula of the problem statement. If $p_1 = p_2 = 1/2$ we have $V = (V_1+V_2)/2$ and thus

$$\sigma_V^2 = \frac{1}{2}\left[\sigma_{V_1}^2 + \sigma_{V_2}^2\right] + \frac{(V_1-V_2)^2}{4}.$$

Notice that this mathematical relation can be applied to both space mean and time mean averages.

### 5.3 Analytical Fundamental Diagram

We have to distinguish between free and congested traffic.

*Free traffic.*

$$V^{\text{free}}(\rho) = V_0 = \text{const}.$$

Flow by using the hydrodynamic relation:

$$Q^{\text{free}}(\rho) = \rho V^{\text{free}}(\rho) = \rho V_0.$$

*Congested traffic.* The speed-dependent equilibrium gap between vehicles, $s(v) = s_0 + vT$, leads to the gap-dependent equilibrium speed $V^{\text{cong}}(s)$:

$$V^{\text{cong}}(s) = \frac{s-s_0}{T}.$$

Using the definition of the density $\rho$, we replace the gap $s$:

$$\begin{aligned}\rho &= \frac{\text{number of vehicles}}{\text{road length}} \\ &= \frac{\text{one vehicle}}{\text{one distance headway (front-to-front distance)}} \\ &= \frac{1}{\text{vehicle length + gap (bumper-to-bumper distance)}} = \frac{1}{l+s}.\end{aligned}$$

Thus $s(\rho) = \frac{1}{\rho} - l$ and therefore

$$V^{\text{cong}}(\rho) = \frac{s - s_0}{T} = \frac{1}{T}\left[\frac{1}{\rho} - (l + s_0)\right].$$

The flow-density relation is obtained again by the hydrodynamic relation:

$$Q^{\text{cong}}(\rho) = \rho V^{\text{cong}}(\rho) = \frac{1}{T}\left[1 - \rho(l + s_0)\right].$$

The sum $l_{\text{eff}} = l + s_0$ of vehicle length and minimum gap can be interpreted as an *effective* vehicle length (typically 7 m in city traffic, somewhat more on highways). Accordingly, the maximum density is

$$\rho_{\max} = \frac{1}{l + s_0} = \frac{1}{l_{\text{eff}}}.$$

To obtain the critical density $\rho_{\text{C}}$ separating free and congested traffic, we determine the point where the free and congested branches of the fundamental diagram intersect:

$$Q^{\text{cong}}(\rho) = Q^{\text{free}}(\rho) \;\Rightarrow\; \rho V_0 T = 1 - \rho(l + s_0) \;\Rightarrow\; \rho_{\text{C}} = \frac{1}{V_0 T + l_{\text{eff}}}.$$

This is the "tip" of the triangular fundamental diagram, and the corresponding flow is the capacity $C$ (the maximum possible flow):

$$C = Q^{\text{cong}}(\rho_{\text{C}}) = Q^{\text{free}}(\rho_{\text{C}}) = \frac{1}{T}\left(\frac{1}{1 + \frac{l_{\text{eff}}}{V_0 T}}\right). \tag{1}$$

The capacity $C$ is of the order of (yet always less than) the inverse time gap $T$. The lower the free speed $V_0$, the more pronounced the discrepancy between the "ideal" capacity $1/T$ and the actual value.

Given the numeric values stated in the problem, we obtain the following values for $\rho_{\max}$, $\rho_{\text{C}}$, and $C$:

$$\rho_{\max} = 143\,\text{veh/km},\;\; \rho_{\text{C}} = 16.6\,\text{veh/km},\;\; C = 0.552\,\text{veh/s} = 1{,}990\,\text{veh/h}.$$

### 5.4 Estimating the Velocity of Traffic Waves

1. We can use the minima of the speeds even if they are biased provided that the relation between the real and biased speed is strictly monotonous (which is the case) since we are interested in the *argument* of the minimum (the time) which is unchanged in this case.
2. Taking the first speed minima (with the difference D07-D09 marked in the figure of the problem statement) of detector pairs, we obtain

   - D07-D08: $\Delta x = -1{,}000\,\mathrm{m}$, $\Delta t = 210\,\mathrm{s}$, $w = \Delta x/\Delta t = -4.76\,\mathrm{m/s}$
   - D08-D09: $\Delta x = -1{,}000\,\mathrm{m}$, $\Delta t = 240\,\mathrm{s}$, $w = \Delta x/\Delta t = -4.17\,\mathrm{m/s}$
   - D07-D09: $\Delta x = -2{,}000\,\mathrm{m}$, $\Delta t = 450\,\mathrm{s}$, $w = \Delta x/\Delta t = -4.44\,\mathrm{m/s}$

   The observations are around $-4.5\,\mathrm{m/s} \approx -16\,\mathrm{km/h}$.
3. The errors are rather large because of the short distances between the detectors and the aggregation time interval of 1 min. Graphically estimating the slope of the traffic waves in spatiotemporal plots such as Fig. 5.11 or analyzing the cross correlation function (5.31) gives more precise results.

**5.5 Fundamental Diagram Estimated from Stationary Detector Data**

The free velocity can be read off the speed-density diagram (at low densities):

$$V_{\mathrm{A8}}^{\mathrm{free}} = 125\,\mathrm{km/h}, \quad V_{\mathrm{A9}}^{\mathrm{free}} = 110\,\mathrm{km/h}.$$

(Dutch police is very rigorous in enforcing speed limits and uses automated systems to do so. This explains why few people drive faster than 110 km/h.)

The flow-density diagram immediately shows the maximum density (the density where the flow data drop to zero at the right-hand side) and the capacity (maximum flow):

$$\rho_{\mathrm{A8}}^{\max} = 80\,\mathrm{veh/km}, \quad \rho_{\mathrm{A9}}^{\max} = 110\,\mathrm{veh/km},$$
$$C_{\mathrm{A8}} = 1{,}700\,\mathrm{veh/h}, \quad C_{\mathrm{A9}} = 2{,}400\,\mathrm{veh/h}.$$

The headways can be calculated by solving the capacity equation (1) for $T$,

$$T = \frac{1 - \frac{l_{\mathrm{eff}} C}{V_0}}{C} = \frac{1 - \frac{C}{V_0 \rho_{\max}}}{C},$$

and thus

$$T_{\mathrm{A8}} = 1.91\,\mathrm{s}, \quad T_{\mathrm{A9}} = 1.27\,\mathrm{s}.$$

One cautionary note is in order: If the data of the scatter plots are derived from arithmetic time mean speeds via the relation $\rho = Q/V$ (as it is the case here), the density of congested traffic flow, and in the consequence $T$, will be underestimated, although not so drastically. To a lesser extent, this also applies to harmonic averages (cf. Fig. 5.15). In the Sections 9.6.3 and 17.4, we will learn about more robust estimation methods based on propagation velocities.

# Problems of Chapter 6

## 6.1 Reconstruction of the Traffic Situation Around an Accident

*Part 1.* In the space-time diagram below, thin dashed green lines mark confirmed free traffic while all other information is visualized using thicker lines and different colors. The respective information is denoted in the key. The signal "zero flow" means "I do not know; either empty road or stopped traffic".

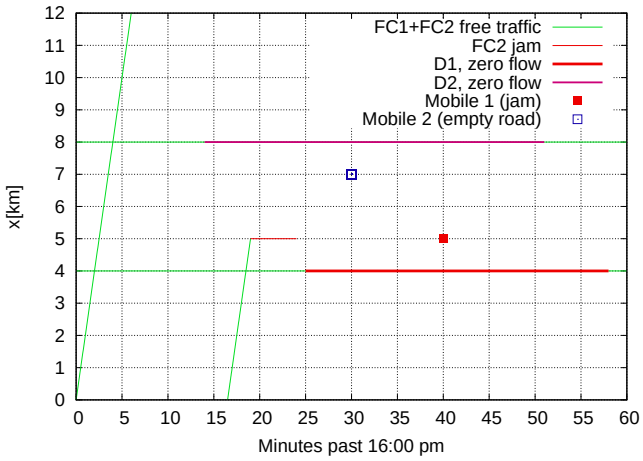


*Part 2.* The information of the first floating car (FC1) tells us the speed in free traffic, $V_{\text{free}} = 10\,\text{km}/5\,\text{minutes} = 120\,\text{km/h}$. From the second floating car (FC2) we know that an upstream jam front passes $x = 5\,\text{km}$ at 4:19 pm.

The stationary detectors D1 at $x = 4\,\text{km}$ and D2 at 8 km both report zero flows in a certain time interval but this does not tell apart whether the road is maximally congested or empty. However, we additionally know by the two mobile phone calls that the road is fully congested at 5 km while it is empty at 7 km. The congestion at 5 km is also consistent with the trajectory of the second floating car. Since downstream jam fronts (transition jam $\rightarrow$ free traffic) are either stationary or propagate upstream at velocity $c \approx -15\,\text{km/h}$ but never downstream (apart from the special case of a moving bottleneck), we know that the missing vehicle counts of D1 are the consequence of standing traffic while that of D2 reflect an empty road (at least when ignoring the possibility that there might be another obstruction more downstream causing a second jam).

With this information, we can estimate the motion of the upstream jam front. Assuming a constant propagation velocity $c^{\text{up}}$, we determine this velocity from the spatiotemporal points where detector D1 and the second floating car encounter congestion, respectively:

$$c^{\text{up}} = \frac{-1\,\text{km}}{6\,\text{min}} = -10\,\text{km/h}\,.$$

The motion of this front is another strong evidence that D2 does not measure a transition from free to fully congested traffic but from free traffic to no traffic at all at $x = 8\,\text{km}$ and $t = 4{:}14\,\text{pm}$: Otherwise, the propagation velocity $c^{\text{up}}$ would be $-4\,\text{km}/5\,\text{min} = -48\,\text{km/h}$ in this region which is not possible even if we do not require $c^{\text{up}}$ to be constant: The largest possible negative velocity $c^{\text{up}}$, realized under conditions of maximum inflow against a full road block, is only insignificantly larger in magnitude than $|c^{\text{down}}| \approx 15\,\text{km/h}$.

Now we have enough information to determine location and time of the initial road block (accident). Intersecting the line

$$x^{\text{up}}(t) = 4\,\text{km} + c^{\text{up}} t - 25\,\text{min}) = 4\,\text{km} - \frac{t - 25\,\text{min}}{6}\,\text{km/min}$$

characterizing the upstream front with the trajectory $x_{\text{last}}(t)$ of the last vehicle that made it past the accident location,

$$x_{\text{last}}(t) = 8\,\text{km} + v_0(t - 14\,\text{min}) = 8\,\text{km} + (t - 14\,\text{min})\,2\,\text{km/min}$$

yields location and time of the road block:

$$x_{\text{crash}} = 6\,\text{km}, \quad t_{\text{crash}} = 4{:}13\,\text{pm}\,.$$

*Part 3.* After the accident site is cleared, the initially stationary downstream jam front (fixed at the accident site) starts moving at the characteristic velocity $c^{\text{down}} = -15\,\text{km/h} = -1\,\text{km}/4\,\text{min}$. Since the detector at $x = 4\,\text{km}$ (D1) detects non-zero traffic flow from 4:58 pm onwards, the front is described by

$$x^{\text{down}}(t) = 4\,\text{km} + c^{\text{down}}(t - 58\,\text{min}).$$

Obviously, the accident location ($x_{\text{crash}} = 6\,\text{km}$) is cleared exactly at the time where the moving downstream jam front crosses the accident site (cf. the figure), i.e., at $t_{\text{clear}} = 4{:}50\,\text{pm}$.

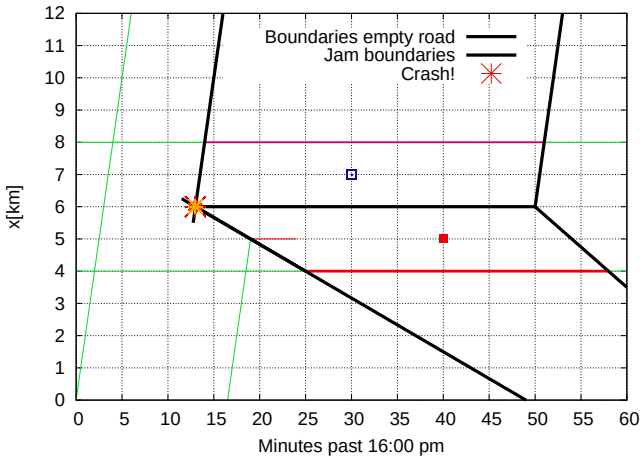


### 6.2 Dealing with Inconsistent Information

Using equal weights, $V = \frac{1}{2}(V_1 + V_2)$, the error variance is

$$\sigma_V^2 = \frac{1}{4}\left(\sigma_1^2 + \sigma_2^2\right) = \frac{1}{4}\left(\sigma_1^2 + 4\sigma_1^2\right) = \frac{5}{4}\sigma_1^2\,,$$

assuming negligible systematic errors and independent random errors. Consequently, the error increases by a factor of $\sqrt{5/4}$ due to the inclusion of the noisy floating-car data. Using optimal weights,

$$V_{\text{opt}} = \frac{1}{5}(4V_1 + V_2)\,,$$

yields the error variance

$$(\sigma_V^2)_{\text{opt}} = \frac{1}{25}\left(16\sigma_1^2 + \sigma_2^2\right) = \frac{1}{25}\left(16\sigma_1^2 + 4\sigma_1^2\right) = \frac{4}{5}\sigma_1^2.$$

This means, adding floating-car data with a small weight to the stationary detector data *reduces* the uncertainty by a factor of down to $\sqrt{4/5}$, in spite of the fourfold variance of the floating-car data compared to the stationary detector data.

## Problems of Chapter 7

### 7.1 Speed Limit on the German Autobahn?

The *safety aspect* of speed limits cannot be modeled or simulated by traffic-flow models simply because these models are calibrated to normal situations (including traffic jams). However, accidents are typically the consequence of a series of unfortunate circumstances and extraordinary driving behavior which is not included in the models. In contrast, the effect on *fuel consumption* can be modeled and simulated

reliably by combining microscopic or macroscopic traffic flow models with the corresponding models for fuel consumption or emissions, cf. Chapter 23. To assess the *economic effect* of speed limits, including social welfare or changed traffic patterns, one needs models for traffic demand and route choice, i.e., models of the domain of transportation planning. Traffic flow models are suited, however, to investigate certain environmental and societal aspects on a smaller scale. For example, traffic flow models in connection with consumption/emission models describe the direct effect of speed limits on emissions. Furthermore, since speed limits change the propensity for traffic breakdowns and traffic flow/emission models can describe this influence as well as the changed emissions in the jammed state, these models also describe the indirect effect via traffic breakdowns.

## Problems of Chapter 8

### 8.1 Flow-Density-Speed Relations

We require

$$Q^{\mathrm{tot}} = \sum_i Q_i = \sum_i \rho_i V_i = \rho^{\mathrm{tot}} V$$

which we can fulfil by suitably defining the effective average $V$ of the local speed across all lanes. Solving this condition for $V$ directly gives

$$V = \sum_i \frac{\rho_i}{\rho^{\mathrm{tot}}} V_i = \sum_i w_i V_i,$$

i.e., the definition (8.7) of the main text.

### 8.2 Conservation of Vehicles

In a closed ring road, the vehicle number $n(t)$ is the integral of the total vehicle density $\rho^{\mathrm{tot}} = I(x)\rho$ over the complete circumference of the ring. Applying Eq. (8.17) for $v_{\mathrm{rmp}} = 0$ and the hydrodynamic relation $\rho V = Q$, we obtain for the rate of change of the vehicle number

$$\frac{\mathrm{d}n}{\mathrm{d}t} = -\oint \left( I(x)\frac{\partial Q(x,t)}{\partial x} + Q(x,t)\frac{\mathrm{d}I}{\mathrm{d}x} \right) \mathrm{d}x = -\oint \frac{\partial (I(x)Q(x,t))}{\partial x} \mathrm{d}x = IQ|_{x_{\mathrm{a}}}^{x_{\mathrm{e}}}.$$

If the road is closed, we have $x_{\mathrm{e}} = x_{\mathrm{a}}$, so $\frac{\mathrm{d}n}{\mathrm{d}t} = 0$ and the total vehicle number $n$ does not change over time.

### 8.3 Continuity Equation I

(i) The continuity equation for $x < 0$ or $x > L = 300\,\mathrm{m}$, i.e., outside of the merging region, has no source terms and reads

$$\frac{\partial \rho}{\partial t} + \frac{\partial Q}{\partial x} = 0.$$

In the merging region $0 \le x \le L$, we have an additional source term $\nu_{\text{rmp}}(x,t)$ that generally depends on space and time:

$$\frac{\partial \rho}{\partial t} + \frac{\partial Q}{\partial x} = \nu_{\text{rmp}}(x,t).$$

Now we assume that $\nu_{\text{rmp}}$ is constant with respect to $x$ over the merging region $L$. In view of the definition of $\nu$, this means that the differential merging rate on a small segment of the merging lane, divided by the number of main-road lanes, is constant. We obtain the connection between the ramp flow $Q_{\text{rmp}}$ and $\nu_{\text{rmp}}$ by integrating $\nu$ over the merging region and requiring that the result is equal to the ramp flow (if there are several ramp lanes, the total ramp flow) divided by the number $I$ of main-road lanes. Thus,

$$\frac{Q_{\text{rmp}}}{I} = \int_0^L \nu_{\text{rmp}}\, dx = \nu_{\text{rmp}} \int_0^L dx = \nu_{\text{rmp}} L,$$

so

$$\nu_{\text{rmp}} = \frac{Q_{\text{rmp}}}{IL} = \frac{1}{2}\,\frac{600\,\text{veh/h}}{300\,\text{m}} = 1\,\text{veh/m/hour}.$$

(ii) It is easy to generalize the source term $\nu_{\text{rmp}}(x)$ to inhomogeneous differential merging rates. In the most general case, we prescribe a distribution function of the merging points[5] over the length of the merging lane by its probability density $f(x)$:

$$\nu_{\text{rmp}}(x,t) = \frac{Q_{\text{rmp}}(t)}{I}\, f(x).$$

For case (i) (constant differential changing rates),

$$f_{\text{uniform}}(x) = \begin{cases} 1/L & \text{if } 0 \le x \le L, \\ 0 & \text{otherwise,} \end{cases}$$

i.e., the merging points are uniformly distributed over the interval $[0,L]$. To model drivers who, in their majority, merge in the first half of the length of the merging lane, we prescribe a distribution $f(x)$ which takes on higher values at the beginning than near the end of the lane, e.g., the triangular distribution

$$f_{\text{early}}(x) = \begin{cases} \frac{2(L-x)}{L^2} & \text{if } 0 \le x \le L, \\ 0 & \text{otherwise.} \end{cases}$$

If we want to describe a behavior where drivers change to the main road near the end (which applies for some situations of congested traffic, we mirror $f_{\text{early}}(x)$ at

[5] Later on, when we explicitly model lane changes by microscopic models, we will assume instantaneous lane changes, so the merging point is well-defined. For real continuous changes, one can define $x$ to be the first location where a vehicle crosses the road marks separating the on-ramp from the adjacent main-road lane.

$x = L/2$ to arrive at

$$f_{\text{late}}(x) = \begin{cases} \frac{2x}{L^2} & \text{if } 0 \le x \le L, \\ 0 & \text{otherwise.} \end{cases}$$

*Remark*: A temporal dependency is modeled directly by a time-dependent ramp flow $Q_{\text{rmp}}(t)$.

### 8.4 Continuity Equation II

A stationary traffic flow is characterized by zero partial time derivatives, particularly,

$$\frac{\partial \rho(x,t)}{\partial t} = 0, \quad \frac{\partial Q(x,t)}{\partial t} = 0.$$

This simplifies the continuity equation (8.17) for the effective (lane-averaged) flow and density for the most general case including ramps and variable lane numbers to

$$\frac{\mathrm{d}Q}{\mathrm{d}x} = -\frac{Q(x)}{I(x)} \frac{\mathrm{d}I}{\mathrm{d}x} + \nu_{\text{rmp}}(x). \tag{2}$$

By the condition of stationarity, the partial differential equation (8.17) for $\rho(x,t)$ and $Q(x,t)$ with the independent variables $x$ and $t$ changes to an ordinary differential equation (ODE) for $Q$ as a function of $x$. Stationarity also implies that the traffic inflow at the upstream boundary is constant, $Q(x = 0, t) = Q_0$.

(i) We can solve the ODE (2) for $\nu_{\text{rmp}} = 0$ by the standard method of *separating the variables*:

$$\frac{\mathrm{d}Q}{Q} = -\frac{\mathrm{d}I}{I} \frac{\mathrm{d}x}{\mathrm{d}x} = -\frac{\mathrm{d}I}{I}.$$

Indefinite integration of both sides with respect to the corresponding variable yields $\ln Q = -\ln I + \tilde{C}$ with the integration constant $\tilde{C}$. Applying the exponentiation on both sides results in

$$Q(x) = \frac{C}{I(x)}$$

where $C = \exp(\tilde{C})$. The new integration constant is fixed by the spatial initial conditions $C = I(x = 0)Q(x = 0) = I_0 Q_0$ where $I_0$ is the number of lanes at $x = 0$. This also determines the spatial dependency of the flow:

$$Q(x) = \frac{I_0 Q_0}{I(x)}. \tag{3}$$

Notice that this is consistent with the stationarity condition $Q^{\text{tot}} = I(x)Q(x) = I_0 Q_0 = \text{const}$.

(ii) To describe an on-ramp or off-ramp merging to or diverging from a main road with $I$ lanes with a constant differential rate, we set

$$\nu_{\text{rmp}} = \frac{Q_{\text{rmp}}}{IL} = \text{const},$$

where $Q_{\text{rmp}} < 0$ for off-ramps. Applying the condition of stationarity to the continuity equation (8.17) assuming a constant number $I$ of lanes results in the ODE

$$\frac{\mathrm{d}Q}{\mathrm{d}x} = \begin{cases} \nu_{\text{rmp}} & \text{parallel to merging/diverging lanes,} \\ 0 & \text{otherwise,} \end{cases}$$

with prescribed and constant $Q(x=0) = Q_0 = Q^{\text{tot}}/I$ at the upstream boundary. In our problem with an off-ramp upstream of an on-ramp (which is the normal configuration at an interchange), we have

$$\frac{\mathrm{d}Q}{\mathrm{d}x} = \begin{cases} -Q_{\text{off}}/(IL_{\text{off}}) & \text{if } 300\,\text{m} \le x < 500\,\text{m}, \\ Q_{\text{on}}/(IL_{\text{on}}) & \text{if } 700\,\text{m} \le x < 1\,00\,\text{m}, \\ 0 & \text{otherwise.} \end{cases}$$

where $L_{\text{off}} = 200\,\text{m}$, and $L_{\text{on}} = 300\,\text{m}$. We calculate the solution to this ODE by simple integration:

$$Q(x) = \begin{cases} Q_0 & \text{if } x < 300\,\text{m}, \\ Q_0 - Q_{\text{off}}(x - 300\,\text{m})/(IL_{\text{off}}) & \text{if } 300\,\text{m} \le x < 500\,\text{m}, \\ Q_0 - Q_{\text{off}}/I & \text{if } 500\,\text{m} \le x < 700\,\text{m}, \\ Q_0 - Q_{\text{off}}/I + Q_{\text{on}}(x - 700\,\text{m})/(IL_{\text{on}}) & \text{if } 700\,\text{m} \le x < 1{,}000\,\text{m}, \\ Q_0 + (Q_{\text{on}} - Q_{\text{off}})/I & \text{if } x \ge 1{,}000\,\text{m}. \end{cases}$$

### 8.5 Continuity Equation III

The highway initially has $I_0 = 3$ lanes, and a lane drop to 2 lanes over the effective length $L$:

$$I(x) = \begin{cases} 3 & x < 0, \\ \left(3 - \frac{x}{L}\right) & 0 \le x \le L, \\ 2 & x > L. \end{cases}$$

Since the traffic demand (inflow) is constant, $Q_{\text{in}} = Q^{\text{tot}}(0) = 3{,}600\,\text{veh/h}$, and there is no other explicit time dependence in the system, the traffic flow equilibrates to the stationary situation characterized by $\frac{\partial}{\partial t} = 0$:

$$\frac{\mathrm{d}Q}{\mathrm{d}x} = -\frac{Q(x)}{I(x)}\,\frac{\mathrm{d}I}{\mathrm{d}x}.$$

1. The solution for the section with a variable lane number reads (cf. Eq. (3)):

$$Q(x) = \frac{I_0 Q_0}{I(x)} = \frac{Q_{\text{tot}}}{I(x)}.$$

Upstream and downstream of the lane drop, we have $I(x)$=const., i.e.,

$$Q(x) = \frac{Q_{\text{tot}}}{I}.$$

In summary, this results in

$$Q(x) = \begin{cases} Q^{\text{tot}}/3 & x < 0, \\ \frac{Q^{\text{tot}}}{3-\frac{x}{L}}, & 0 \le x \le L \\ Q^{\text{tot}}/2 & x > L. \end{cases}$$

Furthermore, the hydrodynamic relation $Q = \rho V$ with $V = 108\,\text{km/h}$ gives the density

$$\rho(x) = \frac{Q}{V} = \begin{cases} 11.11\,/\text{km} & x < 0, \\ \frac{33.33}{3-\frac{x}{L}}\,\frac{1}{\text{km}} & 0 \le x \le L, \\ 16.67\,/\text{km} & x > L. \end{cases}$$

2. We insert the relation $I(x) = 3 - x/L$ and $dI/dx = -1/L$ for the lane drop and $Q(x) = Q^{\text{tot}}/(3 - x/L)$ for the flow into the right-hand side of Eq. (2):

$$\frac{\mathrm{d}Q}{\mathrm{d}x} = -\frac{Q^{\text{tot}}}{I^2(x)}\,\frac{\partial I}{\partial x} = \frac{Q^{\text{tot}}}{L\left(3-\frac{x}{L}\right)^2}.$$

The right-hand side can be identified with the searched-for effective ramp term:

$$v_{\text{rmp}}^{\text{eff}} = \frac{Q^{\text{tot}}}{L\left(3-\frac{x}{L}\right)^2}.$$

We determine the effective ramp flow corresponding to $v_{\text{rmp}}^{\text{eff}}(x)$ from the point of view of the two remaining through lanes:

$$\begin{aligned} Q_{\text{rmp}}^{\text{eff}} &= 2\int_0^L v_{\text{rmp}}^{\text{eff}}\,\mathrm{d}x = \frac{2Q^{\text{tot}}}{L}\int_0^L \frac{\mathrm{d}x}{\left(3-\frac{x}{L}\right)^2} = \frac{2Q^{\text{tot}}}{L}\left(\frac{1}{3-\frac{x}{L}}\right)\Bigg|_0^L \\ &= \frac{Q^{\text{tot}}}{3} = 1{,}200\,\text{veh/h/lane}. \end{aligned}$$

Here, we used the indefinite integral

$$\int \frac{\mathrm{d}x}{\left(3-\frac{x}{L}\right)^2} = \frac{L}{3-\frac{x}{L}}.$$

### 8.6 Continuity Equation for Coupled Maps

We start from the formulation for global flows and densities:

$$\frac{\partial \rho_k^{\text{tot}}}{\partial t} + \frac{\partial Q_k^{\text{tot}}}{\partial x} = I v_{\text{rmp}}$$

By definition, we have $\rho_k^{\text{tot}} = I_k^{\text{down}}\rho_k$. Assuming constant change rates for a small discrete time interval $\Delta t$, the time derivative term becomes

$$\frac{\partial \rho_k^{\text{tot}}}{\partial t} = \frac{I_k^{\text{down}}(\rho_k(t+\Delta t) - \rho_k(t))}{\Delta t}.$$

Assuming constant flow changes over the length of the merging lane, the gradient term becomes

$$\frac{\partial Q_k^{\text{tot}}}{\partial x} = \frac{I^{\text{down}} Q_k^{\text{down}} - I_k^{\text{up}} Q_k^{\text{up}}}{\Delta x_k}.$$

Finally, we simply have, by definition,

$$I v_{\text{rmp}} = Q^{\text{rmp}} / L^{\text{rmp}} = Q^{\text{rmp}} / \Delta x$$

Putting this together, we obtain

$$\rho_k(t+\Delta t) = \rho_k(t) + \frac{1}{I^{\text{down}} \Delta x_k} \left( I^{\text{up}} Q_k^{\text{up}} + Q_{\text{rmp}} - I^{\text{down}} Q_k^{\text{down}} \right) \Delta t.$$

For the *continuous* steady-state condition, we just derive this expression setting $\frac{\partial \rho_k^{\text{tot}}}{\partial t} = 0$ while, in the discrete case, we just set the $\rho_k(t+\Delta t) = \rho_k(t)$ and multiply Eq. (8.18) by $I^{\text{down}}$. In both cases, we obtain

$$0 = I_k^{\text{up}} Q_k^{\text{up}} - I_k^{\text{down}} Q_k^{\text{down}} + Q_{\text{rmp}}$$

which is the flow balance given in the problem statement. This balance means that, in steady-state conditions, the ramp flow is equal to the total outflow $Q_k^{\text{down}} I^{\text{down}}$ from a cell minus the total inflow $Q_k^{\text{up}} I^{\text{up}}$ which is consistent with vehicle conservation.

### 8.7 Parabolic Fundamental Diagram

For the fundamental diagram

$$Q(\rho) = \rho V(\rho) = \rho V_0 \left( 1 - \frac{\rho}{\rho_{\max}} \right),$$

the maximum flow (capacity per lane) $Q_{\max}$ is at a density $\rho_{\text{C}}$. We determine $\rho_{\text{C}}$, as usual, by setting the gradient $Q'(\rho)$ equal to zero:

$$Q'(\rho_{\text{C}}) = V_0 - 2\frac{V_0 \rho_{\text{C}}}{\rho_{\max}} = 0 \quad \Rightarrow \quad \rho_{\text{C}} = \frac{1}{2}\rho_{\max}.$$

Hence

$$Q_{\max} = Q(\rho_{\text{C}}) = \frac{\rho_{\max} V_0}{4}.$$

## Problems of Chapter 9

### 9.1 Propagation Velocity of a Shock Wave Free → Congested

The triangular fundamental diagram is semi-concave, i.e., the second derivative $Q_e''(\rho)$ is non-positive, and the first derivative $Q_e'(\rho)$ is monotonously decreasing. This means, any straight line connecting two points on the fundamental diagram

always lies below or, at most, on the fundamental diagram $Q_e(\rho)$. Consequently, the slope $c_{12} = (Q_2 - Q_1)/(\rho_2 - \rho_1)$ of this line cannot be greater than $Q'(0) = V_0$ and not less than $Q'(\rho_{\max}) = c$ proving the statement. Since this argumentation only relies on the semi-concavity of the fundamental diagram, it can also be applied to the parabolic fundamental diagram of Problem 8.7 leading to $c_{12} \in [-V_0, V_0]$.

### 9.2 Driver Interactions in Free Traffic

There are not any in this model. If there were interactions, the followers would react to the leaders, so the information of the shock wave would propagate at a lower velocity than the vehicle speed, contrary to the fact.

### 9.3 Dissolving Queues at a Traffic Light

When the traffic light turns green, the traffic flow passes the traffic light in the maximum-flow state. For the triangular fundamental diagram, the speed at the maximum-flow state is equal to the desired speed and the transition from the waiting queue (density $\rho_{\max}$) to the maximum-flow state propagates backwards at a velocity $w = -l_{\text{eff}}/T$ corresponding to the congested slope of the fundamental diagram. In the microscopic picture, every follower starts a time interval $T$ later than its leader and instantaneously accelerates to $V_0$ (Fig. 9.18). This suggests to interpret $T$ as the reaction time of each driver, so $|c|$ is simply the distance between two queued vehicles divided by the reaction time.

We emphasize, however, that the LWR model does not contain any reaction time. Moreover, the above microscopic interpretation no longer holds for LWR models with other fundamental diagrams. Therefore, another interpretation is more to the point. As above, the driver instantaneously starts from zero to $V_0$ which follows directly from the sharp macroscopic shock fronts. However, the drivers only start their "rocket-like" acceleration when there is enough time headway at $V_0$. Thus, $|c|$ is the distance between two queued vehicles divided by the desired time gap $T$ in car-following mode. Similar considerations apply for concave fundamental diagrams (such as the parabola-shaped of Problem 8.7). This allows following general conclusion:

> The fact that not all drivers start simultaneously at traffic lights is not caused by reaction times but by the higher space requirement of moving with respect to standing vehicles: It simply takes some time for the already started vehicles to make this space.

### 9.4 Total Waiting Time During One Red Phase of a Traffic Light

The total waiting time in the queue is equal to the number $n(t)$ of vehicles waiting at a given time, integrated over the duration of the queue: Defining $t = 0$ as the begin of the red phase and $x = 0$ as the position of the stopping line, this means

$$\tau^{\text{tot}} = \int_0^{\tau_r+\tau_{\text{diss}}} n(t)\,\mathrm{d}t = \int_0^{\tau_r+\tau_{\text{diss}}} \int_{x_u(t)}^{x_o(t)} \rho_{\max}\,\mathrm{d}x\,\mathrm{d}t = \rho_{\max} A,$$

i.e., the total waiting time is equal to the jam density times the area of the queue in space-time (cf. the following diagram).

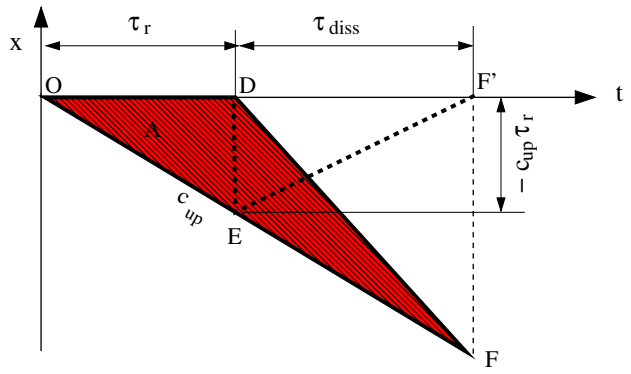


The area of the congested area is equal to the sum of the area of the two right-angled triangles with the legs $(\tau_\mathrm{r}, -c_\mathrm{up}\tau_\mathrm{r})$ and $(\tau_\mathrm{diss}, -c_\mathrm{up}\tau_\mathrm{r})$, respectively:

$$\tau^\mathrm{tot} = \frac{1}{2}\rho_\mathrm{max}\left(-c_\mathrm{up}\tau_\mathrm{r}^2 - c_\mathrm{up}\tau_\mathrm{r}\tau_\mathrm{diss}\right).$$

To obtain the second right-angled triangle DEF', we have shifted the point F of the original triangle DEF to F' which does not change the enclosed area. Furthermore, we have the geometrical relation (cf. the figure again)

$$c_\mathrm{up}\tau_\mathrm{r} = (w - c_\mathrm{up})\tau_\mathrm{diss},$$

i.e., $\tau_\mathrm{diss} = c_\mathrm{up}\tau_\mathrm{r}/(w - c_\mathrm{up})$. Inserting this into the expression for $\tau^\mathrm{tot}$ finally gives

$$\tau^\mathrm{tot} = \frac{1}{2}\rho_\mathrm{max}\tau_\mathrm{r}^2\,\frac{c_\mathrm{up}w}{c_\mathrm{up} - w}$$

with

$$c_\mathrm{up} = \frac{Q_\mathrm{in}}{Q_\mathrm{in}/V_0 - \rho_\mathrm{max}}, \quad w = -\frac{1}{\rho_\mathrm{max}T}.$$

The total waiting time increases with the *square* of the red time.

### 9.5 Jam Propagation on a Highway I: Accident

*Subproblem 1.* With the values given in the problem statement, the capacity per lane reads

$$Q_\mathrm{max} = \frac{V_0}{V_0T + l_\mathrm{eff}} = 2{,}016\,\mathrm{veh/h}.$$

The total capacity of the road in the considered driving direction without accident is just twice that value:

$$C = 2Q_\mathrm{max} = 4{,}032\,\mathrm{veh/h}.$$

This exceeds the traffic demand 3,024 veh/h at the inflow ($x = 0$), so no jam forms before the accident, and only road section 1 exists. Since there are neither changes in the demand nor road-related changes, traffic flow is stationary and the flow per lane is constant:

$$Q_1 = \frac{Q_{\text{in}}}{2} = 1,512\,\text{vehs/h}, \quad V_1 = V_0 = 28\,\text{m/s}, \quad \rho_1 = \frac{Q_1}{V_0} = 15\,\text{veh/km}.$$

This also gives the travel time to traverse the $L = 10\,\text{km}$ long section:

$$t_{\text{trav}} = \frac{L}{V_0} = 357\,\text{s}.$$

*Subproblem 2.* At the location of the accident, only one lane is open, so the bottleneck capacity

$$C_{\text{bottl}} = Q_{\text{max}} = 2,016\,\text{veh/h}$$

does not meet the demand any more, and traffic breaks down at this location. This means, there are now three regions with different flow characteristics:

- Region 1, free traffic upstream of the congestion: Here, the situation is as in Subproblem 1.
- Region 2, congested traffic at and upstream of the bottleneck.
- Region 3, free traffic downstream of the bottleneck.

From the propagation and information velocities of perturbations in free and congested traffic flow, and from the fact that the flow but not the speed derives from a conserved quantity, we can deduce following general rules:

> Free traffic flow is controlled by the flow at the upstream boundary, congested traffic flow and the traffic flow downstream of "activated" bottlenecks is controlled by the bottleneck capacity.

For the congested region 2 upstream of the accident (both lanes are available), this means

$$Q_2 = \frac{C_{\text{bottl}}}{2} = 1,008\,\text{veh/h}.$$

To determine the traffic density, we invert the flow-density relation of the congested branch of the fundamental diagram,[6]

$$\rho_2 = \rho_{\text{cong}}(Q_2) = \frac{1 - Q_2 T}{l_{\text{eff}}} = 72.5\,\text{veh/km}.$$

*Subproblem 3.* To calculate the propagation velocity of the shock (discontinuous transition free $\rightarrow$ congested traffic), we apply the shock-wave formula:

[6] *Beware:* The fundamental diagram and derived quantities (as $\rho_{\text{cong}}(Q)$) are always defined for the lane-averaged effective density and flow.

$$c^{\text{up}} = c_{12} = \frac{Q_2 - Q_1}{\rho_2 - \rho_1} = -8.77\,\text{km/h}.$$

*Subproblem 4.* After lifting the lane closure, the capacity is, again, given by $C = 2Q_{\max} = 4,032\,\text{veh/h}$, everywhere. In the LWR models, the outflow from congestions is equal to the local capacity, so the new outflow from the congestion is characterized by $Q_4 = C/2 = Q_{\max}$, $V_4 = V_0$, and $\rho_4 = Q_4/V_0 = 20\,\text{veh/h}$. Furthermore, the transition from regions 2 to 3 (downstream jam front) starts to move upstream at a propagation velocity again calculated by the shock-wave formula:

$$c^{\text{down}} = c = c_{24} = \frac{Q_4 - Q_2}{\rho_4 - \rho_2} = -19.2\,\text{km/h}.$$

The jam dissolves if the upstream and downstream jam fronts meet. Defining $t$ as the time past 15:00 h, $x$ as in the figure of the problem statement, and denoting the duration of the bottleneck by $\tau_{\text{bottl}} = 30\,\text{minutes}$, we obtain following equations of motion for the fronts,

$$\begin{aligned} x_{\text{up}}(t) &= L + c^{\text{up}}\,t, \\ x_{\text{down}}(t) &= L + c(t - \tau_{\text{bottl}}). \end{aligned}$$

Setting these positions equal results in the time for complete jam dissolution:

$$t_{\text{dissolve}} = \tau_{\text{bottl}}\,\frac{c}{c - c^{\text{up}}} = 3,312\,\text{s}.$$

The position of the last vehicle to be obstructed at obstruction time is equal to the location of the two jam fronts when they dissolve:

$$t_{\text{dissolve}} = L + c^{\text{up}}\,t_{\text{dissolve}} = 1,936\,\text{m}.$$

*Subproblem 5.* In the spatiotemporal diagram, the congestion is restricted by three boundaries:

- Stationary downstream front at the bottleneck position $L = 10\,\text{km}$ for the times $t \in [0, \tau_{\text{bottl}}]$,
- Moving downstream front for $t \in [\tau_{\text{bottl}}], t_{\text{dissolve}}]$ whose position moves according to $x_{\text{down}}(t) = L + c(t - \tau_{\text{bottl}})$,
- Moving upstream front for $t \in [0, t_{\text{dissolve}}]$ whose position moves according to $x_{\text{up}}(t) = L + c^{\text{up}}\,t$

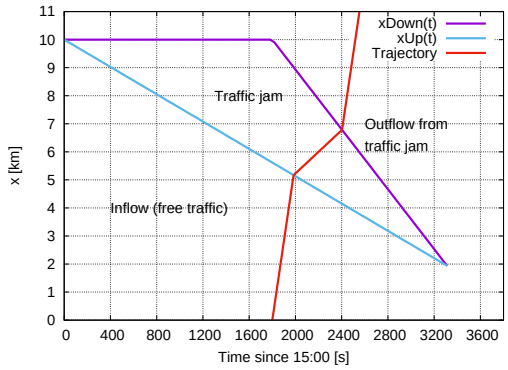


*Subproblem 6.* We follow the vehicle trajectory starting at time $t = t_0 = 1,800\,\mathrm{s}$ at the upstream boundary $x = 0$ by piecewise integrating it through the three regions (cf. the diagram):

1. *Traversing the inflow region*: The vehicle moves at constant speed $V_0$ resulting in the trajectory $x(t) = V_0(t - t_0)$.
2. *Traversing the jam*: To calculate the time $t_{\mathrm{up}}$ of entering the jam, we intersect the free-flow trajectory with the equations of motion $x_{\mathrm{up}}(t) = L + c^{\mathrm{up}}\,t$ for the upstream front:
$$t_{\mathrm{up}} = \frac{L + V_0 t_0}{V_0 - c^{\mathrm{up}}} = 1,984\,\mathrm{s}.$$
The corresponding location $x_{\mathrm{up}} = V_0(t_{\mathrm{up}} - t_0) = 5,168\,\mathrm{m}$. Hence, the trajectory reads
$$x(t) = x_{\mathrm{up}} + v_{\mathrm{cong}}(t - t_{\mathrm{up}}), \quad v_{\mathrm{cong}} = \frac{Q_2}{\rho_2} = 3.86\,\mathrm{m/s}.$$
3. *Trajectory after leaving the jam*: Since, at time $t_{\mathrm{up}}$, the bottleneck no longer exists, we calculate the exiting time by intersecting the trajectory calculated above with the equations of motion of the moving downstream front. This results in
$$t_{\mathrm{down}} = \frac{L - x_{\mathrm{up}} - ct_0 + v_{\mathrm{cong}} t_{\mathrm{up}}}{v_{\mathrm{cong}} - c} = 2,403\,\mathrm{s},$$
$$x_{\mathrm{down}} = x_{\mathrm{up}} + w(t_{\mathrm{down}} - t_{\mathrm{up}}) = 6,783\,\mathrm{m}.$$
After leaving the jam, the vehicle moves according to trajectory $x(t) = x_{\mathrm{down}} + V_0(t - t_{\mathrm{down}})$, so the vehicle crosses the location $x = L = 10\,\mathrm{km}$ at time
$$t_{\mathrm{end}} = t_{\mathrm{down}} + \frac{L - x_{\mathrm{down}}}{V_0} = 2,518\,\mathrm{s}.$$
In summary, we obtain for the total travel time to traverse the $L = 10\,\mathrm{km}$ long section
$$\tau = t_{\mathrm{end}} - t_0 = 718.1\,\mathrm{s}.$$

## 9.6 Jam Propagation on a Highway II: Uphill Grade and Lane Drop

*Subproblem 1.* As in the previous problem, we calculate the capacities with the capacity formula of the triangular fundamental diagram:

$$Q_{\max} = \frac{V_0}{V_0 T + l_{\text{eff}}} = 2,000\,\text{veh/h},$$
$$Q_{\max}^{\text{III}} = \frac{V_{03}}{V_{03} T_3 + l_{\text{eff}}} = 1,440\,\text{veh/h}.$$

*Subproblem 2.* For the *total* quantities, lane drops, gradients, and other flow-conserving bottlenecks are irrelevant, and the continuity equation reads

$$\frac{\partial \rho^{\text{tot}}}{\partial t} + \frac{\partial Q^{\text{tot}}}{\partial x} = \frac{\partial Q^{\text{tot}}}{\partial x} = 0.$$

Since the inflow is constant, $Q_{\text{in}} = 2,000\,\text{veh/h}$, and less the minimum capacity $C^{\text{III}} = 2Q_{\max}^{\text{III}} = 2,880\,\text{veh/h}$, this amounts to stationary free traffic flow in all four regions I - IV with $Q^{\text{tot}} = Q_{\text{in}} = \text{const}$. From this information, we calculate the effective flow of all regions by dividing by the respective number of lanes, and the density by the free part of the fundamental diagram:

| | $V$ [km/h] | $Q^{\text{tot}}$ [veh/h] | $Q$ [veh/h/lane] | $\rho^{\text{tot}}$ [veh/km] | $\rho$ [veh/km/lane] |
|---|---|---|---|---|---|
| Region I | 120 | 2,000 | 667 | 16.7 | 5.55 |
| Region II | 120 | 2,000 | 1,000 | 16.7 | 8.33 |
| Region III | 60 | 2,000 | 1,000 | 33.3 | 16.7 |
| Region IV | 120 | 2,000 | 1,000 | 16.7 | 8.33 |

*Subproblem 3.* Traffic breaks down if the local traffic flow is greater than the local capacity. Thus, the jam forms at a location and at a time where and when this condition is violated, for the first time. Since the capacities in the four regions are given by 6,000, 4,000, 2,880, and 4,000 vehicles/h, respectively, the interface between regions II and III at $x = 3\,\text{km}$ is the first location where the local capacity can no longer meet the new demand $Q_{\text{in}} = 3,600\,\text{veh/h}$. Traffic breaks down if the information of the increased demand reaches $x = 3\,\text{km}$. This information propagates through the regions I and II at $c_{\text{free}} = V_0 = 120\,\text{km/h}$, or at 2 km per minute, so

$$x_{\text{breakd}} = 3\,\text{km}, \quad t_{\text{breakd}} = 16{:}01{:}30\,\text{h}.$$

*Subproblem 4.* To determine density, flow, and speed of congested traffic in the regions I and II, we, again, adhere to the rule that free traffic flow is controlled by the upstream boundary while the total flow of congested regions and of regions downstream of "activated" bottlenecks are equal to the bottleneck capacity at some earlier times determined by the information propagation velocities $c_{\text{free}}$ and $w$, respectively. Furthermore, densities inside congestions are calculated with the congested branch of the fundamental diagram while the free branch is used in all other cases. Denoting with regions Ib and IIb the congested sections of regions I and II, respectively, and

with regions Ia and IIa the corresponding free-flow sections, this leads to following table for the traffic-flow variables:

| | $V$ [km/h] | $Q^{\text{tot}}$ [veh/h] | $Q$ [veh/h/lane] | $\rho^{\text{tot}}$ [veh/km] | $\rho$ [veh/km/lane] |
|---|---|---|---|---|---|
| Ia ($I=3$) | 16 | 3,600 | 1,200 | 30 | 10 |
| Ib ($I=3$) | 120 | 2,880 | 960 | 180 | 60 |
| IIa ($I=2$) | 36 | 3,600 | 1,800 | 30 | 15 |
| IIb ($I=2$) | 120 | 2,880 | 1,440 | 80 | 40 |
| III ($I=2$) | 60 | 2,880 | 1,440 | 48 | 24 |
| IV ($I=2$) | 120 | 2,880 | 1,440 | 24 | 12 |

Notice that the local vehicle speed inside congested two-lane regions is more than *twice* that of three-lane regions.[7]

*Subproblem 5.* To calculate the propagation velocities of the upstream jam front in the regions I and II, we use, again, the shock-wave formula together with the table of the previous subproblem:

$$v_g = \frac{\Delta Q}{\Delta \rho} = \begin{cases} -240/(60-10)\,\text{km/h} = -4.8\,\text{km/h} & \text{Interface Ia-Ib, situation (i),} \\ -360/(40-15)\,\text{km/h} = -14.4\,\text{km/h} & \text{Interface IIa-IIb, situation (ii).} \end{cases}$$

### 9.7 Toll Plaza

*Subproblem 1.* The free-flow speed $V_0 = 25\,\text{m/s}$ is given directly. With the relation $w = -l_{\text{eff}}/T$ between the wave speed and the effective length $l_{\text{eff}} = 1/\rho_{\max}$, the triangular FD has a maximum flow

$$Q_{\max} = \frac{V_0}{V_0 T + l_{\text{eff}}} = \frac{V_0}{l_{\text{eff}}\left(1 - \frac{V_0}{w}\right)}$$

which can be solved for the effective vehicle length:

$$l_{\text{eff}} = \frac{1}{\rho_{\max}} = \frac{V_0}{Q_{\max}\left(1 - \frac{V_0}{w}\right)} = 8.33\,\text{m}.$$

Then, the maximum density $\rho_{\max} = 1/l_{\text{eff}} = 120\,\text{veh/km}$ and the time gap $T = -l_{\text{eff}}/w = 1.67\,\text{s}$ can be calculated easily.

*Subproblem 2.* With a serving capacity of 300 veh/h per booth, the total serving capacity is $C_B = 4,500\,\text{veh/h}$ which is greater than the inflow $Q_{\text{in}} = 4,200\,\text{veh/h}$, so no breakdown occurs.

[7] When being stuck inside jams without knowing the cause, this allows to draw conclusions about the type of bottleneck, e.g., whether it is a three-to-two, or three-to-one lane drop.

*Subproblem 3.* With the surge in the demand, the bottleneck capacity $C_b = 4,500\,\text{veh/h}$ does no longer meet the demand $Q_{\text{in}} = 5,400\,\text{veh/h}$ and a breakdown occurs. In LWR models this means that a shockwave appears. Because the drivers always use the shortest line, the upstream jam front free $\rightarrow$ congested has the same location $x^{\text{up}}$ on all lanes, the congested flow per lane is given by the servicing capacity and the congested density per lane by the inverse of the congested branch of the triangular fundamental diagram:

$$\begin{aligned} Q_{\text{cong}} &= 300\,\text{veh/h} = 1/12\,\text{veh/s}, \\ \rho_{\text{cong}} &= \rho_{\max}(1 - Q_{\text{cong}}T) = \rho_{\max} + Q_{\text{cong}}/w = 103.3\,\text{veh/km}. \end{aligned}$$

The free flow in the plaza upstream of the jam front distributes on all 15 lanes, hence

$$Q_{\text{free}} = Q_{\text{in}}15 = 360\,\text{veh/h}, \quad \rho_{\text{free}} = \frac{Q_{\text{free}}}{V_0} = 4\,\text{veh/km}.$$

The time until the toll plaza of length $L = 200\,\text{m}$ fills up, can be calculated in two means. (i) Vehicle conservation:

$$T_{\text{fill}} = \frac{\Delta n}{\Delta Q} = \frac{15(\rho_{\text{cong}} - \rho_{\text{free}})L}{Q_{\text{in}} - C_b} = 1\,192\,\text{s}.$$

(ii) With the shockwave formula:

$$c_{\text{up}} = \frac{Q_{\text{cong}} - Q_{\text{free}}}{\rho_{\text{cong}} - \rho_{\text{free}}} = -0.1678\,\text{m/s}, \quad T_{\text{fill}} = \frac{L}{-c_{\text{up}}} = 1\,192\,\text{s}.$$

*Subproblem 4.* Average speed in the congested lines in the plaza: $V_{\text{cong}} = Q_{\text{cong}}/\rho_{\text{cong}} = 0.8065\,\text{m/s}$, queuing time $L/V_{\text{cong}} = 248\,\text{s}$.

*Subproblem 5.* Calculation as in Subproblem 3, only with 3 instead of 15 lanes,

$$\begin{aligned} Q_{\text{cong}} &= \frac{4,500\,\text{veh/h}}{3} = 1,500\,\text{veh/h}, \quad Q_{\text{free}} = \frac{5,400\,\text{veh/h}}{3} = 1,800\,\text{veh/h}, \\ \rho_{\text{cong}} &= \rho_{\max}(1 - Q_{\text{cong}}T) = 36.7\,\text{veh/km}, \quad \rho_{\text{free}} = \frac{Q_{\text{free}}}{V_0} = 25\,\text{m/s} \end{aligned}$$

results in a congested speed $V_{\text{cong}} = Q_{\text{cong}}/\rho_{\text{cong}} = 11.36\,\text{m/s}$ and a propagation velocity of the upstream front of $c_{\text{up}} = w = -5\,\text{m/s}$. Notice that we do not even need to use the shockwave formula to calculate $c_{\text{up}}$ because the free section is at capacity, i.e., at the tip of the triangular FD, hence $c_{\text{up}} = w$.

*Subproblem 6.* For ideal lane synchronization and diverging to the new lanes, and assuming $x = 0$ at the beginning of the widening, the fractional lane number at position $x$ is given by

$$I(x) = 3 + \frac{12x}{L_{\text{w}}}$$

where $L_w = 160\,\mathrm{m}$. Then, the position dependent congested speed in the widening section is given by

$$V(x) = \frac{Q}{\rho_{\mathrm{cong}}(Q)} = \frac{\frac{C_b}{I(x)}}{\rho_{\max}\left(1 - \frac{C_b T}{I(x)}\right)} = \frac{C_b}{\rho_{\max}\left(I(x) - C_b T\right)}.$$

*Subproblem 7.* The travel time through the fully congested widening section is the space integral over the inverse of the speed,

$$\begin{aligned} T_{\mathrm{w}} &= \int_{x=0}^{L_w} \frac{\mathrm{d}x}{V(x)} \\ &= \int_{x=0}^{L_w} \frac{\rho_{\max}\left(I(x) - C_b T\right)}{C_b} \mathrm{d}x \\ &= -\rho_{\max} T L_w + \int_{x=0}^{L_w} \frac{\rho_{\max}}{C_b}\left(3 + \frac{12}{L_w} x\right) \mathrm{d}x \\ &= \rho_{\max} L_w \left(\frac{9}{C_b} - T\right) = 106.24\,\mathrm{s}. \end{aligned}$$

**9.8 Diffusion-Transport Equation**

Inserting the initial conditions into Eq. (9.57) results in

$$\rho(x,t) = \rho_0 \int_0^L \frac{1}{\sqrt{4\pi D t}} \exp\left[\frac{-(x - x' - \tilde{c}t)^2}{4Dt}\right] \mathrm{d}x'.$$

Since the integrand is formally identical to the density function $f_N(x')$ of a $(\mu, \sigma^2)$ Gaussian distribution (with space and time dependent expectation $\mu(t) = x - \tilde{c}t$ and variance $\sigma^2(t) = 2Dt$), we can the above integral write as[8]

$$\rho(x,t) = \rho_0 \int_0^L f_N^{(\mu,\sigma^2)}(x')\,\mathrm{d}x'.$$

Since the integrand is the density of a Gaussian distribution function, the integral itself can be expressed in terms of the (cumulated) Gaussian or normal distribution

$$F_N(x) = \int_{-\infty}^{x} f_N(x')\,\mathrm{d}x',$$

resulting in

$$\rho(x,t) = \rho_0 \left[F_N^{(\mu,\sigma^2)}(L) - F_N^{(\mu,\sigma^2)}(0)\right].$$

[8] When doing the integral, watch out that the variable to be integrated is $x'$ rather than $x$.

Since this is no elementary function, we express the result in terms of the tabulated standard normal distribution $\Phi(x) = F_N^{(0,1)}(x)$ by using the relation $F(x) = \Phi((x-\mu)/\sigma)$ taught in statistics courses. With $\mu = x - \tilde{c}t$ and $\sigma^2(t) = 2Dt$, this results in

$$\begin{aligned}\rho(x,t) &= \rho_0 \left[ \Phi\left(\frac{L-\mu}{\sigma}\right) - \Phi\left(\frac{-\mu}{\sigma}\right)\right] \\ &= \rho_0 \left[ \Phi\left(\frac{L-x+\tilde{c}t}{\sqrt{2Dt}}\right) - \Phi\left(\frac{-x+\tilde{c}t}{\sqrt{2Dt}}\right)\right] \\ &= \rho_0 \left[ \Phi\left(\frac{x-\tilde{c}t}{\sqrt{2Dt}}\right) - \Phi\left(\frac{x-\tilde{c}t-L}{\sqrt{2Dt}}\right)\right],\end{aligned}$$

In the last line, we have used the symmetry relation $\Phi(x) = 1 - \Phi(-x)$. In the limiting case of zero diffusion, the two standard normal distribution functions degenerate to jump functions with jumps at the positions $\tilde{c}t$ and $L + \tilde{c}t$. This is consistent with the analytic solution of the triangular LWR model, $\rho(x,t) = \rho_0(x - \tilde{c}t)$ where $\rho_0(x)$ denotes the initial density given in the problem statement. For finite diffusion constants, the initially sharp density profiles smear out over time (cf. Fig. 9.29).

## Problems of Chapter 10

### 10.1 Ramp Term of the Acceleration Equation

Macroscopically, the total derivative $\frac{\mathrm{d}V}{\mathrm{d}t}$ of the local speed denotes the rate of change of the average speed of all $n = \rho\,\Delta x$ vehicles in a (small) road element of length $\Delta x$ comoving with the local speed $V$,

$$\frac{\mathrm{d}V}{\mathrm{d}t} = \frac{\mathrm{d}E\,(v_i)}{\mathrm{d}t} = \frac{\mathrm{d}}{\mathrm{d}t}\left(\frac{1}{n}\sum_{i=1}^{n} v_i\right). \tag{4}$$

Without acceleration of single vehicles ($\frac{\mathrm{d}v_i}{\mathrm{d}t} = 0$), the rate of change is solely caused by vehicles entering or leaving this road element at a speed $V_{\mathrm{rmp}} \neq V$ (cf. Fig. 10.5). Assuming that the position of the merging vehicles is uniformly distributed over the length $L_{\mathrm{rmp}}$ of the merging region, the rate of change of the vehicle number is given by

$$\frac{\mathrm{d}n}{\mathrm{d}t} = q = Q_{\mathrm{rmp}}\frac{\Delta x}{L_{\mathrm{rmp}}} \tag{5}$$

whenever the moving road element is parallel to the merging section of an on-ramp. When evaluating the time derivative (4), we notice that both the prefactor $\frac{1}{n}$ and the sum itself depend explicitly on time. Specifically,

$$\frac{\mathrm{d}}{\mathrm{d}t}\left(\frac{1}{n}\right) = -\frac{q}{n^2}, \quad \frac{\mathrm{d}}{\mathrm{d}t}\left(\sum_i v_i\right) = qV_{\mathrm{rmp}}.$$

The second equation follows from the problem statement that all vehicles enter the road at speed $V_{\text{rmp}}$ and no vehicles (including the ramp vehicles) accelerate ($v_i = \text{const}$). Using these relations and $\sum_i v_i = nV$, we can write the rate of change of the local speed as

$$\begin{aligned} A_{\text{rmp}} &= \frac{\mathrm{d}E\,(v_i)}{\mathrm{d}t} = \frac{\mathrm{d}}{\mathrm{d}t}\left(\frac{1}{n(t)}\sum_{i=1}^{n(t)} v_i\right) \\ &= -\frac{qnV}{n^2} + \frac{qV_{\text{rmp}}}{n} \\ &= \frac{q(V_{\text{rmp}} - V)}{n} \\ &= \frac{Q_{\text{rmp}}\Delta x(V_{\text{rmp}} - V)}{nL_{\text{rmp}}} \\ &= \frac{Q_{\text{rmp}}(V_{\text{rmp}} - V)}{I\rho L_{\text{rmp}}}. \end{aligned}$$

In the last step, we have used $n = I\rho\,\Delta x$.

### 10.2 Kinematic Dispersion

*Subproblem 1.* The lane-averaged local speed is given by

$$V = \frac{1}{\rho_1 + \rho_2}\left(\rho_1 V_1 + \rho_2 V_2\right).$$

First, we calculate the initial speed variance across the lanes ($k = 1$ and 2 for the left and right lanes, respectively):

$$\begin{aligned} \sigma_V^2(x,0) &= E\left((V_k(x,0) - V)^2\right) \\ &= \frac{\rho_1(V_1 - V)^2 + \rho_2(V_2 - V)^2}{\rho_1 + \rho_2}, \end{aligned}$$

or, for the special case $\rho_1 = \rho_2$,

$$\sigma_V^2(x,0) = \frac{(V_1 - V_2)^2}{4} = 100\,(\text{m/s})^2 = \text{const}.$$

Notice that these expressions give the true spatial (instantaneous) variance. In contrast, when determining the time mean variance at a given location from data of a stationary detector station, we would obtain for lane 1 the weighting factor $Q_1/(Q_1 + Q_2) = 1/3$ instead of the correct value $\rho_1/(\rho_1 + \rho_2) = 1/2$ resulting in a biased estimate for the true variance (cf. Chapter 5).

*Subproblem 2.* The kinematic part $P_{\text{kin}} = \rho\sigma_V^2$ of the pressure term leads to a following contribution of the local macroscopic acceleration,

$$A_{\text{kin}} = -\frac{1}{\rho}\frac{\partial P}{\partial x} = -\frac{1}{\rho}\frac{\mathrm{d}}{\mathrm{d}x}\left(\rho(x,t)\sigma_V^2\right) = \begin{cases} \frac{0.01\,\mathrm{s}^{-2}}{\rho} & 0 \le x \le 100\,\mathrm{m}, \\ 0 & \text{otherwise.} \end{cases}$$

(The factor $0.01\,\mathrm{s}^{-2}$ result from the gradient $\frac{\partial\rho}{\partial x} = 10^{-4}\,\mathrm{m}^{-2}$ multiplied by the variance $100\,(\mathrm{m/s})^2$.) Consequently, a finite speed variance implies that a negative density gradient leads to a positive contribution of the macroscopic acceleration. This will be discussed at an intuitive level in the next subproblem.

*Subproblem 3.* If there is a finite variance $\sigma_V^2$ *and* a negative density gradient (a transition from dense to less dense traffic), then the vehicles driving faster than the local speed $V$ go from the region of denser traffic to the less dense region while the slower vehicles are transported backwards (in the comoving system!) to the denser region. Due to the density gradient, the net inflow of faster vehicles is positive and that of slower vehicles negative. This is illustrated in the following figure, the upper graphics of which depicting the situation in the stationary system, and the lower one in a system comoving with $V$. As a result, the averaged speed $V$ is increasing although *not a single vehicle* accelerates while the total number of vehicles in the element, i.e., the density, is essentially constant.

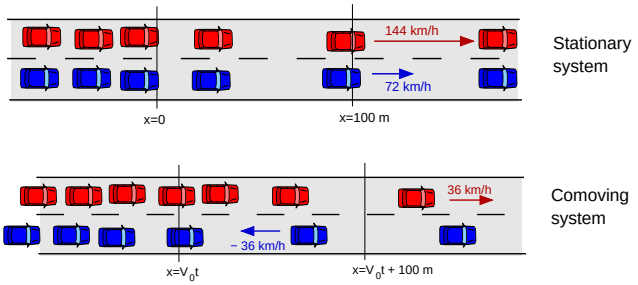


*Subproblem 4.* Assuming that higher actual speeds are positively correlated with higher desired speeds, the mechanism described in Subproblem 3 leads to a *segregation* of the desired speeds such that the fast tail of the desired speed distribution tends to be found further downstream than the slow tail. This is most conspicuous in multi-lane queues of city traffic waiting behind a red traffic light when the light turns green: If there is one lane with speeding drivers, these drivers will reach first a given position downstream of the stopping line of the traffic light. At this moment, the traffic composition at this point consists exclusively of speeding drivers. Macroscopically, this can only be modeled by multi-class macroscopic models where the desired speed $V_0(x,t)$ becomes another dynamical field with its own dynamical equation. Because of their complexity, such *Paveri-Fontana models* are rarely used.

### 10.3 Modeling Anticipation by Traffic Pressure

*Subproblem 1.* Since, by definition, the traffic density is equal to the number of vehicles per distance, one vehicle distance, i.e., the distance headway $d$, can be expressed by the density:

$$d = \frac{1}{\rho((x+x_\mathrm{a})/2,t)} \approx \frac{1}{\rho(x,t)}.$$

The first expression to the right of the equal sign is accurate to second order in $x_\mathrm{a} - x = d$. The second expression $1/\rho(x,t)$ is accurate to first order which is sufficient in the following.

*Subproblem 2.* We expand the nonlocal part $V_e(\rho(x_\mathrm{a},t)) = V_e(\rho(x+d,t))$ of the adaptation term to first order around $x$:

$$\begin{aligned} V_e(\rho(x+d,t)) &= V_e(\rho(x,t)) + \frac{\mathrm{d}V_e(\rho(x,t))}{\mathrm{d}x}\, d + \mathscr{O}(d^2) \\ &= V_e(\rho(x,t)) + \frac{1}{\rho}\frac{\mathrm{d}V_e(\rho(x,t))}{\mathrm{d}x} + \mathscr{O}(d^2)\,. \end{aligned}$$

Inserting this into the speed adaptation term results in

$$\begin{aligned} \left(\frac{\mathrm{d}V}{\mathrm{d}t}\right)_{\text{relax+antic}} &\approx \frac{V_e(\rho(x,t)) - V(x,t)}{\tau} + \frac{1}{\rho\tau}\frac{\mathrm{d}V_e(\rho(x,t))}{\mathrm{d}x} \\ &\stackrel{!}{=} \frac{V_e(\rho(x,t)) - V(x,t)}{\tau} - \frac{1}{\rho}\frac{\mathrm{d}P(x,t)}{\mathrm{d}x}, \end{aligned}$$

where, in the last step, we set the result equal to the general expression for the acceleration caused by $P$. The comparison yields

$$P(x,t) = -\frac{V_e(\rho(x,t))}{\tau}.$$

*Subproblem 3.* According to the problem statement, the density profile obeys (with $\rho_0 = 20\,\mathrm{veh/km} = 0.02\,\mathrm{veh/m}$, $c = 100\,\mathrm{veh/km^2} = 10^{-4}\,\mathrm{veh/m^2}$)

$$\rho(x,t) = \begin{cases} \rho_0 & x < 0, \\ \rho_0 + cx & 0 < x \le 200\,\mathrm{m}, \\ 2\rho_0 & x > 200\,\mathrm{m}. \end{cases} \tag{6}$$

(i) Acceleration by anticipation when using the original relaxation term:

$$\left(\frac{\mathrm{d}V}{\mathrm{d}t}\right)_{\text{relax}} = \frac{V_e(\rho(x+1/\rho(x,t),t)) - V_e(\rho(x,t))}{\tau},$$

where $V_e(\rho) = V_0(1-\rho/\rho_\mathrm{max})$ is given in the problem statement (such a relation is rather unrealistic; it serves to show the principle in the easiest possible way). Inserting Eq. (6), we obtain

$$\left(\frac{\mathrm{d}V}{\mathrm{d}t}\right)_{\text{relax}} = \begin{cases} 0 & x \le -1/\rho_0 \text{ or } x > 200\,\text{m}, \\ \frac{-V_0 c}{\tau\rho_{\max}}\left(\frac{1}{\rho_0} + x\right) & -\frac{1}{\rho_0} < x \le 0, \\ \frac{-V_0 c}{\tau\rho_{\max}\rho} & 0 < x \le 200\,\text{m} - \frac{1}{2\rho_0}, \\ \frac{-V_0}{\tau\rho_{\max}}(2\rho_0 - \rho) & 200\,\text{m} - \frac{1}{2\rho_0} < x \le 200\,\text{m}, \end{cases}$$

where the criterion separating the last two cases is only approximately valid.

(ii) Expressing the acceleration contribution by the pressure term, we obtain

$$\left(\frac{\mathrm{d}V}{\mathrm{d}t}\right)_{\text{pressure}} = \begin{cases} 0 & x \le 0 \text{ or } x > 200\,\text{m}, \\ \frac{-V_0 c}{\tau\rho_{\max}\rho} & 0 < x \le 200\,\text{m} - \frac{1}{2\rho_0}. \end{cases}$$

Except for the transition regions at the beginning and end of the density gradient, this agrees with the acceleration derived from the original relaxation term. However, in contrast to the pressure term, the nonlocal anticipation term provides "true" anticipation everywhere, including the region $-1/\rho_0 \le x < 0$ where the local approximation by the pressure term does not "see" anything. In summary, the nonlocal route to modeling anticipation is more robust.

### 10.4 Steady-State Speed of the GKT Model

In the steady state on homogeneous roads, all spatial and temporal derivatives vanish, so the GKT acceleration equation (10.25) reduces to $V = V_e^*$. Furthermore, the homogeneity associated with the steady state implies $V_\mathrm{a} = V$ and $\rho_\mathrm{a} = \rho$, and the Boltzmann factor is given by $B(0) = 1$. Using these conditions and the definition (10.28) for $V_e^*$, we can write the condition $V = V_e^*$ as

$$\frac{V}{V_0} = 1 - \frac{\alpha(\rho)}{\alpha(\rho_{\max})}\left(\frac{\rho_\mathrm{a} V T}{1 - \rho_\mathrm{a}/\rho_{\max}}\right)^2.$$

This is a quadratic equation in $V$. Its positive root reads

$$V = V_e(\rho) = \frac{\tilde{V}^2}{2V_0}\left(-1 + \sqrt{1 + \frac{4V_0^2}{\tilde{V}^2}}\right)$$

with the abbreviation

$$\tilde{V} = \sqrt{\frac{\alpha(\rho_{\max})}{\alpha(\rho)}}\,\frac{(1 - \rho/\rho_{\max})}{\rho T}.$$

For densities near the maximum density we have $\tilde{V} \ll V_0$ and $\alpha(\rho) \approx \alpha(\rho_{\max})$. With the micro-macro relation $s = 1/\rho - 1/\rho_{\max}$, we can write the steady-state speed in this limit as

$$V_e(\rho) \approx \tilde{V} \approx \frac{(1 - \rho/\rho_{\max})}{\rho T} = \frac{s}{T}.$$

Notice that this implies that $T$ has the meaning of a (bumper-to-bumper) time gap in heavily congested traffic.

**10.5 Flow-Conserving Form of Second-Order Macroscopic Models**

We start by setting $V = Q/\rho$ in the continuity equation:

$$\frac{\partial \rho}{\partial t} + \frac{\partial Q}{\partial x} = -\frac{Q}{I}\frac{\mathrm{d}I}{\mathrm{d}x} + \nu_{\mathrm{rmp}}.$$

Multiplying the acceleration equation (10.11) by $\rho$ and inserting $V = Q/\rho$ gives the intermediate result

$$\rho\frac{\partial V}{\partial t} + Q\frac{\partial V}{\partial x} = \frac{\rho V_e^* - Q}{\tau} - \frac{\partial P}{\partial x} + \frac{\partial}{\partial x}\left(\mu\frac{\partial (Q/\rho)}{\partial x}\right) + \rho A_{\mathrm{rmp}}.$$

Now we substitute the time derivative of the local speed by the time derivative of the flow and replace the resulting time derivative of the density with the flow-conservative continuity equation. The left-hand side of the last equation then reads

$$\begin{aligned}\rho\frac{\partial V}{\partial t} + Q\frac{\partial V}{\partial x} &= \frac{\partial Q}{\partial t} - V\frac{\partial \rho}{\partial t} + Q\frac{\partial V}{\partial x} \\ &= \frac{\partial Q}{\partial t} + V\frac{\partial Q}{\partial x} + V\frac{Q}{I}\frac{\mathrm{d}I}{\mathrm{d}x} - V\nu_{\mathrm{rmp}} + Q\frac{\partial V}{\partial x} \\ &= \frac{\partial Q}{\partial t} + \frac{\partial (QV)}{\partial x} + V\frac{Q}{I}\frac{\mathrm{d}I}{\mathrm{d}x} - V\nu_{\mathrm{rmp}}.\end{aligned}$$

Substituting again $V = Q/\rho$ and grouping the spatial derivatives together, we obtain

$$\frac{\partial Q}{\partial t} + \frac{\partial}{\partial x}\left[\frac{Q^2}{\rho} + P - \mu\frac{\partial}{\partial x}\left(\frac{Q}{\rho}\right)\right] = \frac{\rho V_e^* - Q}{\tau} - \frac{Q^2}{\rho I}\frac{\mathrm{d}I}{\mathrm{d}x} + \frac{Q\nu_{\mathrm{rmp}}}{\rho} + \rho A_{\mathrm{rmp}}.$$

**10.6 Numerics of the GKT Model**

Neglecting the pressure term (its maximum relative influence is of the order of $\sqrt{\alpha} = 10\%$), the first CFL condition (10.46) for the convective numerical instability reads

$$\Delta t < \frac{\Delta x}{V_0} = 1.5\,\mathrm{s}\,. \tag{7}$$

Since the GKT model does not contain diffusion terms, the second CFL condition is not relevant. However, the relaxation instability must be tested: The characteristic equation $\det(\underline{\mathbf{L}} - \lambda\underline{\mathbf{1}}) = 0$ for the eigenvalues of the matrix $\underline{\mathbf{L}}$ of the linear equation (10.42) reads

$$-\lambda(L_{22} - \lambda) = -\lambda\left[\frac{1}{\tau}\left(-1 + \rho\frac{\partial \tilde{V}_e(\rho, Q)}{\partial Q}\right) - \lambda\right] = 0$$

resulting in the eigenvalues

$$\lambda_1 = 0, \quad \lambda_2 = -\frac{1}{\tau}\left(1 - \rho\frac{\partial \tilde{V}_e(\rho, Q)}{\partial Q}\right),$$

where

$$\tilde{V}_e(\rho, Q) = V_e^*(\rho, Q, \rho, Q) = V_0\left[1 - \frac{\alpha(\rho)}{\alpha_{\max}}\left(\frac{Q_e T}{1 - \rho/\rho_{\max}}\right)^2\right].$$

With this result, the condition $\Delta t < |\lambda_2^{-1}|$ to avoid relaxation instability becomes

$$\Delta t < \frac{\tau}{1 + \frac{2\alpha(\rho)V_0\rho Q_e}{\alpha_{\max}}\left(\frac{T}{1-\rho/\rho_{\max}}\right)^2},$$

i.e., Eq. (10.51) of the main text. In the limit of high densities $\rho \to \rho_{\max}$ we make use of the approximate relation (cf. Problem 10.4)

$$V_e(\rho) \approx \frac{1}{T}\left(\frac{1}{\rho} - \frac{1}{\rho_{\max}}\right)$$

to arrive at

$$\Delta t < \frac{\tau(\rho)}{1 + 2\frac{V_0}{V_e}},$$

which is Eq. (10.52) of the main text. Inserting $\rho_{\max,\mathrm{sim}} = 0.1\,\mathrm{m}^{-1}$ from the problem statement and $V_e(\rho_{\max,\mathrm{sim}}) = 4.14\,\mathrm{m/s}$ (watch out for the units! If in doubt, always use the SI units m, kg, and s), we finally obtain

$$\Delta t < \frac{1}{|\lambda_2|} = 1.32\,\mathrm{s}. \tag{8}$$

The definitive limitation of the time step is given by the more restrictive one of the conditions (7) and (8), so $\Delta t < 1.32\,\mathrm{s}$.

The expression (10.57) for the numerical diffusion of both equations at $V = 20\,\mathrm{m/s}$ and $\Delta t = 1\,\mathrm{s}$ (i.e., the conditions for linear numerical stability are satisfied) evaluates to

$$D_{\mathrm{num}} = V\frac{\Delta x}{2}\left(1 - V\frac{\Delta t}{\Delta x}\right) = 300\,\mathrm{m/s^2}.$$

This is only about $1/30$ of the (real) diffusion introduced to the Kerner-Konhäuser model by the term proportional to $D_v$ (assuming standard parameterization).

## Problems of Chapter 11

### 11.1 Dynamics of a Single Vehicle Approaching a Red Traffic Light

*Subproblem 1 (parameters).* The free acceleration is the same as that of the OVM. Hence, $v_0$ is the desired speed and $\tau$ the adaptation time. If the model decelerates, it does so with the deceleration $b$. Since, at this deceleration, the kinematic braking distance to a complete stop is given by $\Delta x_{\text{brake}} = v^2/(2b)$, the vehicle stops at a distance $s_0$ to the (stopping line of) the red traffic light. This explains the meaning of the last parameter. Notice that, in this model, vehicles would follow any leading vehicle driving at a constant speed $v_l < v_0$ at the same gap $s_0$, i.e., the model does not include a safe gap. Nor does it contain a reaction time. The model is accident-free with respect to stationary obstacles, but not when slower vehicles are involved.

*Subproblem 2 (free acceleration phase).* Here, the first condition of the model applies, so we have to solve the ordinary differential equation (ODE) for the speed

$$\frac{\mathrm{d}v}{\mathrm{d}t} = \frac{v_0 - v}{\tau} \quad \text{with } v(0) = 0.$$

The exponential ansatz $\mathrm{e}^{\lambda t}$ for the homogeneous part $\frac{\mathrm{d}v}{\mathrm{d}t} = -v/\tau$ gives the solvability condition $\lambda = 1/\tau$. Furthermore, the general solution for the full inhomogeneous (ODE) reads

$$v(t) = A\mathrm{e}^{-t/\tau} + B.$$

The asymptotic $v(\infty) = B = v_0$ yields the inhomogeneous part $B$. Determining the integration constant $A$ by the initial condition $v(0) = A + B = A + v_0 = 0$ gives $A = -v_0$, so the speed profile reads

$$v(t) = v_0 \left(1 - \mathrm{e}^{-\frac{t}{\tau}}\right).$$

Once $v(t)$ is known, we determine the trajectory $x(t)$ by integrating over time. With $x(0) = 0$, we obtain

$$\begin{aligned} x(t) &= \int_0^t v(t')\,\mathrm{d}t' = v_0 \int_0^t \left(1 - \mathrm{e}^{-\frac{t'}{\tau}}\right) \mathrm{d}t' \\ &= v_0 \left[t' + \tau \mathrm{e}^{-\frac{t'}{\tau}}\right]_{t'=0}^{t'=t} = v_0 t + v_0 \tau \left(\mathrm{e}^{-\frac{t}{\tau}} - 1\right). \end{aligned}$$

By identifying parts of this expression with $v(t)$, this simplifies to

$$x(t) = v_0 t - v(t)\tau.$$

Finally, to obtain the acceleration profile, we either differentiate $v(t)$, or insert $v(t)$ into the right-hand side of the ODE. In either case, the result is

$$\dot{v} = \frac{v_0 - v}{\tau} = \frac{v_0}{\tau}\, \mathrm{e}^{-1/\tau}.$$

*Subproblem 3 (braking phase).* The red traffic light represents a standing virtual vehicle of zero length at the stopping line, so $\Delta v = v$. This phase starts at a distance

$$s_c = s_0 + \frac{v^2}{2b} = 50.2\,\mathrm{m}$$

to the stopping line, and the vehicle stops at a distance $s_0$ to this line.

*Subproblem 4 (trajectory).* For the accelerating phase, the trajectory has already been calculated. The deceleration phase begins at the location

$$x_c = L - s_c = L - s_0 - \frac{v^2}{2b} \approx 450\,\mathrm{m}.$$

To approximately determine the time $t_c$ at which the deceleration phase begins, we set $v(t_c) = v_0$ to obtain

$$x_c(t_c) = v_0 t_c - v(t_c)\tau \approx v_0(t_c - \tau) \quad \Rightarrow \quad t_c = \frac{x_c}{v_0} + \tau = 32.4\,\mathrm{s} + 5.0\,\mathrm{s} = 37.4\,\mathrm{s}.$$

With the braking time $v_0/b$, this also gives the stopping time

$$t_{\mathrm{stop}} = t_c + \frac{v_0}{b} = 44.3\,\mathrm{s}.$$

In summary, the speed profile $v(t)$ can be expressed by (cf. the graphics below)

$$v(t) = \begin{cases} v_0\left(1 - \mathrm{e}^{-t/\tau}\right) & 0 \le t < t_c, \\ v_0 - b(t - t_c) & t_c \le t \le t_{\mathrm{stop}}, \\ 0 & \text{otherwise.} \end{cases}$$

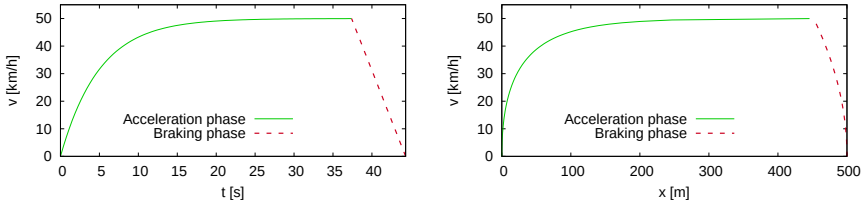


## 11.2 OVM Acceleration on an Empty Road

(i) The maximum acceleration $a_{\max} = v_0/\tau$ is reached right at the beginning, $t = 0$.
(ii) Prescribing $a_{\max} = 2\,\mathrm{m/s^2}$ and a desired speed $v_0 = 120\,\mathrm{km/h}$ determines the speed relaxation time by

$$\tau = \frac{v_0}{a_{\max}} = 16.7\,\mathrm{s}.$$

(iii) We require that, at a time $t_{100}$ to be determined, the speed should reach the value $v_{100} = 100\,\mathrm{km/h}$:

$$v(t_{100}) = v_{100} = v_0\left(1 - \mathrm{e}^{-\frac{t_{100}}{\tau}}\right).$$

Solving this condition for $t_{100}$ gives

$$\frac{v_{100}}{v_0} = 1 - \mathrm{e}^{-\frac{t_{100}}{\tau}} \quad \Rightarrow \quad t_{100} = -\tau \ln\left(1 - \frac{100}{120}\right) \approx 29.9\,\mathrm{s}.$$

### 11.3 Optimal Velocity Model on a Ring Road

The problem describes a situation with evenly spaced identical vehicles on a ring road which, initially, are at rest. This means, traffic flow is not stationary (since the initial gaps are greater than the minimum gap) but homogeneous: Since the road is homogeneous, and the vehicle fleet consists of identical vehicles, the homogeneity imposed by the initial conditions is not destroyed over time. For microscopic models, homogeneity implies that the dynamics depend neither on $x$ nor on the vehicle index $i$. So, dropping $i$, the OVM reads

$$\frac{\mathrm{d}v}{\mathrm{d}t} = \frac{v_{\mathrm{opt}}(s(0)) - v}{\tau}.$$

The solution to this ODE is analogously to Problem 11.2, only $v_0$ is replaced by the steady-state speed $v_e = v_{\mathrm{opt}}(s(0))$.

### 11.4 Full Velocity Difference Model

General plausibility arguments require the steady-state speed $v_{\mathrm{opt}}(s)$ to approach the desired speed $v_0$ when the gap $s$ tends to infinity. However, for an arbitrarily large distance to the red traffic light modeled by a standing virtual vehicle ($\Delta v = v$), the FVDM vehicle accelerates according to

$$\dot{v} = \frac{v_0 - v}{\tau} - \gamma v = \frac{v_0}{\tau} - \left(\frac{1}{\tau} + \gamma\right) v.$$

From this it follows that the acceleration $\dot{v}$ becomes zero for a terminal speed

$$v^* = \frac{v_0}{1 + \gamma\tau}.$$

This is the maximum speed an initially standing FVDM vehicle can reach in this situation. It is significantly lower than $v_0$. For the parameter values of the problem statement, $v^* = 13.5\,\mathrm{km/h}$ which agrees with Fig. 11.6.

### 11.5 A Simple Model for Emergency Braking Maneuvers

*Subproblem 1 (identifying the parameters).* $T_r =$ denotes the reaction time, and $b_{\max}$ is the maximum deceleration in emergency cases.

*Subproblem 2 (braking and stopping distance).* Assuming a fixed reaction timer $T_r$ and a constant deceleration $b_{\max}$ in the braking phase, elementary kinematic relations yield following expressions for the braking and stopping distances $s_B(v)$ and $s_{\mathrm{stop}}(v) = vT_r + s_B(v)$, respectively:

$$s_B(v) = \frac{v^2}{2b_{\max}}, \quad s_{\text{stop}}(v) = vT_r + s_B(v)$$

with the numerical values

$$\begin{aligned} v = 50\,\text{km/h}: &\quad s_B(v) = 12.1\,\text{m},\ s_{\text{stop}}(v) = 25.9\,\text{m}, \\ v = 70\,\text{km/h}: &\quad s_B(v) = 23.6\,\text{m},\ s_{\text{stop}}(v) = 43.1\,\text{m}. \end{aligned}$$

*Subproblem 3 (emergency braking).* At first, we determine the initial distance such that a driver driving at $v_1 = 50\,\text{km/h}$ just manages to stop before hitting the child:

$$s(0) = s_{\text{stop}}(v_1) = 25.95\,\text{m}.$$

Now we consider a speed $v_2 = 70\,\text{km/h}$ but the same initial distance $s(0) = 25.95\,\text{m}$ as calculated above. At the end of the reaction time, the child is just

$$s(T_r) = s(0) - v_2 T_r = 6.50\,\text{m}$$

away from the front bumper. Now, the driver would need the additional braking distance $s_B(v_2) = 23.6\,\text{m}$ for a complete stop. However, only 6.50 m are available resulting in a difference $\Delta s = 17.13\,\text{m}$. With this information, the speed at collision can be calculated by solving $\Delta s = (\Delta s)_B(v) = v^2/(2b_{\max})$ for $v$, i.e.,

$$v_{\text{coll}} = \sqrt{2b_{\max}\Delta s} = 16.56\,\text{m/s} = 59.6\,\text{km/h}.$$

*Remark:* This problem stems from a multiple-choice question of the theoretical exam for a German driver's licence. The official answer is 60 km/h.

## Problems of Chapter 12

### 12.1 Conditions for the Microscopic Fundamental Diagram

The plausibility condition (12.5) is valid for any speed $v_l$ of the leading vehicle. This also includes standing vehicles where Eq. (12.5) becomes $f(s,0,0) = 0$ for $s \le s_0$. This corresponds to the steady-state condition $v_e(s) = 0$ for $s \le s_0$.

Conditions (12.1) and (12.2) are valid for any speed $v_l$ of the leader as well, including the steady-state situation $v_l = v$ or $\Delta v = 0$. For the alternative acceleration function $\tilde{a}(s, v, \Delta v)$, this means

$$\frac{\partial \tilde{f}(s,v,0)}{\partial s} \ge 0, \quad \frac{\partial \tilde{f}(s,v,0)}{\partial v} < 0.$$

Along the one-dimensional manifold of steady-state solutions $\{v_e(s)\}$ for $s \in [0,\infty[$, we have $\tilde{f}(s, v_e(s), 0) = 0$, so the differential change $\mathrm{d}\tilde{f}$ along the equilibrium curve $v_e(s)$ must vanish as well:

$$\mathrm{d}\tilde{f} = \frac{\partial \tilde{f}(s, v_e(s), 0)}{\partial s}\mathrm{d}s + \frac{\partial \tilde{f}(s, v_e(s), 0)}{\partial v} v_e'(s)\mathrm{d}s = 0,$$

hence

$$v_e'(s) = \frac{-\partial \tilde{f}(s, v, 0)/\partial s}{\partial \tilde{f}(s, v, 0)/\partial v} \geq 0.$$

If the leading vehicle is outside the interaction range, we have $v_e'(s) = 0$ (second condition of Eq. (12.2)). Finally, the condition $\lim_{s\to\infty} v_e(s) = v_0$ follows directly from the second part of condition (12.1).

### 12.2 Rules of Thumb for the Safe Gap and Braking Distance

*Subproblem 1.* One mile corresponds to 1.609 km. However, the US rule does not give explicit values for a vehicle length. Here, we assume $15\,\mathrm{ft} = 4.572\,\mathrm{m}$. In any case, the gap $s$ increases linearly with the speed $v$, so the time gap $T = s/v$ is independent of speed. Implementing this rule, we obtain

$$T = \frac{s}{v} = \frac{15\,\mathrm{ft}}{10\,\mathrm{mph}} = \frac{4.572\,\mathrm{m}}{16.09\,\mathrm{km/h}} = \frac{4.572\,\mathrm{m}}{4.469\,\mathrm{m/s}} = 1.0\,\mathrm{s}.$$

Notice that, in the final result, we rounded off generously. After all, this is a rule of thumb and more significant digits would feign a non-existent precision.[9] Notice that this rule is consistent with typically observed gaps (cf. Fig. 5.7).

*Subproblem 2.* Here, the speedometer reading is in units of km/h, and the space gap is in units of meters. Again, the quotient, i.e., the time gap $T$ is constant and given by (watch out for the units)

$$T = \frac{s}{v} = \frac{\frac{1}{2}\mathrm{m}\left(\frac{v}{\mathrm{km/h}}\right)}{v} = \frac{\frac{1}{2}\mathrm{m}}{\mathrm{km/h}} = \frac{0.5\,\mathrm{h}}{1{,}000} = \frac{1{,}800\,\mathrm{s}}{1{,}000} = 1.8\,\mathrm{s}.$$

*Subproblem 3.* The kinematic *braking distance* is $s(v) = v^2/(2b)$, so the cited rule of thumb implies that the braking deceleration does not depend on speed. By solving the kinematic braking distance for $b$ and inserting the rule, we obtain (again, watch out for the units)

$$b = \frac{v^2}{2s} = \frac{v^2}{0.02\,\mathrm{m}}\left(\frac{\mathrm{km}}{\mathrm{h}\,v}\right)^2 = \frac{50}{3.6^2}\mathrm{m/s^2} = 3.86\,\mathrm{m/s^2}.$$

For reference, comfortable decelerations are below $2\,\mathrm{m/s^2}$ while emergency braking decelerations on dry roads with good grip conditions can be up to $10\,\mathrm{m/s^2}$, about $6\,\mathrm{m/s^2}$ for wet conditions, and less than $2\,\mathrm{m/s^2}$ for icy conditions. This means, the above rule could lead to accidents for icy conditions but is okay, otherwise.

### 12.3 Reaction to Vehicles Merging into the Lane

[9] There is also a more conservative variant of this rule where one should leave one car length every five mph corresponding to the "two-second rule" $T = 2.0\,\mathrm{s}$.

*Reaction for the IDM.* For $v = v_0/2$, the IDM steady-state space gap reads

$$s_e(v) = \frac{s_0 + vT}{\sqrt{1 - \left(\frac{v}{v_0}\right)^\delta}} = \frac{s_0 + \frac{v_0 T}{2}}{\sqrt{1 - \left(\frac{1}{2}\right)^\delta}}.$$

The prevailing contribution comes from the prescribed time headway (for $s_0 = 2\,\mathrm{m}$ and $\delta = 4$, the other contributions only make up about 10%). This problem assumes that the merging vehicle reduces the gap to the considered follower to half the steady-state gap, $s = s_e/2 = v_0 T/4$, while the speed difference remain zero. The new IDM acceleration of the follower (with $a = 1\,\mathrm{m/s^2}$ and $\delta = 4$) is therefore

$$\begin{aligned}
\dot{v}_{\mathrm{IDM}} &= a\left[1 - \left(\frac{v}{v_0}\right)^\delta - \left(\frac{s_0 + vT}{s}\right)^2\right] \\
&\overset{(v=v_0/2,\, s=s_e/2)}{=} a\left[1 - \left(\frac{1}{2}\right)^\delta - \left(\frac{s_0 + v_0 T/2}{s_e/2}\right)^2\right] \\
&\overset{s_e(v)=s_e(v_0/2)}{=} -3a\left[1 - \left(\frac{1}{2}\right)^\delta\right] = -\frac{45}{16}\,\mathrm{m/s^2} = -2.81\,\mathrm{m/s^2}.
\end{aligned}$$

*Reaction for the simplified Gipps' model.* For this model, the steady-state gap in the car-following regime reads $s_e(v) = v\Delta t$. Again, at the time of merging, the merging vehicle has the same speed $v_0/2$ as the follower, and the gap is half the steady-state gap, $s = (v\Delta t)/2 = v_0 \Delta t/4$. The new speed of the follower is restricted by the safe speed $v_{\mathrm{safe}}$:

$$v(t + \Delta t) = v_{\mathrm{safe}} = -b\Delta t + \sqrt{b^2(\Delta t)^2 + \left(\frac{v_0}{2}\right)^2 + \frac{b v_0 \Delta t}{2}} = 19.07\,\mathrm{m/s}.$$

This results in an effective acceleration

$$\left(\frac{\mathrm{d}v}{\mathrm{d}t}\right)_{\mathrm{Gipps}} = \frac{v(t + \Delta t) - v(t)}{\Delta t} \approx -0.93\,\mathrm{m/s^2}.$$

We conclude that the Gipps' model describes a more relaxed driver reaction compared to the IDM. Notice that both the IDM and Gipps' model would generate significantly higher decelerations for the case of slower leading vehicles (dangerous situation).

### 12.4 The IDM Braking Strategy

A braking strategy is self-regulating if, during the braking process, the *kinematically necessary deceleration* $b_{\mathrm{kin}} = v^2/(2s)$ approaches the comfortable deceleration $b$. In order to show this, we calculate the rate of change of the kinematic deceleration (applying the quotient and chain rules of differentiation when necessary) and set $\dot{s} = -v$ and $\dot{v} = -b_{\mathrm{kin}}^2/b = -v^4/(4bs^2)$, afterwards. This eventually gives Eq. (12.27) of

the main text:

$$\frac{\mathrm{d}b_{\mathrm{kin}}}{\mathrm{d}t} = \frac{\mathrm{d}}{\mathrm{d}t}\left(\frac{v^2}{2s}\right) = \frac{4vs\dot{v} - 2v^2\dot{s}}{4s^2}$$
$$= \frac{v^3}{2s^2}\left(1 - \frac{v^2}{2sb}\right) = \frac{v\,b_{\mathrm{kin}}}{s\,b}\left(b - b_{\mathrm{kin}}\right),$$

### 12.5 Analysis of a Microscopic Model

*Subproblem 1 (parameters).* For interaction-free accelerations, $v_{\mathrm{safe}} > v_0$, so $v_{\mathrm{safe}}$ is not relevant. Hence $v_0$ denotes the desired speed, and $a$ the absolute value of the acceleration and deceleration for the cases $v < v_0$ and $v > v_0$, respectively. The steady-state conditions $s = \text{const.}$ and $v = v_l = v_e = \text{const.}$ give

$$v_e = \min(v_0, v_{\mathrm{safe}}).$$

Without interaction, $v_{\mathrm{safe}} > v_0$, so $v_e = v_0$. With interactions, the safe speed becomes relevant and the above condition yields

$$v_e = v_{\mathrm{safe}} = -aT + \sqrt{a^2T^2 + v_e^2 + 2a(s - s_0)}$$

which can be simplified to

$$s = s_0 + v_e T.$$

Thus, $s_0$ is the minimum gap for $v = 0$, and $T$ the desired time gap. The model produces a deceleration $-a$ not only if $v > v_0$ (driving too fast in free traffic) but also if $v > v_{\mathrm{safe}}$ (driving too fast in congested situations). Furthermore, the model is symmetrical with respect to accelerations and decelerations. Obviously, it is not accident free.

*Subproblem 2 (steady-state speed).* We have already derived the steady-state condition

$$v_e(s) = \min\left(v_0, \frac{s - s_0}{T}\right).$$

Macroscopically, this corresponds to the triangular fundamental diagram

$$Q_e(\rho) = \min\left(v_0\rho, \frac{1 - \rho\, l_{\mathrm{eff}}}{T}\right)$$

where $l_{\mathrm{eff}} = 1/\rho_{\max} = l + s_0$. The capacity per lane is given by $Q_{\max} = (T + l_{\mathrm{eff}}/v_0)^{-1} = 1{,}800\,\mathrm{veh/h}$ at a density $\rho_{\mathrm{C}} = 1/(l_{\mathrm{eff}} + v_0 T) = 25\,/\mathrm{km}$. For further properties of the triangular fundamental diagram, see Section 9.6.

*Subproblem 3.* The acceleration and braking distances to accelerate from 0 to $20\,\mathrm{m/s}$ or to brake from $20\,\mathrm{m/s}$ to 0, respectively, are the same:

$$s_\mathrm{a} = s_b = \frac{v_0^2}{2a} = 200\,\mathrm{m}.$$

At a minimum gap of 3 m and the location $x_\mathrm{stop} = 603\,\mathrm{m}$ of the stopping line of the traffic light, the acceleration takes place from $x = 0$ to $x_1 = 200\,\mathrm{m}$, and the deceleration from $x_2 = 400\,\mathrm{m}$ to $x_3 = 600\,\mathrm{m}$. The duration of the acceleration and deceleration phases is $v_0/a = 20\,\mathrm{s}$ while the time to cruise the remaining stretch of 200 m at $v_0$ amounts to 10 s. This completes the information to mathematically describe the trajectory:

$$x(t) = \begin{cases} \frac{1}{2}at^2 & t \le t_1 = 20\,\mathrm{s}, \\ x_1 + v_0(t - t_1) & t_1 < t \le t_2 = 30\,\mathrm{s}, \\ x_2 + v_0(t - t_2) - \frac{1}{2}a(t - t_2)^2 & t_2 < t \le t_3 = 50\,\mathrm{s}, \end{cases}$$

where $t_1 = 20\,\mathrm{s}$, $t_2 = 30\,\mathrm{s}$ and $t_3 = 50\,\mathrm{s}$.

### 12.6 Heterogeneous Traffic

The simultaneous effects of heterogeneous traffic and several lanes with lane-changing and overtaking possibilities results in a curved free part of the fundamental diagram even for models that would display a triangular fundamental diagram for identical vehicles and drivers (as the Improved Intelligent Driver Model, IIDM). This can be seen as follows: For heterogeneous traffic, each vehicle-driver class has a different fundamental diagram. Particularly, the density $\rho_C$ at capacity is different for each class, so a simple weighted average of the individual fundamental diagrams would result in a curved free part and a rounded peak. However, without lane-changing and overtaking possibilities, all vehicles would queue up behind the vehicles of the slowest class resulting in a straight free part of the fundamental diagram with the gradient representing the lowest free speed.[10] So, both heterogeneity and overtaking possibilities are necessary to produce a curved free part of the fundamental diagram.

### 12.7 City Traffic in the Improved IDM

[10] Even when obstructed, drivers can choose their preferred gap (in contrast to the desired speed), so the congested branch of the fundamental diagram is curved even without overtaking possibilities.

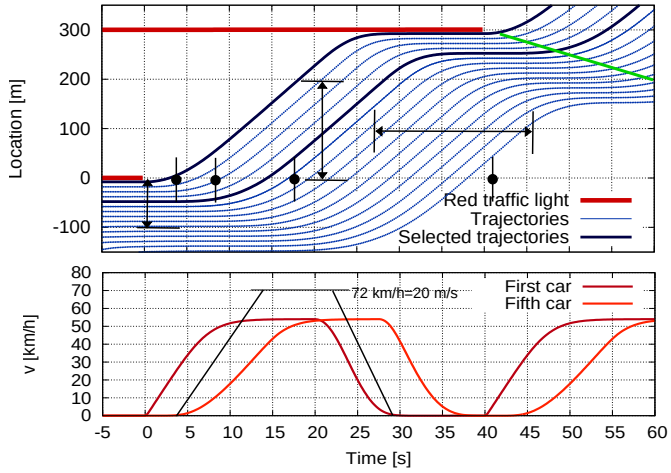


1. For realistic circumstances, the maximum possible flow is given by the *dynamic* capacity, i.e., the outflow from moving downstream congestion fronts. In our case, the "congestion" is formed by the queue of standing vehicles behind a traffic light. Counting the trajectories (horizontal double-arrow in the upper diagram) yields
$$C = Q_{\max} \approx \frac{9\,\text{veh}}{20\,\text{s}} = 1,620\,\text{veh/h}.$$
2. Counting the trajectories passing $x = 0$ for times less than 5 s, 15 s, and 40 s (black bullets in the upper diagram) gives
$$n(5) = 1,\ n(15) = 5,\ n(40) = 15,$$
respectively. We determine $\beta$ by the average time headway after the first vehicles have passed,
$$\beta = \frac{1}{C} = \frac{40\,\text{s} - 15\,\text{s}}{15 - 5} = 2.5\,\text{s/veh}.$$
We observe, that $\beta$ denotes the inverse of the capacity. The obtained value agrees with the result of the first subproblem within the "measuring uncertainty" of one vehicle.[11] This also gives the *additional time* until the first vehicle passes: $\tau_0 = 15\,\text{s} - 5\beta = 2.5\,\text{s}$. (Notice that this is *not* a reaction time since the IIDM does not have one.)
3. The propagation velocity of the position of the starting vehicles in the queue is read off from the upper diagram:
$$w = -\frac{100\,\text{m}}{20\,\text{s}} = -5\,\text{m/s} = -18\,\text{km/h}.$$

[11] One could have calculated $\beta$ as well using the pairs $\{n(15), n(5)\}$ or $\{n(40), n(5)\}$ with similar results.

4. We estimate the desired speed by the maximum speed of the speed profile (lower diagram): $v_0 = 15\,\mathrm{m/s} = 54\,\mathrm{km/h}$. The effective length $l_{\mathrm{eff}}$ is equal to the distance between the standing vehicles in the upper diagram: $\rho_{\max} = 1/l_{\mathrm{eff}} = 10\,\mathrm{s}/100\,\mathrm{m} = 100\,\mathrm{veh/km}$, i.e., $l_{\mathrm{eff}} = 10\,\mathrm{m}$. Since the steady state of this model corresponds to a triangular fundamental diagram, the time gap parameter $T$ is determined by the propagation speed and the maximum density: $T = -l_{\mathrm{eff}}/c = 2\,\mathrm{s}$. Finally, the maximum acceleration $a$ and the comfortable deceleration $b$ can be read off the lower diagram by estimating the maximum and minimum gradient of the speed profile:

$$a = \frac{20\,\mathrm{m/s}}{10\,\mathrm{s}} = 2\,\mathrm{m/s^2}, \quad b = \frac{20\,\mathrm{m/s}}{7\,\mathrm{s}} = 2.9\,\mathrm{m/s^2}.$$

**12.8 Statistical Properties of the Ornstein-Uhlenbeck Process**

To determine the expectation $E(\eta(t)\eta(t'))$ from the given formal solution $\eta(t)$ to the stochastic differential equation of the Ornstein-Uhlenbeck process, we insert the formal solution into $E(\eta(t)\eta(t'))$ carefully distinguishing the arguments $t$ and $t'$ from the formal integration variables $t_1$ and $t_2$. This gives the double integral

$$E(\eta(t)\eta(t')) = \frac{2}{\tilde{\tau}} \int_{t_1=-\infty}^{t} \int_{t_2=-\infty}^{t'} \mathrm{e}^{-(t-t_1+t'-t_2)/\tilde{\tau}} E(\xi(t_1)\xi(t_2))\,\mathrm{d}t_1\mathrm{d}t_2.$$

Notice that the operations of integration and averaging (expectation value) are exchangeable. We now consider the case $t > t'$. Setting $E(\xi(t_1)\xi(t_2)) = \delta(t_1 - t_2)$ and using the definition $\int f(t)\delta(t)\mathrm{d}t = f(0)$ of the Dirac $\delta$-distribution to eliminate the integral over $t_1$[12] yields

$$E(\eta(t)\eta(t')) = \frac{2}{\tilde{\tau}} \int_{t_2=-\infty}^{t'} \mathrm{e}^{(2t_2-t-t')/\tilde{\tau}}\,\mathrm{d}t_2$$

which can be analytically solved resulting in

$$E(\eta(t)\eta(t')) = \mathrm{e}^{-(t-t')/\tau}.$$

If $t < t'$, the derivation proceeds analogously resulting in $E(\eta(t)\eta(t')) = \mathrm{e}^{-(t'-t)/\tau}$. Consolidating these two cases, we arrive at

$$E(\eta(t)\eta(t')) = \mathrm{e}^{-|t-t'|/\tau}.$$

As important special case, we obtain the variance $E\left(\eta^2(t)\right) = 1$. Finally, when we apply the averaging operation $E(\cdot)$ to the formal solution $\eta(t)$ itself using the condition $E(\xi(t)) = 0$, we obtain $E(\eta(t)) = 0$, i.e., the second condition (12.46).

[12] Since $t \geq t'$ and the above integration property of the $\delta$-distribution only applies if the integration interval includes zero (i.e., $t_1 = t_2$), we cannot use this property to eliminate the integral over $t_2$.

This concludes the derivation of the statistical properties of the Ornstein-Uhlenbeck process.

### 12.9 Driving in Curves

1. Anticipation is needed because some time may be needed to reduce the speed from the actual speed to $v_0^{\text{curve}}$. Moreover, for safety reasons, one should have finished the deceleration maneuver before entering the curve.
2. For a finite lateral slope angle $\beta$, the lateral acceleration relative to the road surface consists of two components.
   - Inertial acceleration $v^2/r$ multiplied with the projection factor $\cos\beta$ parallel to the road surface.
   - Lateral slope force: gravitational acceleration $g$ multiplied with the projection factor $-\sin\beta$ (for a proper lateral slope, the slope force is directed oppositely to the inertial force).

   This gives $\dot{v}_{\text{lat}} = v^2/r\ \cos\beta - g\sin\beta$ and, setting $\dot{v}_{\text{lat}} = b$, the safe speed

$$v_{\text{safe}} = \sqrt{\frac{r(b+g\sin\beta)}{\cos\beta}} = 12.2\,\text{m/s} = 44.0\,\text{km/h}.$$

3. The speed becomes critical if the ratio of the lateral and normal acceleration (relative to the road surface) reaches the friction coefficient $\mu$. As the lateral component, also the normal component has two contributions, one from the gravitation ($g\cos\beta$) and one from the inertial acceleration ($v^2/r\ \sin\beta$). This gives a critical speed

$$v_{\text{crit}} = \sqrt{\frac{rg(\mu\cos\beta+\sin\beta)}{\cos\beta-\mu\sin\beta}} = 23.2\,\text{m/s} = 83.6\,\text{km/h}.$$

   When restricting to the lateral comfortable deceleration, the speed safety factor until one slides out of the curve is nearly 2. Notice that the critical speed tends to infinity for $\tan\beta = 1/\mu$ which is realized on some racing courses or test tracks.

## Problems of Chapter 13

### 13.1 Consequences of Estimation Errors

Overestimating the gap by 10%, i.e., by the factor 1.1 results in a *smaller* steady-state gap. With the values of the problem statement, we obtain

$$1.1 s_e = s_0 + vT \quad \Rightarrow \quad s_e = \frac{s_0+vT}{1.1} = 28.3\,\text{m}$$

instead of the "true" steady-state $s_e = 31.1\,\text{m}$. When there is a constant additive acceleration component $a_{\text{thr}} = 0.4\,\text{m/s}^2$, the steady-state condition reads

$$\dot{v} = a_{\text{thr}} + \frac{\frac{s_e - s_0}{T} - v}{\tau} \stackrel{!}{=} 0,$$

or $s_e = s_0 + vT - \tau a_z = 30.9\,\text{m}$. Notice that the surprisingly small amount of change can be tracked back to the "rigidity" of the OVM reaction caused by the small relaxation time $\tau$.

### 13.2 Multi-Anticipation for the IDM

Applying the general equation (13.12) for multi-anticipative effects to the IDM gives

$$c \sum_{j=1}^{n_\text{a}} a \left( \frac{s_0 + vT}{js} \right)^2 = a \left( \frac{s_0 + vT}{s} \right)^2,$$

hence $c = 1/(\sum_{j=1}^{n_\text{a}} \frac{1}{j^2})$, i.e., Eq. (13.13). Instead of introducing $c$, it is obviously possible for the IDM to *renormalize* the parameters $s_0$ and $T$ by multiplying them with a common factor. For this purpose, we write the left-hand side of above equation as

$$\sum_{j=1}^{n_\text{a}} a \left( \frac{\sqrt{c} s_0 + v\sqrt{c} T}{js} \right)^2,$$

so the factor $\sqrt{c}$ of the problem statement is evident. The factor $\sqrt{c}$ assumes values between 1 (no multi-anticipation) and $\sqrt{6}/\pi \approx 0.78$ (multi-anticipation to infinitely many leaders). This means, the numerical values of $s_0$ and $T$ are reduced by no more than 22%.

### 13.3 Wiedemann Model

1. Without the Heaviside function $\Theta(\Delta v + \Delta v_0)$ in (13.28), the plausibility condition (12.4) would be violated for $\Delta v < -\Delta v_0$ because, then, the acceleration would decrease for increasing leading speed. The leading *acceleration* has been added because only then this equation (for $\Delta v_0 = 0$) is based on the constant-acceleration heuristic: The follower brakes in a way that, under this heuristic, the minimum gap $s = s_\text{AX}$ is realized. ($\Delta v_0$ acts as a safety contribution representing an uncertainty in estimating relative speeds.) Finally, adding the term $-b_0$ to (13.28) makes sure that, at least for $\dot{v}_l \le 0$, $\dot{v}_\text{following} > \dot{v}_\text{brake}$ holds at the boundary between the following and the deceleration regime satisfying (12.1) and also between the following and approaching regime satisfying (12.1) and (12.4).
2. W-74 and W-99 accelerations for $v_0 = 100\,\text{km/h}$, $\dot{v}_l = 0$:
   (i) If $v = v_l = 20\,\text{m/s}$, and $s = 15\,\text{m}$, both the W-74 and W-99 models are in the braking regime and the acceleration (assumed to be the same) is given by $\dot{v}_\text{W-74} = \dot{v}_\text{W-99} = -0.95\,\text{m/s}^2$.
   (ii) If $v = 21.5\,\text{m/s}$, $v_l = 20\,\text{m/s}$, and $s = 40\,\text{m}$, the W-74 model is in the approaching regime resulting in $\dot{v}_\text{W-74} = -0.66\,\text{m/s}^2$ while the W-99 model is in the free regime with $\dot{v}_\text{W-99} = 0.79\,\text{m/s}^2$

## Problems of Chapter 14

### 14.1 Dynamic Properties of the Nagel-Schreckenberg Model

To obtain physical units, we multiply the dimensionless desired speed of the NSM with $\Delta x/\Delta t$. Thus, $v_0 = 2$ (city traffic) corresponds to 54 km/h, and $v_0 = 5$ (highways) to 135 km/h. Likewise, multiplying the dimensionless accelerations with $\Delta x/(\Delta t)^2 = 7.5\,\mathrm{m/s^2}$ yields the physical accelerations. In the deterministic NSM, $a = 1$, so $a_{\mathrm{phys}} = 7.5\,\mathrm{m/s^2}$ resulting in an acceleration time of

$$\tau_{0\to 100} = \frac{v_{\mathrm{phys}}}{a_{\mathrm{phys}}} = 3.7\,\mathrm{s}.$$

In the stochastic model, the acceleration $a$ is realized only with a probability $(1-p)$. So, the average acceleration time increases by a factor $(1-p)^{-1}$ to 6.2 s.

### 14.2 Approaching a Red Traffic Light

The driver approaches with the desired speed $v_0$ until the distance to the traffic light falls below the "interaction distance" $g = v_0$. Then, there are two possibilities for the deceleration process: (i) stopping in one step (if, after crossing the interaction point, the gap in the next time step is already zero), (ii) stopping in two steps $v_0 \to v_1 \to 0$ (if the gap after crossing the interaction point is $v_1 > 0$). If $v_0 = 2$, the realized decelerations are (i) $-15\,\mathrm{m/s^2}$ or (ii) $-7.5\,\mathrm{m/s^2}$.

### 14.3 Fundamental Diagram of the Deterministic Nagel-Schreckenberg Model

Without stochastic components, the steady-state speed as a function of the gap $g$ is well-defined:

$$v_e(g) = \max(v_0, g)$$

meaning that the macroscopic fundamental diagram (in physical units) has the well-known triangular shape given by[13]

$$Q_e(\rho) = \min\left[V_0^{\mathrm{phys}}\rho, \frac{1}{T}\left(1 - \frac{\rho}{\rho_{\max}}\right)\right].$$

The values of its three parameters are

$$V_0^{\mathrm{phys}} = v_0 \Delta x/\Delta t = \begin{cases} 54\,\mathrm{km/h} & \text{cities,} \\ 135\,\mathrm{km/h} & \text{highways,} \end{cases}$$

$$T = \Delta t = 1\,\mathrm{s}, \quad \rho_{\max} = \frac{1}{\Delta x} = 133\,\mathrm{veh/km}.$$

In the stochastic model ($p > 0$), the average flow $E\,(Q(\rho))$ as a function of the local density is below that of the deterministic case. The fundamental diagram is no longer triangular, and also the gradients at zero and maximum density are different. In the following two problems, we will derive

[13] We drop the superscripts "phys" denoting physical quantities where no confusion is possible, i.e., for $\rho$ and $Q$. We will retain the superscripts for speeds and velocities.

$$V_0^{\text{phys}} = Q_e'(0) = (v_0 - p)\frac{\Delta x}{\Delta t}, \quad w^{\text{phys}}(\rho_{\max}) = Q_e'(\rho_{\max}) = -(1-p)\frac{\Delta x}{\Delta t}.$$

**14.4 Macroscopic Desired Speed**

Without interaction and after a sufficient time, the vehicle speed is either $v_0$ (no dawdling in the last time step), or $v_0 - 1$ (dawdling). If $v = v_0$, then the speed will be reduced in the next time step to $v_0 - 1$ with probability $p$. If $v = v_0 - 1$, the speed in the next time step will reach $v_0$ with probability $1 - p$. The situation is stationary in the stochastic sense if expectation values do not change over time, $E(v(t+1)) = E(v(t))$. Here, this means that the probabilities for the speeds $v_0$ and $v_0 - 1$ do not change over time, i.e., the unconditional "probability fluxes" from $v_0$ to $v_0 - 1$ and from $v_0 - 1$ to $v_0$ balance to zero.[14] Setting up the balance for the speed state $v = v_0$ and denoting by $\theta$ the probability for this state, the probability flux $v_0 \to v_0 - 1$ away from $v_0$ is $-\theta p$ (probability $\theta$ times conditional probability $p$; negative sign because the flux is outflowing). The "inflowing" probability flux $v_0 - 1 \to v_0$ is $(1-\theta)(1-p)$ (probability $1-\theta$ times conditional probability $1-p$) . So, stationarity implies

$$\frac{\mathrm{d}}{\mathrm{d}t}\left(\text{Prob}(v = v_0)\right) = -\theta p + (1-\theta)(1-p) \stackrel{!}{=} 0 \;\Rightarrow\; \theta = 1 - p,$$

or

$$E(v) = \theta v_0 + (1-\theta)(v_0 - 1) = v_0 - p.$$

In physical units, this means $V^{\text{phys}} = E(v)\Delta x/\Delta t$, i.e., the result displayed above in the solution to Problem 14.4.

**14.5 Propagation Velocity of Downstream Jam Fronts**

Assume a queue of standing vehicles where only the first vehicle has space to accelerate. This first vehicle will accelerate with probability $1 - p$ (with probability $p$, dawdling occurs). Only if this vehicle accelerates, the next vehicle in the queue has the possibility to accelerate in the next time step, which it does, again, with probability $1 - p$. This means, the "starting wave" propagates at an average wave velocity $w = -(1-p)\Delta x/\Delta t$. For $p = 0.4$, this yields the reasonable value $w = -16.2\,\text{km/h}$.

## Problems of Chapter 15

**15.1 Why the Grass is Always Greener on the Other Side?**

We assume two lanes with staggered regions of highly congested traffic $(\rho_1, V_1)$ and less congested traffic ($\rho_2 < \rho_1$, $V_2 > V_1$) of the same length: Whenever there is highly congested traffic on lane 1, congestion is less on lane 2, and vice versa (cf. the figure in the problem statement). Since traffic in both regions is (more or less) congested and the fundamental diagram is triangular by assumption, the transitions from region 1 and 2 and from 2 to 1 remain sharp and propagate according to the

[14] Mathematically, this balance of probability fluxes is called a *Master equation*.

shock-wave formula (9.9) at a constant velocity

$$c = \frac{Q_2 - Q_1}{\rho_2 - \rho_1} = -\frac{l}{T} = -5\,\mathrm{m/s}.$$

The fraction of time in which drivers are stuck in the highly congested regions is obviously equal to the fraction of time spent in regions of type 1. Denoting by $\tau_i$ the time intervals $\tau_i$ to pass one region $i = 1$ or 2, we express this fraction by

$$p_{\text{slower}} = p_1 = \frac{\tau_1}{\tau_1 + \tau_2}\,.$$

When evaluating $\tau_i$, it is crucial to realize that the regions propagate in the opposite direction to the vehicles, so the relative velocity $V_i + |c|$ is relevant. Assuming equal lengths $L$ for both regions, the passage times are $\tau_i = L/(V_i + |c|)$, so

$$p_1 = \frac{\frac{L}{V_1+|c|}}{\frac{L}{V_1+|c|} + \frac{L}{V_2+|c|}} = \frac{V_2 + |c|}{V_2 + V_1 + 2|c|}.$$

For example, if $V_1 = 0$ and $V_2 = 10\,\mathrm{m/s}$, the fraction is

$$p_1 = \frac{10+5}{10+10} = \frac{3}{4},$$

i.e., drivers are stuck in the slower lane 75% of the time – regardless which lane they choose or of whether they change lanes or not.

Alternatively, one picks out a vehicle at random. Since the less and highly congested regions have the same length, the fraction of vehicles in the highly congested region, i.e., the probability of picking one from this region, is given by

$$p_1 = \frac{\rho_1}{\rho_1 + \rho_2} = \frac{200}{200 + 200/3} = \frac{3}{4}.$$

**15.2 Amber Time Intervals – Stop or Cruise?**

We distinguish two cases: (i) Drivers can pass the traffic light at unchanged speed in the amber/yellow phase, i.e.,

$$s < s_1 = v\tau_y.$$

(ii) When cruising, drivers would pass the traffic light in the red phase, so stopping is mandatory. In this case, drivers need a reaction time $T_r$ to perceive the signal, make a decision, and stepping on the braking pedal. Afterwards, we assume that they brake at a constant deceleration $b$ so as to stop just at the stopping line. This results in the *stopping distance*

$$s = vT_r + \frac{v^2}{2b}. \tag{9}$$

Obviously, the *worst case* for the initial distance $s$ to the stopping line at switching time green-yellow is the threshold $s = s_1$ between (i) and (ii), i.e., cruising is just no more legal. Inserting $s = s_1$ into Eq. (9) and solving for $b$ gives

$$b = \frac{v}{2(\tau_y - T_r)} \; = \; 3.47\,\mathrm{m/s^2}.$$

This is a significant, though not critical, deceleration. It is slightly below the deceleration $3.86\,\mathrm{m/s^2}$ implied by the stopping or braking distance rule "speedometer reading in km/h squared divided by 100" (Problem 12.2) but above typical comfortable decelerations of the order of $2\,\mathrm{m/s^2}$. We conclude that the legal minimum duration of amber phases is consistent with the driver and vehicle capabilities.

### 15.3 Trajectory Planning of a Lane Change

The trajectory and its derivatives are given by

$$\begin{aligned} y(t) &= c_0 + c_1 t + c_2 t^2 + c_3 t^3 + c_4 t^4 + c_5 t^5, \\ y'(t) &= c_1 + 2c_2 t + 3c_3 t^2 + 4c_4 t^3 + 5c_5 t^4, \\ y''(t) &= 2c_2 + 6c_3 t + 12c_4 t^2 + 20c_5 t^3. \end{aligned}$$

Setting $w = \tau = 1$, we have the fixed constraints

$$y(0) = y'(0) = y''(0) = 0, \quad y(1) = 1, \quad y'(1) = y''(1) = 0.$$

The conditions at $t = 0$ give immediately $c_0 = c_1 = c_2 = 0$. The remaining coefficients are given by the restraints at $t = 1$ (end of lane change),

$$\begin{aligned} c_3 + c_4 + c_5 &= 1, \\ 3c_3 + 4c_4 + 5c_5 &= 0, \\ 6c_3 + 12c_4 + 20c_5 &= 0. \end{aligned}$$

Solving this linear equation with three unknowns give

$$c_3 = 10, \quad c_4 = -15, \quad c_5 = 6.$$

The unscaled coefficients of (15.13) are given by multiplying the found coefficients $c_j$ with $w/\tau^j$.

### 15.4 Stop or Cruise Decisions Implied by Car-Following Models

1. This MOBIL decision criterion means that one brakes to a stop whenever the braking deceleration at decision time is smaller than the safe braking deceleration. Otherwise one cruises through the intersection. In sensible models as the IDM, one tries to bring the situation under control whenever the required braking deceleration is above the comfortable deceleration $b$. Assuming $b_{\mathrm{safe}} > b$ this means that the initial deceleration is the highest, so a safe deceleration to a stop is guaranteed.

2. If the decision is "stop", one assumes a virtual standing vehicle of length zero at the stopping line, i.e., $v_l = 0$ or $\Delta v = v$. Evaluating the decision criterion for the IDM gives

$$\begin{aligned} \frac{\mathrm{d}v}{\mathrm{d}t} = -a\left(\frac{s^*(v,v_l)}{s}\right)^2 &> -b_{\text{safe}} \\ a\left(\frac{s^*(v,v_l)}{s}\right)^2 &< b_{\text{safe}} \\ a\frac{(s^*(v,v_l))^2}{b_{\text{safe}}} &< s^2. \end{aligned}$$

   This means, the general critical gap is given by

$$s > s_{\text{safe}}(v) = s^*(v,0)\sqrt{\frac{a}{b_{\text{safe}}}}. \tag{10}$$

3. For $a = b = b_{\text{safe}}$, we obtain for $v = v_0$

$$s > s_{\text{safe}}(v) = s^*(v,0) = s_0 + v_0 T + \frac{v_0^2}{2b}.$$

   If the time gap parameter $T$ also gives the reaction time, this is precisely the minimum gap $s_0$ plus the stopping distance with its components reaction distance $vT$ and braking distance $v^2/(2b)$. Specific values:

   - $v_0 = 50\,\text{km/h}:\ s_{\text{safe}} = s^*(v_0,0) = 62\,\text{m},\ \Delta t_{\text{safe}} = s_{\text{safe}}/v_0 = 4.47\,\text{s}$
   - $v_0 = 70\,\text{km/h}:\ s_{\text{safe}} = s^*(v_0,0) = 114\,\text{m},\ \Delta t_{\text{safe}} = s_{\text{safe}}/v_0 = 5.86\,\text{s}$

4. The above critical distances and associated critical time intervals till passing are too great. Considering that the minimum amber times for 50 km/h and 70 km/h are given by 3 s and 4 s, respectively, this strategy may lead to crossing red traffic lights. Of course, the reason is that the legislation imposes on the driver a safe deceleration $b_{\text{safe}}$ that is somewhat greater than the comfortable deceleration $b$. In this case, we obtain from the above general formula (10) for $b_{\text{safe}} = 4\,\text{m/s}^2$,

   - $v_0 = 50\,\text{km/h}:\ s_{\text{safe}} = 44\,\text{m},\ \Delta t_{\text{safe}} = s_{\text{safe}}/v_0 = 3.16\,\text{s}$
   - $v_0 = 70\,\text{km/h}:\ s_{\text{safe}} = s^*(v_0,0) = 81\,\text{m},\ \Delta t_{\text{safe}} = s_{\text{safe}}/v_0 = 4.14\,\text{s}$

   There is still a minimal chance of passing a red traffic light if the amber/yellow times are at their minimum allowed values of 3 s and 4 s, respectively. This is due to an IDM imperfection: At the beginning of a stopping maneuver, the IDM tends to "brake" a little too hard.
5. For the OVM, we have the critical gap

$$\dot{v}_{\text{OVM}} = \frac{v_{\text{opt}}(s) - v}{\tau} < -b_{\text{safe}}.$$

   Because only the interacting range $s < v_0 T$ is relevant, this leads to

$$\dot{v}_{\mathrm{OVM}} = \frac{s/T - v}{\tau} > -b_{\mathrm{safe}}, \quad \Rightarrow \quad s > s_{\mathrm{safe}} = T\,(v - \tau b_{\mathrm{safe}})$$

or $s > s_{\mathrm{safe}} = T(v - \tau b_{\mathrm{safe}})$. For $v = v_0 = 72\,\mathrm{km/h} = 20\,\mathrm{m/s}$, $\tau = T/2 = 0.5\,\mathrm{s}$, and $b_{\mathrm{safe}} = 4\,\mathrm{m/s^2}$, this results in $s_{\mathrm{safe}} = 9.0\,\mathrm{m}$. This is much too low: For example, one would brake if $s = 10\,\mathrm{m}$. However, at this gap, the kinematic braking deceleration to avoid crossing the stopping line (and stopping mid-intersection instead) is given by $b_{\mathrm{kin}} = v^2/(2s) = 20\,\mathrm{m/s^2}$.

**15.5 Entering a Highway with Roadworks**

In this situation, we can apply both the safety criterion (15.4) of the general lane-changing model or the safety criterion of the decision model (15.37) for entering a priority road. With the notations of Fig. 15.7, we obtain for a defensive driver ($b_{\mathrm{safe}} = 0$)

$$s_{\mathrm{f}} > s_{\mathrm{safe}}(v_{\mathrm{f}}, v) = s_{\mathrm{opt}}(v_{\mathrm{f}}) = v_{\mathrm{f}} T = 20\,\mathrm{m}.$$

Here, we have dropped all hats, consistent with the convention adopted in Section 15.6. In the "worst case", the driver decides to merge if the vehicle on the highway is just $s_{\mathrm{safe}} = 20\,\mathrm{m}$ away. Now we calculate the minimum deceleration $b_{\mathrm{min}}$ the driver on the main road has to adopt to avoid a crash. Applying the kinematic braking distance $s = \Delta v^2/(2b)$ to the critical distance $s_{\mathrm{safe}} = 20\,\mathrm{m}$, the initial speed difference $\Delta v = v_{\mathrm{f}} = 20\,\mathrm{m/s}$, and the relative deceleration $b = b_{\mathrm{min}} + a$ (assuming that the merging vehicle accelerates at $a = 2\,\mathrm{m/s^2}$), and solving for $b_{\mathrm{min}}$ results in

$$b_{\mathrm{min}} = \frac{v_{\mathrm{f}}^2}{2s} - a = 8\,\mathrm{m/s^2}.$$

We observe that, in spite of the very conservative assumption $b_{\mathrm{safe}} = 0$ in the decision model, the *actually* necessary deceleration of the main-road vehicle corresponds to an emergency braking maneuver. This discrepancy can be traced back to the OVM whose braking strategy is inconsistent with kinematic constraints and does not contain the speed difference although this is a crucial exogenous factor (in fact, the OVM simulation will lead to crashes in this situation). As shown in the next problem, drivers modeled by the Gipps' model or the IDM family will make a consistent decision in this situation.

**15.6 An IDM Vehicle Entering a Priority Road**

In this situation (Fig. 15.7 for $v_i = 0$), the IDM safety criterion (15.37) reads

$$s_{\mathrm{f}} > s_{\mathrm{safe}}^{\mathrm{IDM}}(v_{\mathrm{f}}, 0) = \frac{s_0 + v_{\mathrm{f}} T + \frac{v_{\mathrm{f}}^2}{2\sqrt{ab}}}{\sqrt{\frac{a_{\mathrm{free}}(v_{\mathrm{f}})}{a} + \frac{b_{\mathrm{safe}}}{a}}},$$

or, with $s_0 = 0$, $v_{\mathrm{f}} = v_0$, and $a = b = b_{\mathrm{safe}}$ (then, the square root is equal to 1)

$$s_{\mathrm{f}} > s_{\mathrm{safe}}^{\mathrm{IDM}} = v_{\mathrm{f}} T + \frac{v_{\mathrm{f}}^2}{2b_{\mathrm{safe}}}.$$

This means, the minimum gap to allow merging corresponds to the *stopping distance* of the follower on the main road (braking distance $v^2/(2b)$ plus distance $vT_r$ driven during the reaction time) when the desired time headway is set equal to the reaction time, $T = T_r$. Consequently, the IDM safety criterion for merging is consistent with the driver capabilities and kinematic constraints. For $T = 1\,\mathrm{s}$, $b_{\mathrm{safe}} = 2\,\mathrm{m/s^2}$, and $v_0 = 50\,\mathrm{km/h}$, we obtain as safe distance for merging $s_{\mathrm{safe}}^{\mathrm{IDM}} = 31\,\mathrm{m}$.

### 15.8 Overtaking on the Lane for the Opposite Direction

1. For the rural road environment, the minimum safe gap to the oppositely driving vehicle for a positive safety criterion is given by $s_{\mathrm{safe}} = 736\,\mathrm{m}$ resulting from a displacement distance $s_{\mathrm{displ}} = 82\,\mathrm{m}$ and the total overtaking time $\tau_{\mathrm{overtake}} = 10.1\,\mathrm{s}$.
2. The minimum initial gap to the oppositely driving vehicle when overtaking a bicycle in the given city environment is given by $s_{\mathrm{safe}} = 162\,\mathrm{m}$ resulting from a displacement distance $s_{\mathrm{displ}} = 34\,\mathrm{m}$ and the total overtaking time $\tau_{\mathrm{overtake}} = 3.4\,\mathrm{s}$. Remarkably, in the above typical cases, overtaking a truck on a rural road requires more than four times the safe distance to the opposite driver than that required when overtaking a bicycle in a city.

## Problems of Chapter 16

### 16.1 Characterizing the Type of Instability

The displayed traffic flow is locally stable since, after a sufficient time, each driver reverts to the steady state (he or she stops, at most, once). At the same time, the dynamics is string unstable since the amplitude of the oscillations increase from vehicle to vehicle. The string instability is convective (of the upstream type) since there is only a single traffic wave: After a sufficiently long time, traffic flow reverts to the steady state at any fixed location.

### 16.2 Propagation Velocity of Traffic Waves in Microscopic Models

At first, we transform the microscopic propagation velocity given in the comoving (Lagrangian) coordinate system to a stationary coordinate system:

$$\tilde{c} = v_e + \tilde{c}_{\mathrm{rel}} = v_e - (s_e + l)v_e'(s_e) = v_e - \frac{v_e'(s_e)}{\rho_e}.$$

Here, we used the relation $s_e + l = 1/\rho_e$. Now we express the microscopic gradient $v_e'(s)$ by the corresponding macroscopic quantity $V_e'(\rho)$. Using the identity $v_e(s) = V_e(\rho(s))$ and the micro-macro relation $\rho = 1/(s+l)$, we obtain

$$v_e'(s) = \frac{\mathrm{d}v_e}{\mathrm{d}s} = \frac{\mathrm{d}V_e}{\mathrm{d}\rho}\frac{\mathrm{d}\rho}{\mathrm{d}s} = -\frac{V_e'(\rho)}{(s+l)^2} = -\rho^2 V_e'(\rho). \tag{11}$$

Inserting this into the expression for $\tilde{c}$ gives the final result

$$\tilde{c} = v_e - \frac{v_e'(s_e)}{\rho_e} = V_e + \rho_e V_e'(\rho_e) = \frac{\mathrm{d}}{\mathrm{d}\rho_e}(\rho_e V_e) = Q_e'(\rho_e).$$

### 16.3 Instability Limits for the Full Velocity Difference Model

*Subproblem 1.* The local stability criterion is satisfied if

$$\tilde{f}_v + \tilde{f}_{\Delta v} = -\frac{1}{\tau} - \gamma \leq 0 \quad \Rightarrow \quad \gamma \geq -\frac{1}{\tau} = -0.2\,\mathrm{s}^{-1}.$$

This is true even for slightly negative values of the sensitivity $\gamma$ to speed differences (although this implies accelerations in response to positive approaching rates which is no reasonable behavior). As such, it reflects the result that all reasonable (and even some unreasonable) models without explicit delays (reaction times) are locally stable.

*Subproblem 2:* For $v \geq v_0$, there are no interactions and, therefore, no instabilities. If $v < v_0$, we have $v_e'(s) = 1/T$, $\tilde{f}_v = -1/\tau$, and $\tilde{f}_{\Delta v} = -\gamma$. Inserting these relations into condition (16.27) for an oscillation-free local car-following characteristics yields

$$\frac{1}{T} \leq \frac{1}{4\tau}(1+\gamma\tau)^2.$$

Solving this quadratic inequality for $\gamma$ results in

$$\gamma \geq -\frac{1}{\tau} \pm \frac{2}{\sqrt{T\tau}} = 0.69\,\mathrm{s}^{-1}.$$

Here, we used the general plausibility condition $\gamma \geq 0$ to select the positive sign of the square root when calculating the numerical value.

*Subproblem 3.* To determine the limits of string instability, we use criterion (16.78). Solving the resulting inequality for $\gamma$ yields

$$\gamma > \frac{1}{T} - \frac{1}{2\tau} = 0.9\,\mathrm{s}^{-1}.$$

We observe that car-following schemes may be string unstable even if they do not produce *any* kind of oscillations (damped or otherwise) when following a single leader. Here, this applies to the parameter range $0.69\,\mathrm{s}^{-1} < \gamma \leq 0.9\,\mathrm{s}^{-1}$. This is highly relevant when investigating the effects of adaptive cruise control systems on traffic flow.

### 16.4 Stability Properties of the Optimal Velocity Model Compared to Payne's Model

The OVM criterion for string stability reads $v_e'(s) \leq 1/(2\tau)$, and the corresponding criterion for flow stability in Payne's model $-V_e'(\rho) \leq 1/(2\rho^2\tau)$. Using the micro-macro relation $v_e'(s) = 1/\rho_e^2 V_e'(\rho)$ already needed for Problem 16.2, we show the equivalence by direct substitution:

$$\frac{1}{2\tau} \geq v_e'(s_e) = -\rho_e^2 V_e'(\rho_e(s_e)) \quad \Rightarrow \quad -V_e'(\rho) \leq \frac{1}{2\rho^2\tau} \text{ q.e.d.}$$

### 16.5 OVM with "Pushing" from Behind

The long-wavelength stability criterion (16.94) can be written as

$$v_{\text{opt}}'(s) \leq \frac{1}{2\tau} \frac{1+\lambda}{(1-\lambda)^2}.$$

For $\lambda = 0.5$, the second factor is equal to 6 increasing the string stability sixfold. However, for very low leading speeds, the follower "pushes" the subject vehicle into the leader even in the semi-static situation because the steady-state gap can drop below zero. For the given triangular fundamental diagram and gaps below $s_0 + (v_0 T$, the steady-state speed of the subject vehicle in the presence of at least one follower is given by

$$v_e(s) = (1-\lambda) v_{\text{opt}}(s) + \lambda v_0 = (1-\lambda) \left( \frac{s - s_0}{T} \right) + \lambda v_0.$$

For a gap equal to zero, this becomes

$$v_e(0) = -\frac{s_0}{T} + \lambda \left( \frac{s_0}{T} + v_0 \right).$$

This means for any $\lambda > (1 + v_0 T / s_0)^{-1}$, we have a finite steady-state speed at zero gap. i.e., collisions. Assuming $v_0 = 19\,\text{m/s}$, $T = 2\,\text{s}$, and $s_0 = 2\,\text{m}$, this is already true for $\lambda > 0.05$.

### 16.6 Flow Instability in Payne's Model and in the Kerner-Konhäuser Model

*Subproblem 1.* We have solved the general flow stability problem for Payne's model already in Problem 16.4. For the triangular fundamental diagram as specified in the problem formulation, the gradient of the speed-density relation reads

$$V_e'(\rho) = \begin{cases} 0 & \rho \leq \rho_C, \\ -\frac{1}{\rho^2 T} & \rho > \rho_C, \end{cases}$$

with the density at capacity $\rho_C = 1/(v_0 T + l_{\text{eff}}) = 20\,\text{veh/km}$. For free traffic ($\rho < \rho_C$) there are no interactions ($V_e'(\rho) = 0$) and therefore unconditional stability. Congested traffic flow ($\rho \geq \rho_C$) is stable if

$$\tau < \frac{T}{2}.$$

This means, Payne's model describes stable congested traffic for unrealistically small adaptation times $\tau$, only.

*Subproblem 2.* For the Kerner-Konhäuser model, the flow stability criterion reads $(\rho V_e'(\rho))^2 < \theta_0$. Inserting the steady-state relation $V_e(\rho) = \max[V_0, 1/T(1/\rho -$

$1/\rho_{\max})]$ gives, again, unconditional stability for free traffic flow ($\rho < \rho_C = 20\,/\mathrm{km}$) which is consistent with the requirements of the problem formulation. For congested traffic ($\rho > \rho_C$), we have

$$\frac{1}{\rho^2 T^2} < \theta_0.$$

From this condition, we determine $\theta$ by demanding that congested traffic flow should be unstable for densities below $\rho_3 = 50\,/\mathrm{km}$, and stable above. With $T = 1.1\,\mathrm{s}$ and $\rho_3 = 50\,/\mathrm{km}$, we finally obtain (cf. the figure below)

$$\theta_0 = \frac{1}{\rho_3^2 T^2} = 331 \frac{\mathrm{m}^2}{\mathrm{s}^2}.$$

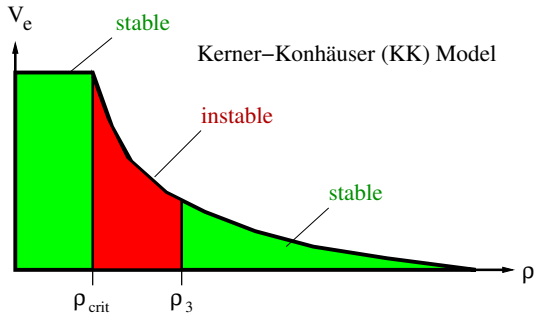


**16.7 Flow Instability of the GKT Model**

For high densities near the maximum density, we can approximate the GKT steady-state flow by $Q_e \approx 1/T(1-\rho/\rho_{\max})$, or $V_e'(\rho) = -1/(T\rho^2) \approx -1/(T\rho_{\max})^2$. Without anticipation ($\gamma = 0$) and assuming a constant speed variance prefactor $\alpha_{\max} = \alpha(\rho) \approx \alpha(\rho_{\max})$ which is equivalent to $P_e' \approx \sigma_V^2 \approx \alpha_{\max} V_e^2$, the GKT stability criterion (16.130) becomes

$$(\rho V_e')^2 - P_e' = \frac{1}{T^2\rho^2} - \alpha_{\max} V_e^2 \le 0.$$

Since, for $\rho \to \rho_{\max}$, the expression $(T\rho)^{-2}$ tends to the squared propagation velocity $c^2$ of moving downstream jam fronts while the speed variance $\alpha_{\max} V_e^2$ tends to zero, the stability criterion cannot be satisfied: Without anticipation, the GKT model is unconditionally unstable for sufficiently high densities!

For a finite anticipation range $s_a = \gamma V_e T$, however, the third term of the stability condition (16.130) can stabilize traffic flow. Sufficiently close to the maximum density, we can approximate the full GKT flow stability criterion to an analytically tractable condition. If $\rho \approx \rho_{\max}$, we have, up to linear order in $V_e$

$$\rho V_e' \approx -\frac{1}{T\rho}, \quad P_e' \approx \alpha_{\max} V_e^2 \approx 0, \quad s_a(V_0 - V_e) \approx \gamma V_e V_0 T.$$

Furthermore, with $\rho_{\max}/(\rho_{\max}-\rho) \approx (\rho V_e T)^{-1}$, we can approximate the bracket of the last term of Eq. (16.130) by

$$\left[\frac{\rho_{\max}}{\rho_{\max}-\rho} - \frac{\rho V_e'}{\sigma_V\sqrt{\pi}}\right] \approx \frac{1}{\rho V_e T}\left(1+\frac{1}{\sqrt{\alpha_{\max}}}\right).$$

Inserting all this into the GKT stability condition (16.130), we find that the GKT model is string stable for densities near the maximum density if the anticipation factor $\gamma$ fulfills

$$\gamma > \frac{\tau}{2T^2\rho_{\max}V_0\left[1+(\alpha_{\max}\pi)^{-1/2}\right]}$$

which is condition (16.131).

### 16.8 IDM Stability Class Diagram for other Parameter Values

In the following, we will denote the scaled dimensionless quantities with a tilde. According to the problem formulation, the scaled time and space coordinates as well as derived variables (speed, acceleration) are related to the unscaled quantities as

$$t = \sqrt{\frac{s_0}{b}}\tilde{t}, \quad x = s_0\tilde{x}, \quad v = \sqrt{bs_0}\tilde{v}, \quad \frac{\mathrm{d}v}{\mathrm{d}t} = b\frac{\mathrm{d}\tilde{v}}{\mathrm{d}\tilde{t}}.$$

Inserting this transformation into the IDM equations results in

$$\frac{\mathrm{d}\tilde{v}}{\mathrm{d}\tilde{t}} = \frac{a}{b}\left[1-\left(\frac{\sqrt{bs_0}\tilde{v}}{v_0}\right)^4 - \left(\frac{\tilde{s}^*}{\tilde{s}}\right)^2\right],$$

$$\tilde{s}^* = \frac{s^*}{s_0} = 1+\sqrt{\frac{b}{s_0}}T\tilde{v} - \sqrt{\frac{b}{a}}\frac{\tilde{v}\Delta\tilde{v}}{2}.$$

As a consequence, the prefactors of the different new terms are dimensionless as well. Moreover, they come in only three combinations of the original IDM parameters which we can identify as the new model parameters:

$$\tilde{v}_0 = \frac{v_0}{\sqrt{bs_0}}, \quad \tilde{f} = \frac{a}{b}, \quad \tilde{T} = T\sqrt{\frac{b}{s_0}}.$$

Thus, the scaled IDM equations read

$$\frac{\mathrm{d}\tilde{v}}{\mathrm{d}\tilde{t}} = \tilde{f}\left[1-\left(\frac{\tilde{v}}{\tilde{v}_0}\right)^4 - \left(\frac{\tilde{s}^*}{\tilde{s}}\right)^2\right], \quad \tilde{s}^* = 1+\tilde{v}\tilde{T} - \frac{\tilde{v}\Delta\tilde{v}}{2\sqrt{\tilde{f}}}.$$

This allows a powerful conclusion:[15] Changing the five physical IDM parameters such that $\tilde{v}_0$, $\tilde{f}$, and $\tilde{T}$ remain unchanged does not change the scaled IDM equations,

[15] In hydrodynamics, such scale relations are the basis to measure the hydrodynamics of big objects (ships, planes etc.) by observing a scaled-down (physical) model of the object in a wind or water channel rather than observing/measuring the real thing.

nor the local dynamics. This allows to reduce the five-dimensional IDM parameter space spanned by $V_0$, $T$, $a$, $b$, and $s_0$ to the three-dimensional space $(\tilde{V}_0, \tilde{T}, \tilde{a})$ spanned by the dimensionless parameters. However, the stability class depends not only on the local dynamics but also on the vehicle length influencing the macroscopic fundamental diagram $Q_e(\rho)$ and the sign of propagation velocities. Therefore, to ensure the same stability class, a forth dimensionless parameter

$$\tilde{l} = l/s_0$$

must be kept constant.

When applying these insights to the concrete problem of where to read off the stability class in the $a$-$T$-class diagram when other IDM parameters are changed, we observe that this is only possible if speed is changed proportionally to changes of $\sqrt{bs_0}$ and the vehicle length changes proportionally to $s_0$. Only then, the two scaled parameters $\tilde{v}_0$ and $\tilde{l}$ containing neither $a$ nor $T$ remain unchanged. This is fulfilled here since $s_0$ does not change anyway and the new values $v_0^* = 139\,\mathrm{km/h}$ and $b^* = 2\,\mathrm{m/s^2}$ of the desired speed and time headway, respectively, satisfy $\tilde{v}_0 = v_0(bs_0)^{-1/2} = v_0^*(b^*s_0)^{-1/2} = \text{const}$. In order to make sure that $\tilde{f}$ and $\tilde{T}$ remain unchanged as well, we read off the old diagram at the coordinate $(T^*, a^*) = (\tau T, \alpha a)$ rather than at $(T, a)$. We fix the scaling factors $\tau$ and $\alpha$ to fulfill the conditions

$$\frac{a}{b} = \frac{a^*}{b^*} = \frac{\alpha a}{b^*}, \quad T\sqrt{\frac{b}{s_0}} = T^*\sqrt{\frac{b^*}{s_0}} = \tau T\sqrt{\frac{b^*}{s_0}}$$

resulting in

$$\tau = \sqrt{\frac{b}{b^*}} = 0.87, \quad \alpha = \frac{b^*}{b} = 1.33.$$

This means, for the new values of $v_0$ and $b$, one reads of the class diagram at 0.87 times the original $T$ coordinate and 1.33 times the original $a$ coordinate.

### 16.9 Fundamental Diagram with Hysteresis

*Subproblem 1.* Maximum free-traffic flow:

$$Q_{\max}^{\text{free}} = v_0\rho_{\max}^{\text{free}} = 2,400\,\mathrm{veh/h}.$$

*Subproblem 2.* The congested part of the fundamental diagram corresponds to the congested part of the triangular fundamental diagram for the parameters $Q_{\text{cong}}(\rho) = 1/T(1-\rho l_{\text{eff}})$ where $l_{\text{eff}} = l + s_0 = 6.67\,\mathrm{m}$. This congested branch intersects the free branch at the same point $(\rho_C, Q_{\max}^{\text{dyn}})$ that would correspond to the maximum of the triangular diagram without hysteresis:

$$\rho_{\min}^{\text{cong}} = \rho_{\text{C}} = \frac{1}{v_0 T + l_{\text{eff}}} = 16.67\,\mathrm{veh/km}.$$

*Subproblems 3 and 4.* The jam outflow is characterized by the dynamic capacity $Q_{\max}^{\mathrm{dyn}} = v_0 \rho_{\mathrm{C}} = 2{,}000\,\mathrm{veh/h}$. This describes a *capacity drop* of

$$\Delta Q = Q_{\max}^{\mathrm{free}} - Q_{\max}^{\mathrm{dyn}} = 400\,\mathrm{veh/h} \quad (\text{or } 16.7\%).$$

The density of the outflow is given by $\rho_C$. This means, hysteretic effects can take place in the density range $\rho \in [\rho_{\mathrm{C}}, \rho_{\max}^{\mathrm{free}}]$, or, numerically, $\rho \in [16.67\,\mathrm{veh/h}, 20\,\mathrm{veh/h}]$.

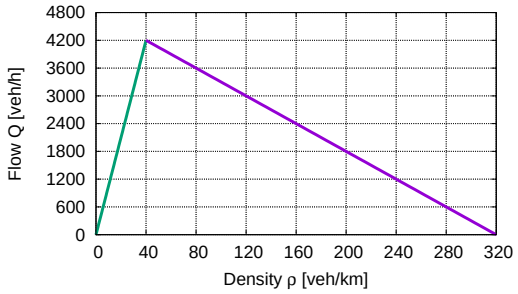


## Problems of Chapter 17

### 17.1 Measures of Performance

Following data are suitable for determining the different measures of performance (MoPs) of the problem statement and running the appropriate simulation

(i) Acceleration of vehicles: Trajectory and extended floating-vehicle data (XFCD). This data also provides the simulation of a microscopic model with the needed inputs gap and leading speed. Normal floating-vehicle data without leading-vehicle information or stationary detectors are not applicable.

(ii) Speed of vehicles: Trajectory data, XFCD, and stationary double-loop data (SDD). With the first two data categories, the simulation setup is the same as above. With double-loop data, local and average speeds as well as speed variances can be calculated and used to estimate microscopic and macroscopic models.

(iii) Gap to the leading vehicle: Data and simulation as for the accelerations as MoP.

(iv) Realized travel time: Of course, travel time series but also trajectory data together with a microscopic simulation or SDD together with a macroscopic simulation. In the microscopic simulation, the travel time is given directly by the corresponding trajectories, in the macroscopic simulation, the realized travel time at time $t$ (cf. Sect. 22.1) is given via the virtual trajectory extracted from the macroscopic speed field $V(x,t)$ by

$$\frac{\mathrm{d}x}{\mathrm{d}t'} = V(x,t')$$

with the final condition

$$x(t) = x_2.$$

Notice that XFC data are unsuited because, then, only leader-follower pairs can be simulated and the follower essentially has the same realized travel time as the leader.

(v) Flow at a given location: Since flow is an extensive quantity, only sources with extensive data are eligible, i.e., Trajectory data or SDD.

(vi) Flow-density data at a given location: Likewise.

(vii) Local lane-changing rate: Microscopic data needed, i.e., trajectory data or XFCD. Since the lane-changing rate is intensive, no extensive input (density or flow) is needed and the local lane-changing rate can also be estimated from the sample of the xFCD provided these data contain sufficiently many lane changes.

### 17.2 Goodness of Fit Functions

Calibration means minimizing (or maximizing) a GoF function $S(\boldsymbol{\beta})$. However, the GoF value itself is not relevant for the calibration but the *argument* $\hat{\boldsymbol{\beta}}$ minimizing or maximizing this function. If $f(\cdot)$ is a strictly monotonously increasing or decreasing function with $f'(x) \neq 0$ everywhere in the allowed range, we have

$$\frac{\partial f(S(\boldsymbol{\beta}))}{\partial \boldsymbol{\beta}} = f'(S)\frac{\partial S}{\partial \boldsymbol{\beta}} = 0 \Leftrightarrow \frac{\partial S}{\partial \boldsymbol{\beta}} = 0,$$

since $f'(S)$ is strictly nonzero, i.e., an unchanged calibration result. Specifically, the square root (going from MSE to RMSE) is such a strictly monotonous function as is multiplication with the constant $\left[\sum_{i=1}^{n}\left(y_i^{\text{data}}\right)^2\right]^{-1/2}$ (going from the RMSE to the SRMSE).

### 17.3 Compatibility of Measures of Performances with Goodness of Fit Functions

*Relative GoFs such as RMSPE or MAPE:* Not any $y_i^{\text{data}}$ may be zero (as it may happen for the speed) because, otherwise, these MoPs are not defined. Possibly negative $y_i^{\text{data}}$ (accelerations) are not allowed either because they contradict the very concept of relative errors denoting "standard deviation divided by expectation". Finally, plausible error measures are translation invariant, i.e., do not change when adding to the positions a global constant (e.g., going from local coordinates to geo-coordinates). This excludes positions from relative and standardized GoFs but not from absolute GoFs (RMSE, MAE) which remain unchanged when going from gaps to positions.

*Standardized GoFs such as SRMSE:* In contrast to relative MoPs, $y_i^{\text{data}} = 0$ is allowed for some $i$ because only the sum and not single data points are in the denominator, i.e., the speed is a valid MoP. Positions and accelerations are excluded for the same reasons as for the relative GoFs.

### 17.4 Influence of Serial Correlations on Measures of Parsimony

Given are 20 data points $(s_i, v_i)$ of which the first ten and the second ten are identical. This means, Model (i) can fit, at least, ten data points exactly, while Model (ii) fits the data to 100%, after calibration. In contrast, if the data were not serially correlated, Models (i) and (ii) will fit at least one and two data points, respectively. This result does not depend on the specific model, since the same would apply to, say, the models (i) $\hat{v}(s) = \ln(\beta_0/s)$ and (ii) $\hat{v}(s) = \ln(\beta_0/s + \beta_1)$. This means, even completely nonsensical models fit one additional data point per parameter if the data points are independent, but they fit ten additional points if they are serially correlated as in this example. Now assume a nonsensical addition to a given model introducing one new parameter. For i.i.d. errors in the data, a parsimony test such as the likelihood-ratio test would yield a negative result for the augmented model since each parameter can always fit one additional data point without increasing its predictive value which such tests take care of. However, for correlated data as above, this parameter explains ten additional points. For robustness tests assuming i.i.d. errors, this corresponds to nine nontrivial fits which such tests may erroneously interpret as worth the additional parameter.

## Problems of Chapter 18

### 18.1 Phase Diagram for Stability Class 3

For class 3, there are no traffic-flow instabilities and no hysteresis. Therefore, one just distinguishes between free traffic and homogeneous congested traffic:

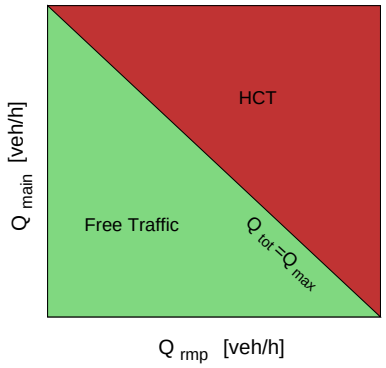


Furthermore, since no instability also implies no hysteresis effects, there is only one phase diagram valid for both small and large initial perturbations.

### 18.2 Boundary-Induced Phase Diagram

The kind of extended congested pattern (TSG, OCT, HCT) is directly defined by the supply restriction $Q_{\text{out}}$. Because of the oscillatory nature of the congested states for comparatively high values of $Q_{\text{out}}$ (OCT and TSG), significant perturbations arrive at the upstream boundary activating the "inflow-bottleneck" if $Q_{\text{in}} > C_{\text{dyn}}$ (remem-

ber that we have $I = 1$ lane). If, additionally, $Q_{\text{out}} \geq C_{\text{dyn}}$, the potential outflow is higher than the inflow restricted by the activated inflow-bottleneck. This means there is free traffic in the bulk of the investigated road section corresponding to the maximum-flow state. If, however, $Q_{\text{out}} < C_{\text{dyn}}$, congested traffic will arise everywhere and the inflow-bottleneck (whether activated or not) is no longer relevant. Therefore, the maximum-flow state requires both $Q_{\text{in}} > C_{\text{dyn}}$ and $Q_{\text{out}} \geq C_{\text{dyn}}$. This results in following boundary-induced phase diagram:

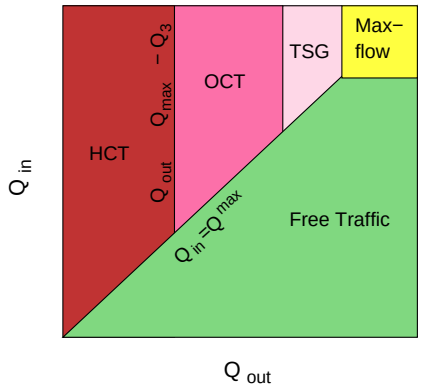


The situation with an activated inflow bottleneck corresponds to the stationary front of a bottleneck in inhomogeneous systems. However, since no upstream region is simulated here, the stationary front appears as a "standing wave". In simulations, activated inflow bottlenecks are a serious problem since they introduce bottlenecks not corresponding to anything in reality. Dedicated and very complex upstream boundary conditions (not discussed here) are necessary to avoid them.

## Problems of Chapter 19

### 19.1 Assessing a Mass Event

1. The bottleneck is the region with the lowest local capacity. Without counterflow and obstacles, the capacity is given by

$$C = J_{\max} w^{\text{tot}}, \quad J_{\max} = 1.25\,\text{ped}(\text{ms})^{-1},$$

where the value for the maximum flow density has been read off the maximum of the Weidmann flow density depicted in Fig. 19.2. In the tunnel sections, we have a total width $w^{\text{tot}} = 40\,\text{m}$ while, in the ramp section, there is only one pedestrian stream with a width of 30 m. Therefore, the bottleneck is at the (beginning of) the ramp section and its capacity is given by

$$C = 1.25\,\text{ped}(\text{ms})^{-1} 30\,\text{m} = 37.5\,\text{ped}/\text{s} = 135\,000\,\text{ped}/\text{h}.$$

2. With a capacity of 135 000 ped/h, the approach network can manage the initial demand. After a surge to $Q_{\text{in}} = 170\,000\,\text{ped/h}$, the tunnels are still able to manage the demand (since their total capacity is $1.25\,\text{ped(ms)}^{-1}50\,\text{m} = 50\,\text{ped/s} = 180\,000\,\text{ped/h}$) while the ramp is not. Therefore, we expect a breakdown at the begin of the ramp section.[16]
3. On the upstream free-flow side in the tunnel, we have

$$J_1 = \frac{Q_{\text{in}}}{40\,\text{m}} = 1.18\,\text{ped(sm)}^{-1}, \quad \rho_1 = \rho^{\text{free}}(J_1) = 1.1\,\text{ped/m}^2$$

where $\rho_1$ has been read off Fig. 19.2(left) for the Weidmann FD. Likewise, we have on the congested downstream side in the tunnel

$$J_2 = \frac{C}{40\,\text{m}} = 0.94\,\text{ped(sm)}^{-1}, \quad \rho_2 = \rho^{\text{cong}}(J_2) = 3.5\,\text{ped/m}^2.$$

With the shockwave-formula, the propagation of the congestion front is given by

$$c_{12} = \frac{J_2 - J_1}{\rho_2 - \rho_1} = -0.101\,\text{m/s}$$

and, after one hour of increased demand, the congested region in the tunnels is $-c_{12}3\,600\,\text{s} = 365\,\text{m}$ long.

### 19.2 Weidmann's Fundamental Diagram

1. The three parameters of the Weidmann model (19.7) have following meaning
   - $v_0$: desired speed (since this is the steady-state speed for $\rho \to 0$)
   - $\rho_{\max}$: maximum density (since at this density the steady-state speed tends to zero)
   - $\lambda$: form factor. For small values, the density at capacity is rather low while for high values ($\lambda = \rho_{\max}$ or higher), the $e$ function of the Weidmann model only leads to significantly decreasing flows for densities near the maximum density.
2. Comparing the Weidmann model (19.7) with the steady-state solution of the Social-force model (SFM) (19.54) for a series of single files, we can identify the effective radius $R$ of an SFM pedestrian and the range parameter $B$ as

$$R = \frac{1}{2\sqrt{\rho_{\max}}} = 0.215\,\text{m}, \quad B = \frac{\sqrt{\rho_{\max}}}{\lambda} = 1.21\,\text{m}.$$

### 19.3 Kinetic and Potential Energy of the Social Force Model

Without free-flow forces and for a pedestrian moving straight to a standing pedestrian (assuming, without loss of generality, a motion in direction of the $x$ axis), the acceleration of the moving pedestrian reads

[16] In fact, this was the location of the accidents caused by the stampede of the *Loveparade* event.

$$\frac{\mathrm{d}v_x}{\mathrm{d}t} = -\frac{\partial \Phi}{\partial x}.$$

For a circular or elliptical I specification, the social-force potential exerted by the standing pedestrian is constant. So, by multiplying both sides of the above equation with $v_x$, we can integrate the equation as follows

$$\begin{aligned}
\frac{\mathrm{d}v_x}{\mathrm{d}t} v_x &= -\frac{\partial \Phi}{\partial x} v_x = -\frac{\partial \Phi}{\partial x}\frac{\mathrm{d}x}{\mathrm{d}t} \\
\frac{\mathrm{d}}{\mathrm{d}t}\left(\frac{1}{2}v_x^2\right) &= -\frac{\mathrm{d}\Phi}{\mathrm{d}t} \\
\frac{1}{2}v_x^2 &= -\Phi(x) + C.
\end{aligned}$$

The integration constant can be determined by assuming an initial speed $v_\infty$ sufficiently far away from the target pedestrian ($x \to -\infty$) where $\Phi(x) = 0$, so $C = 1/2\, v_\infty^2$ and

$$v_x^2(x) = v_\infty^2 - 2\Phi(x).$$

In order to not collide or touch with the pedestrian (assumed to be circular with radius $R$), the moving pedestrian needs to stop before reaching $|x| = 2R$ (pedestrian radius $R$), so

$$\Phi(2R) > \frac{1}{2}v_\infty^2$$

which is (19.19) for $\mathscr{C}_j : |x| \leq 2R$.

**19.4 Limits of the Self-Driving Force of the Social Force Model**
In the *best case*, a pedestrian $i$ driven by the free-flow acceleration $(v_0 - v_i)/\tau$ in $x$ direction ($x < 0$) towards another pedestrian $j$ at $(x, y) = \mathbf{0}$ is already standing immediately at pedestrian $j$, i.e., $x_i = -R$. In this situation, the static repulsion force $-\Phi'(x)$ needs to overcompensate the free driving force:

$$\frac{v_0 - v_i}{\tau} = \frac{v_0}{\tau} < \Phi'(x) = Ae^{-|x|/B}.$$

With a radius $R$ for both pedestrians, we need to require for the relaxation time $\tau$ the condition

$$\tau > \tau = \frac{v_0}{A} e^{-2R/B}.$$

which is Eq. (19.23) for $R_1 = R_2$. In order to avoid collisions for other cases as well (moving instead of standing pedestrians), the relaxation time $\tau$ should be significantly higher than $\tau_c$.

**19.5 Consistency Order of the Velocity Verlet Scheme** As in Chapter 16, we define a function $f(\tau)$ to be of the "order" symbol $\mathscr{O}(\tau^n)$ if $\lim_{\tau \to 0} f(\tau^m)$=0 for any $m < n$. For notational simplicity, we ignore the sums, indices and vector properties of the SFM equations of motion (neither of them does influence the numerical properties) and write the Velocity Verlet scheme as

$$\begin{aligned} x' &= x + v\Delta t + \tfrac{1}{2} f \Delta t^2, \\ f' &= f(x', v^{\mathrm{E}}), \quad v^{\mathrm{E}} = v + f\Delta t, \\ v' &= v + \tfrac{1}{2}(f + f')\Delta t, \end{aligned} \tag{12}$$

where the dashed quantities are the numerical approximations taken at the time $t + \Delta t$ and the not dashed ones at time $t$. Obviously, due to its ballistic nature, the positional discretization error

$$\Delta x = x^{\mathrm{real}}(t + \Delta t) - x'$$

where $x^{\mathrm{real}}(t + \Delta t)$ is the exact solution of the SFM for the initial conditions $x(t) = x$ and $v(t) = v$ is already of $\mathscr{O}(\Delta t^3)$ while the Euler predictor $v^{\mathrm{E}}$ for the speed is only $\mathscr{O}(\Delta t^2)$, i.e., the *ballistic* scheme with the Euler speed update is only of local order $\mathscr{O}(\Delta t^2)$ and global order $\mathscr{O}(\Delta t)$.

In order to assess the consistency order of

$$\Delta v = v^{\mathrm{real}}(t + \Delta t) - v'$$

we make use of the assumption that the first partial derivatives of the forces,

$$\frac{\partial f}{\partial x} \equiv f_x, \quad \frac{\partial f}{\partial v} \equiv f_v,$$

are finite and expand $f$ to first order in $x$ and $v$,

$$f(x + \Delta x, v + \Delta v) = f + f_x \Delta x + f_v \Delta v + \mathscr{O}(\Delta x, \Delta v)^2$$

With the second line of (12), we transform this in an expansion around $t$:

$$f' = f(x', v^{\mathrm{E}}) = f + f_x v \Delta t + f_v f \Delta t + \mathscr{O}(\Delta t)^2$$

Notice that we have already ignored the term $\frac{1}{2} f_x f (\Delta t)^2$ which is of $\mathscr{O}(\Delta t)^3$. Inserting this into the velocity update of (12) finally gives

$$v' = v + \frac{1}{2}(f + f')\Delta t = v + f\Delta t + \frac{1}{2}\left(f_x v + f_v f\right)(\Delta t)^2 + \mathscr{O}(\Delta t)^3.$$

So, both the positional and velocity updates of the Velocity Verlet scheme are of third local and thus of second global consistency order. This derivation also indicates that a higher consistency order is not always better. If we have physical interactions, the equations of motion are *stiff* meaning that the gradients $f_x$ and $f_v$ are of high absolute value making the global error to *scale* with $(\Delta t)^2$ but with a very big *prefactor* particularly relating to the $f_v f$ product term.

### 19.6 Free-Flow Speed of a Pedestrian Cellular Automaton

The three allowed cells are associated with the displacement vectors

$$\Delta \boldsymbol{r}_0 = \begin{pmatrix} 0 \\ 0 \end{pmatrix}, \quad \Delta \boldsymbol{r}_1 = \begin{pmatrix} \Delta x_1 \\ \Delta y_1 \end{pmatrix}, \quad \Delta \boldsymbol{r}_2 = \begin{pmatrix} \Delta x_2 \\ \Delta y_2 \end{pmatrix},$$

where the components are related to the absolute displacement 0, $L$, or $L\sqrt{2}$ (with the cell size $L$) multiplied by straightforward trigonometric functions. For a given desired velocity $\boldsymbol{v}_0 = v_0 \boldsymbol{e}_x$, we have three equations for the three unknowns $p_0$, $p_1$, and $p_2$ corresponding to the expected displacement vectors and the probability sum condition,

$$\begin{aligned} E(\Delta x) &= p_1 \Delta x_1 + p_2 \Delta x_2 = v_0 \tau_a, \\ E(\Delta y) &= p_1 \Delta y_1 + p_2 \Delta y_2 = 0, \\ p_0 + p_1 + p_2 &= 0. \end{aligned}$$

If $\Delta y_1 = 0$, we have from the second equation $p_2 = 0$, hence

$$\Delta y_1 = 0: \qquad p_2 = 0, \quad p_1 = \frac{v_0 \tau_q}{\Delta x_1}, \quad p_0 = 1 - p_1, \quad \Delta x_1 = L \text{ or } L\sqrt{2}$$

Likewise, if $\Delta y_2 = 0$, the probabilities are

$$\Delta y_2 = 0: \qquad p_1 = 0, \quad p_2 = \frac{v_0 \tau_q}{\Delta x_2}, \quad p_0 = 1 - p_2, \quad \Delta x_2 = L \text{ or } L\sqrt{2}$$

If neither $\Delta y_1 = 0$ nor $\Delta y_2 = 0$, the grid is not oriented towards the destination and the non-degenerated solution of the above equation system reads

$$p_1 = \frac{v_0 \tau_q \Delta y_2}{\Delta x_1 \Delta y_2 - \Delta x_2 \Delta y_1}, \quad p_2 = -p_1 \frac{\Delta y_1}{\Delta y_2}, \quad p_0 = 1 - p_1 - p_2.$$

Obviously, we need to require $v_0 \tau_q / L \leq 1$. Otherwise, the probabilities are not always restricted in the range $0 \leq p_i \leq 1$.

## Problems of Chapter 20

### 20.1 Overtaking Two Slower Vehicles

1. For $\lambda = 0$, followers have no influence on the leaders, so the two leaders will not make space for the motorcyclist to pass.
2. The lateral dynamics of the follower is driven by the lateral repulsive forces from both leaders. Because they both have the same speed and the same longitudinal position, the situation is symmetric and the follower will be laterally centered with equal lateral gaps $s_y$ to both leaders.
3. Once laterally centered, the passing will succeed if, at a speed $v = v_1$, the longitudinal acceleration is positive during the time of longitudinal overlap where the two vehicles are still the leaders (greater coordinate $x$). From Eq. (20.12) we obtain

$$\frac{\mathrm{d}v}{\mathrm{d}t} = f^{\text{free}} + f^{\text{int}} = f^{\text{free}}(v) - b_{\max} \exp\left(-\frac{s_y}{s_{0y}}\right) > 0$$

and solving for the critical lateral gap giving a positive acceleration at speed $v_1$,

$$s_y^{\text{crit}} = s_{0y} \ln\left(\frac{b_{\max}}{f^{\text{free}}(v_1)}\right).$$

Notice that only the most interacting leader is considered, also if, as here, both leaders exert the same force.

4. Inserting the numerical values $f^{\text{free}}(v_1) = 1\,\text{m/s}^2$, $b_{\max} = 9\,\text{m/s}^2$, and $s_{0y}^{\text{lat}} = 0.2\,\text{m}$ gives $s_y^{\text{crit}} = 0.44\,\text{m}$.

### 20.2 Fundamental Diagram for Single-File Traffic

1. Because only the most interacting leader and follower matters for the longitudinal dynamics, the acceleration consists of five forces: free-flow force, interacting force from leader and follower, and the two boundary forces. Because of the lateral boundary forces, the subject vehicle will center itself on the road with equal gaps $s_{yb}$ to the boundary:

$$\dot{v} = f^{\text{free}}(v) + f^{\text{CF,int}}(s, v, v_l) - \lambda f^{\text{CF,int}}(s_f, v_f, v_l) - 2f_{\text{b,max}} \exp\left(-\frac{s_{yb}}{s_{0b}}\right)\left(\frac{v}{v_0}\right).$$

In the steady state, we have $\dot{v} = 0$, same speeds $v = v_l = v_f$ of subject, leader, and follower, and same gaps $s = s_f$ of the subject to the leader and the follower to the subject. Thus,

$$0 = f^{\text{free}}(v) + (1-\lambda) f^{\text{CF,int}}(s, v, v) - 2f_{\text{b,max}} \exp\left(-\frac{s_{yb}}{s_{0b}}\right)\left(\frac{v}{v_0}\right).$$

2. The FVDM interaction force at the steady state for gaps $s_0 \le s \le s_0 + v_0 T$ is given by

$$f^{\text{FVDM,int}} = f^{\text{FVDM}} - f^{\text{FVDM,free}} = \frac{v_{\text{opt}}(s) - v}{\tau} - \frac{v_0 - v}{\tau} = \frac{1}{\tau}\left(\frac{s - s_0}{T} - v_0\right).$$

Notice that the FVDM relative-speed term proportional to $\gamma$ drops out at the steady state.

3. We consider separately the case of free traffic flow (only interactions with the road boundaries) and interacting traffic.

*Free traffic.* Here, we have $f^{\text{CF,int}}(s, v, v) = 0$ and we obtain the condition

$$\begin{aligned} 0 &= f^{\text{free}}(v) - 2f_{\text{b,max}} \exp\left(-\frac{s_{yb}}{s_{0b}}\right)\left(\frac{v}{v_0}\right) \\ &= \frac{v_0 - v}{\tau} - 2f_{\text{b,max}} \exp\left(-\frac{s_{yb}}{s_{0b}}\right)\left(\frac{v}{v_0}\right) \end{aligned}$$

which can be solved for $v$ as

$$v = v_0^* = v_0/f, \quad f = \left[1 + 2\tau \frac{f_{\text{b,max}}}{v_0} \exp\left(-\frac{s_{yb}}{s_{0b}}\right)\right].$$

*Interacting traffic.* For $\lambda = 0$, we do not need a decomposition of the FVDM in a free and interacting force. At steady state with a gap $s_0 \le s \le s_0 + v_0^* T$, the force balance reads

$$0 = \frac{1}{\tau}\left(\frac{s - s_0}{T} - v\right) - 2 f_{\text{b,max}} \exp\left(-\frac{s_{yb}}{s_{0b}}\right)\left(\frac{v}{v_0}\right).$$

Solving for $v$ gives

$$v = v_e = \frac{s - s_0}{T^*}, \quad T^* = Tf = T\left[1 + 2\tau \frac{f_{\text{b,max}}}{v_0} \exp\left(-\frac{s_{yb}}{s_{0b}}\right)\right].$$

This means, the time gap $T^*$ is increased by a factor of $f > 1$ by the boundaries, and the steady-state speed is reduced by the factor $1/f$.

4. Even without leading vehicles, the boundaries reduce the desired speed and the factor $1/f$ shrinks exponentially when increasing the gaps to the boundary which both is plausible: Drivers generally do not traverse very narrow roads at the same desired speed that they would use for a wider road. With leading vehicles, the influence of the road boundaries increases the desired gap by the factor $f$ or, at a given gap, the speed is reduced by the factor $1/f$ as in the free-flow scenario.
5. Numerical value for $f$ if the road is as wide as the vehicle ($s_{yb} = 0$): $f = 2.0$.
6. If there are solid structures at the sides of the road, it would not be a good idea to drive at half the desired speed grazing the structures. For this case, the boundary interaction needs to be changed, e.g., by an additional factor $s_{0b}/s_{yb}$ diverging for lateral gaps tending to zero.

## Problems of Chapter 21

### 21.1 Locating a Temporary Bottleneck

From the data of floating car 3, we know that this car leaves a jam, i.e., crosses its downstream boundary, at the spatiotemporal point A depicted in the diagram below. From the data of detector 2 (point B), we know that this front is moving. We can exclude that the transition from congested to free traffic recorded by detector 2 at point B corresponds to a downstream moving upstream front because (i) detector D1 records essentially constant traffic flow, (ii) the data of the detector D2 and the floating car 3 imply an upstream propagating upstream jam front, i.e., a growing jam. Hence, the upstream front is propagating backwards as long as it exists.

From Stylized Fact 2 we know that downstream fronts are either stationary or move at a constant velocity $c_{\text{cong}}$. Hence, the set of possible spatiotemporal points indicating when and where the road closure is lifted, lies on a line connecting the

points A and B at a position $x > x_A$. The end of the road block not only sets the downstream jam front into motion but also leads to a transition empty road $\rightarrow$ maximum-flow state. The shockwave formula (9.9) implies that this front propagates with the desired free-flow speed $v_0$. Microscopically, this transition is given by the first car passing the accident site. This car is recorded as first trajectory of the trajectory data from the bridge at point C. Assuming, for simplicity, an instantaneous acceleration to the speed $v_0$, another set of possible spatiotemporal points for the removal of the road block is given by a line parallel to the first trajectory and touching it at point C (dashed line in the diagram). Intersecting the lines $\overline{AB}$ and the line parallel to the trajectories and going through C gives us the location and time of the lifting of the road block by the intersecting set of the two lines (point D), and also the location of the accident.

To estimate the time when the accident occurred, we determine the intersection F of the line $x = x_D$ of the temporary bottleneck, and the line representing the extrapolation of the last trajectory (point E) to locations further upstream (dashed line). Finally, because of the constant inflow recorded by D1, we know from the shockwave formula that the upstream jam front propagates essentially at a constant velocity, i.e., it is given by the line intersecting F and G. The jam dissolves when the upstream and downstream fronts meet at point H.

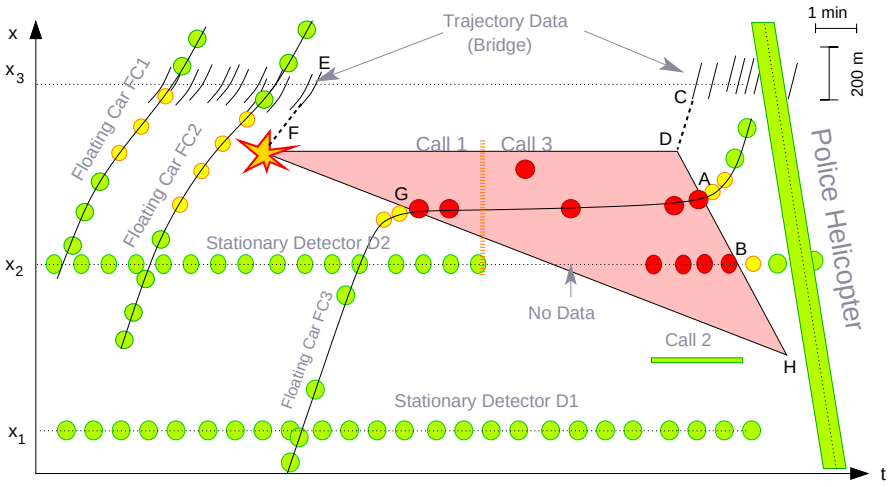


**21.2 Estimating the Location of a Jam Front from Stationary Detector Data**
The qualitative situation is depicted in following figure:

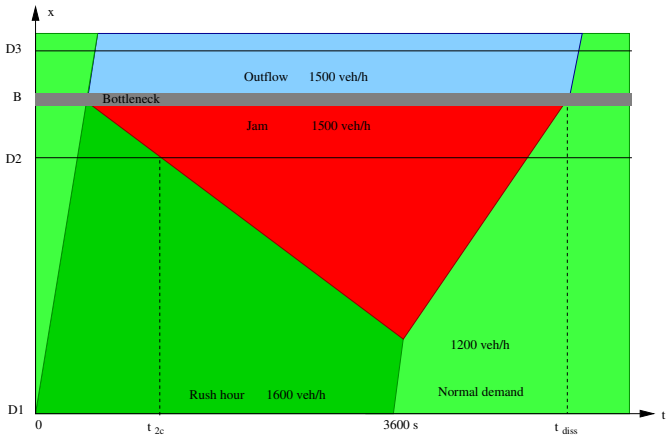


1. The transition between the two free-flow states "normal demand" (light green in the figure) and "rush hour" (dark green) propagates at the velocity $V_0 = 4\,\mathrm{km}/120\,\mathrm{s} = 120\,\mathrm{km/h}$. The same propagation velocity also applies to the boundary between free flow and outflow confirming $V_0 = 2\,\mathrm{km}/60\,\mathrm{s} = 120\,\mathrm{km/h}$. Furthermore, the outflow is equal to the bottleneck capacity, hence $C_\mathrm{B} = 1,500\,\mathrm{veh/h}$.
2. Since the velocity of the transition jam-outflow is zero, the flows of the two states must be the same. Hence, the reading $Q_2 = 1,500\,\mathrm{veh/h}$ of Detector D2 after $t_{c2} = 1,270\,\mathrm{s}$ confirms the bottleneck capacity. To calculate the velocity $c_\mathrm{up}$ of the transition rush-hour flow to congestion, one needs to solve the equation for the propagation times of the transition fronts,

$$t_{2c} = \frac{x_\mathrm{B}}{V_0} + \frac{x_2 - x_\mathrm{B}}{c_\mathrm{up}},$$

for $c_\mathrm{up}$ resulting in

$$c_\mathrm{up} = \frac{x_2 - x_\mathrm{B}}{t_{2c} - \frac{x_\mathrm{B}}{V_0}} = -0.893\,\mathrm{m/s}.$$

The traffic breakdown occurs always at the bottleneck, so, we go along the jam front back in time to arrive at

$$t_\mathrm{breakd} = t_{2c} - \frac{x_\mathrm{B} - x_\mathrm{D2}}{|c_\mathrm{up}|} = 150\,\mathrm{s}.$$

3. With $w = -5\,\mathrm{m/s}$, the shockwave propagation formula for $t > t_{2c}$ gives the same result:

$$c_\mathrm{up} = \frac{Q_\mathrm{rush} - Q_\mathrm{B}}{\frac{Q_\mathrm{rush} - Q_\mathrm{max}}{V_0} + \frac{Q_\mathrm{max} - Q_\mathrm{B}}{w}} = -0.893\,\mathrm{m/s}$$

(One could also solve the shockwave formula for $w$ to obtain the estimate directly).

4. The information from the upstream Detector D1 that the rush hour is over propagates with $V_0$ towards the upstream jam front. The time where this transition fronts meets the upstream jam front defines the time $t_m$ of the maximum jam extension: With respect to the observed transition time $t_{2c}$ at D2, the crossing condition reads

$$x_2 + c_{\text{up}}\,(t_m - t_{2c}) = x_{\text{D1}} + V_0(t_m - 3,600\,\text{s}).$$

Solving for $t_m$ gives $t_m = 3,656\,\text{s}$. Vehicles arriving at the jam at time $t_m$ (or passing D1 at the time 3,600 s where the rush hour ends) will encounter a jam of length

$$l_{\max} = |c_{\text{up}}|(t_m - t_{\text{breakd}}) = 3,130\,\text{m}$$

resulting in a time delay of

$$\tau_{\text{delay}} = l_{\max}\left(\frac{\rho_{\text{jam}}}{Q_{\text{jam}}} - \frac{1}{V_0}\right) = 240\,\text{s},$$

where $Q_{\text{jam}} = Q_{\text{B}} = 1,500\,\text{veh/h}$ and $\rho_{\text{jam}} = Q_{\max}(1/V_0 - 1/w) + Q_{\text{jam}}/w = 44.4\,\text{veh/km}$ have been used. Notice that, in order to get the delay time, we need to subtract the free-flow travel time $L/V_0$ from the "jam time" $l_{\max}\rho_{\text{jam}}/Q_{\text{jam}}$.

5. The dissolution time is easily obtained by the crossing time of the downstream moving jam front after the rush hour ($Q_{\text{in}} = 1,200\,\text{veh/h}$, propagation velocity $c'_{\text{up}} > 0$) with the bottleneck location:

$$c'_{\text{up}} = \frac{Q_{\text{in}} - Q_{\text{B}}}{\frac{Q_{\text{in}} - Q_{\max}}{V_0} + \frac{Q_{\max} - Q_{\text{B}}}{w}} = 2.419\,\text{m/s},$$

$$t_{\text{diss}} = t_m + \frac{l_{\max}}{c'_{\text{up}}} = 4,950\,\text{s}.$$

Once the jam has dissolved, the front between the states outflow ($Q = 1,500\,\text{veh/h}$) and the normal demand ($Q_{\text{in}} = 1,200\,\text{veh/h}$) propagates at velocity $V_0$, i.e., reaches D3 just a time interval $\Delta t = (x_3 - x_{\text{B}})/V_0 = 30\,\text{s}$ after the dissolution.

6. Additional FC trajectories give information $(x_i^{\text{up}}, t_i^{\text{up}})$ about the location of the jam front at a given time. These additional data points can be used to calibrate the LWR parameters of the shock-wave formula (9.45) in real time using as MoP the location of the jam front. Of course, in reality, we have fluctuating demand and predicting the jam front at the FCD times $t_i^{\text{up}}$ using (9.45) implies solving a delay-differential equation. Still, this is straightforward.

## Problems of Chapter 22

### 22.1 Criteria for Estimating Travel Times by N-Curves

This method works exactly on roads with a single lane per driving direction and

without ramps or other non-flow-conserving bottlenecks. Without floating cars, initialization and corrections of the cumulated vehicle numbers are possible on a heuristic basis, only. If the past speed data indicate free-flow speed and there are no fast-growing differences $N_i - N_j$ between the N-curves of the detectors $i$ and $j$, one assumes that there is free traffic in between, and initializes/corrects the N-curves by Eq. (22.10) with the density estimated by the average flow divided by the average speed. During the evolution of a jam (indicated by fast growing differences $N_i - N_{i+1}$), there are no correction possibilities without floating cars.

## 22.2 Estimating Travel Times from Aggregated Detector Data

*Subproblem 1.* The following figure displays two possibilities leading to the observed zero traffic flow at detector D2 between 16:00 and 16:30 h: (1) The accident happens upstream of D2 causing a temporarily empty road ($\rho = 0$, $Q = 0$) near the detector location D2. (2) The accident happens downstream of D2 causing temporarily blocked traffic ($\rho = \rho_{\max}$, $Q = 0$) near the detector location D2.

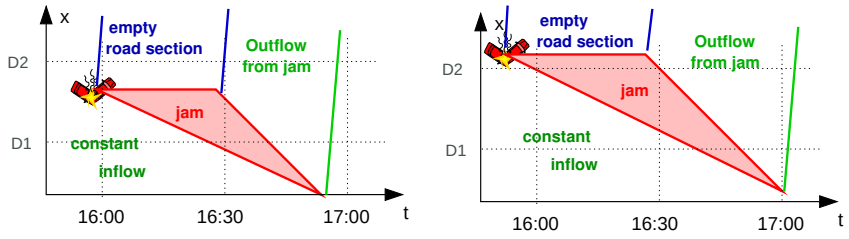


*Subproblem 2.* Assuming a free-flow speed of 120 km/h, it takes $\tau_{12} = 2\,\text{min} = 120\,\text{s}$ to pass the 4 km long section between the detectors D1 and D2. In this time interval, $\Delta n = 60$ vehicles have passed D1. Setting the cumulated vehicle count $N_1(0) = 0$ for the time 16:00 h (corresponding to $t = 0$), we obtain $N_2(0) = 60$. With this initialization, we calculate the cumulated vehicle count as a function of time, i.e., the N-curves, $N_1(t)$ and $N_2(t)$, by piecewise integration of the flows given in the problem statement:

$$N_1(t) = \begin{cases} 60 + 0.5\,t & t < 2{,}520, \\ 1{,}320 & 2{,}520 \le t < 3{,}000, \\ 1{,}320 + (t - 3{,}000) = t - 1{,}680 & 3{,}000 \le t < 3{,}480, \\ 1{,}800 + 0.5\,(t - 3{,}480) = 60 + 0.5\,t & t \ge 3{,}480, \end{cases}$$

and

$$N_2(t) = \begin{cases} 0.5\,t & t < 0, \\ 0 & 0 \le t < 1{,}800, \\ t - 1{,}800 & 1{,}800 \le t < 3{,}600, \\ 0.5\,t & t \ge 3{,}600. \end{cases}$$

*Subproblem 3.* Sketch of the N-curves:

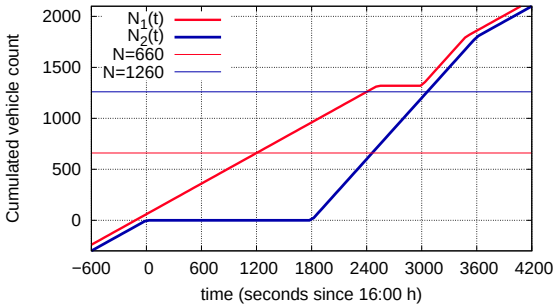


The realized travel time $\tau_{12}(t)$ at time $t = 2{,}400\,\mathrm{s}$ can be read from the diagram by the length of the horizontal line at height $N = N_2(2{,}400) = 600\,\mathrm{s}$ intersecting the curves $N_1(t)$ and $N_2(t)$: $\tau_{12}(t = 2{,}400) \approx 1{,}300\,\mathrm{s}$ (exactly: 1260, see below). The expected travel time $\tilde{\tau}_{12}(t)$ at time $t = 2{,}400\,\mathrm{s}$ is equal to the length of the horizontal line at height $N_1(2{,}400) = 1{,}250$ intersecting the two N-curves: $\tilde{\tau}_{12}(t) \approx 600\,\mathrm{s}$ (exactly: 660).

*Subproblem 4.* The diagram of the *N-curves* shows that, when estimating $\tilde{\tau}_{12}(t)$ within the time interval $-120\,\mathrm{s} \le t < 2{,}520\,\mathrm{s}$, the horizontal line intersecting the N-curves has a height $N$ between $N_1(-120) = 0$ and $N_1(2520) = 1320$. We determine its length between the intersections with the N-curves using the results of subproblem 2:

$$\begin{aligned} N_1(t) &= N_2(t + \tilde{\tau}_{12}) \\ 60 + \frac{t}{2} &= (t + \tilde{\tau}_{12}) - 1{,}800 \quad \Rightarrow \quad \tilde{\tau}_{12} = 1{,}860 - \frac{t}{2}\,. \end{aligned}$$

For $t < -120\,\mathrm{s}$, we have $\tilde{\tau}_{12} = 120\,\mathrm{s}$, i.e., equal to the free-flow travel time. At $t = -120\,\mathrm{s}$, there is a jump from 120 to 1,920, i.e., by 1,800 s or 30 min. This corresponds to the waiting time difference between the last vehicle that can pass before the road closure becomes active (possibly the car causing the accident), and the car after it having to wait the full duration of the road block.

For $\tau_{12}(t)$ within the time interval $1{,}800\,\mathrm{s} \le t < 3{,}120\,\mathrm{s}$, we obtain analogously

$$\begin{aligned} N_1(t - \tau_{12}) &= N_2(t) \\ 60 + \frac{1}{2}(t - \tau_{12}) &= t - 1{,}800 \quad \Rightarrow \quad \tau_{12} = 3{,}720\,\mathrm{s} - t\,. \end{aligned}$$

*Subproblem 5.* Since, according to the problem statement, the floating car slows down sharply when passing D2 at 16:00 h, the accident happened downstream of D2 somewhat before 16:00 h. This corresponds to situation (2) discussed in subproblem 1 above.

### 22.3 Costs of Motorway Congestion Estimated from Floating-Car Data

1. The total vehicle travel time (22.3) inside jams can be expressed by $\tau_{\mathrm{tot}} = \sum_t \sum_{s_t} n_{ts} \Delta t$ as sum over all updates $\Delta t$ and all congested road segments $s$ with

$n_{ts}$ vehicles in each at time $t$. The delay time is calculated by subtracting the travel times for free traffic,

$$\tau_{\text{delay}} = \tau_{\text{tot}} - \tau_{\text{free}} = \sum_t \sum_{s_t} \left( n_{ts} - n_{ts}^{\text{free}} \right) \Delta t = \sum_t \sum_{s_t} n_{ts} \left( 1 - \frac{V_{ts}}{V_{ts}^0} \right) \Delta t$$

where the last expression follows from vehicle conservation assuming steady states and a known free-flow speed $V_{ts}^0$. The number of vehicles $n_{ts}$ in each congested road segment of length $L_s$ with the number of lanes $I_s$ known from a digital map is given by $n = \rho^{\text{tot}} L_s = I_s \rho L_s = I_s \rho_{\text{cong}}(V_{ts}) L_s$. To estimate the congested density per lane, we assume a triangular fundamental diagram whose congested speed-density relation is given by Eq. (9.33),

$$V(\rho_{\text{cong}}) = \frac{Q(\rho_{\text{cong}})}{\rho_{\text{cong}}} = \frac{Q_{\max}}{\rho_{\text{cong}}} \left( 1 - \frac{w}{V_0} \right) + w$$

with measurable parameters for the free-flow speed $V_0$, the maximum flow per lane $Q_{\max}$ (approximately 2,000 veh/h/lane on highways), and the wave speed $w \approx -15\,\text{km/h}$. With the known speed $V_{ts}$ and the inverse relation

$$\rho_{\text{cong}}(V) = \frac{Q_{\max} \left( 1 - \frac{w}{V_0} \right)}{V - w},$$

the number of vehicles in a congested road segment at time $t$ can be estimated as

$$n_{ts} = I_s L_s \rho_{\text{cong}}(V_{ts}),$$

and the total and additional travel times by summing over all times and congested segments.[17]

2. The socioeconomic costs of congestion include loss of time, changed fuel consumptions/emissions, additional accidents, delay costs (e.g., missed appointments or broken just-in-time supply chains), and other external costs. Focussing on direct costs (time loss and increased fuel costs) we will show in Chapter 23 that increased fuel consumption is negligible (there may even be a *decreased* fuel consumption). Estimating the costs of loss of time from the delayed vehicle-hours, we need to assume an average value of time (VoT), 10 €/h for instance, and an average occupancy of 1.2 persons/veh for example. Then, the monetary costs are just the delayed vehicle-hours multiplied with the VoT and the occupancy according to following table.

[17] Note that, unlike the congested density, the free-flow density can *not* be estimated from local speeds if the penetration level is unknown. Conversely, the penetration level could be estimated from the absolute number of vehicles in congested segments (cf. Sect. 4.7.1).

| Country | Motorways (km) | $\tau_{\text{delay}}$ (mill. h/year) | Direct Costs (mill. €/year) | Motorway Specific Costs (€/km/year) |
|---|---|---|---|---|
| NLD | 5,500 | 62.0 | 744 | 135,000 |
| GBR | 7,500 | 61.0 | 732 | 97,600 |
| DEU | 27,400 | 195 | 2340 | 85,400 |

## Problems of Chapter 23

### 23.1 Coefficients of a Statistical Modal Consumption Model

Assuming a constant specific consumption $C_{\text{spec}} = 1/(\gamma w_{\text{cal}})$ (purely analytic physics-based model) and inserting Eqs. (23.13), (23.7), and (23.5) into Eq. (23.15) gives following function for the instantaneous model consumption:

$$\begin{aligned}\dot{C} = C_{\text{spec}} P &= C_{\text{spec}} \max\left[0, P_0 + Fv\right] \\ &= C_{\text{spec}} \max\left[0, P_0 + mv\dot{v} + m(\mu+\phi)gv + \frac{1}{2} c_d \rho A v^3\right].\end{aligned}$$

Apart from the maximum condition, this is a parameter-linear function whose parameters $\beta_j$ can be easily estimated by conventional multivariate regression. Comparing this function with the statistical model specified in the problem statement and using Table 23.2 gives following relations and values for the model parameters:

$$\begin{aligned}\beta_0 &= C_{\text{spec}} P_0 && = 242 \cdot 10^{-6}\,\text{liters/s} \\ \beta_1 &= C_{\text{spec}} mg\mu && = 11.9 \cdot 10^{-6}\,\text{liters/m} \\ \beta_2 & && = 0 \\ \beta_3 &= \tfrac{1}{2} C_{\text{spec}} c_d \rho A && = 31.4 \cdot 10^{-9}\,\text{liters}\,\text{s}^2/\text{m}^3 \\ \beta_4 &= C_{\text{spec}} m && = 121 \cdot 10^{-6}\,\text{liters}\,\text{s}^2/\text{m}^2 \\ \beta_5 &= C_{\text{spec}} mg && = 1.19 \cdot 10^{-3}\,\text{liters/s}.\end{aligned}$$

The following figure gives a plot of this function:

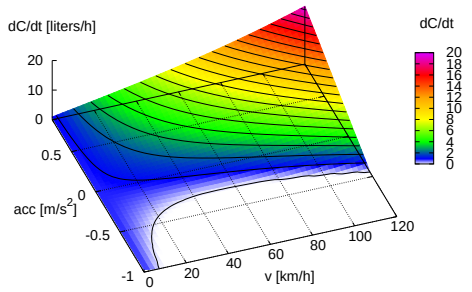

### 23.2 Coefficients of the *VT-micro* Model

The VT-micro model (23.3) reads

$$\dot{C} = e^P, \quad P = \begin{cases} \sum_{i,j} L_{ij} v^i \dot{v}^j & \dot{v} \geq 0 \\ \sum_{i,j} M_{ij} v^i \dot{v}^j & \dot{v} < 0 \end{cases}$$

and the physics-based model (23.15) with constant efficiency factor or specific consumption $c_{\text{spec}}$

$$\dot{C} = C_{\text{spec}} \left( P_0 + \mu m g v + m_{\text{dyn}} v \dot{v} + \frac{1}{2} c_d \rho A v^3 \right)$$

with the physical parameters explained in Table 23.2. In order to find the terms of the *VT-micro* model for $\dot{v} \geq 0$ corresponding to the physics-based model, we write the *VT-micro* model as

$$\dot{C} = e^{L_{00}} \exp \left( \sum_{i,j} L_{ij} v^i \dot{v}^j - L_{00} \right)$$

which, for the limit $v \to 0$ and $\dot{v} \to 0$, allows to immediately identify $e^{L_{00}} = C_{\text{spec}} P_0$, so

$$L_{00} = \ln(C_{\text{spec}} P_0) = -8.33\,.$$

To identify the remaining parameters $L_{10}$, $L_{11}$, and $L_{30}$, we could identify

$$\dot{C}_{\text{VTmicro}} = C_{\text{spec}} P_0 \exp\left( l_{10} v + L_{20} v^2 + L_{30} v^3 + L_{11} v \dot{v} + \ldots \right)$$

with

$$\dot{C}_{\text{phys}} = C_{\text{spec}} P_0 \left( \frac{\mu m g}{P_0} v + \frac{c_d \rho A}{2 P_0} v^3 + \frac{m_{\text{dyn}}}{P_0} v \dot{v} \right)$$

and perform a Taylor expansion around $v = 0$ and $\dot{v} = 0$. However, because of the nonlinear exponential function, such an expansion will only be valid for very low speeds and accelerations. In fact, the *VT-micro* model only produces valid results for a complete set of factors and quickly will result in unphysical values outside its calibrated range.

### 23.3 An Acceleration Model for Trucks

To solve this problem, we only need the power module of the physics-based modal consumption/emissions model. Assuming a constant engine power $P$ and solving Eq. (23.7) for the acceleration gives

$$\dot{v}_P(v, \phi) = \frac{P - P_0}{m v} - g(\mu + \phi) - \frac{1}{2} c_d \rho A v^2.$$

To include the restraints "maximum acceleration $a_{\max}$" and "no positive acceleration at speed $v > v_0$", we obtain the final form of the free-flow truck acceleration model:

$$\dot{v}(v,\phi) = \begin{cases} \min\left(a_{\max}, \dot{v}_P(v,\phi)\right) & v \le v_0 \\ \min\left(0, \dot{v}_P(v,\phi)\right) & v > v_0. \end{cases}$$

Following plot shows that the engine power is just sufficient to drive the truck at 80 km/h along a 2% uphill gradient with maximum power.

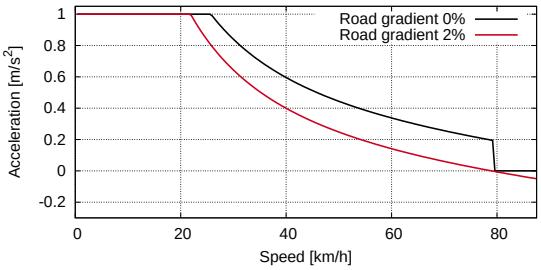


### 23.4 Characteristic Map of Engine Speed and Power

"Full throttle" corresponds to the top part of the allowed operating region for a given engine speed, i.e., to the top contour line of Fig. 23.3(c) or (d). At 3,000 rpm, it corresponds to 70 kW. For a power demand of 60 kW, an engine speed $f = 3,300$ rpm (or the speed nearest to this value allowed by the transmission) results in most efficient fuel usage (determine this again using Fig. 23.3(c) or (d)).

### 23.5 Characteristic Map of Engine Speed and Mean Effective Pressure

(i) 60 kW; (ii) An engine speed of $2,600\,\mathrm{min}^{-1}$ results in a specific consumption of about 300 ml per kWh while, at $4,000\,\mathrm{min}^{-1}$, the specific consumption is $\approx 350\,\mathrm{ml/kWh}$. The first option is more efficient although the throttle pedal needs to be pressed down further than for the higher engine speed because, for 2,600 rpm, the distance to the full-throttle maximum is lower than for 4,000 rpm).

### 23.6 Does Jam Avoidance Save Fuel?

At high vehicle speeds, the aerodynamic drag becomes dominant and the consumption per kilometer increases nearly quadratically. Therefore, the savings potential decreases and can even become negative (when comparing homogeneously flowing congested traffic with high-speed free traffic).

### 23.7 Influencing Factors of Fuel Consumption

Combining Eqs. (23.19), (23.13), (23.7), and (23.5) for the purely analytical physics-based model (constant specific consumption), we obtain following relation for the consumption per travel distance:

$$C_x = \frac{\mathrm{d}C}{\mathrm{d}x} = C_{\mathrm{spec}} \max\left[0, \left(\frac{P_0}{v} + m\dot{v} + (\mu+\phi)mg + \frac{1}{2}c_d\rho A v^2\right)\right]. \qquad (13)$$

*1. Air condition.* Correct. The additional power $\Delta P_0$ results in an additional consumption $\Delta C_x = C_{\mathrm{spec}}\Delta P_0/v$ which increases for decreasing speed. (Numerical values for $\Delta P_0 = 4\,\mathrm{kW}$: 2.9 l/100 km at 40 km/h and 1.45 l/100 km at 80 km/h.)

*2. Roof rack:* False. It is true that the increased $c_d$ value increases the consumption per distance by $\Delta C_x = C_{\text{spec}} \Delta c_d \rho A v^2/2$. However, this increase grows *quadratically* with the vehicle speed, i.e., it is lowest for city traffic. (Numerical values for $\Delta c_d = 0.08$: 0.41 l/100 km at 80 km/h and 1.65 l/100 km at 160 km/h.)

*3. Disconnecting the clutch when driving downhill.* False. If the clutch is disconnected, the driving shaft is decoupled from the generator and the overrun fuel cut-off cannot operate. In this case, the instantaneous consumption rate is given by the idling consumption rate $\dot{C}_0 = C_{\text{spec}} P_0$ leading to $C_{x0} = C_{\text{spec}} P_0/v$ for the consumption per distance. With the clutch connected, the fuel consumption $C_x$ is less than $C_{x0}$ if $F < 0$, and the overrun fuel cut-off is fully operative, i.e., $C_x = 0$, if $F < -P_0/v$. (Numerical values at 50 km/h: $C_{x0} = 1.74\,\text{l}/100\text{km}$; downhill gradient where the driving resistance $F$ is equal to zero: $-1.51\%$; downhill gradient where the overrun fuel cut-off is fully operative: $-2.98\%$.)

*4. Only use half the capacity of the tank.* False. At a tank capacity of 60 liters, the average fuel volume is 30 liters for the cycle full–empty–full etc., and 15 liters for the cycle half-filled–empty–half-filled etc. This corresponds, on average, to a savings of the total mass by $\Delta m < 15\,\text{kg}$ (since the specific mass of fuels is less than 1 kg/liter). The resulting effect on the consumption per distance, $\Delta C_x = -C_{\text{spec}} \Delta m g \mu < 0.0119\ \text{l}/100\text{km}$, is independent of the speed $v$ and negligible (but the risk to run out of fuel increases).

*5. Reduce speed from 50 km/h to 30 km/h.* False. At speeds below the optimal value of about $50 - 60\,\text{km/h}$ (cf. the figure), the consumption (13) per distance increases with decreasing speed. Specifically, $C_x = 4.31/100\text{km}$ at 30 km/h and 3.5 l/100 km at 50 km/h.

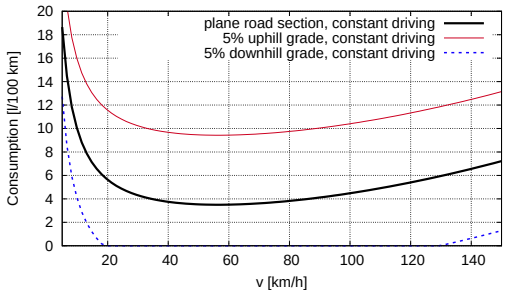


*6. Reduce speed from 150 km/h to 130 km/h.* Correct. $C_x = 7.21/100\text{km}$ at 150 km/h and 6.0 l/100 km at 130 km/h (cf. the figure).

### 23.8 Start-Stop System

The total waiting time is 360 s which, at 0.87 l/h for idling the engine means 87 ml saved fuel. In relation to the covered distance of 5 km, this is a fuel saving of 1.74 l/100 km.

**23.9 Highway vs. Mountain Pass: Which Route Needs More Fuel?**
When choosing alternative 1, i.e., driving the level highway at 150 km/h, one needs 7.2 liter per 100 km (cf. Solution to Problem 23.7).

When choosing alternative 2, i.e., driving the mountain pass at 70 km/h, one needs fuel only for the 50% of the route going uphill while the downhill gradient of 8% is more than enough to fully activate the overrun fuel cut-off (cf. the figure at the solution to Problem 23.7). With Eq. (13), we obtain for the uphill sections ($\phi = 0.08$) a consumption $C_x = 13.11/100\text{km}$. For the complete mountain pass (uphill and downhill), the consumption halves to $C_x = 6.51/100\text{km}$ which is less than the consumption on the highway! (The balance tips over to the other side for gradients of more than 10% or when driving more slowly on the highway.)

**23.10 Four-Way-Stops vs. Intersection with Priority Rules**
The analysis of situation II (constant speed $v_0 = 16\,\text{m/s}$) is easy: With Eq. (13), we obtain for the 500 m long stretch between two intersections $C_{\text{II}} = LC_x = 24.2\,\text{ml}$.

For situation I, we separate the driving cycle between two intersections into three driving modes: (i) accelerating from zero to $v_0$, (ii) cruising at $v_0$, and (iii) decelerating to a full stop at the next intersection.

*(i) Acceleration phase.* With $\dot{v} = a = 2\,\text{m/s}^2$, this phase lasts a time interval of $t_a = 8\,\text{s}$ during which a distance of $L_a = v_0^2/2a = 64\,\text{m}$ is covered. Because both $C_x$ and $\dot{C}$ are variable during the acceleration phase, explicit integration is necessary. We choose integration over time. With Eq. (23.15) and $C_{\text{spec}} = 1/(\gamma w_{\text{cal}})$, the integrand $\dot{C}$ reads

$$\dot{C}(t) = \frac{\mathrm{d}C}{\mathrm{d}t} = C_{\text{spec}} \left( P_0 + m\dot{v}v(t) + (\mu + \phi) mgv(t) + \frac{1}{2} c_d \rho A v^3(t) \right). \tag{14}$$

With $v(t) = at$, the integration can be evaluated analytically:

$$\begin{aligned} C_{\text{acc}} &= \int_0^{t_a} \dot{C}(t)\mathrm{d}t \\ &= C_{\text{spec}} \int_0^{t_a} \left( P_0 + ma^2 t + \mu mgat + \frac{1}{2} c_d \rho A a^3 t^3 \right) \mathrm{d}t \\ &= C_{\text{spec}} \left( P_0 t_a + \frac{1}{2} ma(a + \mu g) t_a^2 + \frac{1}{8} c_d \rho A a^3 t_a^4 \right). \end{aligned}$$

Using $t_a = v_0/a$ and $L_a = \frac{1}{2} a t_a^2$, we simplify this expression to

$$C_{\text{acc}} = C_{\text{spec}} W_{\text{acc}} = C_{\text{spec}} \left( P_0 t_a + \frac{1}{2} m v_0^2 + m\mu g L_a + \frac{1}{4} c_d \rho A v_0^2 L_a \right) = 17.8\,\text{ml}.$$

The terms in the parenthesis of the last equation have the following meanings: $P_0 t_a$ is the energy necessary to operate all the secondary appliances during the acceleration phase, $\frac{1}{2} m v_0^2$ is the kinetic energy at the end of this phase, $m\mu g L_a$ is the energy lost

(or, more precisely, transformed to heat) by the solid-state friction, and $\frac{1}{4}c_d\rho A v_0^2 L_a$ is the energy lost by the aerodynamic drag.

*(ii) Cruising phase.* Since both the acceleration and deceleration phases cover a road section of $L_a = 64\,\mathrm{m}$, a distance $L_c = L - 2L_a = 372\,\mathrm{m}$ remains for the cruising phase. Correspondingly, $C_{\mathrm{cruise}} = C_{\mathrm{spec}} W_{\mathrm{cruise}} = L_c C_x(v_0, \dot{v} = 0) = 11.1\,\mathrm{ml}$.

*(iii) Deceleration phase.* Due to overrun fuel cut-off, no fuel is consumed in this phase, so $C_{\mathrm{brake}} = 0$.[18]

*Result for situation I.* The total consumption between two intersections for the traffic rules of situation I equals $C_{\mathrm{I}} = C_{\mathrm{acc}} + C_{\mathrm{cruise}} + C_{\mathrm{brake}} = 31.4\,\mathrm{ml}$ which has to be compared with $C_{\mathrm{II}} = 17.5\,\mathrm{ml}$.

In summary, the fuel saving potential of changing the traffic rules from that of situation I to that of situation II is more than 40% which is massive.

### 23.11 Fuel Consumption for an OVM-Generated Speed Profile

*Subproblem 1.* The OVM free acceleration $\dot{v} = (v_0 - v)/\tau$ is maximal at $v = 0$. Prescribing $\dot{v}_{\max} = v0/\tau = 2\,\mathrm{m/s^2}$ gives the relaxation time $\tau = v_0/a = 16.67\,\mathrm{s}$.[19]

*Subproblem 2.* We calculate the instantaneous power at a given speed $v$ from Eq. (23.7) with Eq. (23.5):

$$P(v,\dot{v}) = \frac{\dot{C}(v,\dot{v})}{C_{\mathrm{spec}}} = P_0 + m\dot{v}v + (\mu + \phi)mgv + \frac{1}{2}c_d\rho A v^3 .$$

Inserting the OVM free acceleration $\dot{v} = (v_0 - v)/\tau$, we obtain $P_{\mathrm{OVM}}(v) = A_0 + A_1 v + A_2 v^2 + A_3 v^3$ where

$$\begin{aligned} A_0 &= P_0 = 3\,\mathrm{kW}, & A_1 &= m\left(g\mu + \frac{v_0}{\tau}\right) = 3,147\,\mathrm{Ws/m}, \\ A_2 &= -\tfrac{m}{\tau} = -90\,\mathrm{W(s/m)^2}, & A_3 &= \frac{1}{2}c_d\rho A = 0.39\,\mathrm{W(s/m)^3}. \end{aligned}$$

*Subproblem 3.* As usual, we calculate extremal values by setting the derivative with respect to the interesting variable (here, the speed $v$) equal to zero:

$$\frac{\mathrm{d}P_a}{\mathrm{d}v} = A_1 + 2A_2 v + 3A_3 v^2 \stackrel{!}{=} 0 .$$

This quadratic equation has two solutions and corresponding extremal power requirements $P_{\mathrm{OVM}}$:

[18] Strictly speaking, this is not true for the very last part of the deceleration phase when the speed (ignoring aerodynamic drag) drops below $v_c = P_0/[m(|\dot{v}| - \mu g)] \approx 7\,\mathrm{km/h}$. This is neglected here.

[19] At this value, the OVM is extremely unstable and cannot be used for simulating interacting or congested traffic.

$$v_1 = 133.7\,\mathrm{m/s} = 481.4\,\mathrm{km/h},\;\; P_{\mathrm{OVM}}(v_1^*) = -254\,\mathrm{kW},$$
$$v_2 = 20.1\,\mathrm{m/s} = 72.4\,\mathrm{km/h},\;\; P_{\mathrm{OVM}}(v_2^*) = 33.1\,\mathrm{kW}.$$

Obviously, the second solution is the correct one since the power (and the OVM acceleration) is negative for the first one.[20] The maximum power during the acceleration phase is reached at 76 km/h. Its value is 32.1 kW.

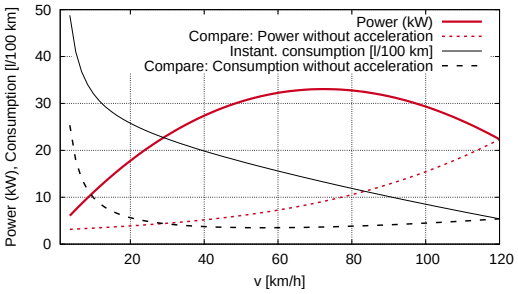


## 23.12 Trucks at Uphill Gradients

*1. Engine power.* With Eqs. (23.7) and (23.5), we obtain for the necessary power to maintain a speed $v = v_{\mathrm{limit}} = 80\,\mathrm{km/h}$ at level roads

$$P_{\mathrm{dyn}} = P - P_0 = vF(v) = \mu mgv + \frac{1}{2}c_d\rho Av^3 = 249\,\mathrm{kW} + 57\,\mathrm{kW} = 306\,\mathrm{kW}.$$

*2. Initial deceleration.* The two new forces entering the balance are the uphill-slope force and the inertial force. Since, initially, all other forces remain unchanged, the two new forces must cancel each other, i.e.,

$$\phi g + \dot{v} = 0 \Rightarrow \dot{v} = -\phi g = \begin{cases} -0.49\,\mathrm{m/s^2} & \text{at } 5\% \text{ gradient,} \\ -0.39\,\mathrm{m/s^2} & \text{at } 4\% \text{ gradient.} \end{cases}$$

*3. Terminal speed.* Equation (23.7) also delivers the terminal speed at a gradient $\phi$ by setting $\dot{v} = 0$ and solving for $v$. Neglecting the aerodynamic drag, we obtain

$$P_{\mathrm{dyn}} = (\mu + \phi)gmv \;\Rightarrow\; v_\infty = \frac{P_{\mathrm{dyn}}}{(\mu+\phi)gm} = \begin{cases} 10.2\,\mathrm{m/s} & \text{at } 5\% \text{ gradient,} \\ 11.7\,\mathrm{m/s} & \text{at } 4\% \text{ gradient.} \end{cases}$$

*4. Estimating the OVM parameters in the uphill section.* Since the OVM speed approaches asymptotically the desired speed $v_\infty$, we can set the OVM "desired speed" in the uphill sections equal to the terminal speed $v_\infty$. The initial accelerations calculated in subproblem 2 at the desired speed $v_0$ of the *level* section serve to estimate $\tau$ via $\dot{v} = (v_\infty - v_0)/\tau$, i.e., $\tau = (v_\infty - v_0)/\dot{v}$, resulting in

$$\tau = \begin{cases} 24.4\,\mathrm{s} & \text{at } 5\% \text{ gradient,} \\ 26.8\,\mathrm{s} & \text{at } 4\% \text{ gradient.} \end{cases}$$

[20] This solution represents the minimum power requirement.

*5. Speed and distance over time.* The solution to the inhomogeneous ordinary differential equation $\frac{dv}{dt} = (v_\infty - v)/\tau$ for the initial condition $v(0) = v_0$ reads (cf. the following figure)

$$v(t) = v_\infty + (v_0 - v_\infty)\,e^{-t/\tau},$$
$$x(t) = v_\infty(t-\tau) + v_0\tau - (v_0 - v_\infty)\,\tau e^{-t/\tau}.$$

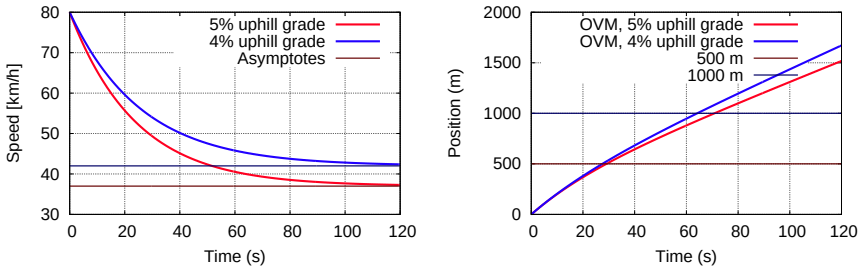


For the uphill section 1 of length $L_1 = 500\,\text{m}$ and gradient $\phi_1 = 5\%$, we obtain for the time $t = t_1 = 29.1\,\text{s}$ given in the problem statement:

$$v(t_1) = 13.8\,\text{m/s} = 49.8\,\text{km/h}.$$

(Test: $x(t_1) = 500.5\,\text{m}$.) Analogously, we obtain for the uphill section 2 of length $L_2 = 1{,}000\,\text{m}$ and gradient $\phi_2 = 4\%$ at time $t = t_2 = 64.2\,\text{s}$:

$$v(t_2) = 12.6\,\text{m/s} = 45.2\,\text{km/h}.$$

(Test: $x(t_2) = 1{,}000.2\,\text{m}$)

*Discussion.* Although the uphill section 1 is steeper, the speed of the trucks at its end is higher than at the end of the less steep but longer uphill section 2. Therefore, it makes sense to allow higher gradients on shorter uphill sections.

### 23.13 Maximum Deceleration Capability of Regenerative Braking

The maximum regenerative deceleration is proportional to the maximum torque in the generator regime which is constant below a critical engine speed $f_c$ and corresponding vehicle speed $v_c$, and proportional to $1/v$ for higher speeds. Using Eq (23.17) at the transition point, $P_{\max} = 2\pi f_c M_{\max}$, we find

$$f_c = \frac{P_{\max}}{2\pi M_{\max}} = 47.7\,\text{s}^{-1}, \quad v_c = \frac{2\pi f_c}{i_{\text{BEV}}} = 23.5\,\text{m/s}.$$

At 50 km/h (13.9 m/s), we are at the torque limited regime and the maximum regenerative deceleration is given by

$$b^{\text{reg}}_{\max}(v \le v_c) = \frac{F}{m} = \frac{i_{\text{BEV}} M_{\max}}{r_{\text{tire}}} = 3.67\,\text{m/s}^2.$$

For $v = 100\,\mathrm{km/h} = 27.8\,\mathrm{m/s}$, we are in the power limited regime, so, with $P = mv\dot{v}$, we have

$$b_{\max}^{\mathrm{reg}}(v > v_c) = \frac{P}{mv} = 3.09\,\mathrm{m/s^2}.$$

Notice that we also could have calculated this deceleration by $b_{\max}^{\mathrm{reg}}(v > v_c) = b_{\max}^{\mathrm{reg}}(v \le v_c)\, v_c/v$. In summary, regenerative braking (recuperation) is possible for most everyday braking situations but not for emergency braking maneuvers ($\approx 10\,\mathrm{m/s^2}$) or stronger decelerations at high speeds.

### 23.14 Driving Patterns of Battery-Electric Vehicles

*1. Basic elements of the driving patterns.*

- *Cruising at constant speed $v_0$ over a distance L.* Clearly, $P_0 + vF > 0$ for a level terrain. Since state variables are independent of $x$ in this driving element, we use Eq. (23.30) with (23.5). With the travel time $T = L/v_0$ and the abbreviation $c = 1/2 c_d \rho A$ ($c = 0.897\,\mathrm{kg/m}$ in our example), we have

$$W_{\mathrm{c}}(v_0, L) = \frac{P_0 T + mg\mu L + \frac{1}{2} c v_0^2 L}{\eta_{\mathrm{batt}}^2 \eta_{\mathrm{mot}}} = \frac{\left(\frac{P_0}{v_0} + mg\mu + \frac{1}{2} c v_0^2\right) L}{\eta_{\mathrm{batt}}^2 \eta_{\mathrm{mot}}}$$

  corresponding to an energy demand per distance of $W_{\mathrm{plug}}/L$.
- *Accelerating from zero to the speed $v_0$.* For the $P_0$ term, we need the time $T_a = v_0/a$. For the constant rolling friction term, we use Eq. (23.30) resulting in $\int F(x)\mathrm{d}x = mg\mu L_a$ with the acceleration distance $L_a = v_0^2/(2a) = v_0 T_a/2$ (corresponding to the braking distance at $-a$). For the inertial part, we use Eq. (23.29) with

$$\int_0^{T_a} m_{\mathrm{dyn}} v\dot{v}\mathrm{d}t = \frac{m_{\mathrm{dyn}}}{2} \int_0^{T_a} \frac{\mathrm{d}}{\mathrm{d}t}(v^2)\mathrm{d}t = \frac{m_{\mathrm{dyn}}}{2} \left[v^2\right]_{v=0}^{v=v_0} = \frac{m_{\mathrm{dyn}}}{2} v_0^2.$$

  Finally, for the wind-drag part, we use the time integral of Eq. (23.29) as well:

$$\begin{aligned} \int_0^{T_a} v \left(\frac{c}{2} v^2(t)\right) \mathrm{d}t &= \frac{c}{2} \int_0^{v_0/a} a^3 t^3 \mathrm{d}t \\ &= \frac{ca^3}{8} \left[t^4\right]_{t=0}^{t=v_0/a} \\ &= \frac{c v_0^4}{8a} = \frac{c v_0^3}{8} T_a = \frac{c v_0^2}{4} L_a, \end{aligned}$$

  where $L_a = v_0 T_a/2$ has been used at the last equality sign. Putting all together, we have

$$W_{\mathrm{a}}(v_0, a) = \frac{\left(\frac{2P_0}{v_0} + mg\mu + \frac{1}{4} c v_0^2\right) L_a + \frac{1}{2} m_{\mathrm{dyn}} v_0^2}{\eta_{\mathrm{batt}}^2 \eta_{\mathrm{mot}}}, \quad L_a = \frac{v_0^2}{2a}.$$

- *Decelerating from speed $v_0$ to zero.* Assuming that one is always in the regenerative braking regime, the derivation is along the lines of the acceleration regime resulting in the above expression with a reversed sign for the dynamic contribution and the $\gamma$ value for recuperation,

$$W_{\mathrm{b}}(v_0,b) = \left[\left(\frac{2P_0}{v_0} + mg\mu + \frac{1}{4}cv_0^2\right)L_b - \frac{1}{2}m_{\mathrm{dyn}}v_0^2\right]\eta_{\mathrm{mot}}, \quad L_b = \frac{v_0^2}{2b}.$$

  The approximation of always being in the regenerative braking regime is valid as long as $v > v_c$ given by $P_0 + mg\mu v_c - m_{\mathrm{dyn}}v_c b = 0$ resulting in

$$v_c = \frac{P_0}{m_{\mathrm{dyn}}b - mg\mu}$$

  evaluating to $v_c = 0.25\,\mathrm{m/s}$, in our case. Therefore, this approximation only entails minimal errors.
- *Waiting a time $T_{stop}$.* This is just given by

$$W_{\mathrm{w}}(T) = \frac{P_0 T}{\eta_{\mathrm{batt}}^2\eta_{\mathrm{mot}}}.$$

*2. Driving patterns "residential area" and "arterial".*

- *Pattern 1: Residential area.* We have a total length of $L = 1{,}000\,\mathrm{m}$, a maximum speed $v_0 = 30/3.6\,\mathrm{m/s}$, and $n = 5$ acceleration and deceleration phases at $a = b = 2\,\mathrm{m/s^2}$. Hence

$$\begin{aligned} W_{\mathrm{plug}}^{\mathrm{residential}} &= 5W_{\mathrm{b}}(v_0,b) + 5W_{\mathrm{a}}(v_0,a) + W_{\mathrm{c}}(v_0, L - 5(L_a + L_b)) \\ &= 655\,000\,\mathrm{Ws} = 0.182\,\mathrm{kWh} \end{aligned}$$

  where $L_a = L_b = v_0^2/a = 17.4\,\mathrm{m}$ has been used.
- *Pattern 2: City arterial.* In analogy to above, we have

$$\begin{aligned} W_{\mathrm{plug}}^{\mathrm{arterial}} &= W_{\mathrm{b}}(v_0,b) + W_{\mathrm{w}}(T_w) + W_{\mathrm{a}}(v_0,a) + W_{\mathrm{c}}(v_0, L - (L_a + L_b)) \\ &= 618\,000\,\mathrm{Ws} = 0.172\,\mathrm{kWh} \end{aligned}$$

  where $v_0 = 50/3.6\,\mathrm{m/s}$, $L_a = L_b = v_0^2/a = 48.2\,\mathrm{m}$, and $T_w = 30\,\mathrm{s}$ has been used.

**23.15 Under Which Conditions Do All-Electric Cars Save $CO_2$ Emissions?**
For the BEV, the indirect $CO_2$ emissions per km can be calculated from the definition of the carbon intensity $C_{\mathrm{CO_2}}^{\mathrm{el}} = 0.35\,\mathrm{kg\ CO_2/kWh}$ of the used mix of electricity generation and the fact that the values for $W_{\mathrm{plug}}$ already calculated in the previous problem 23.14 and in the main text Section 23.4.4 directly give the electricity demand including charging losses,

$$e_{\mathrm{CO_2}}^{\mathrm{BEV}} = C_{\mathrm{CO_2}}^{\mathrm{el}} W_{\mathrm{plug}}.$$

For the ICE, the $CO_2$ emissions are calculated using the definition of the specific consumption $C_{\text{spec}} = 0.291/\text{kWh}$ (transforming the needed energy for driving and appliances into used fuel) and the well-to-wheel carbon intensity (sum of well-to-tank and tank-to-wheel emissions) $C_{\text{CO}_2}^{\text{w2w}} = 2.79\,\text{kg}\,\text{CO}_2/\text{l}$ transforming used fuel into $CO_2$:

$$e_{\text{CO}_2}^{\text{ICE}} = C_{\text{CO}_2}^{\text{w2w}} C_{\text{spec}} W_{\text{ICE}}.$$

Since all engine losses are already characterized in the specific consumption and "charging" the ICE (i.e., filling it up) is lossless, the expressions for the ICE energy demand in the five patterns are that for BEVs with $\eta_{\text{batt}}$ and $\eta_{\text{mot}}$ set to unity. Furthermore, because ICEs cannot recuperate, all negative energy/power contributions are set to zero (overrun fuel cut-off). The results are given in Table 23.4 in the main text.

## Problems of Chapter 24

### 24.1 Discrete-Choice Models for the Routing Decision

*1. General binary discrete-choice model.* Since a *homo oeconomicus* will always choose the alternative with the highest total utility $U_i$, the probability of choosing alternative $i = 1$ out of two alternatives is just given by $P_1 = \text{prob}(U_1 \geq U_2)$. Inserting the decomposition $U_i = V_i + \varepsilon_i$, separating the deterministic and random terms and using the definition of the cumulative distribution function $F(x) = \text{prob}(X \leq x)$ of a random variable $X$, we obtain

$$\begin{aligned} P_1 &= \text{prob}(V_2 + \varepsilon_2 \leq V_1 + \varepsilon_1) \\ &= \text{prob}(\varepsilon_2 - \varepsilon_1 \leq V_1 - V_2) \\ &= F_{\varepsilon_2 - \varepsilon_1}(V_1 - V_2). \end{aligned}$$

*2. Binary Logit model.* With $F_{\varepsilon_2-\varepsilon_1}(x) = F_{\varepsilon_1-\varepsilon_2}(x) = 1/(1+e^{-x})$, we obtain

$$P_1 = \frac{1}{1+e^{V_2-V_1}} = \frac{e^{V_1}}{e^{V_1}+e^{V_2}}.$$

*3. Meaning of the model parameters.* If the travel time of alternative $i$ increases by $\Delta T_i$, the utility increases by $\beta_T \Delta T_i$, so, obviously, $\beta_T < 0$. Since $\varepsilon_i$ is dimensionless with a variance near unity,[21] this means that an increment $\Delta V_i = \beta_T \Delta T_i = 1$ essentially corresponds to a change by one standard deviation of the random utility. Hence, $1/\beta_T$ essentially corresponds to the standard deviation of the random utility if measured in minutes. The parameter $\beta_1$ gives an ad-hoc "bonus" for alternative 1 for the case of equal travel times in multiples of the standard deviation of the ran-

[21] The precise value depends on the model but it is always near 1. For the Logit model, we have $\text{Var}(\varepsilon_i) = \pi^2/6$.

dom utility. We expect $\beta_1 \geq 0$ since, generally, driving an unknown deviation is more stressful than just following the main route.

*4. Application to the route-choice decision.* Only the fraction $\alpha$ of drivers is "in the know" and willing to potentially use the deviation is eligible for the discrete choice. Hence, the probability $P_2$ of drivers actually using the deviation is the product of the probability for being eligible and the conditional probability of choosing route 2 if eligible, hence

$$P_2 = \alpha P_2^{\text{Logit}} = \frac{\alpha e^{V_2(t)}}{e^{V_1(t)} + e^{V_2(t)}}, \quad P_1(t) = 1 - P_2(t),$$

which is Eq. (24.2) of the main text.

### 24.2 User Equilibrium and System Optimum in Dynamic Navigation

*1. Travel times.* In an empty network, the maximum speed $V_0$ (which here is the same on both routes) can be driven, so

$$T_{01} = \frac{L_1}{V_0} = 750\,\text{s}, \quad T_{02} = \frac{L_2}{V_0} = 800\,\text{s}.$$

*2. User equilibrium I: Qualitative considerations.* Once an inflow $Q_{\text{in}} = 5,400\,\text{veh/h}$ arrives, all drivers will first choose R1 since $T_{10} < T_{20}$. However, since $Q_{\text{in}} > C_1^{\text{B}}$, a traffic jam will form behind the bottleneck. New incoming drivers with a perfect knowledge of the instantaneous travel times on both routes will still select R1 until the travel time $T_i$ has increased near $T_{20}$. Then, some drivers will select R2 such that the length of the jam on R1 remains constant at $T_1 \approx T_{20}$. However, this will only happen in the presence of noise, $\sigma_T > 0$. Otherwise, we have a *bang-bang control* which, in the presence of delays, will always lead to oscillations. Since there is no hysteresis or capacity drop in LWR models, the flow on R1 in the user equilibrium (UE) and the corresponding flow on R2 are given by

$$Q_1^{\text{tot,UE}} = C_1^{\text{B}} = 4,860\,\text{veh/h}, \quad Q_2^{\text{tot,UE}} = Q_{\text{in}} - Q_1^{\text{tot,UE}} = 540\,\text{veh/h}.$$

The resulting flow $Q_2^{\text{tot,UE}}$ is well below the bottleneck capacity $C_2^{\text{B}}$, so no jam will form on R2.

*Length of the congestion on R1 in user equilibrium.* The length $x$ of the congestion on R1 in user equilibrium is given by the condition of equal travel times on both routes:

$$T_1 = \frac{x}{V_{\text{cong}}} + \frac{L_1 - x}{V_0} \stackrel{!}{=} T_{20},$$

or

$$x = \frac{T_{20} - \frac{L_1}{V_0}}{\frac{1}{V_{\text{cong}}} - \frac{1}{V_0}}.$$

In order to obtain the speed $V_{\text{cong}}$ in the congestion, we observe that the congested flow per lane on the three-lane road is given by $Q_{\text{cong}} = C_1^{\text{B}}/3$. Since the wave speed $w$ is the slope of the congested branch of the triangular fundamental diagram, and $Q_{\text{cong}} = 0$ for $\rho = \rho_{\max}$, the associated density is determined by $Q_{\text{cong}} = w(\rho - \rho_{\max})$ or

$$\rho_{\text{cong}} = \rho_{\max} + \frac{Q_{\text{cong}}}{w} = \rho_{\max} + \frac{C_1^{\text{B}}}{3w} = 60\,\text{veh/km},$$

whence

$$V_{\text{cong}} = \frac{Q_{\text{cong}}}{\rho_{\text{cong}}} = 7.5\,\text{m/s}, \quad x = 600\,\text{m}.$$

*3. System optimum (SO).* Since $T_{10} < T_{20}$, the system optimum implies that as many vehicles as possible take R1 without producing a jam. This means $Q_1^{\text{tot,SO}} = C_1^{\text{B}}$ as in the user equilibrium. However, vehicles are sent on R2 *before* a jam can form, so that $T_2 > T_1$ which means, the SO is no equilibrium configuration, whether stable or unstable. In summary, we have

$$Q_1^{\text{tot,SO}} = Q_1^{\text{tot,UE}} = 4,860\,\text{veh/h}, \quad Q_2^{\text{tot,SO}} = Q_2^{\text{tot,UE}} = 540\,\text{veh/h},$$

and

$$\begin{aligned} T_1 &= T_{10} = 750\,\text{s}, \quad T_2 = T_{20} = 800\,\text{s}, \\ \bar{T} &= \frac{Q_1^{\text{tot,SO}}}{Q_{\text{in}}} T_1 + \frac{Q_2^{\text{tot,SO}}}{Q_{\text{in}}} T_2 = 0.9T_1 + 0.1T_2 = 755\,\text{s}. \end{aligned}$$

*4.1 Necessary conditions for a UE* as calculated previously, both the UE and SO require that a percentage

$$P_2^{\text{SO}} = \frac{Q_{\text{in}} - C_1^{\text{B}}}{Q_{\text{in}}} = 10\%$$

diverts to the deviation. If the uncertainty $\sigma_T$ is sufficiently small, $\sigma_T \ll T_{02} - T_{01}$, all equipped drivers will divert as soon as the jam on Route 1 reaches its UE length but not earlier thus stabilizing the UE. Obviously, this is only possible if there are enough equipped vehicles, $\alpha > P_2^{\text{SO}}$. If, however, $\alpha$ is significantly greater than $P_2^{\text{SO}}$, oscillation instabilities will form. If $\sigma_T$ is no longer $\ll T_{02} - T_{01}$, oscillations are suppressed but some drivers will already use Route 2 before the UE length of the jam is reached leading to a situation between the UE and SO.

*4.2 Necessary conditions for a SO.* In order that a SO is sustained, a fraction $P_2^{\text{SO}}$ of drivers must use Route 2 right at the beginning, i.e., use a route which is longer by the time difference $T_{02} - T_{01}$. In order to do this, the uncertainty must be at a certain level given by

$$P_2 = \frac{\alpha}{e^{V_{01} - V_{02}} + 1} = \frac{\alpha}{e^{\frac{T_{02} - T_{01}}{\sigma_T}} + 1}$$

which can be solved for $\alpha$ resulting in Eq. (24.21) of the main text,

$$\alpha = P_2^{\mathrm{SO}} \left( e^{\frac{\tau_{02}-\tau_{01}}{\sigma_T}} + 1 \right).$$

Additionally, we must require $P_2 < 50\%$ because, otherwise, Condition (24.21) can never be met.

*Necessary conditions for no jam on Route 2.* Congestions on both routes are avoided in the steady state if $P_s^{\mathrm{SO}} \leq P_2 \leq P_2^{\max}$ where $P_2^{\max}$ is calculated from the maximum flow $Q_{\mathrm{in}} P_2^{\max} = C_2^{\mathrm{B}}$ that Route 2 can accommodate without becoming congested, so

$$P_2^{\max} = \frac{C_2^{\mathrm{B}}}{Q_{\mathrm{in}}} = 20\%.$$

In terms of $\alpha$, this means

$$\alpha \leq P_2^{\max} \left( e^{\frac{\tau_{02}-\tau_{01}}{\sigma_T}} + 1 \right)$$

which is the second condition of (24.21).